DEVELOPMENT OF A NEW TYPE OF SIMULATED SCALAR FEED

A THESIS SUBMITTED BY

STEPHEN RODRIGUES

IN PARTIAL FULFILMENT OF THE REQUIREMENTS
FOR THE DEGREE OF

DOCTOR OF PHILOSOPHY

COCHIN UNIVERSITY OF SCIENCE AND TECHNOLOGY
FACULTY OF TECHNOLOGY
DEPARTMENT OF ELECTRONICS
COCHIN – 682 022
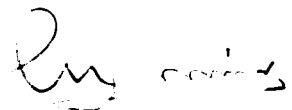**INDIA**

OCTOBER 1992

dedicated

to

my parents

CERTIFICATE

This is to certify that the thesis entitled "DEVELOPMENT OF A NEW TYPE OF SIMULATED SCALAR FEED" is a bona fide record of the research work carried out by Mr.Stephen Rodrigues under my supervision in the Department of Electronics, Cochin University of Science and Technology. The results embodied in this thesis or part of it have not been presented for any other degree.

Dr.K.G.Nair
(Supervising Teacher)
Professor and Head of the
Department of Electronics
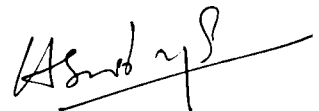Cochin University of Science
and Technology

Kochi 682022

23 October 1992

DECLARATION

I hereby declare that the work presented in the thesis entitled "DEVELOPMENT OF A NEW TYPE OF SIMULATED SCALAR FEED" is based on the original work done by me under the supervision of Dr.K.G.Nair, in the Department of Electronics, Cochin University of Science and Technology, and that no part thereof has been presented for the award of any other degree.

Kochi 682022

23 October 1992

STEPHEN RODRIGUES.

ACKNOWLEDGEMENTS

CONTENTS

Chapter 1

INTRODUCTION

1

Chapter 1

INTRODUCTION

Horns have been used as accoustical instruments, for thousands of years to amplify sound waves. As a microwave antenna, the forerunner of the horn, namely, the hollow pipe radiator has been used first by Sir Oliver Lodge in June 1894. He demonstrated the use of a hollow pipe radiator for radiating and receiving microwaves.

In 1897, the famous Indian scientist, Prof.J.C.Bose demonstrated a "Microwave spectrometer" operating at a frequency of 60 GHz, at the Royal Institution of London. The receiver of the microwave spectrometer was a pyramidal horn called "The Collecting Funnel". In the same year, Lord Rayleigh published his famous paper on waveguide transmission.

After these works, the interest in microwave pipe radiators and horn radiators did not receive much attention until late 1930's. Though the concept of electromagnetic waveguide radiator was suggested in 1936, the first experimental and theoretical analysis of the waveguide radiator was reported by W.L.Barrow and F.M.Green in 1938.

2

Regarding the electromagnetic horn, the first theoretical analysis of its operation was reported by W.L.Barrow and L.J.Chu in 1939. Although the analysis applies specifically to sectoral horns, it provides a clear picture of the operation of electromagnetic horns of any shape. After the late 1930's the exigencies of World War II produced a veritable explosion in the development of efficient radiators of electromagnetic energy.

1.1 ELECTROMAGNETIC HORN ANTENNAS

There are different types of electromagnetic horn antennas suitable for different applications. Pyramidal horns, sectoral horns, conical horns etc., are the commonly used conventional electromagnetic horn antennas.

The flaring of both the principal planes of a rectangular waveguide results in a pyramidal horn. Since the waveguide is flared in both the principal planes, the beamwidths are narrow in both the principal planes. The beamwidth in any one of the principal planes can be controlled by varying the flare angle in that plane.

If the rectangular waveguide is flared in the direction of the E-field, keeping the other dimension

constant, an E-plane sectoral horn is obtained. On the other hand if the flaring is in the direction of the H-field without changing the other, a H-plane sectoral horn is formed. The sectoral horns radiate a fan shaped beam whose width is very narrow in the flared plane and very broad in the orthogonal plane.

A conical horn is derived by flaring a circular waveguide. Conical horns are usually preferred as feeds for symmetric reflectors due to their axially symmetric radiation characteristics. Both the pyramidal and the conical horns are used as standard gain antennas to standardise other antennas.

Advancements in satellite communication, radio astronomy and radar technology have triggered research in the field of antenna theory and design. For most of these systems, a feed whose aperture field distribution is matched with the focal plane field of the reflector is required. In the next sections, the earlier developments in the field of electromagnetic horn antennas are briefly discussed.

1.2 APERTURE MATCHED HORNS

The attachment of suitable curved sections to the outside of the aperture edges of an ordinary horn forms an aperture matched horn. The attachment of curved sections reduces the diffractions which occur at the sharp edges of the horn aperture and provides smooth matching section between the horn modes and the free space. Compared to ordinary conventional horns, this leads to smoother radiation patterns with reduced backlobes, sidelobes and VSWR.

The aperture matching technique with curved surfaces can be used in a wide variety of horns. This type of horns with elliptical, circular or other curved surfaces can easily attain a large bandwidth.

1.3 MULTIMODE HORNS

The E-plane radiation characteristics of the dominant single mode horns, both the pyramidal and the conical, are considerably different from the H-plane radiation characteristics. This is due to the fact that the aperture electric field distribution in the H-plane is tapered, while that in the E-plane is constant. This will

illuminate the aperture edges of the E-plane boundary walls strongly and results in high sidelobe and backlobes. By the introduction of additional higher order modes, along with the dominant mode, the same tapered aperture electric field distribution can be achieved in both the planes. This technique is employed in multimode horns. Hence the edge diffractions are minimised and results in radiation patterns with beam symmetry, phase centre coincidence for the E and H-planes, low sidelobe and cross-polar levels. Some of the multimode horns are briefly discussed in the following sections.

1.3.1 The Diagonal Horn

The electric field vector in a small flare angle diagonal horn is parallel to one of the diagonals of the horn. This diagonal polarisation of the aperture electric field has given the horn the name "Diagonal horn". The internal fields of a diagonal horn consists of a superposition of the orthogonal TE_{01} and TE_{10} modes in square waveguides. Consequently the horn possesses only some of the desirable characteristics of the usual multimode horns which make use of higher order TE and TM modes.

A diagonal horn reported by A.W.Love exhibits circularly symmetric radiation patterns with low sidelobes

not only in the orthogonal principal planes, but also in the intercardinal planes. These desirable features are achieved only at the expense of increased cross-polarised levels in the intercardinal planes. Hence this type of horns are unsuitable where high polarisation purity is required. Diagonal horns can be converted into circularly polarised horns by inserting a proper phase shifter and an orthomode transducer inside the horn.

1.3.2 Multimode Pyramidal Horn

In multimode pyramidal horns, for beam shaping, apart from the dominant TE_{10} mode, the necessary higher order modes are suitably mixed. Usually a mixture of TE_{12} and TM_{12} modes is used. Since these two modes are having the same propagation constant, they can exist as a hybrid pair. If the relative amplitudes of the TE_{12} and TM_{12} modes are properly adjusted to give a linearly polarised aperture field and when this is added in proper phase with the dominant TE_{10} mode, the resulting aperture electric field distribution will be tapered both in the E and H planes.

Flare angle change technique can be employed to generate the hybrid TE_{12}/TM_{12} pair of modes. The

efficiency of a multimode horn is less than that of a dominant mode horn. This is because of the fact that these horns do not radiate in the axial direction. This class of multimode horns are well matched. The main disadvantage is its low frequency bandwidth of 3 to 4 percent.

1.3.3 Multimode Conical Horn

A multimode conical horn is basically designed to satisfy the same boundary conditions at the horn aperture boundary for all polarisations. For the conversion of the dominant TE_{11} mode, the flare angle change technique can be used. If the two modes are properly phased, in the central region of the aperture the electric field of the TM_{11} mode reinforces that of the TE_{11} mode. Near the aperture boundary the two fields oppose one another. Hence the resulting electric field is heavily tapered in both the E and H planes. Because of the different dispersion characteristics of the two modes, this condition can be satisfied only at a single frequency. Thus it is frequency sensitive and the bandwidth is only 3 to 4 percent.

1.4 CORRUGATED HORNS

In 1964, A.F.Kay in the United States, showed that if grooves or corrugations are made on the walls of a

dominant mode horn antenna, the same boundary conditions will be satisfied for all polarisations. As a result, the electric field distribution at the horn aperture is heavily tapered in all planes. This eliminates the spurious diffractions at the aperture edges of the horn antenna. Hence, its radiation characteristics like sidelobe level, cross-polar level and beam symmetry are considerably improved. He termed this type of feed as "Scalar Feed", since it offers the same boundary conditions for E and H fields.

At about the same time, the scientists at the Commonwealth Scientific and Industrial Research Organisation in Australia showed that the focal region fields of a paraboloidal reflector consist of superposition of cylindrical hybrid modes. These hybrid modes were found to be the natural propagating modes for a circular waveguide with grooved internal walls. These grooved walls impose exactly the same boundary conditions on both the electric and magnetic fields. In 1966, V.H.Rumsey showed that such a boundary condition at the walls of a horn would lead to axially symmetric radiation patterns. H.C.Minnet and B.MacA.Thomas of CSIRO Division of Radiophysics, Australia presented a method of synthesizing radiation patterns with

axial symmetry from the study of the fields at the focus of a circular-aperture paraboloid.

Coincidentally in 1966, R.E.Lawrie and J.Peters Jr., of Ohio State University, reported a rectangular pyramidal horn antenna with corrugated E-plane walls. They used $\lambda/4$ deep corrugations on the walls and obtained E-plane radiation patterns with very low sidelobe and backlobe levels. A rectangular pyramidal horn with corrugated E-plane boundary walls is shown in figure 1.1.

In the United Kingdom, P.J.B.Clarricoats and his colleagues have done a great deal of work in the field of corrugated horn antennas. They have analysed both the cylindrical and spherical hybrid modes, respectively of a corrugated cylindrical waveguide and a corrugated conical horn antenna. They have also pointed out the similarity between the balanced hybrid modes in a corrugated feed antenna and those in an optical fibre waveguide.

In Netherlands, at the Technological University of Eindhoven, research work on corrugated conical horn antennas has been carried out by M.E.J.Jeuken and colleagues. M.E.J.Jeuken and C.W.Lambrechtse have compared
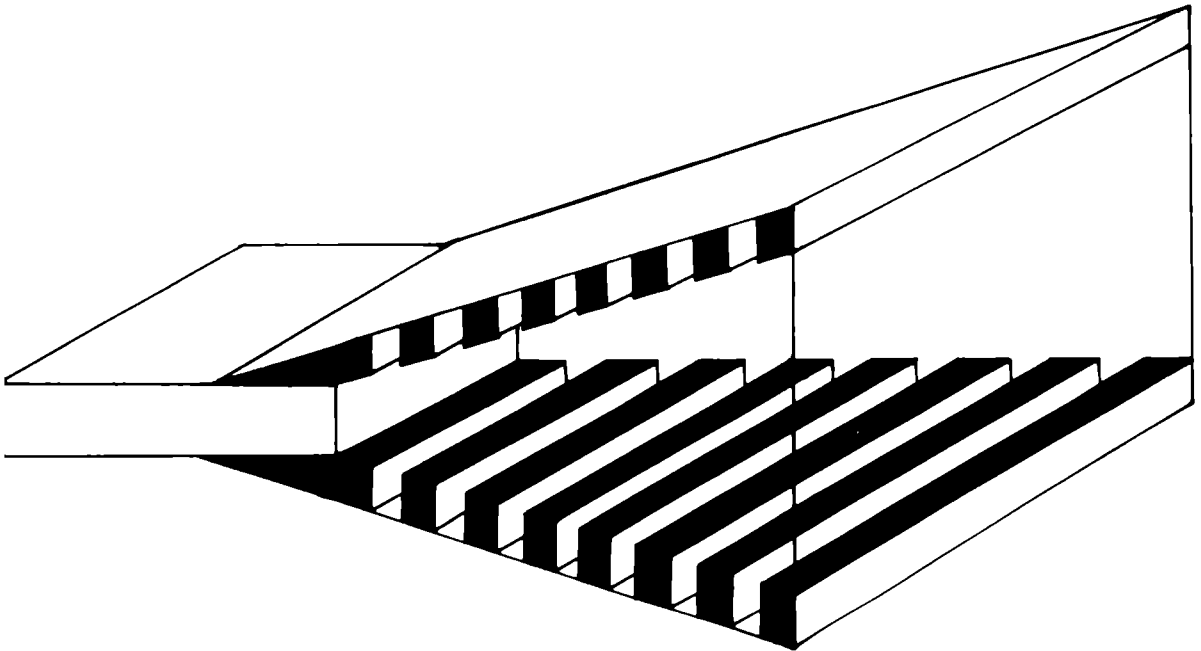
Fig.1.1: Rectangular pyramidal horn with corrugated E-plane
boundary walls

the experimental results with theory for narrow and wide-flare-angle corrugated conical horn antennas, respectively and obtained good agreement with them. A detailed analysis of the operation of Kay's scalar feed is reported by J.K.M.Jansen et al. In this work, the information concerning the design of the scalar feed is also presented.

M.S.Narasimhan and his co-workers at the Indian Institute of Technology, Madras, have analysed both the corrugated conical as well as sectoral horn antennas. They have used a simplified asymptotic solution for analysing the spherical mode fields in a corrugated conical horn for calculating the gain and the radiation patterns. Geometrical Theory of Diffraction (GTD) analysis were carried out for calculating the patterns of corrugated conical and sectoral horn antennas. Good agreement between computed and experimental results were obtained. The design details pertaining to corrugated conical horns of optimum proportions that can be used for illuminating a phased array with a prescribed area are also reported by Narasimhan.

C.Dragone has presented a corrugated rectangular horn antenna with radiation characteristics similar to

those commonly obtained with corrugated horn antenna of circular aperture. The described horn antenna consists of four identical corrugated plates whose corrugations are obtained by numerical machining. As all the four walls of the horn antenna are made of corrugated plates, for both the polarisations, the aperture illumination to a good approximation, is assumed to be having a cosine nature. Measured radiation patterns from 8.7 GHz to 12.2 GHz showed good agreement with the theoretical patterns obtained on the basis of the above distribution. The advantage of this horn antenna over a corrugated conical horn antenna is that different beamwidths are obtainable in the two principal planes.

1.5 DIELECTRIC-LOADED METAL HORNS

Dielectric-loaded metal horn antennas of circular or rectangular shape have many desirable properties. They bring about enhancement of aperture efficiency and gain, have rotationally symmetric beams. Compared to corrugated metallic horn antennas these are light in weight and have low production cost. Hence they are employed as feeds in satellite-borne antennas, in large reflector antennas, in limited scan arrays and in stacked arrays. Different types of dielectric loaded rectangular and circular metal horns are briefly discussed in the following sections.

1.5.1 Dielectric-Loaded Rectangular Metal Horns

The efficiency with which a horn antenna concentrates energy inside the main beam depends on the flatness of the aperture electric field distribution. The symmetrical E-plane loading of a rectangular horn reported by Tsandoulas et al. [123] results in LSE_{10} mode of field distribution. The aperture electric field distribution of this mode is relatively flat. As a result, the aperture efficiency of the horn antenna is considerably improved.

The symmetrical E-plane dielectric loading results in H-plane radiation patterns with reduced beamwidths, but slightly increased sidelobe levels. Aperture efficiencies of the order of 92-96% and good frequency bandwidth can be easily and inexpensively achieved by this technique. An important application of this type of horn antenna is in limited scan arrays.

Chan et al. [139] have reported a trifurcated E-plane metal horn antenna. The dielectric slabs loaded in the E-plane divides the H-plane of the horn into three regions. Two perfectly conducting plates divide the E-plane of the horn into three regions. Compared to

conventional horn antenna, the H-plane radiation patterns of these horn antennas are narrow and the E-plane radiation patterns possess low sidelobe levels. This type of horn antennas find application in H-plane stacked reflector feed arrays.

Sabnani et al. [135] have considered a rectangular horn antenna with an H-plane dielectric slab in the centre. Due to this type of loading, the mode generated is LSM_{11} mode. This results in E-plane radiation patterns with reduced sidelobe levels. This method can be employed for equalising the radiation patterns of a horn antenna in the two principal planes.

A double flare multimode horn antenna with the E-plane walls coated with a dielectric material is presented by Nair et al. [136]. The higher order modes required for beamshaping are generated at the symmetric discontinuity of the oversized square waveguide. Two orthogonal $TE_{10} + TE/TM_{12}$ and $TE_{01} + TE/TM_{21}$ mode sets are used to generate a circularly polarised elliptical shaped beam. The higher order modes produce a tapered aperture field distribiution and make the E-plane far-field beamwidth approximately equal to the H-plane beamwidth of the other

orthogonal set of modes and also results in low off-axis polarisation ratio. Because of the tapered aperture field distribution the radiation patterns possess low sidelobe levels.

1.5.2 Dielectric-Loaded Conical Metal Horns

Rotationally symmetric radiation patterns with low sidelobe levels can be obtained by loading a thin dielectric slab inside a metallic horn antenna as suggested by Satoh [125]. The dielectric band loaded inside the horn antenna excites a series of higher order modes, whose predominant mode is the TM_{11} mode. The loading makes the phases of the TE_{11} and TM_{11} modes the same at the horn aperture. This condition can be satisfied by a single dielectric-band at several frequencies. The radiation patterns of these horn antennas possess low sidelobe levels and the E and H-plane patterns are nearly identical. This type of horn antennas can be used as primary feeds for reflector antennas. The light-weight nature and structural simplicity also make them suitable for satellite borne antennas.

Nair et al. [137] have reported the results of an analytical and experimental study of the propagation and

radiation characteristics of dielectric-coated conical horns with small flare angles. Compared to the uncoated case, the radiation patterns of this type of horn antennas exhibit low sidelobe levels and improved axial directivity. The dielectric coating on the walls results in fields which are no longer purely TE, but hybrid (HE) in nature.

Erik Lier [141] has reported a hybrid mode horn antenna having simple design and excellent electrical performance. This horn antenna conists of a conical metal horn with a dielectric core inside, separated from the metal wall by another dielectric layer with lower permittivity than for the core material. The antenna is found to be exhibiting low cross polarisation and low sidelobes over a wide frequency range.

Recently Lier and Pettersen [146] have reported a new type of strip-loaded hybrid-mode conical feed horn antenna with minimal cross-polarisation at two arbitrarily separated frequencies. This horn antenna is made of a hollow conical dielectric waveguide whose outer surface is completely metallised. The inner surface is loaded with circumferentially oriented thin conducting strips with a periodic variation along the horn. Compared to metallic

corrugated horn antennas, this horn antenna has the potential of very low-weight and cheapness of fabrication cost. A strip-loaded hybrid mode conical feed-horn is illustrated in figure 1.2.

The discussion of different type of feed horn antennas reveals the importance of development of new type of feed horn antennas having added advantages and features over the existing ones. Though the metallic corrugated horn (Scalar feed horn) is considered as an ideal feed by virtue of its excellent radiation characteristics, its high relative weight and the high fabrication cost are the main undesirable features.

The strip-loaded hybrid mode feed horn antenna suggested by Lier et al. [146] can be considered as an alternative to the metallic corrugated horn antenna. But a conical horn antenna cannot be used where different beamwidths are required in the two principal planes. In the present work a strip-loaded, light-weight rectangular pyramidal horn antenna having low production cost is developed. This newly developed horn antenna is found to be simulating the radiation characteristics of an identical metallic corrugated horn antenna. Hence the new horn

Conducting strips

Dielectric

Circular waveguide
section

Metallised
surface
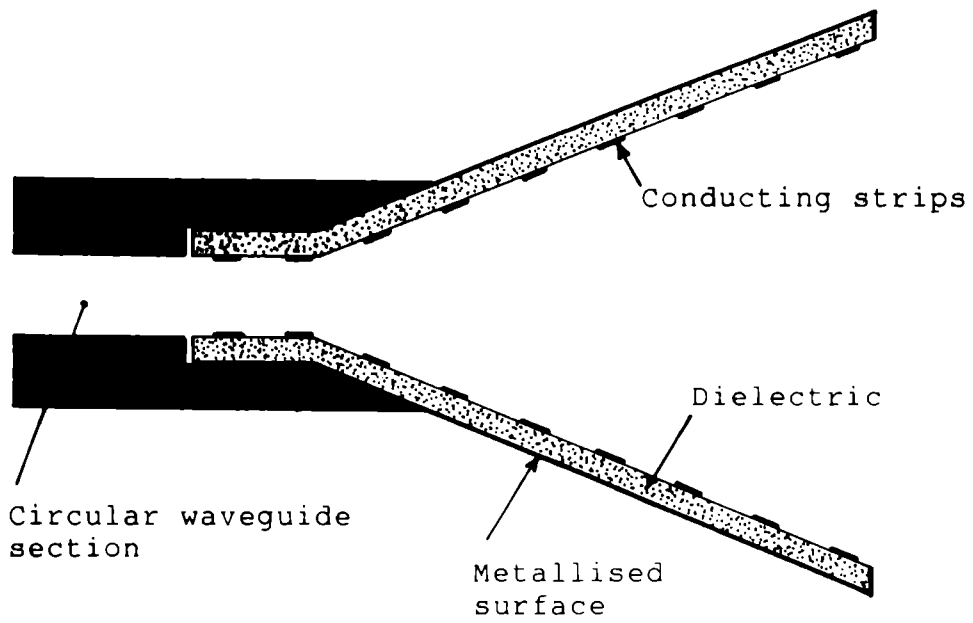
Fig.1.2: A strip-loaded hybrid-mode conical feed horn

antenna is designated as "Simulated Scalar Feed". As the aperture of the horn antenna is rectangular, different beamwidths are obtainable in the two principal planes.

1.6 BRIEF SKETCH OF THE PRESENT WORK

This thesis presents the results of an investigation conducted for the development of a new type of feed horn antenna called "Simulated Scalar Feed". A schematic presentation of the work is given below.

A review of the past important work done in the field of conventional/multimode electromagnetic horn antennas is presented in the first part of the second chapter. The work carried out on corrugated horns and surfaces are included in the second part of the review. In the third part, work on dielectric and dielectric loaded metal horns are reviewed. In all the parts of the review, special emphasis is given to theoretical design considerations.

The methodology adopted for the experimental investigations is presented in the third chapter. The instrumentation utilized and the details of fabrication of

the new simulated scalar feed are described. The method of measurements of radiation characteristics of the antenna are also explained in this chapter.

In the fourth chapter the outcome of the experimental results of the investigations carried out on horn antennas fabricated with different physical dimensions and different parameters for the E-plane boundary walls are highlighted. The theoretical explanation used to explain the experimental results is given in the fifth chapter of the thesis. A comparison between the experimental and the theoretical results is also presented in this chapter.

In chapter six, the conclusions drawn from the experimental as well as the theoretical investigations are discussed. The advantages and features of the newly developed simulated scalar feed is examined in this chapter. Scope of further investigations in this field is also discussed at the end of this chapter.

The experimental results of the investigations in related fields carried out by the author during his research period are incorporated in the thesis as two

Appendices. In Appendix I, the development of a new type
of reflecting polariser for e.m. waves and the experimental
results obtained are presented. The method of antenna
radiation pattern measurement using a vector network
analyser is described in Appendix II.

Chapter 2

REVIEW OF PAST WORK IN THE FIELD

23

Chapter 2

REVIEW OF PAST WORK IN THE FIELD

Extensive efforts have been devoted to the development of efficient feed horn antennas over the past few decades. In this chapter an overview of important works in the field of conventional electromagnetic horn antennas, multimode horn antennas, corrugated horn antennas and surfaces and dielectric loaded metal horn antennas related to the present work are presented.

2.1 CONVENTIONAL ELECTROMAGNETIC HORNS AND MULTIMODE HORNS

The forerunner of the horn, namely, the hollow pipe radiator have been first used by Sir Oliver Lodge. In June 1894, he demonstrated a hollow pipe for radiating and receiving microwaves in London. In 1897, Prof.J.C.Bose, the famous Indian scientist, used a pyramidal horn as a receiver in his spectrometer. He referred it as a "collecting funnel". Ramsay [1] in his classical review paper elaborated these past works before 1900.

Although Southworth [2] and Barrow [3] have suggested the concept of a waveguide radiator, the first

24

experimental and theoretical analysis of waveguide radiator was reported by Barrow and Greene [4] in 1938.

In 1939, Barrow and Chu [5] have theoretically analysed the operation of sectoral horn antennas. Theoretically calculated radiation patterns were in good agreement with the experimental ones reported in a companion paper [6]. Quantitative design curves for sectoral and pyramidal horn antennas were also presented.

Southworth and King [7] have presented the experimental results of directive properties of metal pipes and conical horns. They have measured the on-axis received power with and without the horn in place. The effect of different horn parameters like flare angle, aperture size, horn length etc. on radiation patterns were described. According to them, the horn system can provide 20 dB power gain with respect to a half wave antenna.

At the same time, Chu and Barrow [8] have reported the principles of designing of electromagnetic horn antennas for obtaining the required beamwidth and gain. The design data of sectoral horn antennas having shortest radial length and flare angle for the desired power gain are also discussed.

Using vector Kirchoff's formula, Chu [9] has analysed the radiation properties of hollow pipes and horns. Power gain of a horn antenna compared to a dipole antenna is given and formulae for the radiation fields of TE_{01} and TE_{10} modes in a sectoral horn are also derived.

The variation of H-plane and E-plane radiation patterns of rectangular horns as a function of flare angle for different lengths has been discussed by Rhodes [10]. He has observed the presence of sidelobes in the E-plane patterns and total absence of sidelobes in the H-plane patterns. A qualitative explanation of this phenomenon in terms of the field distribution was given.

In 1949, Woonton et al. [11] have carried out extensive experimental study on radiation patterns of horn antennas. The experimental results were compared with the corrected formula by Stratten and Chu and with Kirchoff's formula. They have showed that principles in physical optics can be used for predicting the magnitude of the E-plane field with an accuracy of 1 dB up to an angle of 20° and that of H-plane field with fairly good accuracy.

Horton [12] has reported a simple integral method for computing the radiation patterns of horn antennas of moderate flare angle. He has showed that when the flare angle is reduced to zero, the modes of vibration in conical and sectoral horns approach to that of circular and rectangular waveguides. The theoretical results were in good agreement with the experimental ones.

Bennet [13] has analysed a sectoral horn by considering it as a non-uniform transmission line called "sectoral transmission line". The experimental curves presented by him are useful for designing sectoral horns. Detailed discussion about the physical significance of the derived normalised functions is also presented.

Rice [14] has used WKB approximation for calculating the reflection coefficient at the junction of a straight waveguide and a sectoral horn. Numerical data for a 60° H-plane sectoral horn is also presented.

Measured radiation characteristics of conical horns having linear rate of flare employing waveguide excitation were presented by King [15]. Graphs for absolute gain of a conical horn as a function of aperture

diameter for a series of axial lengths are given. The optimum design data in terms of wavelengths for fabricating optimum horns are also presented by him.

In the same year, Schorr and Bech [16] have solved Maxwell's equations for a perfectly conducting conical waveguide and calculated the propagation coefficients. They have estimated the field at the mouth of the horn and the radiation patterns were calculated in integral form. According to them the same field equations with appropriate modifications can be used for a pyramidal horn.

Jakes [17] has carried out experimental investigations on the gain of pyramidal horn antennas. He has showed that the error in gain measurements due to the edge effect is less than 0.2 dB, so that the gain may be computed to this accuracy from their physical dimensions and Schelkunoff's curve.

Braun [18] has discussed about the errors in the measurement of gain due to two horns separated by a short distance. From the experimental curves presented by him, the error in gain measured at any distance could be directly obtained. In another paper [19] he has presented

a table connecting the gain and the aperture size of a horn. The design procedure of a pyramidal horn with equal E and H-plane patterns is also given.

Epis [20] has reported a compensated horn having metallic nails radially on the rim of the horn. This technique has reduced the fringes of E-field in the E-plane. Hence E-plane beamwidth is considerably narrowed. The design and development of radiation patterns with beam symmetry for all polarisations is also presented.

Walton and Sundberg [21] have used a dielectric lens for correcting the phase-error at the mouth of a horn and were able to increase the bandwidth.

Russo et al. [22] have used Geometrical Theory of Diffraction (GTD) for calculating the E-plane radiation patterns of a pyramidal horn. It has been shown that, when this theory is applied to a horn, the significant radiation mechanism are direct radiation from the source at the horn apex and diffracted radiation due to the edges. The theoretical E-plane patterns fairly agreed with the measured patterns.

Tingye and Turrin [23] have used a numerical integration method for computing the near-field of a

conical horn. For this they considered the assumption that the field at the mouth of the horn is same as that existing at the mouth of an infinite horn of same cross-section.

Later Yu et al. [24] have computed the E-plane radiation patterns of a pyramidal horn more accurately by considering higher order diffractions at the edges and reflections inside the horn. They have proposed a corner reflector with a magnetic line source at the vertex as a model for E-plane radiation of horn antennas. For appropriate approximations diffraction mechanism were used.

Hamid [25] has also used GTD to investigate the gain and radiation pattern of a conical horn excited by a circular waveguide operating in the TE_{11} mode. A systematic procedure for converting the field of the dominant mode into a geometrical optics ray is presented. The far-field at a point is taken as the sum of the geometrical optics rays and the edge rays passing through the point. Calculated patterns showed good agreement with the experimental ones.

Using the near-field transmission formula Chu and Semplak [26] have calculated the ratio between the

Fraunhoffer and Fresnel gain of pyramidal horns as a function of its dimension and separation distance. The calculated corrections have been applied to absolute gain measurements and obtained an accuracy of ± 0.035 dB.

Jull [27] has carried out accurate gain measurement with revised proximity corrections. He has considered the mismatch of the horn and the aperture edge diffraction effects which were not accounted in Schelkunoff's gain expression. In another paper [28] he has also incorporated the finite range effect in the Fresnel zones into Schelkunoff's gain formula for pyramidal horns. Using this modified expression, the gain can be easily obtained from two single line curves.

Based on a vector approach, Muehldorf [29] has calculated the phase centres of different horn antennas. Different expressions were derived for the phase centres of E and H-planes. The dependence of horn dimension on phase centre is also presented graphically.

Narasimhan and Rao [30] have formulated a simple but sufficiently accurate solution for modes in a conical horn. With the aid of the vector diffraction formula, the

radiation pattern and gain of a conical horn with TE_{11} mode were obtained. The calculated results showed close agreement with experimental results. Using vector diffraction formula, the same authors [31] have calculated the radiation patterns of conical horns with large flare angles excited in the TE_{11} mode. They [32] have also applied a correction to the already available radiation formula for E-plane sectoral horns.

Kerr [33] has reported a short axial length broadband horn antenna. The required H-plane half-power beamwidth is maintained by the use of a grid type H-plane boundary wall.

Jull [34] has used GTD for analysing the on-axis gain of two dimensional E-plane sectoral horns. The modification of the gain equation has been carried out by considering the reflection of diffracted field from the horn and the double diffraction at the horn aperture.

The higher order interaction between two H-plane sectoral horns have been analysed by Iskander and Hamid [35]. They have calculated the field distribution at the horn aperture. A correction for the gain of the horn is also reported.

An accurate method of gain measurement of E-plane sectoral horns is reported by Jull and Allen [36]. They have put forward a new proposal against Kirchoff's theory incorporating the exact TE_{10} mode field of an open ended waveguide.

Mentzer et al. [37] have used slope diffraction function for correcting the errors around the shadow boundary region. In the H-plane pattern analysis, they have included the fields of E-plane edge diffracted rays also.

In 1981, Mather [38] has developed and presented a broad-band horn antenna possessing low sidelobe level characteristics. The antenna is a circular horn whose aperture is flared like a trumpet. The patterns calculated using GTD were fairly agreeing with the experimental patterns. The sidelobe level of this horn antenna was found to be 75 dB down from the mainlobe level.

Based on multiple image model Menendez and Lee [39] have reported analytical expressions for the far-field radiation pattern and reflection coefficient of horn

antennas. The theoretically obtained radiation pattern and reflection coefficient were in good agreement with the experimental results.

In 1962, Love [40] has developed an unusual form of electromagnetic horn antenna with square cross-section, called "the diagonal horn". The electric field vector inside the horn is parallel to one of the diagonals of the horn aperture. The horn antenna is found to be exhibiting rotationally symmetric beams with reduced sidelobes not only in the principal E and H-planes, but also in the intercardinal planes. These desirable features were achieved only at the expense of a pair of increased cross-polarised lobes in the intercardinal planes.

Potter [41,42] has reported a new type of conical horn, referred to as the "dual mode conical horn". Making use of TE_{11} and TM_{11} mode excitation at the throat and by adjusting the relative amplitude and phase of these modes, complete beamwidth equalisation in all planes, complete phase centre coincidence and sidelobe suppression were achieved. He has computed the radiation patterns of this horn theoretically.

A low-noise multimode cassegrain monopulse feed with polarisation purity has been reported by Jensen [43]. The monopulse bridge feeding the common aperture section is a standard four guide monopulse circuit providing dual polarisation capability. The sum and difference patterns of E and H-planes were theoretically calculated and presented.

A definitive development of pattern synthesis for circular aperture horn antennas is given by Ludwig [44]. Using spherical wave theory, maximum performance theoretically obtainable from an antenna is derived as a function of the aperture size. He has showed that the θ and ϕ components of the radiated field may be synthesized, respectively, from TM and TE cylindrical waveguide modes. He has presented examples incorporating upto four modes.

Turrin [45] has reported a dual mode small-aperture horn antenna in which a very compact TM_{11} mode transducer and a circular horn were combined. The relative phase and amplitude of the generated TM_{11} and TE_{11} modes were adjusted to cancel the electric field at the aperture

boundary. As a result, the sidelobe level and other radiation characteristics of the horn were considerably improved.

Tomiyasu [46] has effected the conversion of TE_{11} mode into higher order modes by using a large diameter conical junction. A time-shared computer was employed for determining the relative amplitudes of the higher order modes required to match the TE_{11} mode curved phase front.

Agarval and Nagelberg [47] have analysed and measured the $TE_{11} \longrightarrow TM_{11}$ mode conversion by circularly symmetric transducers in a circular waveguide. The two methods employed by them were (i) the simple step change in radius of the waveguide (ii) a discontinuity covered by a dielectric ring. Measurements have showed that the dielectric loaded transducer is independent of frequency over a wide range.

Small variations of flare angle at one or more points along the horn were used by Cohn [48] to control the radiation patterns of pyramidal or conical horns. This technique has produced a tapered E-plane aperture field and resulted in equal E and H-plane beamwidths with low sidelobes.

Using the same technique Han and Wickert [49] have described a multimode circularly polarised horn antenna radiating an elliptically shaped beam. According to them, axial ratio of less than 2 dB can be achieved over an earth coverage angle of approximately 9°x16°. Experimental patterns were in excellent agreement with the computed patterns.

By a modal analysis of the discontinuity, English [50] has accurately predicted the power conversion coefficients and the phase of the propagating modes excited by a symmetric step discontinuity in a circular waveguide.

Co-axial feeds radiating sector shaped beams for paraboloid antennas producing high aperture efficiency and low spillover have been reported by Koch [51]. Aperture efficiencies of the order of 68% to 80% were achieved by a co-axial feed employing only one ring. This type of feed is found to be producing very little cross-polarisation.

A circularly polarised feed assembly providing efficient prime focus illumination of a reflector antenna has been designed by Gruner [52]. Using a multimode horn, 4 and 6 GHz satellite communication bands were separately

optimised. The corrugations put on the outside of the waveguide was effective in the 4 GHz band and the radial step inside the waveguide was effective in the 6 GHz band. The three components of the feed assembly, the feed horn, polariser, and the orthomode transducer were briefly discussed.

2.2 CORRUGATED HORNS AND SURFACES

In 1966, Simmons and Kay [53] have reported an ideal horn antenna that can be used as a feed for reflector antennas. By putting closely spaced circumferential grooves in the wall of a wide flare-angle conical horn they realised the same boundary conditions for all the polarisations. This created a tapered aperture E-field distribution in all the planes. As a result axially symmetric radiation patterns with low sidelobes with a 2:1 bandwidth were achieved. They termed such horns as "scalar feeds". A comparison between standard horn and scalar feed horn is also presented.

At the same time Lawrie and Peters [54] have reported modifications of horn antennas for low sidelobe levels. They have used choke slots and corrugated surfaces in the E-plane boundary walls of pyramidal horns and

obtained radiation patterns with very low sidelobes and backlobes. Corrugated surfaces are proved to be superior to choke slots.

Rumsey [55] have showed that a linearly polarised horn that has symmetrical radiation patterns in all planes through the axis can be achieved from a synthetic material for which the boundary conditions on E and H are the same. A theoretical analysis for obtaining such patterns from a circular waveguide is presented.

Minnet and Thomas [56] have studied the radiation from a cylindrical hybrid mode guide which results in axially symmetric pattern. The synthesis is developed from a study of the fields at the focal plane of a circular aperture paraboloid.

Clarricoats and Saha [57] have theoretically analysed the cylindrical hybrid modes in a corrugated horn. A procedure for achieving a balanced hybrid condition in the horn aperture is discussed by them. In another paper [58] they have used spherical hybrid modes for analysing the fields in a corrugated horn. A procedure is described for the calculation of the radiation pattern of the horn.

Their calculated radiation patterns were in good agreement with those computed by Kay et al. [53]. Later the same authors [59] have used modal expansion technique and Kirchoff-Huygen method for determining the radiation pattern of a wide flare-angle scalar horn. These two methods fairly agreed over a wide range of observation angles.

Jeuken [60] has carried out experimental investigation on the bandwidth of small flare-angle corrugated conical horn antenna. From the observations, he has concluded that antennas with small diameter have a symmetrical radiation pattern in the frequency range of 1:1.3 only. In another paper he and Lambrechtse [61] have calculated the radiation patterns of small corrugated conical horns with wide flare-angles using Kirchoff-Huygen integration method. Theoretical and experimental results showed good agreement.

MacA.Thomas [62] has carried out investigation on the bandwidth properties of corrugated conical horns. He has showed that the aperture fields of corrugated conical horns remain virtually unchanged over a wide frequency range. The bandwidth is increased as the length of the

horn is increased. In another paper he [65] has discussed the performance of one and two hybrid mode feeds designed to illuminate Parkes 210 ft radio telescope. Measurements have showed that the two hybrid mode feed gave an increased efficiency of 12%.

Narasimhan and Rao [63] have reported a simple solution for spherical hybrid modes in corrugated conical horns. The radiation pattern and gain calculated using this formula yielded accurate results when the flare angle was less than 20°. Later, in another paper [66] they have analysed the radiation pattern of a wide-flare-angle corrugated conical horn. The phase variation of the aperture field was taken into account and using vector diffraction formula the far-field radiation patterns were computed.

Clarricoats et al. [67] have predicted the near-field amplitude and phase patterns of corrugated feed horns by spherical-mode-expansion method which has been previously applied only in the far-field. Theoretical patterns showed good agreement with the experimental ones.

Using cylindrical mode analogy, Clarricoats and Saha [68] have presented a detailed study of the

propagation and radiation characteristics of corrugated waveguide. 1:1.5 bandwidth is reported for such a system. In the second part of the paper [69] they have applied Kirchoff-Huygen integration over a constant phase surface at the mouth of the horn for calculating the radiation pattern. The pattern is also obtained by expanding aperture field in terms of TE and TM spherical modes. Excellent agreement is obtained between the two methods and with the experimental results.

Baldwin and McInnes [64] have discussed the radiation characteristics of a corrugated conical horn. The theoretically computed radiation patterns were in good agreement with the experimental ones.

Jansen et al. [70] have investigated the electromagnetic fields in the grooves of a corrugated conical horn. They have showed that when the width of the grooves is small compared with the wavelength, the dominant mode in the grooves is TM. Experimental results confirmed the theory.

The principle of mode conversion using a tapered reactance cylindrical waveguide surface is described by

MacA.Thomas [71]. The experimental results of a multistage converter, which converts a TE_{11} mode into HE_{11}, TM_{11} and EH_{12} modes in successive stages are presented by him.

Knop and Wiesenfarth [72] have showed that a corrugated pipe with large diameter and $\lambda/4$ teeth carries the HE_{11} mode and radiates as a "scalar feed". It is revealed that the E-plane pattern approaches H-plane pattern and is linearly polarised only if the aperture is sufficiently large. The beam efficiency of this model is found to be higher than that of the same size uncorrugated pipe.

Clarricoats and Seng [73] have used modal matching technique and Kirchoff-Huygen integration method for predicting the radiation patterns of a corrugated horn with oblique angles. The theoretical results have showed good agreement with the experimental results of a horn with semi flare-angle of 110°.

Narasimhan [74] has investigated the fields inside a corrugated conical horn with arbitrary corrugation depth in the interval $0.25\lambda \leq h \leq 0.5\lambda$. When the corrugation depth is equal to $\lambda/2$, the hybrid mode solution

degenerated to the solution for the TE_{11} mode in a conical waveguide. In another paper [81] he has described the design details of corrugated conical horns of optimum proportions that can be used for the uniform illumination of a phased array with a prescribed area.

Narasimhan and Rao [75,80] have carried out analytical and experimental investigations on E-plane corrugated horns. They have computed the far-field radiation patterns by two methods: (i) vector diffraction formula over a constant phase surface at the aperture, (ii) expansion of aperture field in terms of free space cylindrical TE and TM wave function.

Caldecott et al. [76] have discussed a corrugated horn that can be used as a source antenna in a pattern range and also as a standard antenna for calibration purposes.

Vu and Hien [77] have designed a wide band single-horn monopulse feed with a circular waveguide. In this feed, the dominant hybrid mode in the corrugated structure provided the reference signal, whereas the error signal for the servodevice is derived from the TM_{01} mode.

The electromagnetic properties of the corrugated surface and waveguide junction in a corrugated horn are investigated by Mentzer and Peters [78]. They used an integral equation to study the influence of corrugation density and tooth thickness on the power loss, surface current and the scattering from the plane waveguide surface-corrugated surface junction.

Using power loss method and previously successful approximations, Hariri et al. [79] have determined the attenuation coefficient of a rectangular waveguide. The authors have corrected the error in the earlier predictions and identified a region in which the corrugated waveguide exhibits an attenuation advantage over comparable smooth wall rectangular waveguide.

Frank [82] has proposed the use of tapered slots in a corrugated horn for bandwidth greater than 3:1. The experimental result of a test horn operating over the full 7.5 GHz to 18 GHz frequency range is also presented.

Baldwin and McInnes [83,84] have discussed the propagation and radiation characteristics of moderate flare-angle rectangular horns with transverse corrugations.

Considering the hybrid modes inside the horn, the radiation pattern is calculated using Kirchoff-Huygen integration. Experimental results of a square corrugated horn and another fully corrugated small horn with rectangular aperture, producing an elliptical beam for either of the two orthogonally polarised signals are presented.

The theoretical and experimental investigations on cross-polar radiation from open-ended corrugated waveguides are reported by Parini et al. [85]. They have proved that, good agreement between theory and experiment is achieved only if the effects of space harmonics, the waveguide flange and higher order mode are incorporated into the theory.

Takeda and Hashi Moto [86] have used ring loading technique for broadbanding the bandwidth of corrugated conical horns. The investigation has revealed that in the ring-loaded corrugated horn, the useful bandwidth is 1.35 times broader than that in the conventional corrugated horn.

James [87] has used a combination of the method of moments and GTD to predict the radiation properties of 90°

semiflare angle conical horns having a number of annular slots in the aperture flange. The theoretically computed results have showed good agreement with the measured results.

Terzuoli and Peters [88] have evaluated the VSWR of a E-plane dihedral corrugated horn using a moment method solution. They have showed that the use of an appropriate curved horn waveguide geometry in conjunction with a tapered corrugation input results in a very small VSWR over a reasonable band.

Considering the effect of aperture size of horns, slot width-to-pitch ratio and frequency on the cross-polarisation, MacA.Thomas [89] has presented the design details of a corrugated conical horn. The design of slots near the throat of the horn to achieve a low VSWR is also given.

Guy and Ashton [90] have reported the radiation details of a corrugated horn of elliptical cross-section. This horn has exhibited polarisation purity in both the planes.

Worm [91] has reported a feed horn in which the hybrid modes are generated at a corrugated step discontinuity at the aperture of the horn. Compared with feeds developed earlier, this technique has substantially reduced the electrical length of the horn.

Jull [92] has proposed a method to produce circular polarisation using metallic corrugated surface. The normally incident plane-polarised wave is oriented with its plane of polarisation at 45° to the grooves of the corrugated surface. The incident waves on the reflecting surface can be resolved into transverse electric (TE) and transverse magnetic (TM) components, in which the tips of corrugations are parallel to the electric and magnetic fields respectively. During reflection, the TM component travels a quarter wavelength further than the TE component (if the corrugation depth is $\lambda/8$) which is totally reflected from the top of the corrugations. As a result, a differential phase shift of $\pi/2$ radian is obtained between the two orthogonal components. This caused circular polarisation.

Rotation of plane of polarisation of a beam of microwaves by metallic corrugated reflecting surface has been reported by Paul and Nair [97]. The orientation of

the corrugations with the plane of polarisation of the incident beam determines the tilt of polarisation. A 90° rotation of electric field is reported for a surface with $\lambda/4$ deep corrugations.

Using a rigorous solution, James [93] has determined the surface reactance of a corrugated plane illuminated by a plane wave. He has used this result to establish the range of validity of the usual approximate solution. The dependence of the surface reactance on slot depth, width, period and the angle of incidence is also discussed. In another paper [95] he has used modal field matching technique to determine the scattering matrix of a TE_{11} to HE_{11} mode converter of corrugated waveguide with varying slot depth. The predicted results are in good agreement with the experimental data.

James and Thomas [96] have used ring loaded slots in a TE_{11} to HE_{11} mode converter. The theoretical parametric study has revealed that a minimum of five ring-loaded slots are sufficient for obtaining a return-loss of better than -30 dB with a bandwidth ratio of 1.5, which is superior than obtainable from a varying slot depth converter.

Dragone [94] has discussed the assymptotic properties of the fundamental mode, HE_{11}, inside a large waveguide of finite surface impedances. He has applied the analysis to corrugated waveguides, certain optical fibres and waveguides with metal walls coated by a dielectric layer. Approximate expressions for the HE_{11} mode have been derived for rectangular and circular geometry. It has been also shown how surface impedances affect the edge illumination of a feed aperture.

Iskander et al. [98] have used an integral equation method for formulating the problem of scattering by rotationally symmetric horn antennas. They have used this formulation to investigate numerically the radiation from corrugated conical horns by approximating the corrugated surface with anisotropic surface impedances. The obtained results are in good agreement with the experimental results and other existing methods.

Chu and Legg [99] have presented a three horn transmission method for measuring the gain of a corrugated horn designed as a 100 GHz gain standard. The comparison

between the measured and the calculated gains has showed
that the ohmic loss in a corrugated horn is very low.

Morris [100] has reported a broad band constant
beamwidth corrugated rectangular horn. The horn has
constant E and H-plane beamwidth over a band width
of 2.4:1. The broad-band nature is due to the end loaded
T-slots whose capacitive admittance is nearly constant in
the band. A large separation between the E and H-plane
phase centres is also obtained.

James [101] has studied TE_{11}-to-HE_{11} mode
converters using ring loaded slots and varying depth slots.
For a return-loss exceeding -30 dB, bandwidth ratios of
1.45 for the varying depth slot converter and of 1.55 for
the ring-loaded slot converter were achieved.

The design and characteristics of a hybrid mode
corrugated horn with a curved aperture of constant radius
of curvature has been reported by MacA.Thomas [102].
Design details of a mode converter that can be used with
this horn is also presented. At the design frequency, the
cross-polar and sidelobe levels of the horn system are
better than -50 dB.

Dragone [103] has derived the scattering matrix of scattering at a junction of two waveguides with different surface impedances. It is shown that, under certain general conditions, the infinite set of equations specifying the junction scattering coefficients can be solved exactly by the residue-calculus method. Very simple expressions between the scattering coefficients and propagation constants are also obtained.

The propagation characteristics of guided waves in a rectangular waveguide with transverse corrugations on all four walls have been theoretically and experimentally investigated by Obaid et al. [105].

Witebsky et al. [106] have presented the design details of a light-weight rectangular corrugated horn antenna fabricated from sheet metal. The $\lambda/4$ choke slots placed at the aperture of the horn has reduced the E-plane sidelobes below -55 dB at angles greater than 90°.

Olver and Xiang [107] have used spherical modal matching technique to analyse the design of throat region of wide-angle corrugated horns. According to them, the optimum geometry of the throat design depends on the flare-

angle of the horn. The experimental results have verified the validity of the theory.

Recently, Kildal and Lier [108] have reported a conical horn with longitudinal corrugations, called "the hard horn", that can be used as cluster feed in satellite antennas. They have showed that, the use of this type of feed elements reduce the spill over.

Manshadi and Hartop [109] have developed a novel technique to move the phase centre of a corrugated standard feed horn without significant degradation of other major radiation characteristics. For this they have used a corrugated straight section in conjunction with the standard horn.

Toral et al. [110] have reported an outdoor far field measurement technique for radiation patterns, down to levels 90 dB below the main beam maximum. Conical corrugated horn antennas and circular polarisation orthomode transducers were designed and tested.

Arnold and Dendane [111] have applied the concept of intrinsic modes to the theory of propagation in conical

horns. The numerical calculations have showed that the intrinsic mode based on the HE_{11} local normal mode is sufficient for many applications including the calculation of cross-polar radiation.

Clarricoats and Saha [112] have analysed and predicted the attenuation characteristics of the dominant hybrid mode in corrugated circular waveguides. They have showed that, over a substantial frequency band including the optimum frequency used for antenna feed applications, the attenuation of the dominant hybrid mode is lower than that of the dominant mode in smooth wall circular waveguide.

Using finite difference method, Ata et al. [113] have designed a E-plane sectoral horn with channel inserts at the corners. As a result of the tapered E-plane field distribution, the sidelobes are considerably improved. Good agreement is obtained between the predicted and the measured far-field distributions.

MacA.Thomas et al. [114] have reported a wide-band prime-focus horn that can be used for low-noise receiver applications. The horn has exhibited excellent radiation characteristics across a 1.8 to 1 bandwidth.

In 1979 Zachariah et al. [115,116] have used corrugated flanges to modify the radiation patterns of H-plane sectoral horns. The tips of the corrugations of the flanges are normal to the E-vector. The experimental results have proved that the corrugated flanges are more effective than the plane flanges for improving the radiation patterns. On the basis of line sources and ray optics principle, the radiation patterns are theoretically analysed.

Pravinkumar and Mohanan [117] have used a corrugated flanged H-plane sectoral horn for feeding an offset paraboloidal reflector. The feed system has improved the coupling between the feed and the reflector. Experimental data for flanges of varying parameters are presented.

Vasudevan and Nair [118] have analysed the radiation characteristics of corrugated corner reflectors. At the optimum position of the feed, a sharp radiation pattern is obtained. Line source theory and method of images were used to analyse the corrugated corner reflector system and the results were compared with the experimental ones.

By attaching corrugated flanges on E and H-plane sectoral horns, Mohanan et al. [119,120] have obtained axially symmetric radiation patterns. Half power beamwidth and gain of the antenna system were considerably improved. The radiation patterns of the corrugated flanged H-plane sectoral horn were with low sidelobes, backlobes and good matching. In another paper [121] they have reported the design and development of a circularly polarised corrugated flanged H-plane sectoral feed horn. The corrugations were inclined at 45° to the E-vector component parallel to the plane of the flange. Depending upon the position of the flange from the aperture, the flange angle and frequency, the desired polarisation can be synthesized.

2.3 DIELECTRIC-LOADED WAVEGUIDES AND METAL HORNS

In 1966, Bartlett and Moseley [122] have reported a dielectric guiding structure called 'dielguide', that can be employed as a feed for reflectors. This light-weight plastic feed structure reduced the spillover and provided uniform reflector illumination. Aperture efficiencies of 75% have been achieved by this technique.

Tsandoulas and Fitzgerald [123] have investigated theoretically and experimentally the effects of symmetrical

loading of horn apertures with E-plane dielectric slabs. Flat aperture electric field distribution has been achieved by this technique. As a result, aperture efficiency is enhanced to 92% to 96%.

Hamid et al. [124] have reported the design details and test results of a simple and light-weight antenna consisting of a dielectric rod with a conical hole, loading an open-ended waveguide. Different radiation patterns are possible depending on the depth of penetration of the rod into the waveguide.

By loading a thin dielectric band inside a conical horn antenna, Satoh [125] has realised a wide-band dual-mode horn radiating rotationally symmetric radiation patterns with low sidelobe levels. A single dielectric band is required to achieve a wide bandwidth of operation.

James [126] has used semi-empirical method to optimise a dielectric rod antenna and a dielectric horn antenna with variable wall thickness. When the flare angle is reduced to zero, the dielectric walled horn antenna has exhibited similar patterns to the tapered rod antenna.

Ashton and Baldwin [127] have theoretically derived the field distribution in a rectangular horn with a thin dielectric slab placed centrally along the H-plane. The horn has exhibited radiation patterns with constant beamwidth and low sidelobe levels.

Baldwin and McInnes [128] have reported considerable enhancement in the directivity of rectangular horns loaded with dielectric slabs in their E-plane walls. The sidelobe levels are slightly increased due to the loading.

Clarricoats and Salema [129] have developed approximate theory for the propagation and radiation characteristics of dielectric cone that can be used as a feed horn to reduce the spillover beyond a subreflector of small diameter. They have showed that the dominant HE_{11} mode of the dielectric cone is very much similar to the HE_{11} mode of the corrugated horn. In the second part of the paper [130] they have presented a theory for the design of cassegrain reflectors employing dielectric cone feeds. A modal approach is used to describe the aperture field over the sub-reflector, while ray opics is used to determine the profile of the sub and main reflector aperture distributions. Calculated results are in good agreement with the experimental ones.

Brooking et al. [131] have predicted the radiation patterns of pyramidal dielectric waveguides excited by pyramidal metallic horns and compared the results with patterns measured at 9 GHz. Satisfactory agreement is obtained, especially in the region of mainlobe. At wide angles, the pattern corresponds quite closely to that of the launcher, the metallic pyramidal horn.

Using transmission technique, Collier and Potter [132] have made attenuation coefficient measurements of a square-cross-section dielectric waveguide in the 9-18 GHz frequency range. The measured results are in good agreement with the theoretical prediction given by earlier workers.

Vokurka [133] has presented a simple feed with high polarisation purity designed for operating in two arbitrarily located frequency bands. The grooves of the corrugated surface of the horn are partially loaded with a dielectric material.

Martin [134] has reported the radiation patterns of a dielectric sphere fed from a conical horn. He has

used a circular dielectric rod in the horn as a matching device. Improvement in gain and beam symmetry are achieved by this technique.

Kumar [138] has theoretically predicted the radiation patterns of a dielectric lined cylindrical waveguide feed. Experimental patterns are in good agreement with the predicted ones. Rotationally symmetric patterns with good polarisation discrimination and 90% to 96% efficiency are obtained.

Aly and Mahmoud [140] have showed that by filling the slots of a longitudinally slotted horn with a dielectric, the slot depth required for achieving low cross-polarisation is considerably reduced. Design curves for the modal propagation constant of the first two modes against the frequency, the dielectric constant of the slot filling material and the geometrical constants of the horn are presented.

Lier [141] has reported a hybrid mode conical metal horn antenna with a dielectric core inside and separated from the metal wall by another dielectric layer having lower permittivity than the core. The radiation

patterns are found to be with low sidelobes and low cross-polarisation levels over a wide frequency range. Theoretical and experimental results are also presented.

Raghavan et al. [142] have analysed a dual mode dielectric-ring-loaded conical horn by using numerical modal matching technique. The peak cross-polarisation bandwidth of the horn is found to be three times greater than that of a stepped dual mode metal horn.

Using asymptotic technique, Knop et al. [143] have calculated the radiation fields and cross-polarisation discrimination of different types of horns. Comparison of results of a dielectric core, foam-lined horn, a foam core air lined horn and a corrugated horn are also discussed.

Mahmoud and Aly [145] have reported a new version of dielectric lined waveguide with very low cross-polar radiation characteristics. They have realised this by putting periodic transverse slots in the dielectric lining of the waveguide. Compared to the continuously lined waveguide, it has exhibited a very low cross-polar level over a wide band of frequency.

In 1987, Lier and Pettersen [146] have reported a novel type of light-weight hybrid mode conical feed horn antenna. It comprised of a hollow conical dielectric waveguide whose outer surface is metallised, and whose inner surface is coated with circumferentially oriented conducting strips. It is designed to have minimal cross-polarisation at two arbitrarily separated frequencies as for a dual depth corrugated horn.

Lee et al. [147] have described a circular wave-guide horn coated with a lossy magnetic material in its interior wall. This horn is found to be radiating good circularly polarised waves when the diameter of the wave-guide is larger than the free space wavelength.

The gain and cross-polarisation characteristics of hard horns and strip-loaded horns are investigated by Lier [148]. When, the surface waves are neglected, the two representations have exhibited almost identical radiation characteristics.

Definitions for artificially soft and hard surfaces that can be used for electromagnetic waves are presented by Kildal [149]. By an analogy with the soft

surfaces in acoustics, the transversely corrugated and other alternate surfaces having the same anisotropic surface impedance are termed as artificially soft surfaces. In the same way the longitudinally corrugated surface filled with a dielectric is defined as artificially hard surface.

Based on ray theory, Ata and Benson [150] have reported a new design for a phase corrected horn antenna which is shorter than one with a hyberbolic secant refractive index profile.

Kildal and Lier [151] have suggested the use of circular hard horns as cluster elements for minimising the spillover of radiation from contoured beam satellite antennas. Hard horns with square apertures are also suggested by them.

Olver et al. [152] have investigated the characteristics of conical horns loaded with dielectric cones. Horns loaded with cones made of foam or solid dielectric are found to radiate low cross-polarisation over a wide band of frequencies. Using modal matching technique, the behaviour of the excited higher order modes responsible for radiated cross-polarisation is also investigated.

Kumar [153] has described a compact horn coated with a lossy magnetic material, which can be used for earth coverage from a geosynchronous satellite. From 8 GHz to 8.3 GHz, the axial ratio of this antenna is better than 0.7 dB in the earth coverage angle.

The characteristic equation of a square hard horn is presented by Kildal [154]. The results have shown that the cross-polar bandwidth of an open hard waveguide is narrow for large aperture diameters. Within the bandwidth the aperture efficiency is close to 100%.

Horn antennas having soft and hard boundary conditions, denoted by soft and hard horns, respectively are discussed by Lier and Kildal [155]. Calculated aperture field distributions, radiation patterns, directivity and sidelobe level versus edge taper of a conical hard and a soft horn with semiflare angle of 5° are presented.

Based on a simple model in which the fields are expanded into several plane waves, Wang et al. [156] have analysed a magnetically coated horn. By choosing appropriate horn flare angle and coating thickness, performance

close to that of a corrugated horn is achieved. Due to dissipative loss a slight reduction in gain is observed.

Cahill [157] has described a practical design for supporting the inner core of a mm-wave dielectric loaded horn. By this technique a good input impedance match, excellent radiation characteristics and high mechanical strength are achieved.

Singh et al. [158] have investigated both theoretically and experimentally, the amplitude of the aperture field of an E-plane sectoral hollow dielectric horn. They have obtained a reasonable agreement between the theoretical and experimental results.

Ghobrial and Sharobim [159] have achieved a reduction of 7 dB in cross-polarisation in pyramidal horns by covering the walls of the horn with a dissipative material. This in turn reduced the co-polar gain by 1 dB.

Bird and Hay [160] have described a method for calculating the mode reflection and conversion at the aperture of a dielectric-loaded waveguide terminated in a

ground plane. Experimental and theoretical results of the mismatch in a rectangular waveguide with dielectric plates placed parallel to the H-plane walls are also presented.

Using several simplifying assumptions, Singh et al. [161] have attempted to determine theoretically the fields at the aperture of a H-plane sectoral horn with dielectric walls. The theoretical and experimental results showed good agreement.

Based on a circular cylindrical and uniform waveguide model with a periodic strip structure, Lier [162] has analysed strip-loaded horn with transverse (soft) and longitudinal (hard) strips. The results have shown that the soft-strip-loaded horn exhibits the same electrical behaviour as corrugated horns. The hard horn is found to be possessing high gain and low cross-polarisation over a certain frequency range. In another paper [163], using dielectric core approach he has discussed a broad-band elliptical-beamshape horn with low cross-polarisation levels. Experimental results of horns with rectangular and elliptical cross-sections are also presented.

Theoretical and experimental investigations on the effect of placing a dielectric sphere in front of, but

displaced from, the aperture of a corrugated horn are carried out by Nair [164]. The results have established that this system possesses gain and directivity in excess compared to conventional corrugated horns of the same dimensions.

Knop [165] has extended the asymptotic analysis technique for determining the HE_{11} mode e.m fields that can exist inside an across the aperture of a metallic wall conical horn, centrally loaded with a concentric dielectric material. The theoretical results of two other horns, the form-core air-lined and the dielectrically loaded horns agreed well with the experimental results.

The above review of the past work in the field has revealed the importance of development of new type of feed horn antennas with added advantages over the existing ones. Eventhough conical strip-loaded dielectric hybrid-mode feed horn antennas are reported in the literature, no attempt has been made to develop strip-loaded dielectric, rectangular or square pyramidal feed horns so far. This thesis presents the outcome of the investigation carried out to develop a new type of light-weight square pyramidal scalar-feed horn antenna with excellent radiation charact-eristics.

Chapter 3

METHODOLOGY

Chapter 3

METHODOLOGY

This chapter is devoted for highlighting the experimental methodology and the essential facilities used for the investigation of various antenna characteristics. The fabrication techniques and design details of the newly developed 'Simulated Scalar Feed' are also presented.

3.1 FACILITIES UTILISED

3.1.1 Anechoic Chamber

The evaluation of antenna radiation character-istics has to be carried out in an environment devoid of reflections from walls and external electromagnetic interferences. Such conditions are satisfied only if the measurements are carried out in free-space. The free-space conditions can be artificially simulated in laboratory by the use of an anechoic chamber. Eventhough the free-space conditions are not exactly satisfied by an anechoic chamber, it minimises the electromagnetic interferences from external sources and the reflections from the walls.

For antenna radiation characteristics measure-ments, a tapered anechoic chamber is required, whereas for

69

bistatic scattering studies a rectangular chamber is required. The present anechoic chamber is having convertible features. Depending up on the requirement, it can be converted from rectangular to tapered configuration. The schematic representation of an anechoic chamber is shown in figure 3.1.

A rectangular room of 9.00 metre X 5.00 metre is used for the construction of the anechoic chamber. The entire interior surface of the chamber is covered with pyramidal or wedge shaped polyurethane- form based material with microwave absorbing materials dispersed inside. Depending upon the importance of the area of the chamber, different type of absorbing materials are employed.

For covering the ceiling, sidewalls and a major portion of the floor area, small pyramids of base 7.60 cm and height 15.20 cm are employed. The central portion of the back wall, from where reflections are most likely to occur, is covered with large pyramids of base 15.20 cm and height 45.70 cm.

Portions of the chamber, like the tapered surfaces, from where less reflections are expected are covered with wedges of base 10.20 cm and height 5.10 cm.

CONVERTIBLE MICROWAVE ANECHOIC CHAMBER

[view from the top]

hinges

door

Target positioner

Walk ways

door

hinges

wedge
absorber

sliding
opening

door

Terminal
box

plywood
wedge absorber
aluminium sheet

[dimensions in cm.]

100   360   360
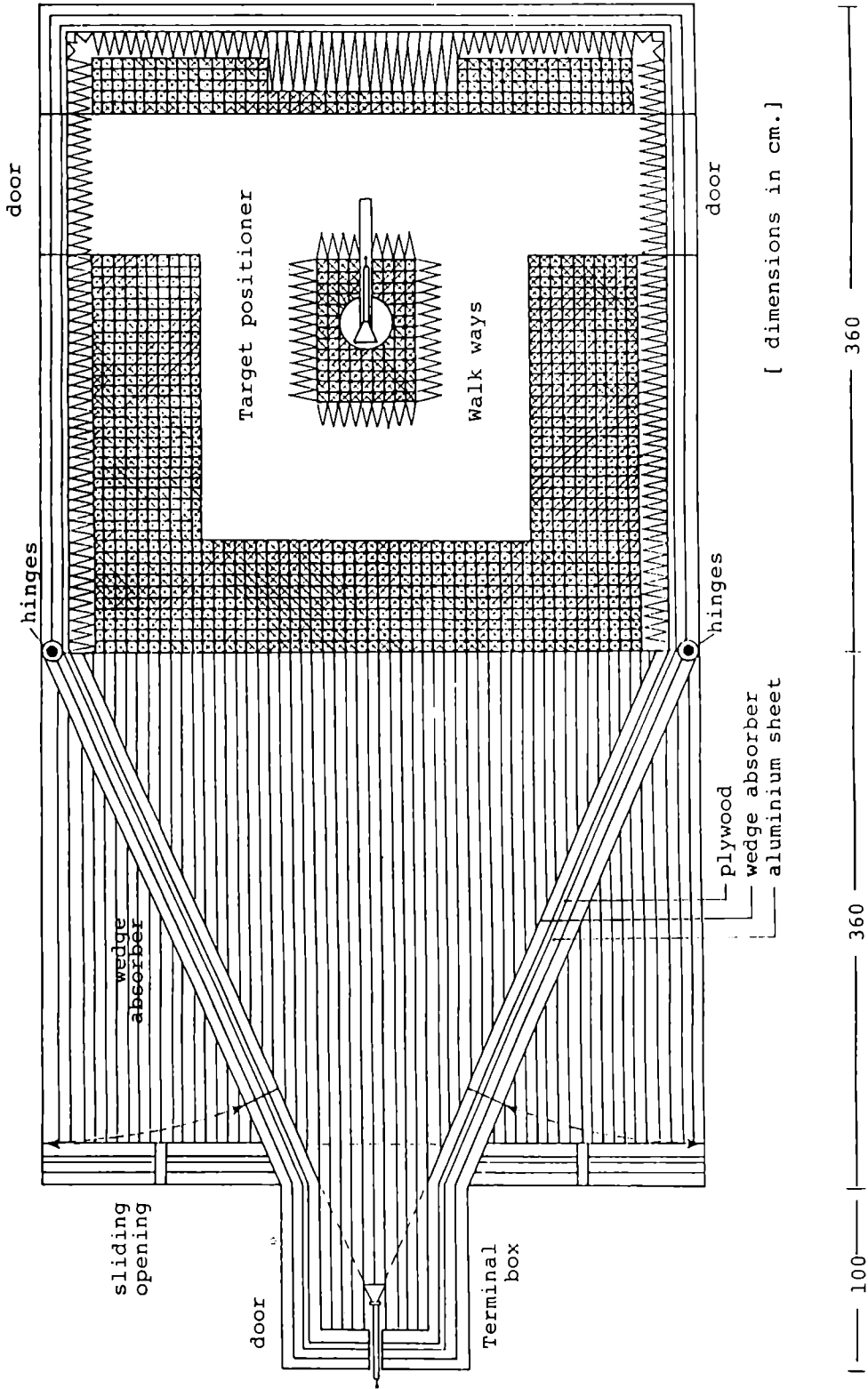
Fig.3.1: Schematic representation of a microwave anechoic chamber

For covering the walkways of the chamber a layered flat sheet absorber having five layers with a total thickness of 15.20 cm is used. Beneath the entire surface, to increase the total absorption, a densely packed flat absorber of thickness 5.10 cm has been used. All these absorbers are finally pasted to the wooden walls of the chamber using quick drying rubber based adhesives.

Electromagnetic interference shielding [EMI] is achieved by covering the entire wooden walls of the chamber by thin aluminium sheets. This is well earthed to prevent the formation of the fringing waves inside the chamber. Irrespective of the rectangular or tapered shape of the chamber, the quiet zone of the chamber is having an area of 1 sq.m. This zone is at a distance in such a way that the distance between the test antenna placed in this zone and the transmitter is greater than the distance required for satisfying the plane wave condition.

The antenna positioner and the associated accessories are housed in a cellar below the floor level, beneath the quiet zone. The test antenna is mounted on the axial rod of the positioner which is protruding above the floor level. The antenna mount is also covered with

microwave absorbing material. Using a remote control, the antenna positioner can be controlled from outside of the chamber. The average reflectivity of the present anechoic chamber is -30 dB.

3.1.2 Antenna Positioner and Controller

The radiation pattern of an antenna is the spacial distribution of electromagnetic energy in the space. In the present work the radiation patterns are measured in the receiver mode. In this mode of radiation pattern measurement, the test antenna has to be rotated about a vertical axis in the azimuthal plane. For this an antenna positioner (turn-table) with a remote controlling facility is required.

The antenna positioner used for the radiation pattern measurements consists of a rotating circular platform which is rotated by an a.c. motor. The speed of rotation of the platform is adjusted using a reduction gear mechanism. In the present case, the speed of rotation is chosen as 0.5 rpm. The axis of rotation of the circular platform passes through its centre and is perpendicular to its plane. The test antenna is fitted to this using a mounting mechanism. The maximum load capacity of the turn-

table is 80 kg. During measurements, to avoid the rotation of the platform beyond the required range, limit switches are provided. Two calibrated level meters, one for reading the azimuthal position and the other for antenna output signal are fitted to the front panel of the turn-table. Provision is also given for giving the antenna output signal to a X-Y recorder for plotting the radiation pattern. This turn-table is kept in the underground cellar which is just below the quiet zone of the anechoic chamber.

During pattern measurements, as the environment is to be reflection free, it is not advisable to operate the turn-table by standing inside the chamber. To avoid this, a remote control facility is required to operate the turn-table from outside the chamber. The remote control unit is having ON/OFF switches and provision for selection of clockwise or anticlockwise rotation of the turn-table. The unit is provided with an analogue meter calibrated in dB for measuring the signal received by the test antenna. Another meter with LED display gives the azimuthal position of the test antenna. This remote control unit along with the other equipments are housed in the control room of the anechoic chamber. The power cable, the control leads and the signal cables are taken to the control room through underground using seperately shielded metallic pipes.

3.1.3 Network Analyser

For the measurement of radiation patterns and impedance characteristics of the antenna, an instrumentation based on microwave vector network analyser is used. In this section a brief description of the microwave network analyser is presented.

The description of parameters like impedance or transfer functions of both the active and passive networks through stimulus response testing is referred as network analysis. Thus using a network analyser, the transmission and reflection characteristics of a test device can be measured. A network analyser consists of a sweep oscillator, a transducer, a harmonic frequency converter (receiver) and a display unit as shown in figure 3.2.

The transducer, which is the transmission/ reflection test unit, is connected between the signal source and the receiver. This has a threefold function. The first is to split the incoming microwave signal into reference and test signals. Secondly, it provides an extension capability for the electrical length of the reference channel so that the distance travelled by the
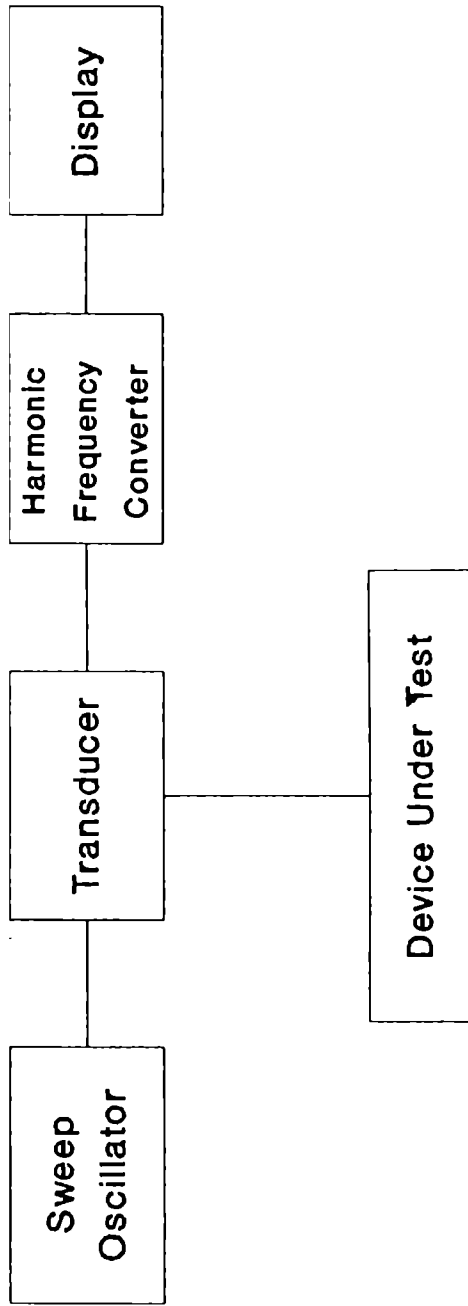
Fig.3.2: Block diagram of a network analyser

test and reference signals are equal. Finally, it connects the system properly for transmission or reflection measurements.

In the receiver, the harmonic frequency converter mixes the RF signal with the output of a local oscillator and the resulting IF signal is given to the display unit.

For measuring the radiation pattern using this system, the device under test (in this case, the test antenna) is to be connected in between the transmitter and the test port of the harmonic frequency converter.

In the present investigation, the network analysers used for the measurements are HP 8410 C and HP 8510 B.

The 8410 C network analyser is a manual system. This system measures the transmission and reflection characteristics of linear networks in the form of gain, impedance, reflection coefficient and S-parameters, in the frequency range of 110 MHz to 18 GHz. A phase-gain display and a polar display units are available with this system.

The HP 8510 B network analyser is a fully computer controlled system. The frequency range of operation of this system is 45 MHz to 26.5 GHz. Compared to HP 8410 C, this system is having a number of advantages and test facilities. For displaying the measured results two independent channels are provided. These channels can be displayed individually or simultaneously, with results displayed in either logarithmic/linear magnitude, phase or group delay format on polar or rectangular co-ordinates. Smith chart format is also provided for the direct measurement of impedance. The displayed results can be directly plotted by a HP 7475 A plotter. Five independent markers are provided in the display. Using these markers, the frequency of measured data can be directly read. The data processing speed of this system is such that, a fully error corrected 801 point trace of data is obtained under two seconds. Hence, adjustments in the device under test can be done while it is being measured. The capability of displaying the time domain response of a network is one of the major advantages of this system.

3.1.4 X-Y Plotter

The signals received by the test antenna at different azimuthal angular positions are graphically

plotted using an X-Y plotter. In the present work, the patterns are plotted using a HP 7047 X-Y plotter. Both the X and Y axes of this plotter are having a maximum sensitive range of 0.02 mV/cm. Depending upon the level of the signal received by the test antenna, various ranges from 0.02 mV/cm to 5 V/cm can be selected by a range selecting switch in both the axes. In addition to this, verniers are also provided for setting intermediate ranges. Time base sweeping is also possible for the axes. Sweep rates from 0.1 sec/cm to 50 sec/cm can be selected.

3.1.5 Rectangular to Square Waveguide Transition

Pyramidal horns with rectangular throat and aperture as well as square throat and aperture are fabricated and their radiation characteristics are investigated. For pyramidal horns with rectangular throat and aperture, conventional X-band waveguides and microwave components are used. But in the case of horns with square throat and aperture, for feeding the horn a rectangular to square waveguide transition is employed.

The sketch of the rectangular to square waveguide transition is shown in the figure 3.3. The transition is fabricated by keeping the broadwall width of
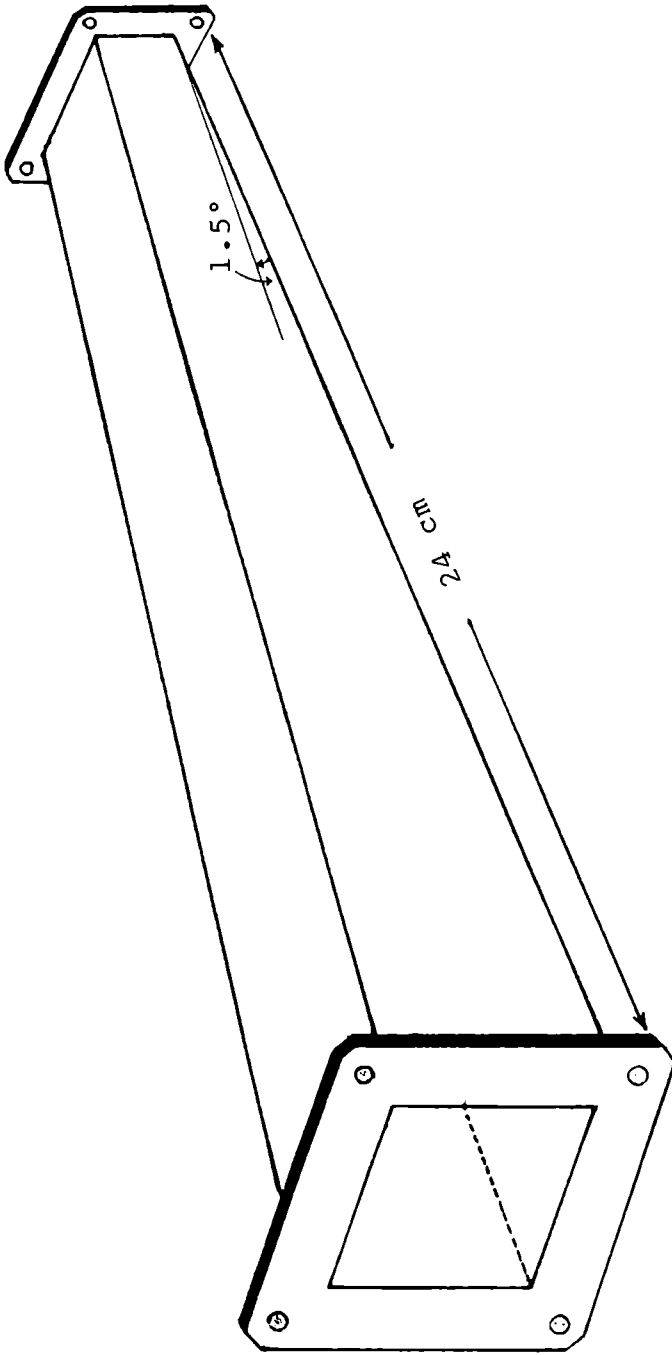
Fig.3.3: Sketch of the rectangular to square waveguide transition

the X-band waveguide constant at the usual value, while the
waveguide wall parallel to the E vector is gradually
flared. The width of this wall is made equal to that of
the broader wall after a flaring length of 24 cm so that the semi-
flare angle of the transition is 1.5°. This ensures good
VSWR characteristics for the transition.

3.2 FABRICATION OF THE SIMULATED SCALAR FEED HORN ANTENNA

The main interest of the present work was to
develop a light-weight pyramidal feed horn antenna with
high gain, good impedance matching, low sidelobe, backlobe
and cross-polarisation levels. In order to reduce the
physical weight of the test horn antenna, the entire
structure of the antenna is made up of a low-loss
dielectric material. Commercially available dieletric
material (perspex) with dielectric constant 2.56 is used
for this purpose.

The dielectric substrate, which is available in
the form of flat plate is machined to the required
thickness using a shaping machine. The flat surface of the
machined dielectric plate is then periodically loaded with
thin conducting wires or strips of width 'a' at a period
'd'. The periodic loading of conducting strips can be very

precisely executed by photolithography and etching technique. The other surface of the dielectric plate is completely metallised. The E-plane boundary walls of the test pyramidal horn are cut from this plate. The H-plane boundary walls are made from a dielectric plate of uniform thickness, which is completely metallised. Now, the horn antenna is constructed in such a way that the loaded dielectric surfaces of the E-walls are at the interior side of the horn. The flange at the throat of the horn is also made from the same dielectric material. Its inner and outer surfaces are completely metallised.

Pyramidal horn antennas of different physical dimensions and with different dielectric thickness and throat profile structures were fabricated. All these antennas were designed to operate in the X-band frequency range.

The radiation characteristics of all the horn antennas were studied. The experimental observations have showed that, when the thickness of the dielectric substrate of the E-plane boundary wall is $\lambda/4\sqrt{\epsilon_r - 1}$, the E-plane radiation pattern of the horn antenna is with very low sidelobe levels. 'λ' is the free-space wavelength and 'ϵ_r' is

the permittivity of the dielectric material. This is the condition for achieving the balanced hybrid mode as suggested by Lier et al. [146]. The measured E-plane aperture electric field distribution of the horn is found to be cosine in nature as in the case of a metallic corrugated horn antenna. As the H-plane boundary walls of the horn antenna are unaltered, the H-plane radiation patterns are exactly similar to that of a conventional horn antenna with identical physical dimensions.

The schematic representation of a square pyramidal horn antenna, fabricated with the optimised thickness for the dielectric substrate of E-plane boundary walls, required for the balanced hybrid condition is given in figure 3.4. This is a 11.8 cm x 11.8 cm square aperture horn antenna with a slant length of 1$\mathbf{3.8}$ cm and a semi-flare angle of 25 degrees in both the principal planes. At the throat region of this horn, a small portion of about 1 cm of the dielectric E-plane boundary walls are metallised. To achieve good impedance matching, after this metallised portion, the thickness 'h_1' of the dielectric substrate is selected as $\lambda/2\sqrt{\epsilon_r - 1}$, so that the surface impedance is infinity. Now, this thickness is gradually tapered to a thickness $h_2 = \lambda/4\sqrt{\epsilon_r - 1}$, at the point P. From
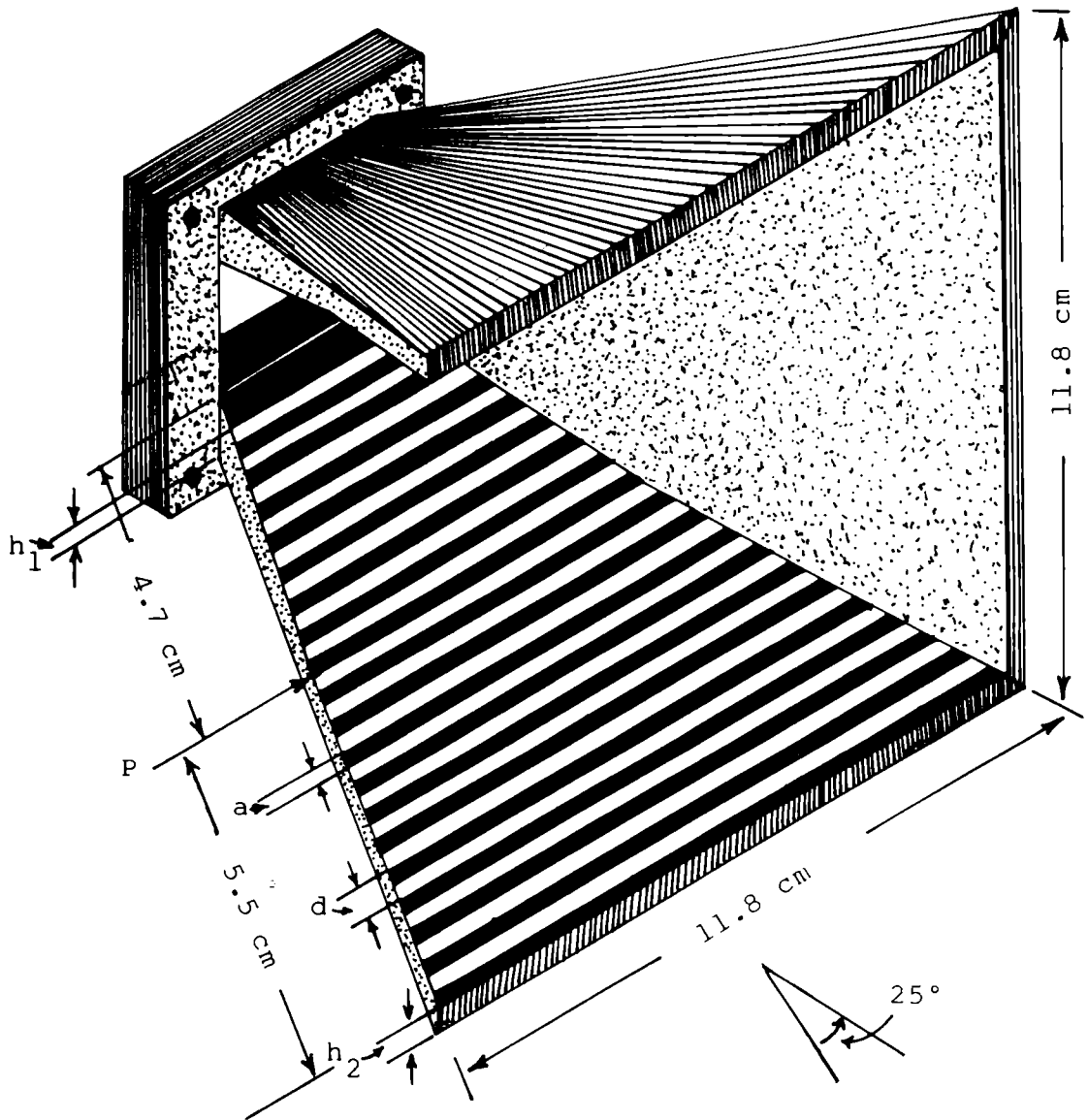
Fig.3.4: Schematic representation of a square pyramidal horn with optimised dielectric thickness for its E-plane walls (Simulated Scalar Feed)

the point P to the aperture of the horn antenna the thickness is kept at $\lambda/4\sqrt{\epsilon_r - 1}$. The remaining inner surface of the E-plane boundary walls are periodically loaded with thin conducting strips of width 'a' = 2 mm at a period of d = 4 mm.

A metallic corrugated horn antenna having identical physical dimensions as the above optimum test horn is also fabricated. Brass plates were used for this purpose. As in the case of the newly developed test horn antenna, the depth of the corrugation after 1 cm of throat region is $\lambda/2$. This is gradually tapered to $\lambda/4$ at the corresponding point P. Thereafter upto the aperture, the corrugation depth is kept constant as $\lambda/4$. The corrugation width 'a' and period 'd' are 2 mm and 4 mm respectively.

The radiation characteristics of both the test horn antenna and the identical metallic corrugated horn antenna were studied. From the experimental results, it is observed that the newly developed test horn is found to be simulating the radiation characteristics of the identical metallic corrugated horn antenna. The experimentally observed results are discussed in detail in the chapter for experimental results.

The basic design parameters of the pyramidal horn are shown in figure 3.5. The design details of all the horn antennas fabricated and investigated are presented in the table 3.1.

3.3 METHOD OF MEASUREMENTS

In the present investigation, the antenna characteristics measured are (i) radiation pattern; (ii) impedance and (iii) gain.

3.3.1 Radiation Pattern

The radiation pattern of an antenna is the graphical representation of the received field intensity/ power by the antenna as a function of direction. A complete representation of the radiation pattern requires a three dimensional representation. Hence, for simplicity, the radiation pattern is often described in terms of principal E and H-planes. According to the reciprocity theorem, the radiation pattern can be measured by two methods: (i) test antenna as receiver, and (ii) test antenna as transmitter. Using the first method, the radiation pattern measurements of the test horn antennas were carried out inside an anechoic chamber. The set-up used for the pattern measurement is shown in figure 3.6.
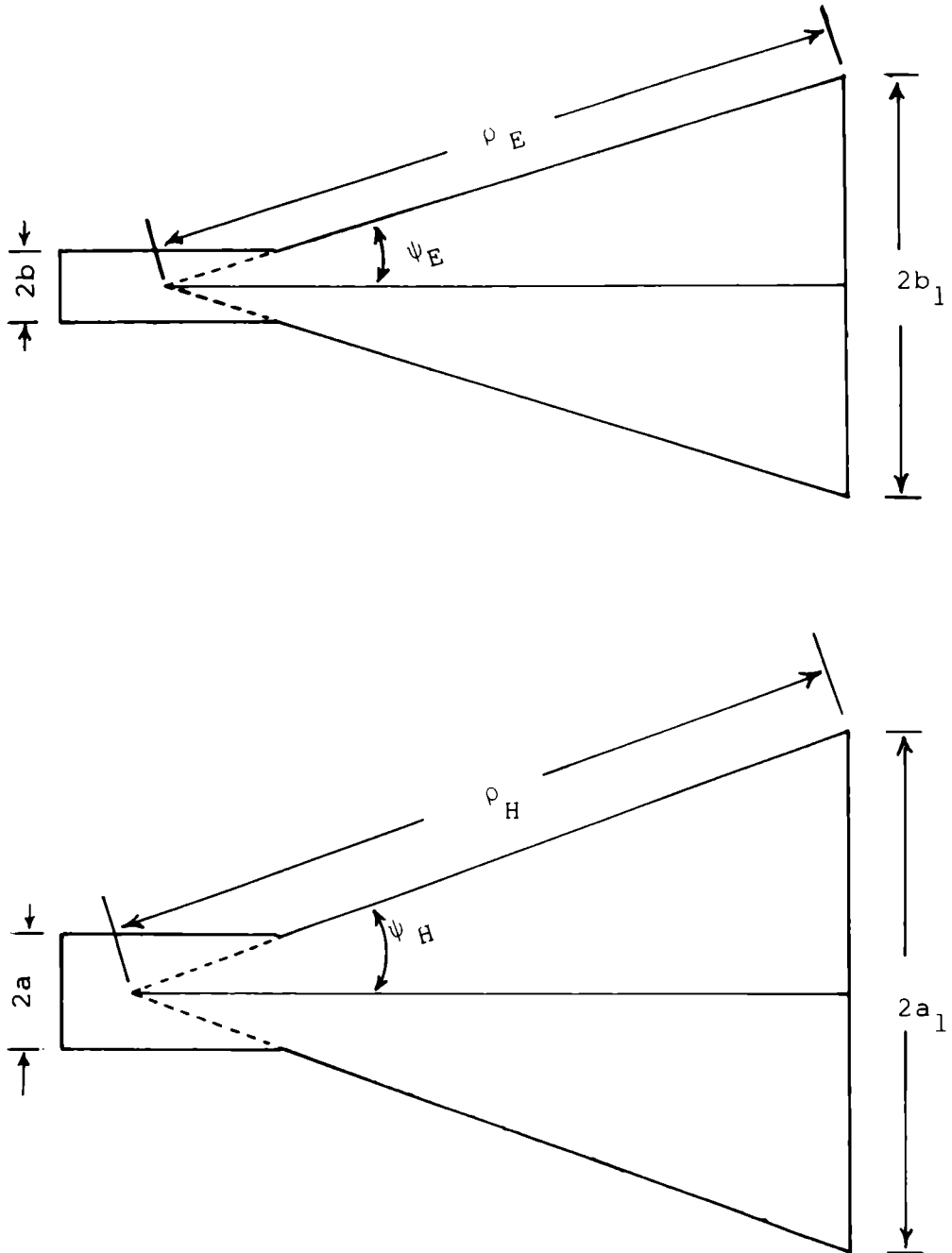
Fig.3.5: Basic design parameters of a pyramidal horn antenna

Horn	Throat dimension (cm)		Aperture dimension (cm)		Slant length (cm)		Semi-flare angle (deg)		Nature of E-plane boundary walls at the throat region	Grating parameters (cm)	
	$2a$	$2b$	$2a_1$	$2b_1$	ρ_E	ρ_H	ψ_E	ψ_H		a	d
H1	2.3	1	9.4	7.4	12.5	14.6	16	17.5	Uniform throat profile	0.025	0.2
H2	2.3	1	11.8	9	11.4	12.3	22	25	'' ''	0.01	0.2
H3	2.3	1	11.8	11.8	11.4	12.1	27	25	Tapered throat profile	0.2	0.4
H3A	2.3	1	11.8	11.8	11.4	12.1	27	25	'' ''	0.025	0.1
H4	2.3	1	11.8	11.8	12.8	12.8	25	25	Uniform throat profile	0.2	0.4
H4A	2.3	1	11.8	11.8	12.8	12.8	25	25	'' ''	0.2	0.4
H5	2.3	1	11.8	11.8	12.8	12.8	25	25	Tapered throat profile	0.1	0.2
H6	2.3	1	11.8	11.8	12.8	12.8	25	25	Tapered throat profile with tapering interior side of horn	0.2	0.4
H6A	2.3	1	11.8	11.8	12.8	12.8	25	25	Tapered throat profile with tapering exterior side of horn	0.2	0.4
H7	2.3	1	7	7	20.3	20.3	9.5	9.5	Tapered throat profile with tapering interior side of horn	0.2	0.4
SSF	2.3	1	11.8	11.8	12.8	12.8	25	25	'' ''	0.2	0.4
MCH	2.3	1	11.8	11.8	12.8	12.8	25	25	Metallic corrugated walls	0.2	0.4

Table 3.1: Design details of horn antennas fabricated and investigated
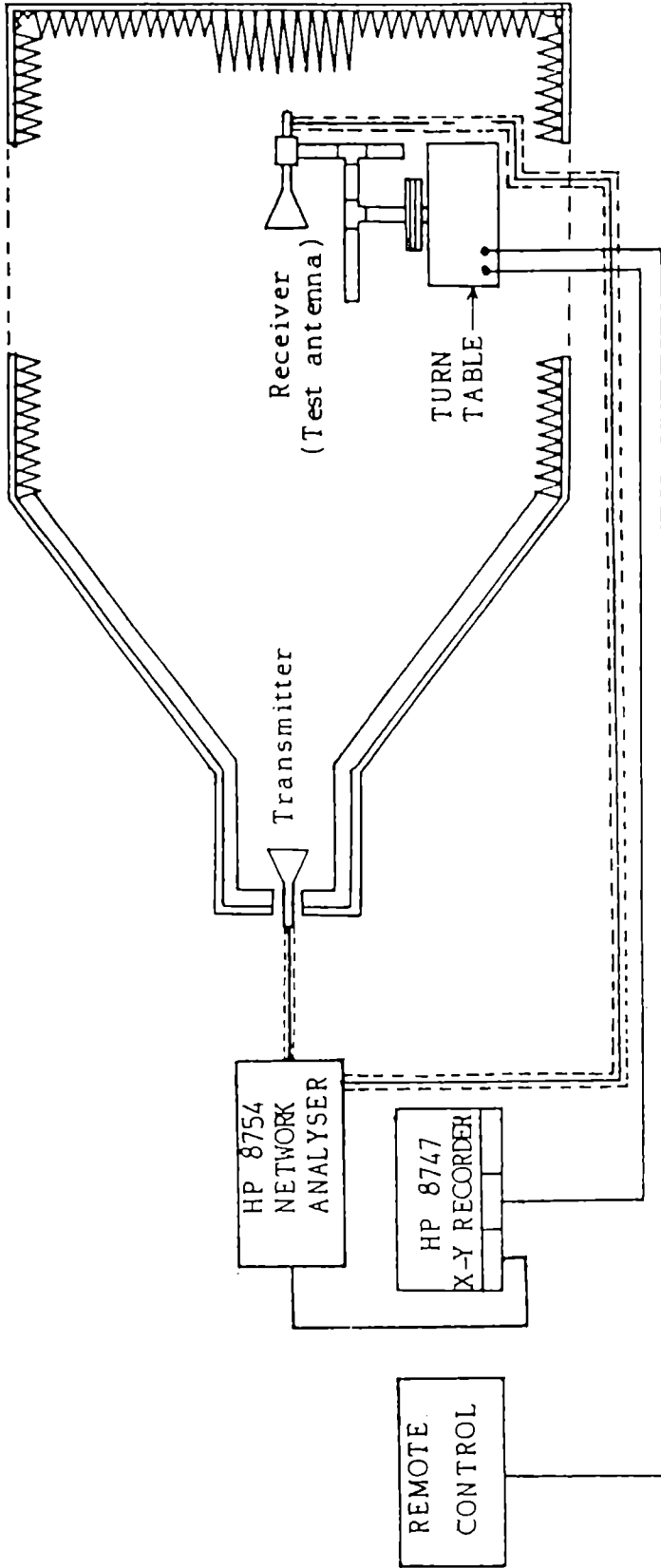
Fig.3.6: Experimental set-up for antenna radiation pattern measurement

The network analysers HP 8410 C and HP 8510 B were utilised for the radiation pattern measurements. The test antenna is mounted on a turn-table which is housed at the silent zone of the anechoic chamber, with its E-plane parallel to the E-plane of the transmitting antenna. A directional coupler is used to derive the required reference signal from the signal source. This reference signal is fed to the reference input of the harmonic frequency converter. The power received by the test antenna is given to the test port of the frequency converter. The output of the frequency converter is given to the network analyser. For plotting the radiation pattern the network analyser is connected to an X-Y plotter. The turn-table is rotated through 360° and the co-polar power pattern is plotted in dB scale. Now the test antenna is rotated through 90° and the cross-polar radiation pattern is plotted in the same paper along with the co-polar pattern. In both the measurements, the input power level to the transmitter is kept constant so that the cross-polar discrimination of the test horn with respect to the co-polar pattern is calculated as the difference in maximum received power levels of the two patterns. The co-polar and cross-polar radiation patterns of all the fabricated test horn antennas were plotted for different

frequencies in X-band. As all the power patterns were plotted in dB scale, the sidelobe and backlobe levels with respect to the maximum level of the main beam can be directly obtained as the difference between the main beam maximum and sidelobe level or backlobe level. Information regarding the 3 dB or 10 dB beamwidth and the position of nulls of the pattern are obtained from the radiation patterns.

3.3.2 Radiation Pattern Measurement Using HP 8510 B Network Analyser

The HP 8510 B Network Analyser system is completely controlled by a HP 98785 A computer. A software is used for measuring and plotting the radiation patterns of the antenna. The software incorporates all the facilities of the network analyser like averaging, time-domain capability etc.

In this method the standard transmitting antenna is connected to Port 1 and the test antenna is connected to Port 2. The test antenna can be rotated along the azimuthal plane by a Scientific Atlanta Positioner and Controller, which are also interfaced to the computer. The computer will automatically control both the network

analyser and positioner and enquire and store the data in it. In one rotation itself, it will acquire the information of 801 frequency points. The computer and the HP 7475 A plotter will give the hard copy of the radiation pattern. A detailed description of the method of measurement of radiation pattern using HP 8510 B Network Analyser is presented in Appendix II.

3.3.3 Antenna Impedance

The knowledge of the impedance of an antenna is of prime importance, because it directly affects the efficiency with which it transfers energy to or from the antenna. When a microwave signal is fed to an antenna, if the antenna impedance is not matched with the impedance of the propagating medium, a part of the signal will be reflected towards inside the antenna itself. This results in a standing wave pattern inside the waveguide.

In the case of horn antennas, the impedance of the antenna and the VSWR are influenced by the reflections from the throat and the aperture of the horn. The reflection is accounted by the parameter "reflection coefficient" (ρ). It is the voltage ratio of the energy reflected to the incident energy. A measure of the

reflection towards inside the horn and hence the formation of standing waves inside the waveguide can also be represented in terms of the parameter "VSWR". It is related to 'ρ' by the relation VSWR = $\frac{1+\rho}{1-\rho}$. For a perfectly matched antenna, which is the ideal case the value of VSWR is unity. On the other hand if the return loss in dB 'R' of the antenna system is measured, then $\rho = 10^{-R/20}$

In the present investigation, the antenna impedance measurements are carried out using the HP 8510 B vector network analyser. The antenna whose impedance is to be measured is connected to the Port 1 of the network analyser. The 'START' and the 'STOP' frequencies of measurement are selected using the 'STIMULUS' menu and 'PARAMETER' menu is used for setting the S_{11} mode. Now using the 'FORMAT' menu, the measured results can be plotted either in 'LOG MAG' format or 'SMITH CHART' format. After presetting, the system characteristic impedance Z_o is set to 50 Ω, so that the centre of the Smith Chart corresponds to 50 Ω. Now, the complex impedance of the device under test is displayed on the screen. By selecting the 'MARKER' and using the knob provided for varying the frequency, the complex impedance in the R ± jX format can

be read from the display. The marker position at the
bottom half of the chart indicates a capacitive impedance,
whereas at the top half indicates an inductive impedance.

If the 'LOG MAG' format is selected, the SWR or
Return loss in dB at a frequency can be directly obtained
from the display. In this format also the marker and the
knob can be used for obtaining the variation of VSWR or
Return loss with frequency in the range of interest.

The impedance plots of the horn antennas
investigated in the present work are presented in the
chapter for experimental results.

3.3.4 Antenna Gain

The ability of an antenna to concentrate the
radiated power in a direction, or conversely to absorb the
incident power effectively from that direction is termed
variously in terms of its gain, power gain, directive gain
or directivity. The gain of the antenna in this thesis
refers to the power gain.

In the present work, for measuring the gain of
test antenna, a pyramidal standard gain horn antenna of

Scientific Atlanta is used. Initially the standard gain horn antenna is placed on the turn-table and the maximum received power is measured with the help of a HP 8510 B network analyser. Then it is replaced by the test antenna and the maximum received power is noted. In both the cases, the input power level given to the transmitter antenna is kept constant. The difference in the power levels received by both the antennas is noted as ± g dB. If the power level of the test antenna is higher than that of the standard gain antenna then the gain of the test antenna is G_T + g dB. In the other case it will be G_T - g dB. G_T is the gain of the standard gain antenna, which is available from the manufacturer.

Chapter 4

EXPERIMENTAL RESULTS

Chapter ·4

EXPERIMENTAL RESULTS

Metallic corrugated horn antennas, by virtue of its scalar boundary wall and radiation characteristics [53,54], are found to be excellent feeds for large reflector antennas used in radar, radio astronomy and satellite tracking. The main disadvantages of these antennas are their high production cost, heavy weight and the tedious fabrication process. In this thesis, an alternate technique for the development of a feed horn antenna, which simulates all the radiation characteristics of a metallic corrugated horn antenna, by a very simple, easy and less time consuming procedure for mass production is presented.

This chapter highlights the experimental results of the investigation carried out for the development of the new simulated scalar feed horn antenna with excellent radiation characteristics. In order to optimise the design parameters of the simulated scalar feed horn antenna, pyramidal horn antennas of different physical dimensions and different grating parameters for the E-plane boundary walls were fabricated. All these horn antennas were

constructed for the operation in X-band frequency range.
The E-plane radiation characteristics of these horn
antennas are compared with that of the corresponding
ordinary metallic conventional horn antennas of identical
physical dimensions. Finally, the E-plane radiation
characteristics of the newly developed simulated scalar
feed horn antenna are compared with that of a metallic
corrugated horn antenna of identical physical dimensions.

As the H-plane boundary walls of all the horn
antennas investigated are unmodified, and since they are
identical to that of a corresponding ordinary metallic
conventional horn antenna, (refer page 101, figure 4.1) no
attempt has been made to study the H-plane radiation
characteristics. The following E-plane radiation charact-
eristics of the horns are studied in detail:

1. Radiation pattern

2. Sidelobe level

3. Backlobe level

4. Cross-polarisation level

5. Half-power (3 dB) and 10 dB beamwidths

6. Return-loss

7. Gain

Variation of these antenna radiation character-
istics of all the horn antennas with frequency are
summarised in the following sections of the thesis. For
convenience, the results of horn antennas of different
physical dimensions and design criteria are presented in
different sections.

4.1   EXPERIMENTAL RESULTS OF HORN H1

The main reason for the presence of high sidelobes
and backlobes in the E-plane radiation patterns of conven-
tional metallic horns are due to the strong diffractions
from the edges of E-plane boundary walls. This strong edge
diffractions can be considerably reduced if the illumina-
tion of the E-plane boundary walls is reduced as in the
case of H-plane walls illumination.

It is well known that when the depth of corruga-
tions on the boundary walls of a metallic corrugated horn
is $\lambda/4$, the surface admittance is zero. This zero wall
admittance forces the E-field to reduce considerably and as
a result, the sidelobe and backlobe levels in the radiation
patterns of such horns are very much reduced. It is also
observed that a dielectric substrate with a strip-grating
structure on its surface is behaving exactly like a

metallic corrugated surface [144]. This has inspired to apply such kind of surfaces as the E-plane walls of a pyramidal horn antenna for improving its radiation characteristics.

With the above idea, a pyramidal horn antenna whose E-plane walls are fabricated with a dielectric substrate of uniform thickness h = $\lambda/4\sqrt{\epsilon_r}$, loaded with a strip-grating structure is constructed. Here ' λ ' is the free-space wavelength at the design frequency 'h' is the dielectric thickness and 'ϵ_r' its dielectric constant. This horn antenna is referred to as horn Hl in this thesis.

The horn Hl is a rectangular pyramidal horn antenna whose selected physical dimensions are that of an optimum horn [170]. The aperture dimensions are a_1 = 4.7 cm, b_1 = 3.7 cm. The slant lengths of the horn antenna in the E and H-planes respectively are ρ_E = 12.5 cm, ρ_H = 14.6 cm, and the corresponding semiflare angles in the above planes are ψ_E = 16°, ψ_H = 17.5°. As stated earlier, the thickness 'h' of the low loss dielectric substrate used for the fabrication of the E-plane walls is 0.55 cm so that the condition h = $\lambda/4\sqrt{\epsilon_r}$ is satisfied at 8.5 GHz. The

entire inner surface of the E-plane boundary wall is periodically loaded with thin conducting wires of diameter a = 0.007 λ at a period d = 0.056 λ, where 'λ' is the free space wavelength at the design frequency, 8.5 GHz. The outer surface of the E-plane boundary walls is completely metallised. No modification is made on the H-plane boundary walls of this horn. They are also fabricated with a uniform thick dielectric substrate whose inner and outer surfaces are completely metallised so that they are identical to the H-plane walls of a conventional metallic horn. The longitudinal cross-sectional view of horn H1 is given in figure 4.1. Unfortunately, the impedance matching of the horn antenna was very poor. Hence, to achieve good impedance matching, at the throat region of the horn, about 3 cm portion of the inner surface of the E-plane boundary walls is completely metallised. This structure is derived after many experimental iterations.

A conventional horn antenna (H1M) of identical physical dimensions as that of the horn H1 is fabricated. The radiation characteristics of the horn H1 are compared with that of the above conventional horn.

The typical E-plane radiation patterns of the horns H1 and H1M at the design frequency 8.5 GHz and at

(a)   E-plane

(b)   H-plane
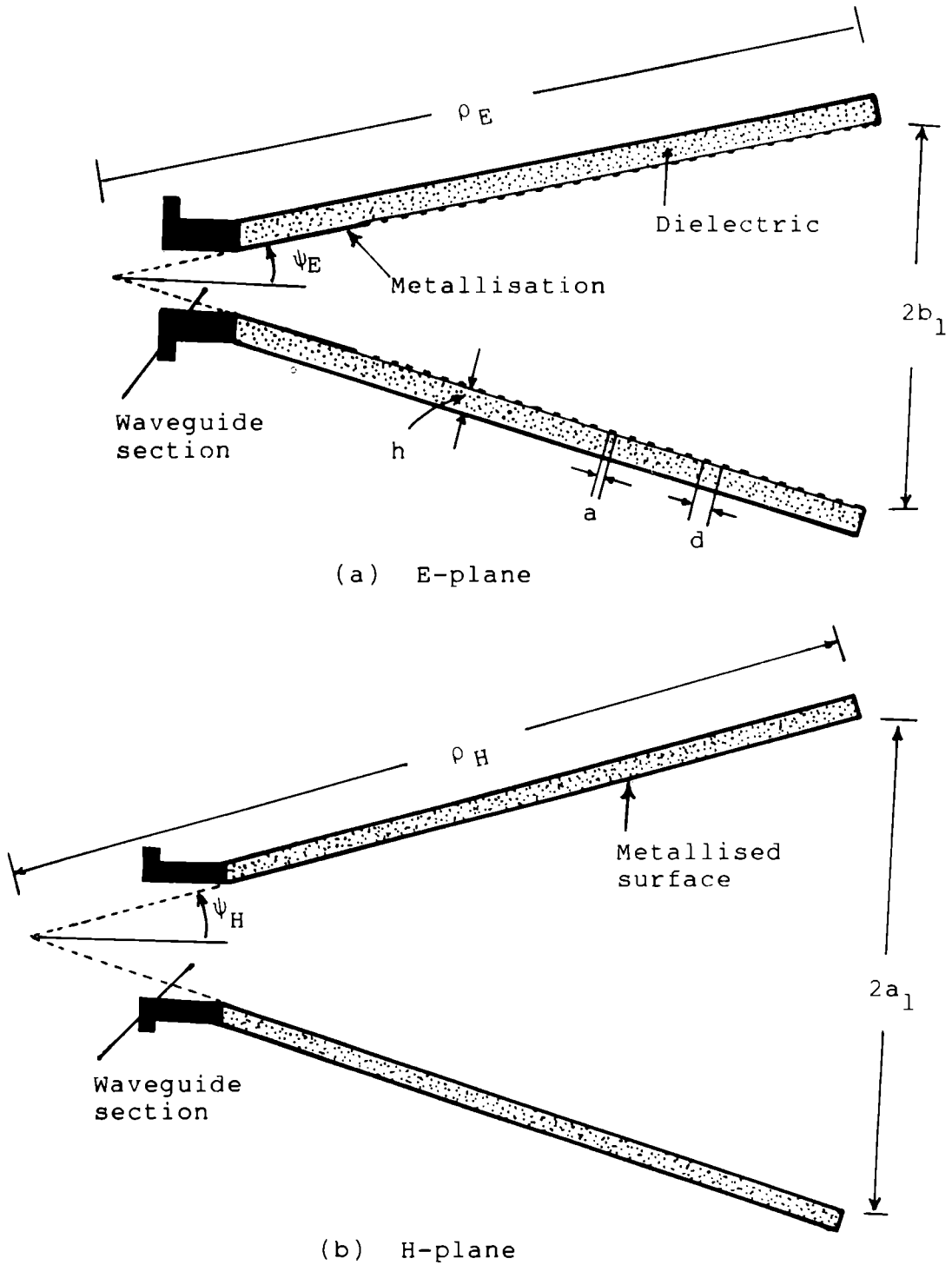
Fig.4.1: Longitudinal cross-sectional view of horn H1

11 GHz are compared in figure 4.2. The radiation pattern
studies showed that at the design frequency (8.5 GHz) the
E-plane radiation pattern is worsened as far as the side-
lobe level is concerned. But at higher band edge it is
found that the horn H1 is better than H1M. The probable
reason for this may be the poor design criteria of
dielectric thickness $h = \lambda / 4\sqrt{\epsilon_r}$. A close look on the
boundary condition shows that the correct design criteria
for the dielectric thickness is $h = \lambda / 4\sqrt{\epsilon_r - 1}$. This design
criteria is discussed in detail in other sections.
Nevertheless, the other radiation characteristics of this
horn H1 are also discussed in this section.

The typical H-plane radiation patterns of the two
horns, at the centre frequency 10 GHz, are compared in
figure 4.3. In other frequencies also, it is found that
the H-plane radiation patterns of the horns H1 and H1M are
almost identical. As stated earlier, this may be due to the
unaltered metallic nature of the H-plane walls of horn H1.
Since, all the horn antennas discussed in the following
sections are with unaltered H-plane boundary walls, their
H-plane radiation characteristics are not presented in the
remaining sections of this thesis.
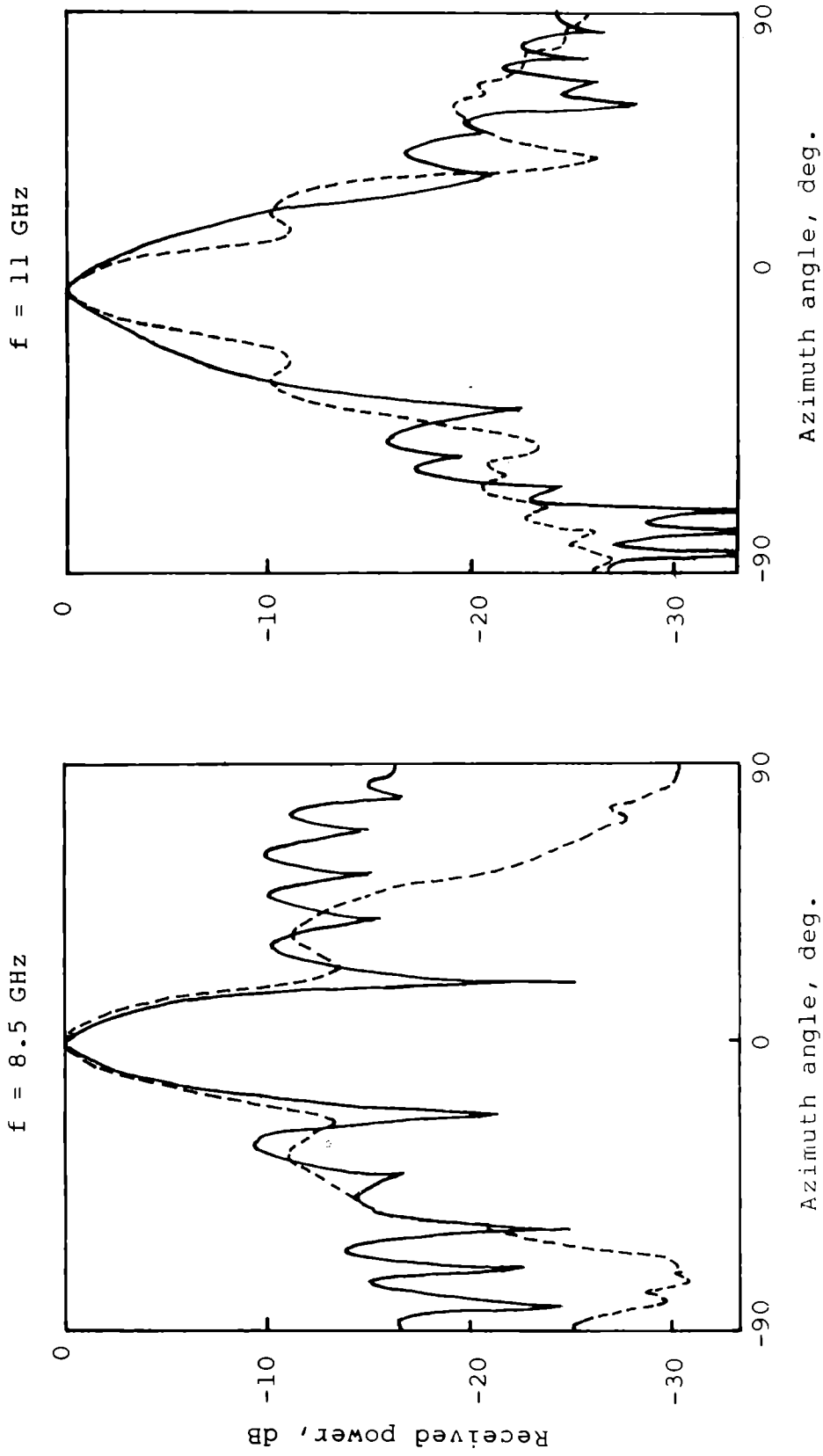
Fig.4.2: E-plane radiation patterns of horns H1 and H1M

——— Horn H1 ; —————— Horn H1M
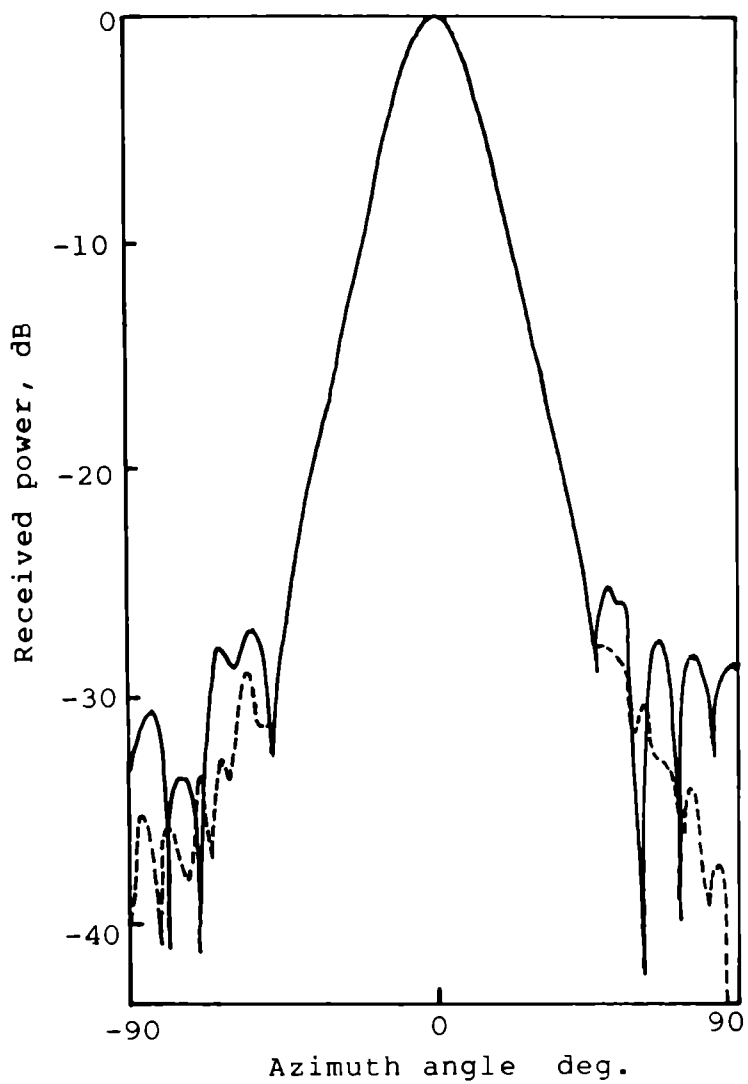
Fig.4.3: Typical H-plane radiation patterns of horns Hl and HlM at 10 GHz

——————— Horn Hl ; ────── Horn HlM

The typical variation of return-loss of the two
horns with frequency is given in figure 4.4. Eventhough
the return-loss characteristics of the horn H1 is poor in
the 8 GHz to 9.8 GHz frequency range, above 9.8 GHz it is
well within the tolerable limit.

The variation of sidelobe and backlobe levels of
the horns H1 and H1M with frequency is shown in figure 4.5.
Though the design frequency of the horn H1 is 8.5 GHz, the
exhibited minimum level of sidelobe is occurring at the
frequency of 11 GHz. In the case of backlobe character-
istics also, it is found to be higher at the design
frequency than at 11 GHz. At the design frequency,
8.5 GHz, the backlobe level of the horn H1 is -21.3 dB,
whereas at 11 GHz, it is -27.6 dB.

The variation of the 3 dB and 10 dB beamwidths of
the horns with frequency is presented in figure 4.6. Upto
10 GHz, no drastic change in the 3 dB or 10 dB beamwidths
of the horn H1 is obtained. However, above 10 GHz, the
3 dB and 10 dB beamwidths of the horn are found to be
increasing considerably. At 12 GHz, the 3 dB beamwidth of
the horn H1 is 35°, which is almost equal to the 10 dB
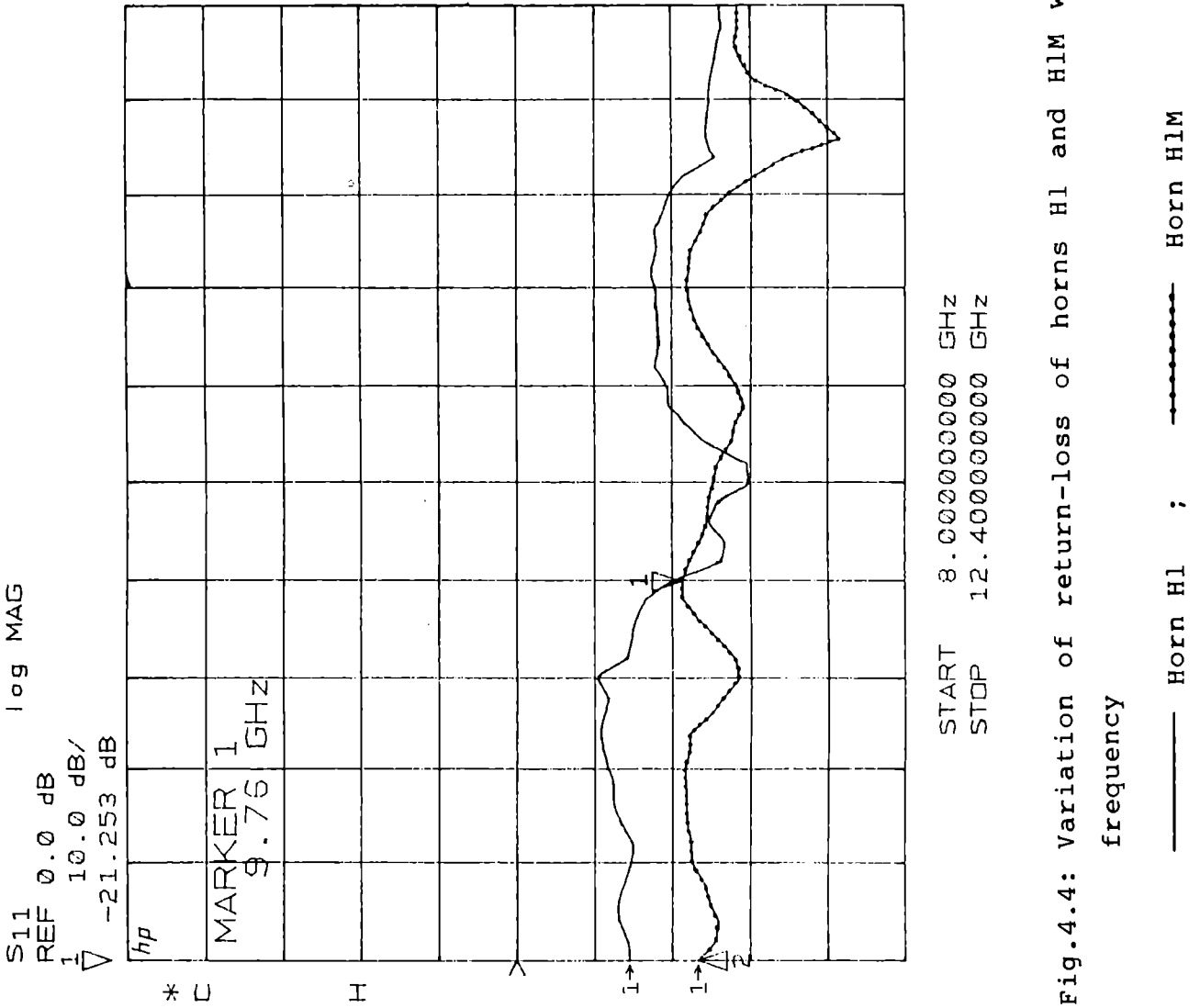
Fig.4.4: Variation of return-loss of horns H1 and H1M with frequency

—— Horn H1 ; ········· Horn H1M

Sidelobe level, dB   Backlobe level, dB

Frequency, GHz

— Sidelobe level, H1   —+— Sidelobe level, H1M

—*— Backlobe level, H1   —□— Backlobe level, H1M
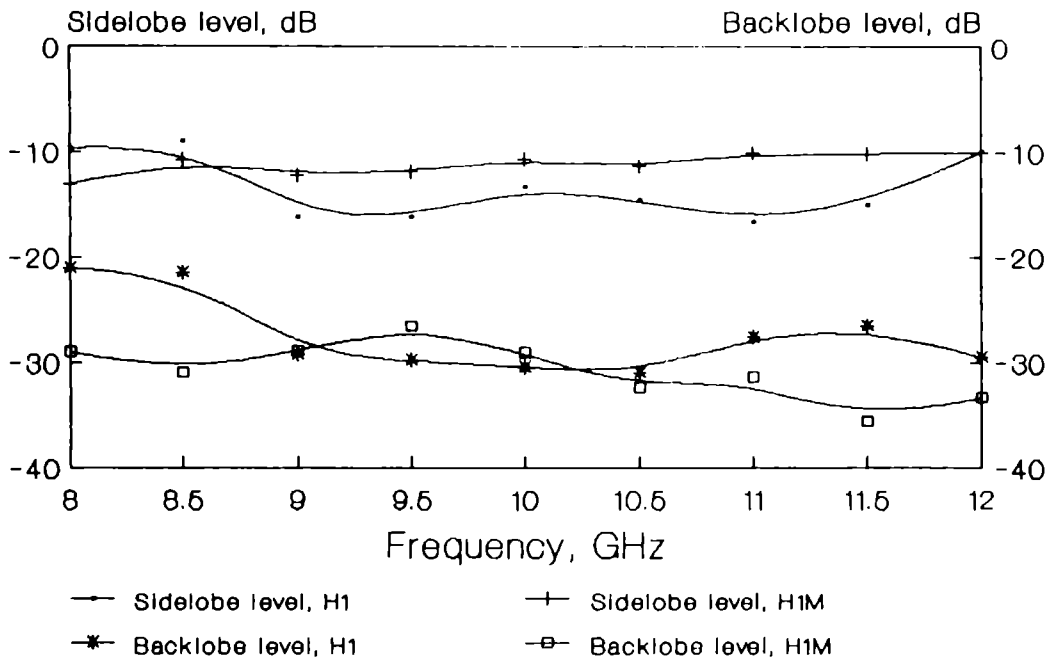
Fig.4.5: Variation of sidelobe and backlobe levels of horns H1 and H1M with frequency

3-dB Beamwidth, deg.   10-dB Beamwidth, deg.

Frequency, GHz

— 3-dB Beamwidth H1   —+— 3-dB Beamwidth H1M

—*— 10-dB Beamwidth H1   —□— 10-dB Beamwidth H1M
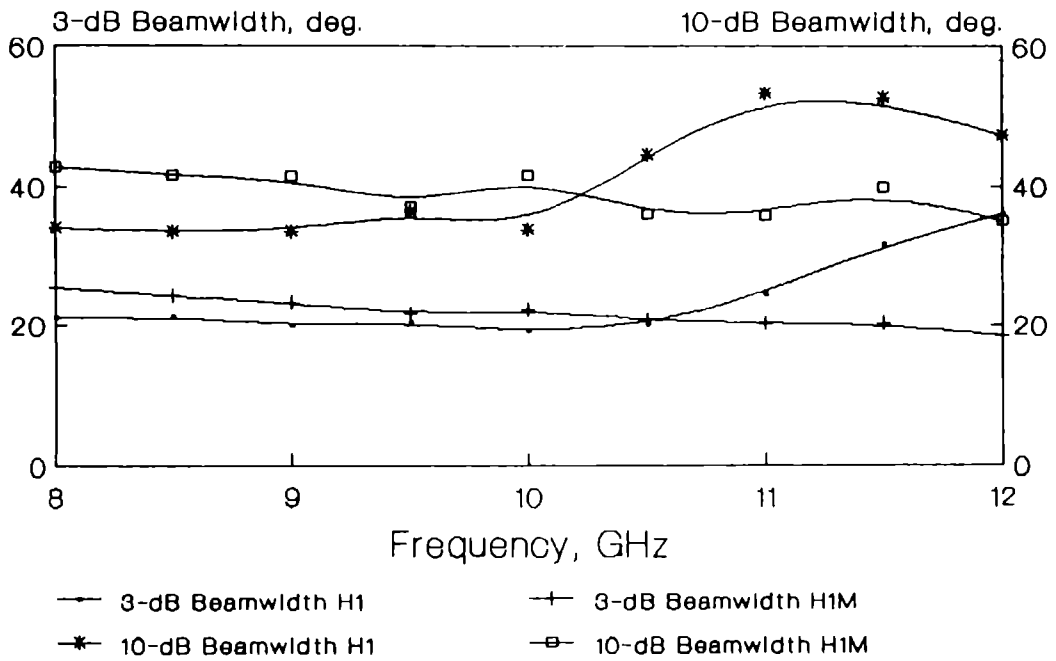
Fig.4.6: Variation of 3 dB and 10 dB beamwidths of horns H1 and H1M with frequency

beamwidth of the conventional horn H1M. The 3 dB and 10 dB beamwidths of the conventional horn H1M, in the entire 8 GHz to 12 GHz frequency range, are more or less found to be decreasing with the increase of frequency.

The frequency response of the cross-polarisation of the horns H1 and H1M is shown in figure 4.7. Although the cross-polarisation levels of the horn H1 are higher than that of the conventional horn H1M, its exhibited cross-polar level at 11 GHz is better than -29 dB.

The gain of the horn H1 and the conventional horn H1M at different frequencies in 8.5 GHz to 12 GHz frequency range is compared in figure 4.8. In the entire above frequency range the gain characteristic of the horn H1 is found to be poorer than that of the conventional horn H1M. From 8.5 GHz to 10 GHz, the 3 dB and 10 dB beamwidths of the horn H1 are narrower than that of the conventional horn H1M. Even then, as normally expected, the gain of the horn H1 is not found to be higher than that of the conventional horn H1M in the above frequency range. Moreover, above 10 GHz, though the 3 dB and 10 dB beamwidths of the horn H1 are considerably increased, the expected corresponding reduction in gain is not observed. On the other hand it is
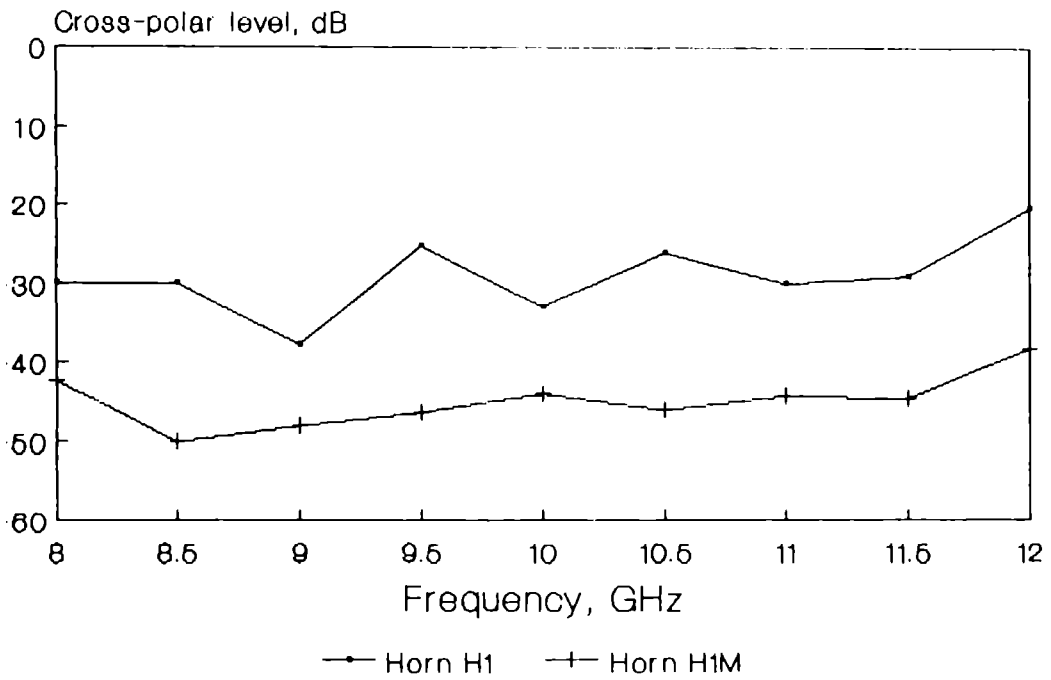
Fig.4.7: Variation of cross-polarisation level of horns
H1 and H1M with frequency
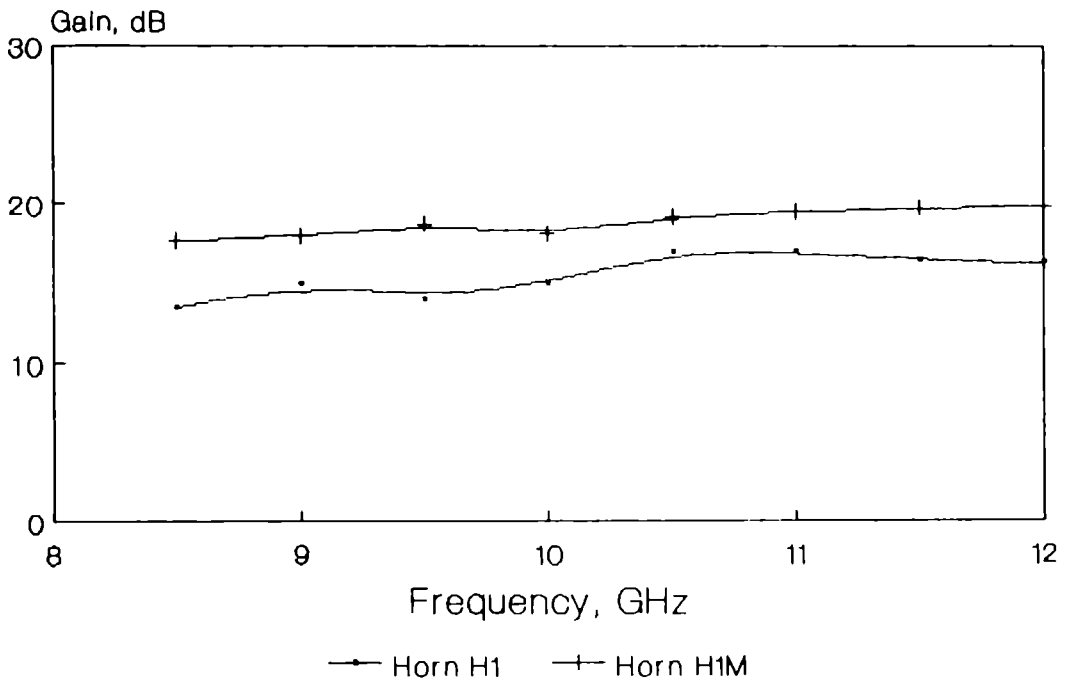
Fig.4.8: Variation of gain of horns H1 and H1M with
frequency

found to be increasing. The overall reduction observed in the gain characteristics of the horn H1 may be due to its increased cross-polar characteristics compared to that of the conventional horn H1M.

From the study of the experimental results of the two horns, it is found that, mainly, except in the case of gain, the horn H1 is preferable to the conventional horn H1M. In order to explore the possibility of achieving further improvements in the radiation characteristics and for validating the experimental results obtained, another rectangular pyramidal horn with different physical dimensions is fabricated. The fabrication details and the experimental results of this horn antenna are presented in the next section.

4.2 EXPERIMENTAL RESULTS OF HORN H2

The second horn (H2) is also a rectangular pyramidal horn, but of different physical dimensions than the earlier horn H1. The aperture dimensions of the present horn H2 are $a_1 = 5.9$ cm $b_1 = 4.5$ cm. Its E and H-plane slant lengths are $\rho_E = 11.4$ cm and $\rho_H = 12.3$ cm respectively. The respective semiflare angles in the above principal planes are $\psi_E = 22°$ and $\psi_H = 25°$.

As in the case of horn H1, the E-plane boundary walls of the present horn H2 are also fabricated with a flat dielectric plate of thickness h = 0.55 cm, so that the condition h = $\lambda/4\sqrt{\epsilon_r}$ is satisfied at 8.5 GHz. Here 'λ' is the free-space wavelength at the design frequency, and 'ϵ_r' is the dielectric constant of the substrate used. At the throat region of the horn, after the 3 cm metallised portion, about 1.8 cm ($\approx \lambda/2$) region of the inner surface of the E-walls are periodically loaded with thin conducting wires of diameter a = 0.007 λ at a period d = 0.028λ. For the entire remaining inner surface of the E-walls, upto the aperture of the horn, the period of loading is 0.056λ. The outer surface of the E-plane walls are completely metallised.

A conventional horn (H2M) of identical physical dimensions as that of the horn H2 is also fabricated. The radiation characteristics of the horns H2 and H2M are compared and the results are presented in the following part of the thesis.

The typical E-plane radiation patterns of both the horns H2 and H2M at the design frequency 8.5 GHz and at 11 GHz are compared in figure 4.9. From the figure it is
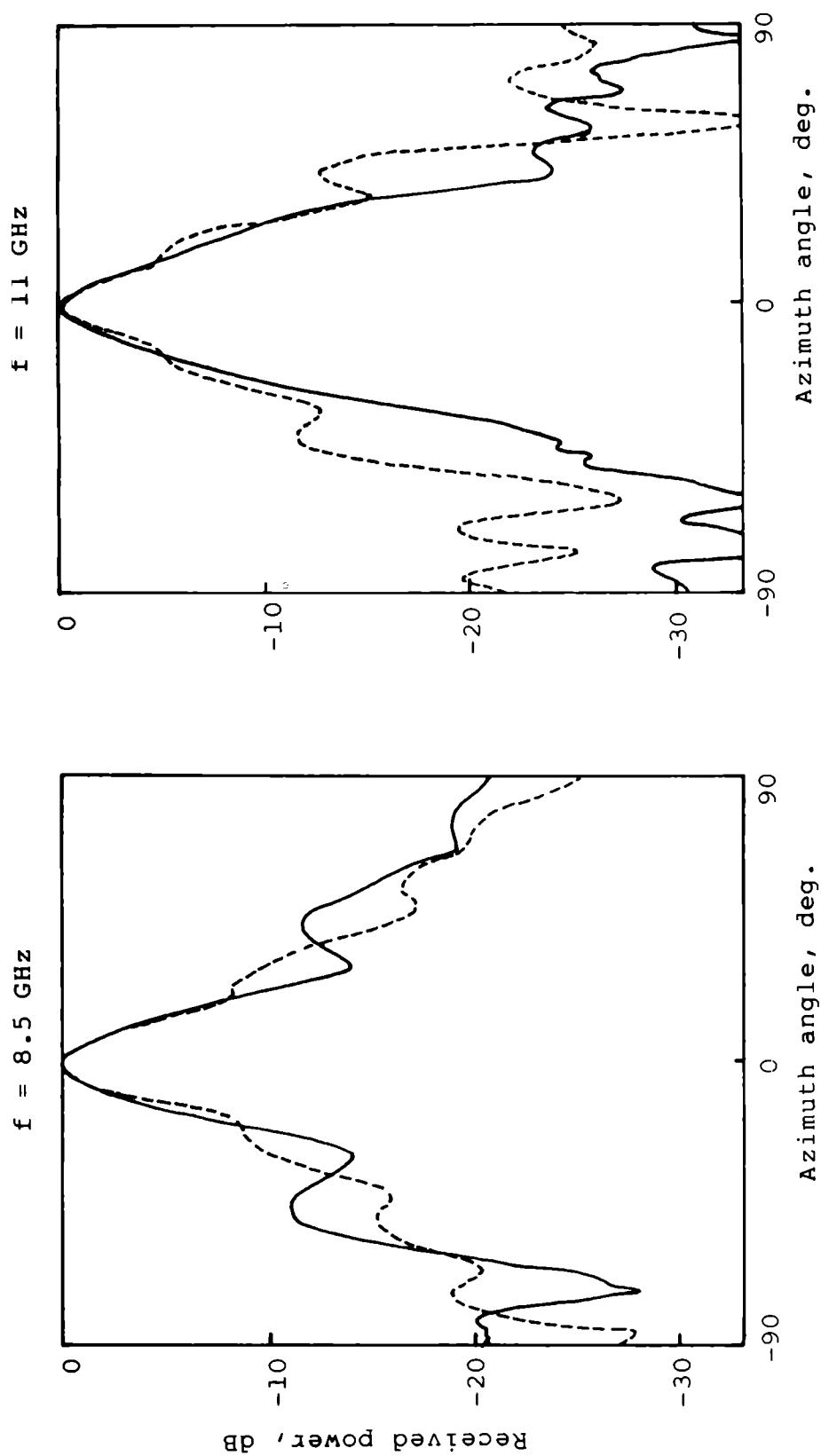
Fig.4.9: E-plane radiation patterns of horns H2 and H2M

——— Horn H2 ; ------ Horn H2M

well understood that the sidelobe levels of the present
horn H2, especially at 11 GHz, is very much lower than that
of the conventional horn H2M. As in the case of horn H1,
here also, considerable variations in the H-plane radiation
patterns of the horns H2 and H2M are not observed. The
typical H-plane radiation patterns of the two horns at
10 GHz are given in figure 4.10.

The frequency response of the return-loss of the
horn H2 in the 7.5 GHz to 14 GHz frequency range is shown
in figure 4.11. Eventhough the return-loss characteristic
of the conventional horn H2M (better than -20 dB in the
entire X-band of frequency) is found to be better than that
of the horn H2, for frequencies from 11 GHz to 12.4 GHz,
the return-loss of horn H2 is within the tolerable limit.
However, in the lower edge of the frequency band
considered, its return-loss characteristics is found to be
poor.

The variation of sidelobe and backlobe levels of
the horns H2 and H2M with frequency is given in figure
4.12. In the 8 GHz to 10.5 GHz frequency range, the
E-plane radiation patterns of the conventional horn H2M are
found to be possessing shoulderlobes in the mainlobe. As
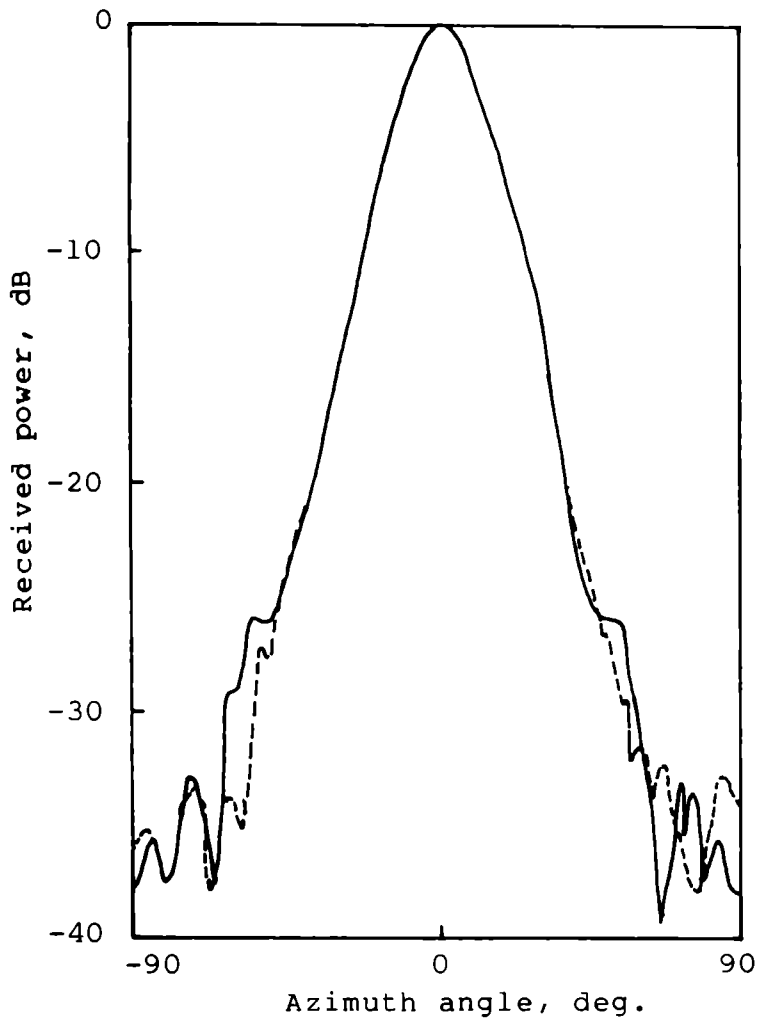
Fig.4.10: Typical H-plane radiation patterns of horns H2 and H2M at 10 GHz

———————— Horn H2 ; ─ ─ ─ ─ ─ ─ ─ Horn H2M

116
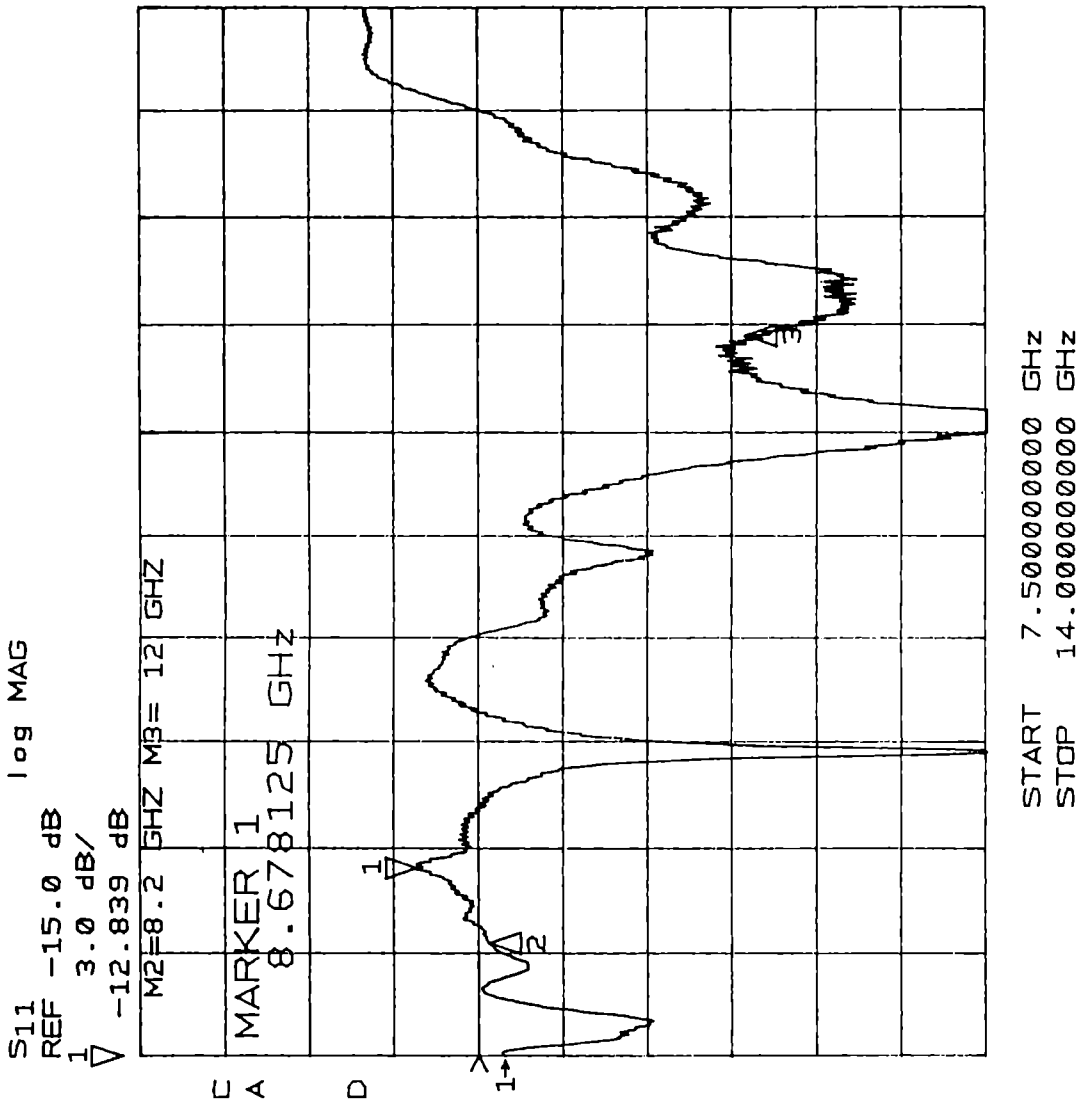
Fig.4.11: Variation of return-loss of horn H2 with frequency

the frequency is increased from 8 GHz, the level of the shoulderlobes are found to be increasing. At 10.5 GHz, the observed shoulderlobe level is -5.5 dB. Moreover, for frequencies above 10.5 GHz, the shoulderlobe levels are found to be considerably reduced. However, in the case of present horn H2, such shoulderlobes are totally absent and its radiation patterns are found to be with very low sidelobes. Here also, as observed in the case of horn H1, the exhibited minimum level of sidelobe is at 11 GHz instead of at the design frequency 8.5 GHz. At 11 GHz, the observed sidelobe level of the horn is -23.4 dB, whereas at 8.5 GHz, it is only -11 dB. The backlobe characteristics of the horn H2 is also found to be better than that of the conventional horn H2M, especially above 9.3 GHz.

The cross-polarisation levels of the two horns at different frequencies in the 8 GHz to 12 GHz frequency range are compared in figure 4.13. As observed in the earlier case, compared to the conventional horn, the cross-polar characteristic of the present horn H2 is found to be slightly poor. However, above 10.5 GHz, its cross-polarisation level is better than -30 dB.

The 3 dB and 10 dB beamwidths of the two horns with frequency are shown in figure 4.14. As expected, the 3 dB and 10 dB beamwidths of the conventional horn H2M are
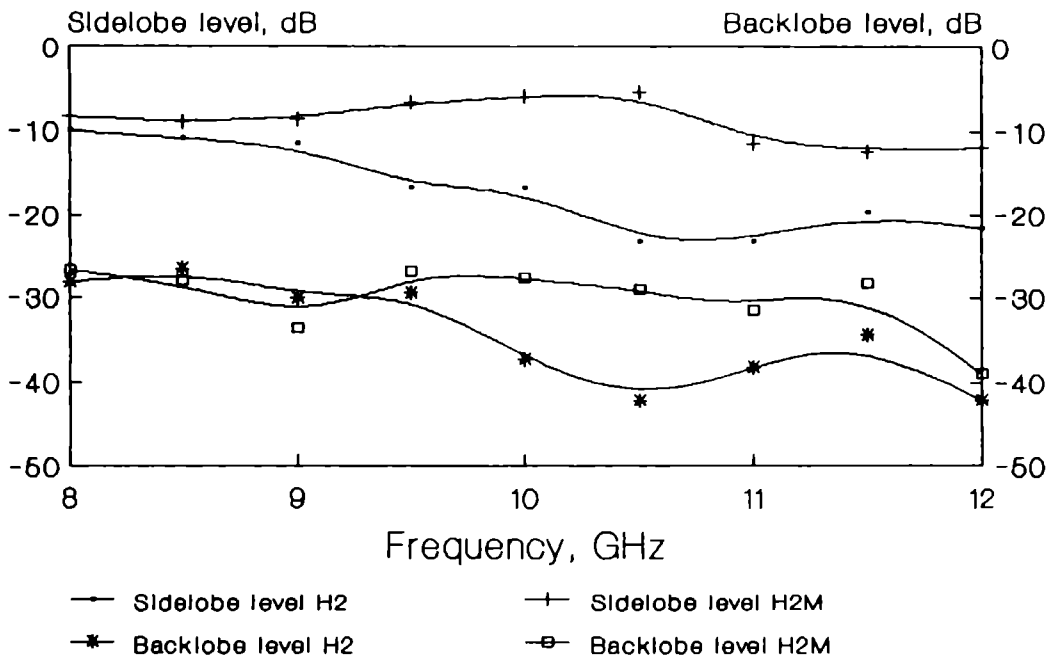
Fig.4.12: Variation of sidelobe and backlobe levels of
horns H2 and H2M with frequency
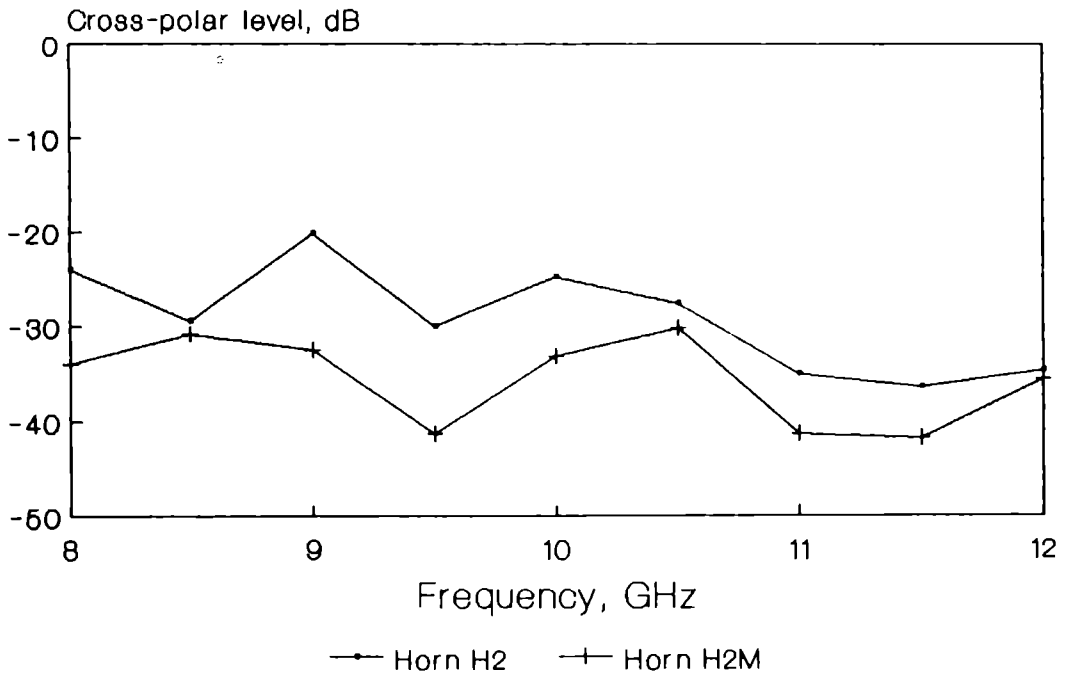
Fig.4.13: Variation of cross-polarisation level of
horns H2 and H2M with frequency

found to be more or less decreasing with the increase of frequency. From 8 GHz to 10 GHz, the horn H2 also exhibits similar variation in beamwidths. However, above 10 GHz, both the 3 dB and 10 dB beamwidths of the horn H2 are found to be increasing with frequency. This may be due to the tapering of the electric field across the E-plane aperture of the horn.

The variation of gain of the two horns with frequency is plotted in figure 4.15. At the central region, the gain of both the horns are found to be almost equal. But, in the lower and upper edges of the frequency band the conventional horn exhibits better gain character-istics than that of the horn H2.

The most important outcome of the analysis of the experimental results of the horn H1 and the horn H2 is regarding the design criteria employed for the fabrication of their E-plane boundary walls. Although the E-plane boundary walls of both the horns were fabricated with a dielectric thickness h = 0.55 cm, satisfying the condition h = $\lambda/4\sqrt{\epsilon_r}$ at 8.5 GHz, they exhibited minimum sidelobe levels at the frequency of 11 GHz. Recently, [146] it has been shown that, for strip-loaded dielectric wall horns, the balanced hybrid mode condition is satisfied only if the
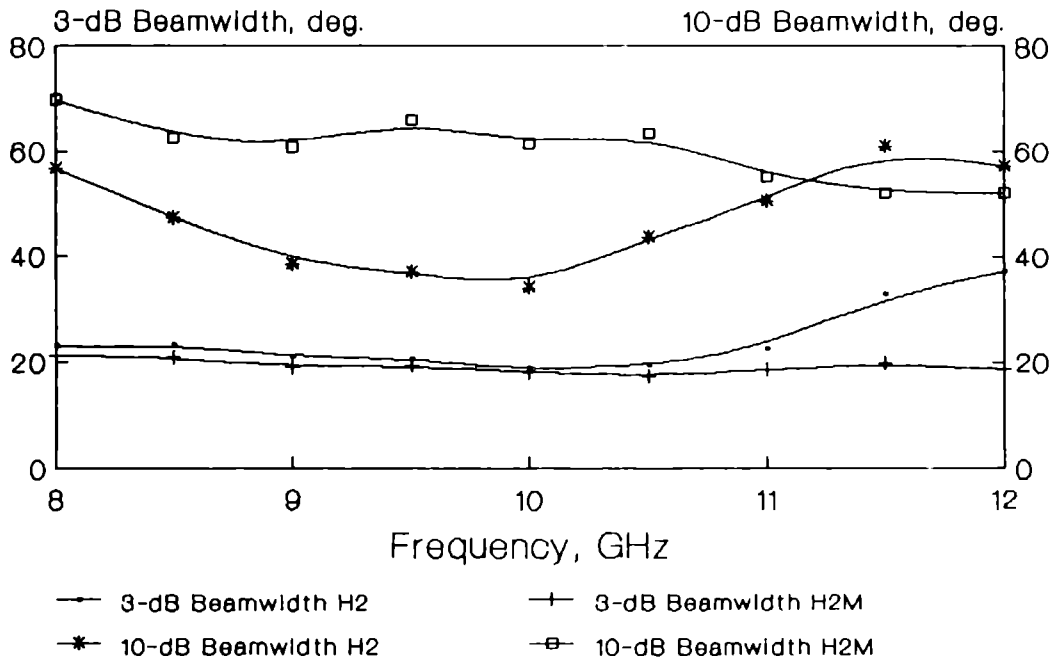
Fig.4.14: Variation of 3 dB and 10 dB beamwidths of horns H2 and H2M with frequency
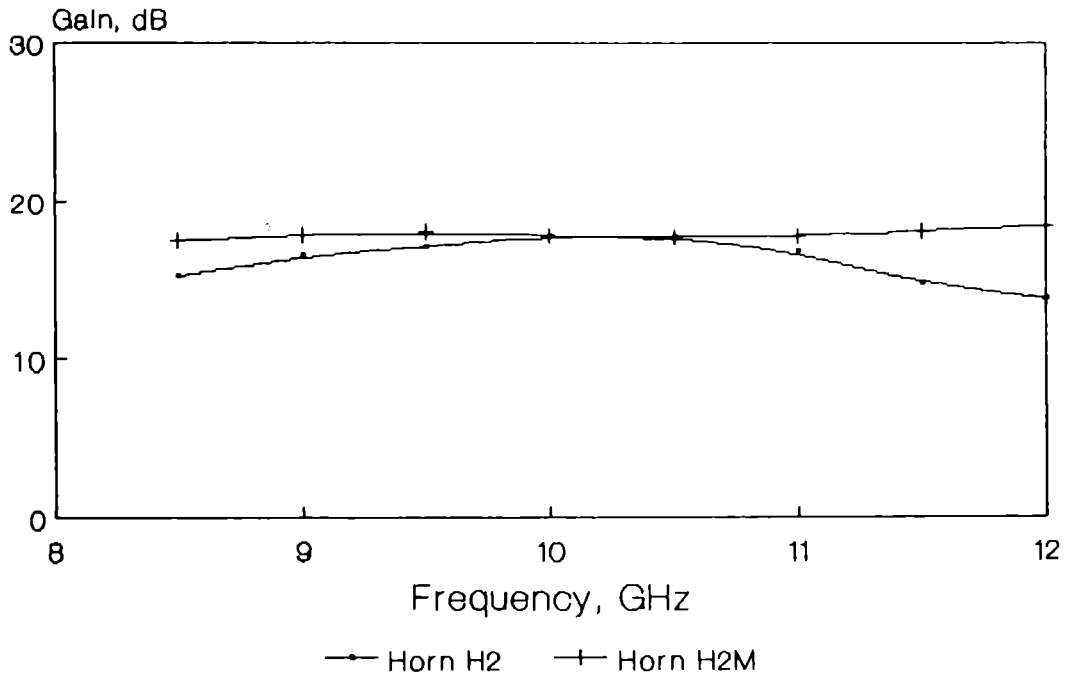
Fig.4.15: Variation of gain of horns H2 and H2M with frequency

substrate thickness satisfies the condition $h = \lambda/4\sqrt{\epsilon_r - 1}$

For h = 0.55 cm, the frequency at which this condition is satisfied is approximately 11 GHz. Moreover, compared to the horn H1 of earlier section, though the horn H2 showed improvements in its sidelobe characteristics, the return-loss study showed poor impedance matching. Hence, with an eye on further improvement of radiation characteristics, especially the impedance matching of the horn, two pyramidal horns of rectangular throat and square aperture are fabricated. The E-plane boundary walls of these horns are fabricated with dielectric substrate having tapered profile structure. The experimental results of these horns are presented in the next section of the thesis.

4.3 OPTIMISATION OF RADIATION CHARACTERISTICS BY TAPERED DIELECTRIC E-PLANE WALLS

The analysis of the experimental results of the horns H1 and H2 have shown that the dielectric thickness 'h' of the E-plane wall of a horn should satisfy the condition $h = \lambda/4\sqrt{\epsilon_r - 1}$ instead of $h = \lambda/4\sqrt{\epsilon_r}$. Both the horns H1 and H2 were fabricated with uniform thick dielectric E-plane boundary walls. This may be the reason for poor impedance matching of these horns. Hence, as stated earlier, in order to explore the possibility of

improving the radiation characteristics, especially the sidelobe and impedance characteristics, two pyramidal horns with tapered dielectric E-plane walls satisfying the balanced hybrid condition are fabricated.

Both the horns, horn 3 (H3) and horn 3A (H3A), are pyramidal horns with rectangular throat and square aperture having identical physical dimensions. The aperture dimensions of the horn antennas fabricated are $a_1 = b_1 = 5.9$ cm. and the slant lengths in the E and H-planes respectively are $\rho_E = 11.4$ cm and $\rho_H = 12.1$ cm. The corresponding semiflare angles in the above planes are $\psi_E = 27°$ and $\psi_H = 25°$ respectively. Different tapered profile structures are employed for the fabrication of the E-plane boundary walls of these horns. The inner surface of the E-plane walls of these horns are loaded with strip-grating structures of different period and strip parameters and the outer surface is completely metallised.

In horn H3, at the throat region, after the 3 cm metallised portion, the thickness of the dielectric substrate is 0.7 cm. This is gradually tapered to a thickness of 0.44 cm at the aperture of the horn so that the mean thickness of the substrate is $h = 0.57$ cm. For

the mean thickness 'h' the balanced hybrid mode condition h = $\lambda/4\sqrt{\epsilon_r - 1}$ is satisfied at the frequency of 10.5 GHz. The entire remaining inner surface of the E-walls are periodically loaded with thin conducting strips of width a = 0.07λ at a period d = 0.14λ. 'λ' is the free-space wavelength at the mean design frequency of 10.5 GHz.

In the case of the horn H3A, the thickness of the dielectric substrate at the corresponding point of the throat region is 0.8 cm. As in the earlier case a gradual tapering makes this thickness equal to 0.4 cm at the aperture of the horn. Here, the mean thickness h = 0.6 cm satisfies the balanced hybrid mode condition at the frequency of 10 GHz. Thin conducting wires of diameter a = 0.0083λ are then periodically loaded on the inner surfaces of the E-walls, at a period of d = 0.033λ. As stated earlier, all other physical dimensions of both the horns H3 and H3A are identical. The radiation characteristics of the horns H3 and H3A are compared with that of a conventional horn (H3M) of same physical dimensions. The conventional horn H3M is derived from the horn H3, by covering its entire strip-loaded E-plane wall surface with thin conducting foil.

The study of the return-loss characteristics of the two horns H3 and H3A with frequency has showed that, in

the entire X-band of frequency, the impedance matching of the horn H3A is better than that of the horn H3. The variation of return-loss of the two horns with frequency is shown in figure 4.16. In the entire X-band of frequency the maximum level of return-loss exhibited by the horn H3 is -12.8 dB, whereas in the case of the horn H3A, it is -17.65 dB.

The typical E-plane radiation patterns of the horns H3 and H3A at their design frequencies, compared with that of the conventional horn H3M are given in figures 4.17 and 4.18. The saddle on the mainlobe of the E-plane radiation patterns of the conventional horn is attributed to the out-of-phase relation of the edge diffracted and the direct rays. However, the E-plane radiation patterns of both the horns H3 and H3A are found to be without such saddles and their sidelobe levels are very much improved than that of the identical conventional horn H3M. The H-plane radiation patterns of both the horns H3 and H3A are found to be identical to the H-plane radiation patterns of the conventional horn H3M (refer page 103). Hence they are not presented in the thesis.

The sidelobe levels of the three horns at different frequencies in the 8 GHz to 12 GHz range are
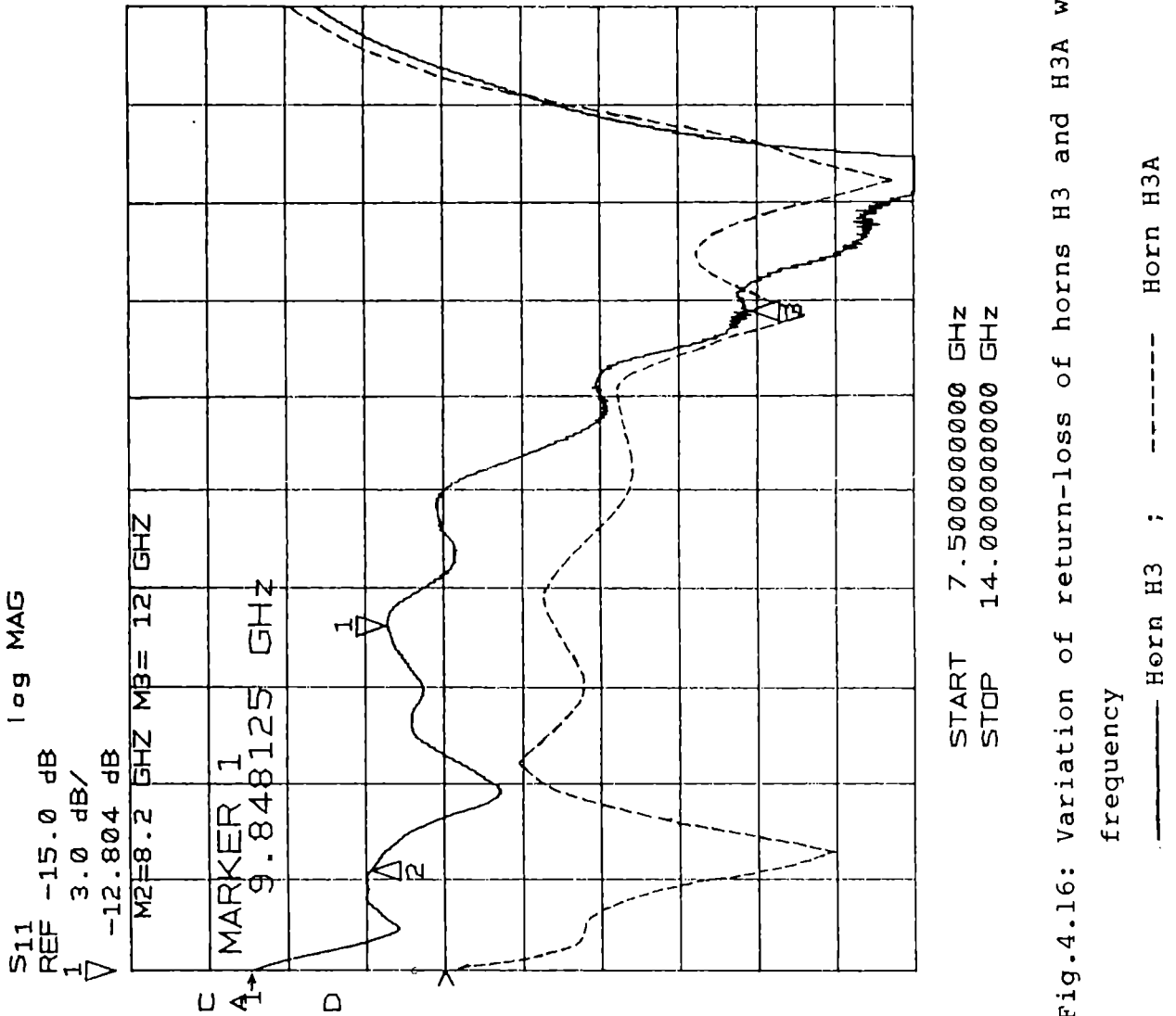
Fig.4.16: Variation of return-loss of horns H3 and H3A with frequency
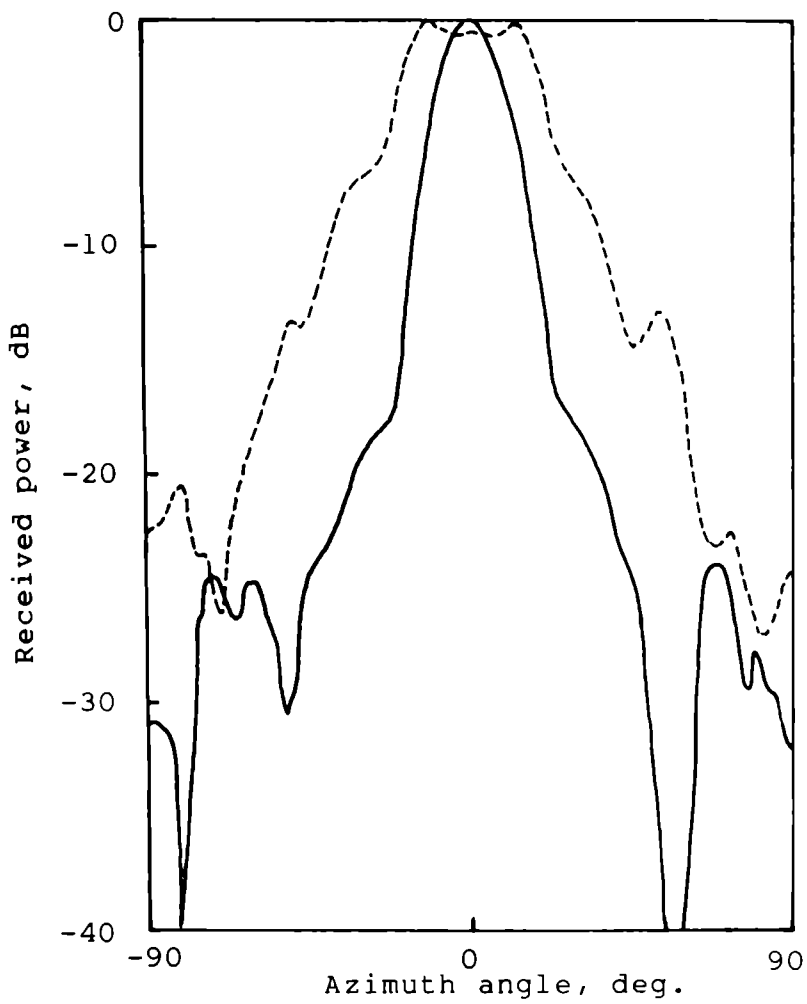
——— Horn H3 ; - - - - - - Horn H3A

Fig.4.17: E-plane radiation patterns of horns H3 and H3M at 10.5 GHz

———————— Horn H3 ;   ——————— Horn H3M
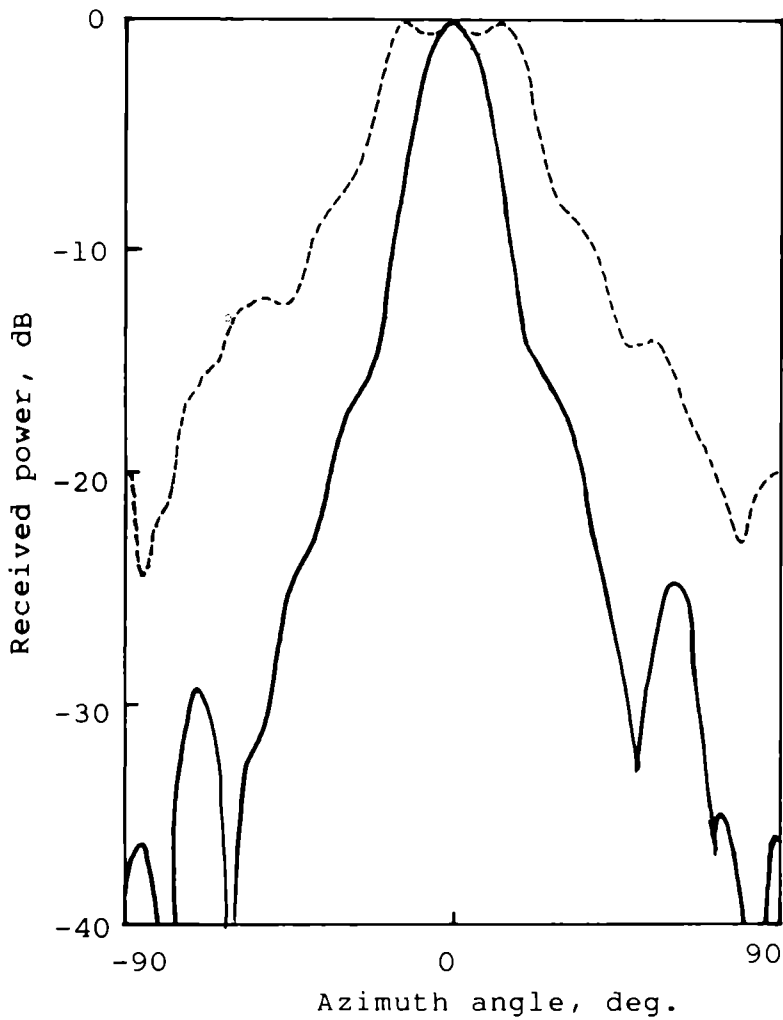
Fig.4.18: E-plane radiation patterns of horns
H3A and H3M at 10 GHz

———————— Horn H3A ; ——————— Horn H3M

shown in figure 4.19. Above 9 GHz, the sidelobe levels of the horns H3 and H3A are found to be very much improved than that of the conventional horn H3M. However, the -20 dB sidelobe bandwidth of the horn H3A is better than that of the horn H3.

The variation of backlobe levels of the three horns with frequency is given in figure 4.20. In the entire 8.5 GHz to 12 GHz frequency range, compared to the backlobe levels of the conventional horn, the horns H3 and H3A show better characteristics. Here also, as in the case of sidelobe characteristics, the horn H3A exhibits better backlobe characteristics than that of the horn H3.

The frequency response of cross-polarisation levels of the horns is presented in figure 4.21. Throughout the frequency range of interest, the cross-polar discrimination characteristics of the horns H3 and H3A are well within the tolerable limit. Moreover, at the design frequencies, the horns H3 and H3A show slight improvement than the corresponding cross-polar levels of the conventional horn H3M.

The 3 dB beamwidths of the three horns in the 8 GHz to 12 GHz frequency band are plotted in figure 4.22.
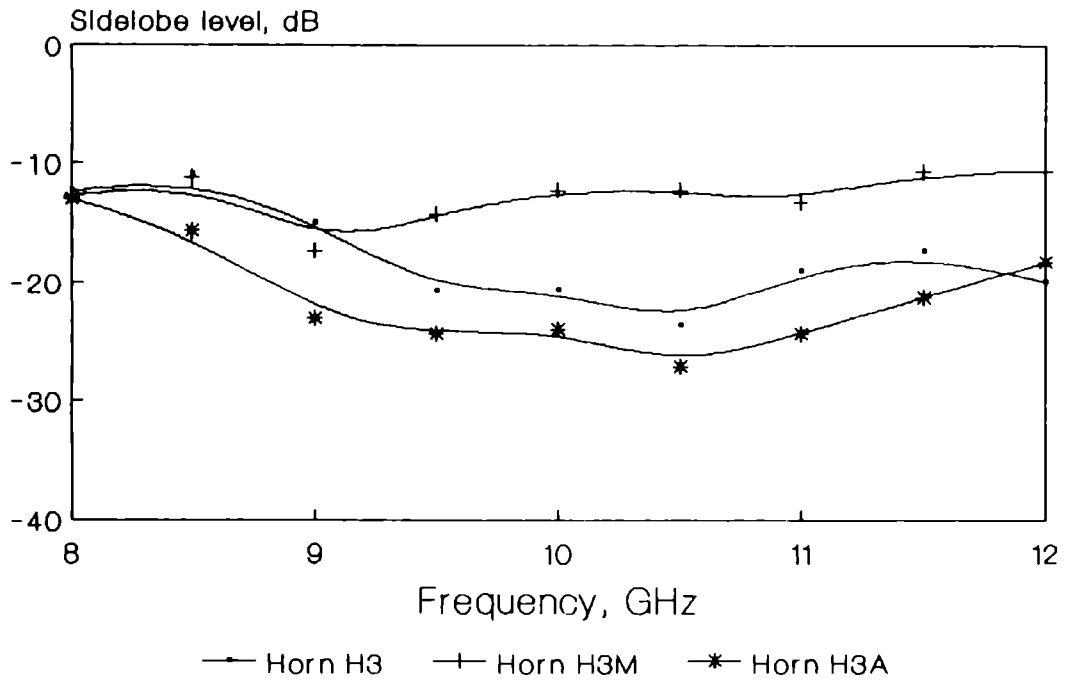
Fig.4.19: Variation of sidelobe level of horns H3, H3M
and H3A with frequency
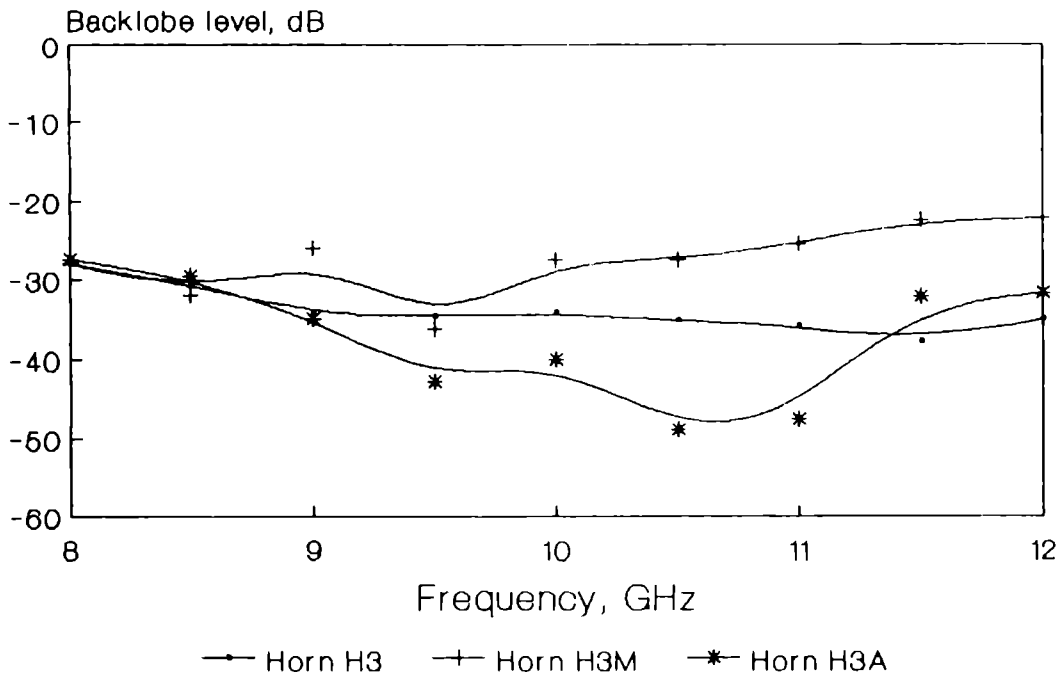
Fig.4.20: Variation of backlobe level of horns H3, H3M
and H3A with frequency

Cross-polar level, dB

Horn H3   Horn H3M   Horn H3A
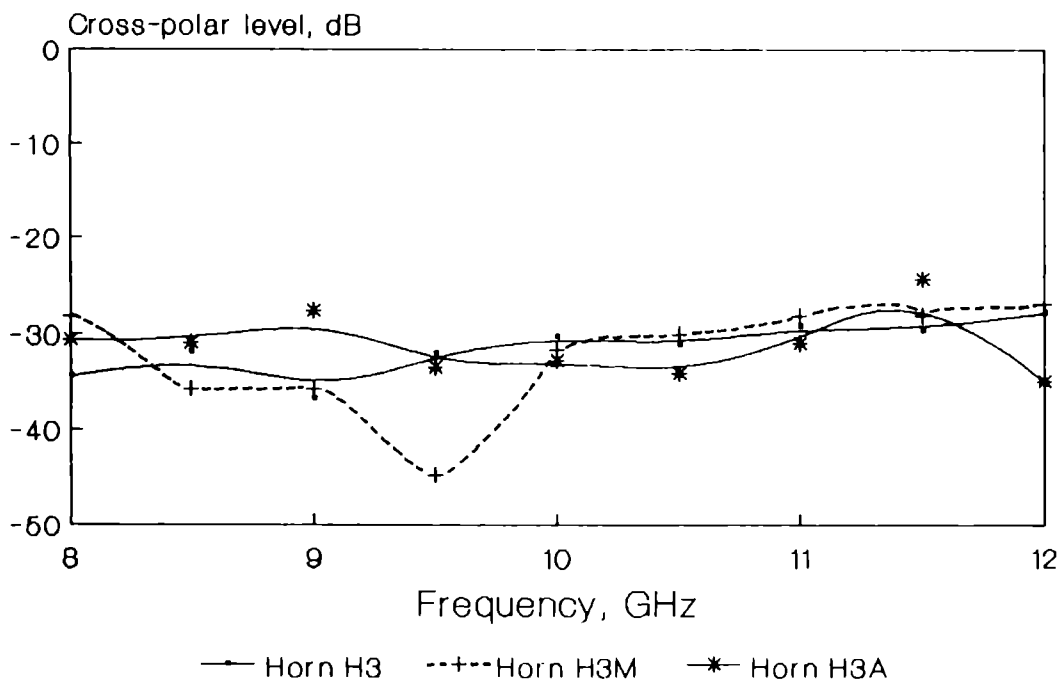
Fig.4.21: Variation of cross-polarisation level of
horns H3, H3M and H3A with frequency

3-dB Beamwidth, deg.

Horn H3   Horn H3M   Horn H3A
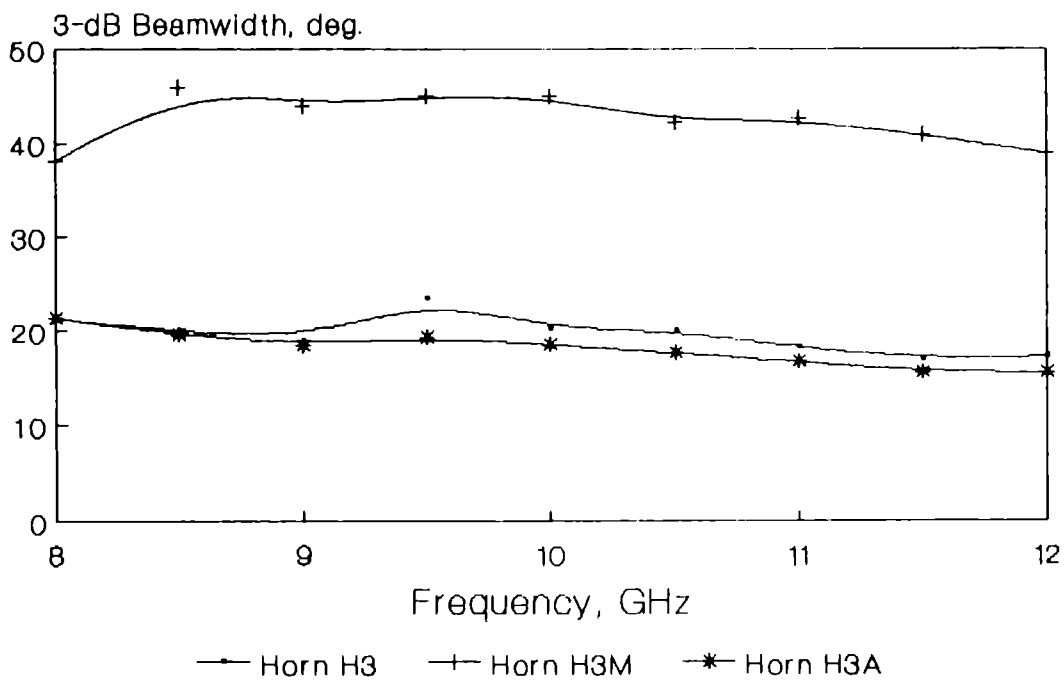
Fig.4.22: Variation of 3 dB beamwidth of horns H3, H3M
and H3A with frequency

As expected, the 3 dB beamwidths of all the three horns are found to be decreasing with the increase of frequency. However, compared to the 3 dB beamwidths of the conventional horn, considerable reduction in the 3 dB beamwidths of both the horns H3 and H3A is observed. The observed wider beamwidth of the conventional horn is due to the presence of saddle on the mainlobe of its radiation patterns. As explained earlier, this is attributed to the out-of-phase relation between the direct and edge diffracted rays. However, in the case of horns H3 and H3A, due to the balanced hybrid mode condition, the E-plane aperture edge diffractions are minimised so that the radiation patterns are void of such saddles on the mainlobe.

The typical variation of the 10 dB beamwidths of all the three horns is shown in figure 4.23. In this case also, as observed in 3 dB beamwidth, the 10 dB beamwidths of the horns H3 and H3A are found to be considerably reduced. Nevertheless, above 11 GHz, the 10 dB beamwidths of the two horns are observed to be increasing with frequency. In the above frequency range, ie., from 11 GHz to 12 GHz, the 10 dB beamwidths of the horn H3A are found to be slightly wider than that of the horn H3.

The gain of the three horns at different frequencies is shown in figure 4.24. In the entire 8.5 GHz to 12 GHz frequency band, the gain characteristics of the horns H3 and H3A are found to be better than that of the conventional horn. In the lower side of the frequency band the horn H3A shows better gain characteristics than the horn H3. On the other hand, in the upper side, the horn H3 shows a slight improvement in its gain than that of the horn H3A.

From the above experimental observations, it is clear that the horn H3A is exhibiting better radiation characteristics than the horn H3. However, to explore the possibility of achieving further improvements in the radiation patterns and the impedance matching, a pyramidal horn with square throat and aperture was fabricated.

4.4 OPTIMISATION OF VSWR BY PROPER METALLISATION OF THE THROAT REGION

A close look on the impedance variation with frequency of the horns H3 and H3A reveals the fact that the impedance matching of the horns are not good in the entire X-band region. However, in the designed frequency region

10-dB Beamwidth, deg.

Frequency, GHz

—•— Horn H3   —+— Horn H3M   —*— Horn H3A
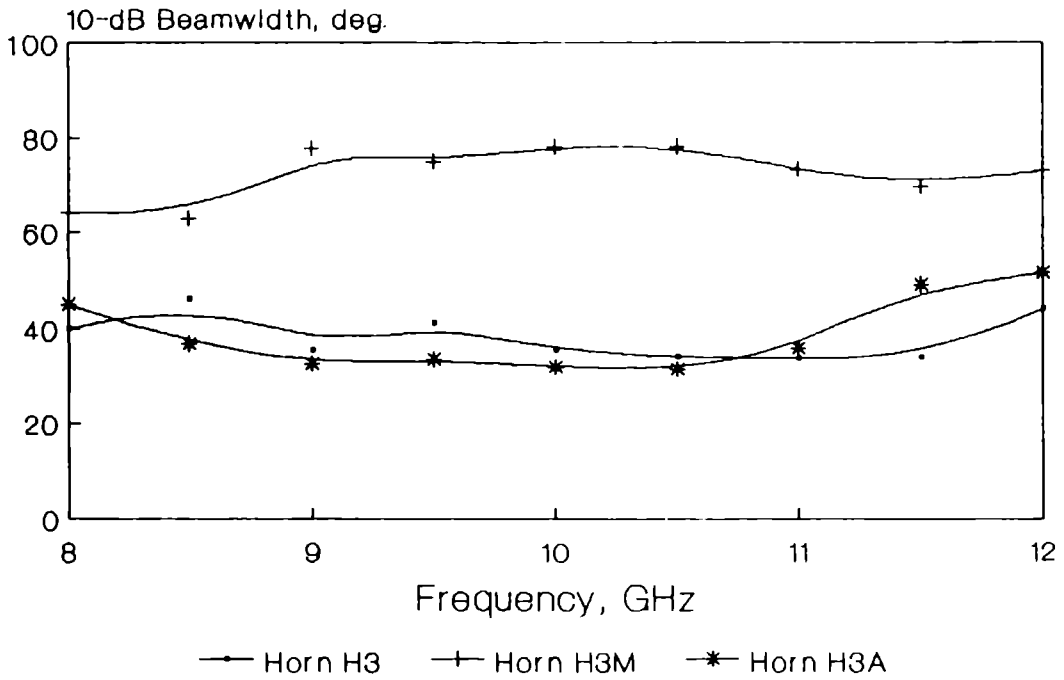
Fig.4.23: Variation of 10 dB beamwidth of horns H3,
H3M and H3A with frequency

Gain,dB

Frequency GHz

—•— Horn H3   —+— Horn H3M   —*— Horn H3A
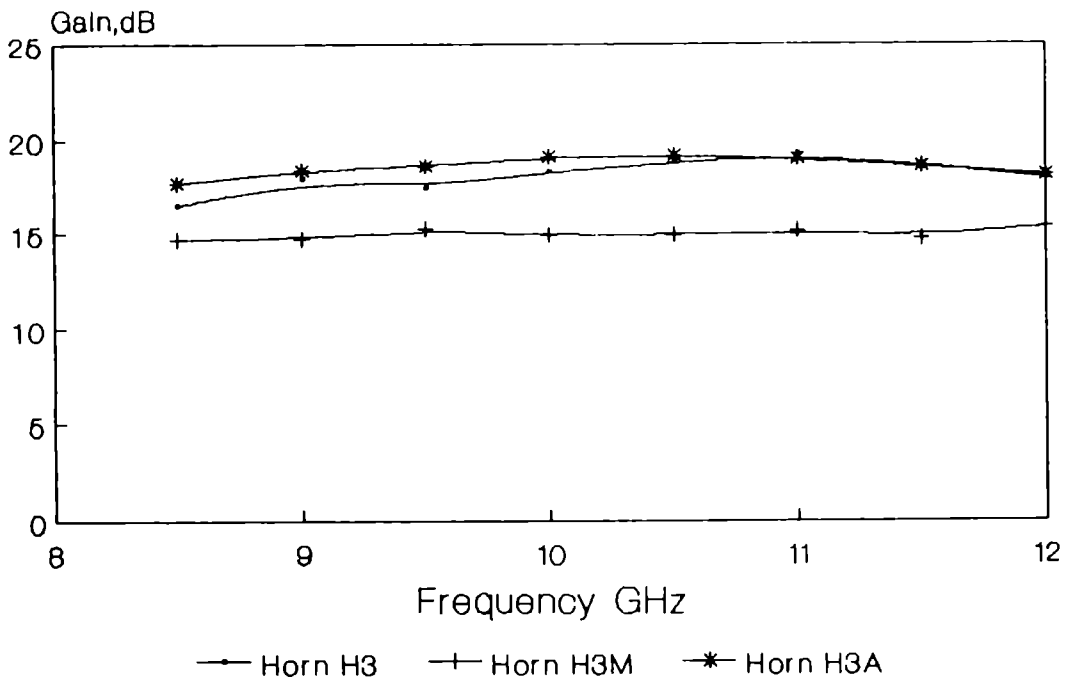
Fig.4.24: Variation of gain of horns H3, H3M and H3A
with frequency

the impedance matching is within the tolerable limit. The main reason for the high VSWR is due to the poor design of the throat region.

Usually in the case of an ordinary conventional metallic pyramidal horn, the impedance matching is found to be good. So to improve the impedance matching characteristics of the present horn, as in the case of an ordinary conventional metallic horn, the immediate vicinity of the throat region is metallised. This section shows the effect of metallisation of the throat region E-plane walls to different extents. Another factor considered here is regarding the physical dimensions of the horn. In the previous section, both the horns investigated, H3 and H3A were with rectangular throat and square aperture. As stated earlier, in order to explore further improvements in the radiation patterns, the impedance matching and the possibility of obtaining symmetrical radiation patterns in the two orthogonal principal planes, a pyramidal horn with square throat and aperture is fabricated.

The aperture dimensions of this square pyramidal horn H4 are $a_1 = b_1 = 5.9$ cm. The E and H-plane slant lengths are $\rho_E = \rho_H = 12.8$ cm respectively. The semiflare

angles of the respective planes are $\psi_E = \psi_H = 25°$. The E-plane boundary walls of this horn are fabricated from a flat dielectric plate of thickness h = 0.52 cm. For this thickness, the balanced hybrid mode condition is satisfied approximately at the frequency of 11.5 GHz. At the throat region of this horn, 3 cm portion of the E-plane wall is completely metallised. The remaining entire E-plane wall surface is periodically loaded with thin conducting strips of width $a = 0.077\lambda$ and period $d = 0.154\lambda$ where 'λ' is the free-space wavelength at the design frequency.

The square pyramidal horn H4A is derived from the horn H4 by reducing its 3 cm metallised portion to 1 cm. The remaining 2 cm portion at the throat region is also periodically loaded with strip gratings of same width and period as in the case of horn H4.

A conventional horn (CH) of identical physical dimensions as that of horn H4 is also fabricated. The radiation characteristics of the horns H4 and H4A are compared with that of the conventional horn in the following part of this section.

Typical E-plane radiation patterns at 11.5 GHz of the two horns H4 and H4A, which are of different throat

metallisation extents, compared with that of the conventional horn are given in figure 4.25. It is observed that compared to the conventional horn, the beamwidths of the present horns H4 and H4A are narrow and are found to be good in all respects. The pattern of the conventional horn at this frequency shows a saddle on the mainlobe. This saddle formed on the mainlobe is attributed to the out-of-phase relations between the direct and diffracted rays. But in the case of the present horns H4 and H4A, due to the balanced hybrid mode condition, the diffracted rays are nearly absent and the minimum on-axis field is eliminated. As explained earlier, the H-plane patterns of both the horns H4 and H4A are almost identical to that of the conventional horn. Hence they are not shown in this section. Throughout the frequency band, the E-plane radiation patterns of the horn H4 are found to be narrower than its H-plane radiation patterns. At the design frequency, 11.5 GHz, the E and H-plane 3 dB beamwidths of the horn H4 are 16.7° and 20.8° and the 10 dB beamwidths are 33° and 46.4° respectively. However, in the case of horn H4A, the 3 dB and 10 dB beamwidths of the E-plane pattern at 11.5 GHz are found to be much larger than those of the corresponding H-plane pattern. At this frequency the E and H-plane 3 dB beamwidths of the horn H4A are 36.8°
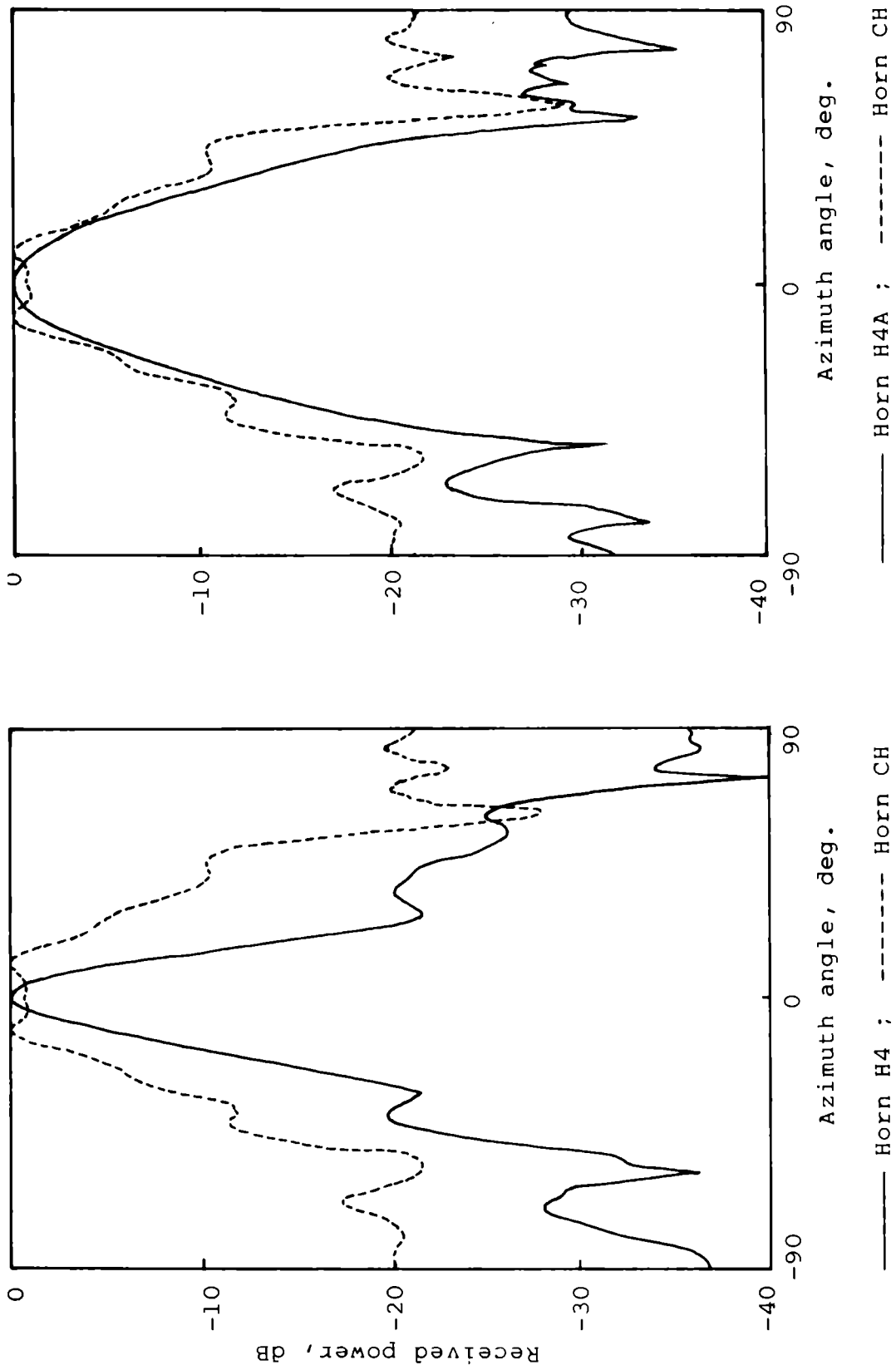
Fig.4.25: E-plane radiation patterns of horns H4, H4A and CH at 11.5 GHz

and 20.8°, whereas the 10 dB beamwidths are 60.3° and 46.4° respectively. Hence as expected [104] the property of beamwidth equilisation in the two orthogonal principal planes is not observed.

The variations of the sidelobe and backlobe levels of the three horns with frequency are shown in figures 4.26 and 4.27. Compared to the sidelobe levels of the conventional horn, the sidelobe characteristics of both the horns H4 and H4A are found to be within reasonable limits. Regarding the backlobe level, the horn H4A which is having a 1 cm metallised portion at the throat region is slightly better for the -30 dB backlobe level bandwidth.

Frequency response of cross-polarisation of the horns is shown in figure 4.28. The -30 dB cross-polarisation bandwidth of the horn H4A is found to be better than that of the other two horns.

Figures 4.29 and 4.30 shows the variation of 3 dB and 10 dB beamwidths of the above horns with frequency. From the studies it is observed that for sharper beams the horn H4 is better than the horn H4A. The beamwidths of the horn H4 are found to be virtually uniform in the 9.5 GHz to

Sidelobe level, dB

Frequency, GHz

——— Horn H4   —+— Horn CH   —*— Horn H4A

Fig.4.26: Variation of sidelobe level of horns H4, CH
and H4A with frequency

Backlobe level, dB

Frequency, GHz

—·— Horn H4   —+— Horn CH   —*— Horn H4A
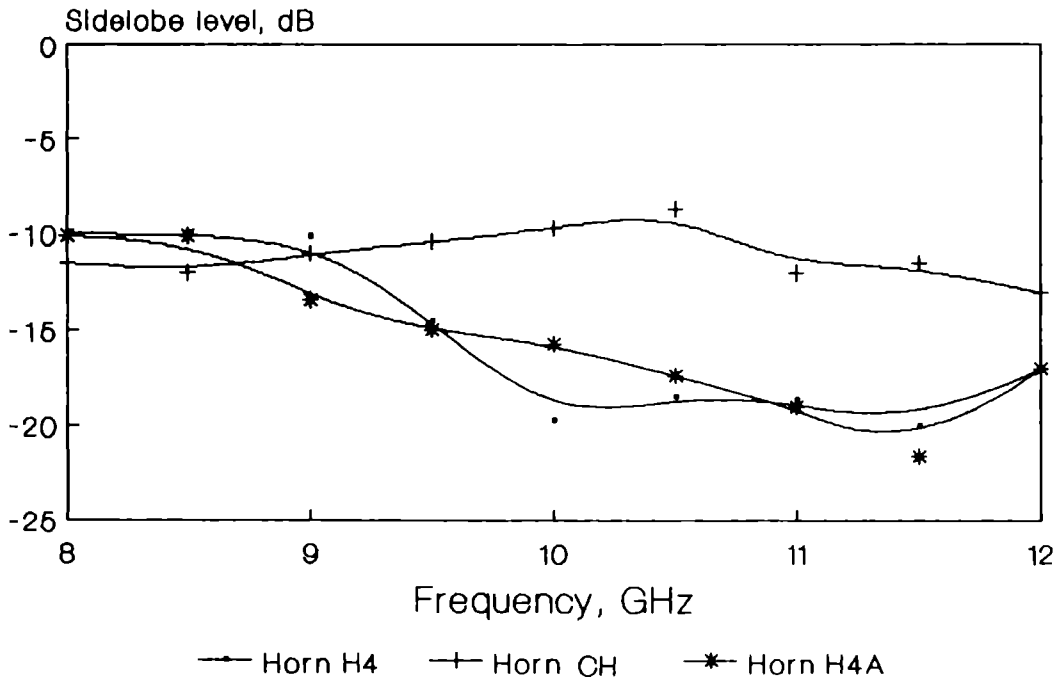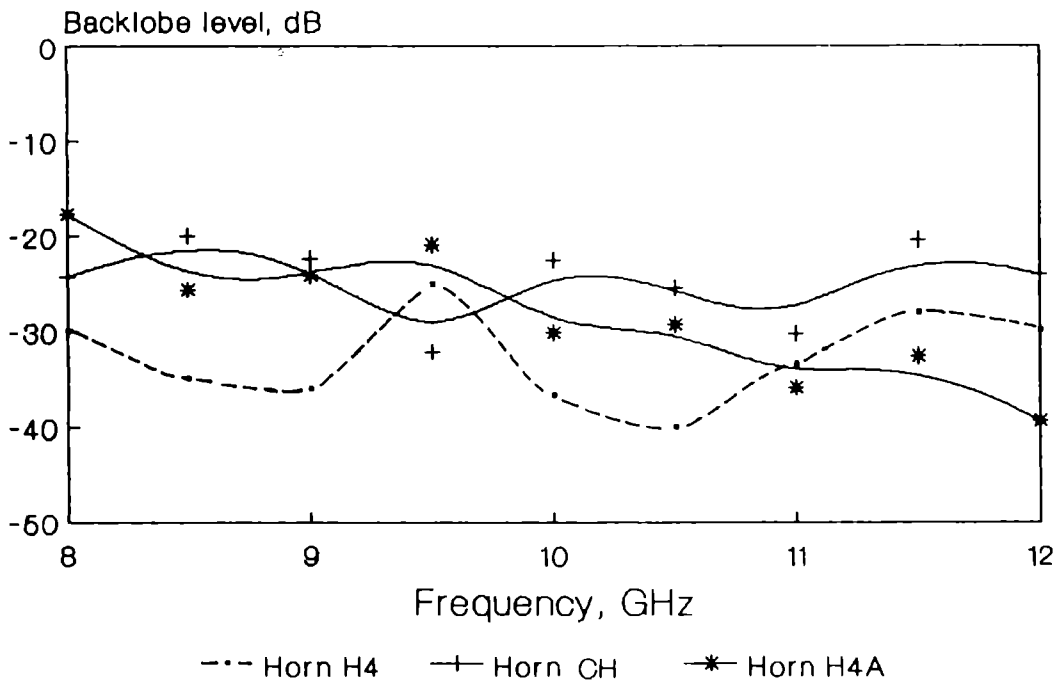
Fig.4.27: Variation of backlobe level of horns H4, CH
and H4A with frequency

Cross-polar level, dB
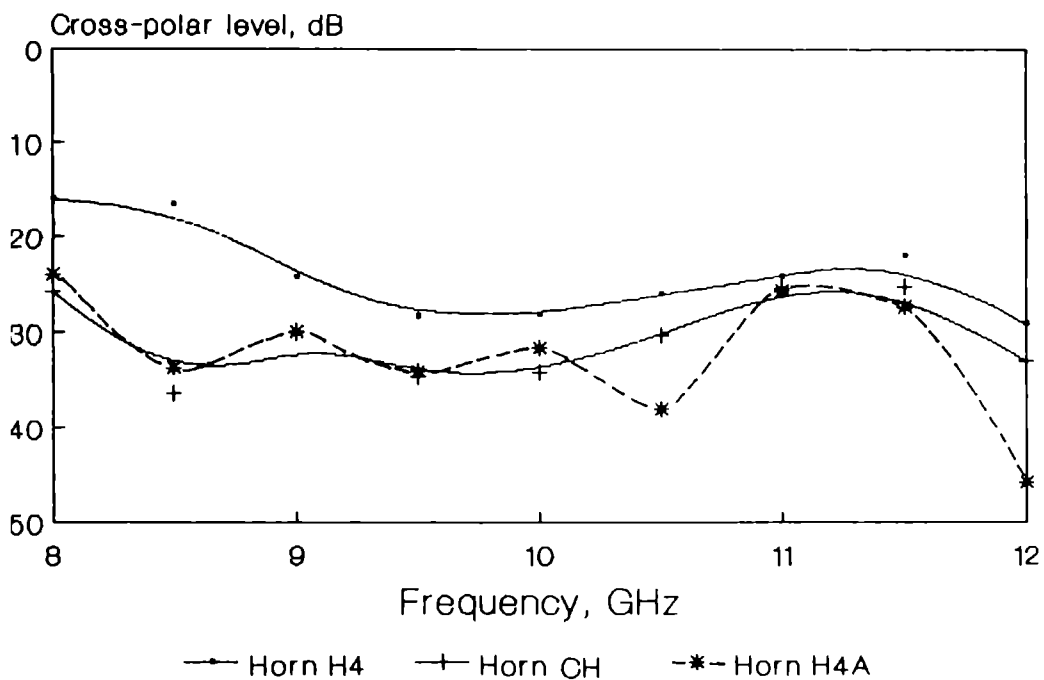
Fig.4.28: Variation of cross-polarisation level of horns H4, CH and H4A with frequency

3-dB Beamwldth, deg.
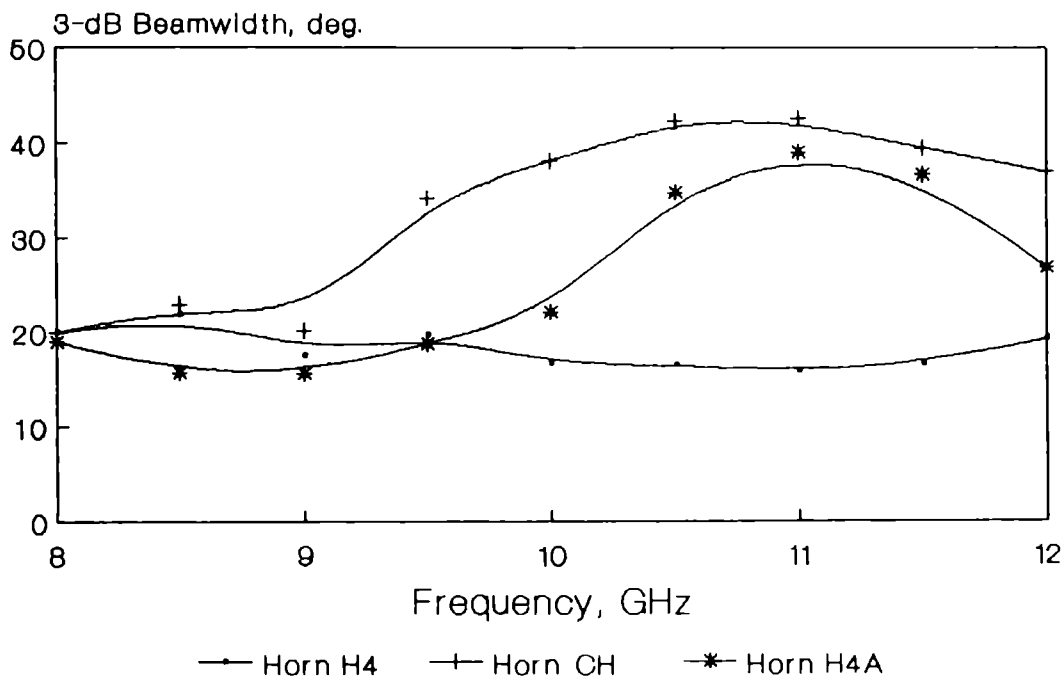
Fig.4.29: Variation of 3 dB beamwidth of horns H4, CH and H4A with frequency

12 GHz frequency range. For frequencies below 9.5 GHz, the large 10 dB beamwidths of this horn are due to the deteriorated shape of the radiation patterns. However, in the case of horn H4A, above 9.5 GHz, considerable changes in the 3 dB beamwidths are observed. Upto 11 GHz, the 3 dB beamwidth increases with frequency whereas above 11 GHz, it decreases with increase in frequency. On the other hand, the 10 dB beamwidths are found to be increasing with frequency. As in the case of 3 dB beamwidth, above 11 GHz, a reduction in 10 dB beamwidths is observed with frequency.

The variation of gain of the three horns with frequency is presented in figure 4.31. As expected, the gain of the horn H4 is found to be higher than that of the other two horns.

Return-loss studies showed that the conventional horn is better than the horns H4 and H4A. In the X-band frequency, the maximum levels of return-loss exhibited by horns H4 and H4A are -13.18 dB and -11.62 dB respectively, whereas for conventional horn it is better than -20 dB. Moreover, it is again found that in the case of horn H4A, the variation of return-loss is smoother and better than that of horn H4 in the X-band of frequency. The return-
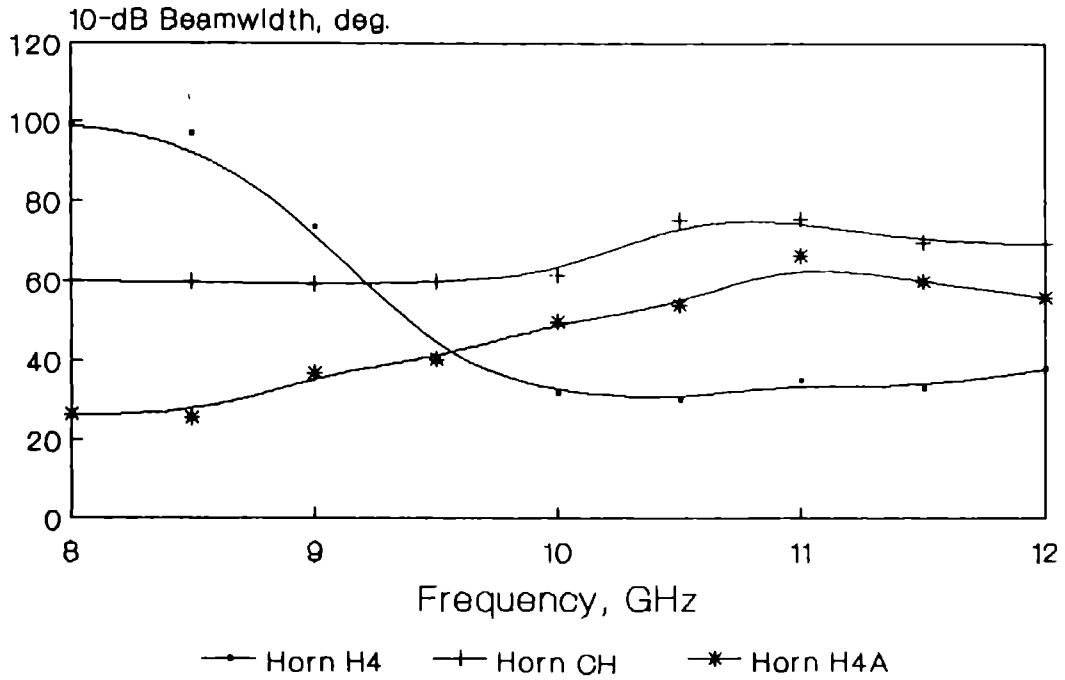
Fig.4.30: Variation of 10 dB beamwidth of horns H4, CH and H4A with frequency
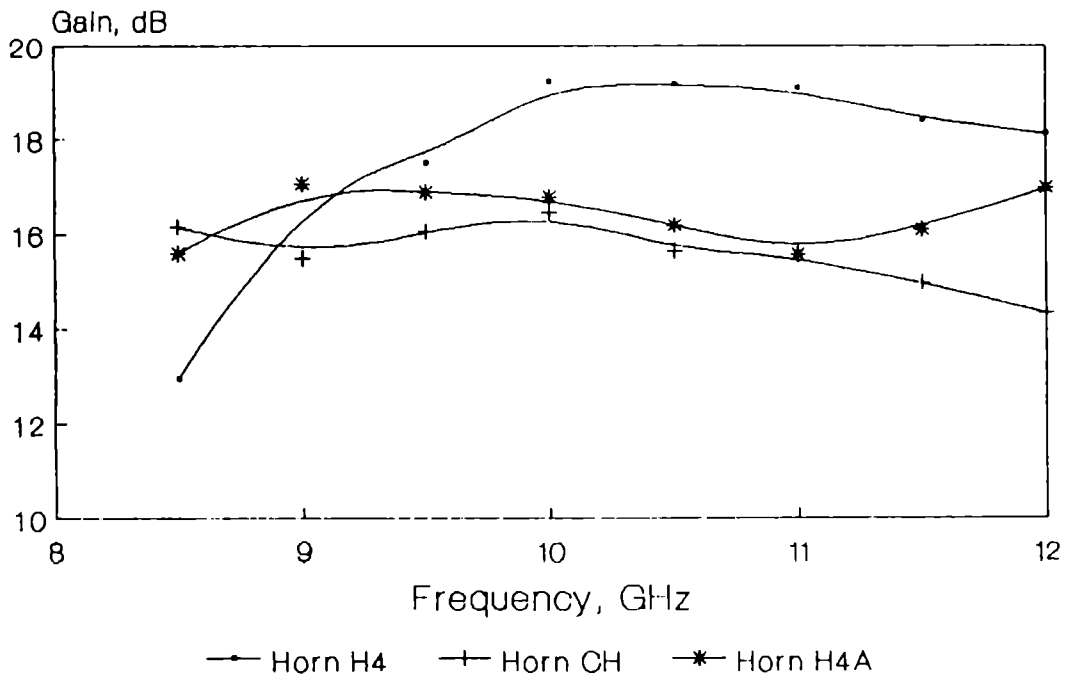
Fig.4.31: Variation of gain of horns H4, CH and H4A with frequency

loss variations of the horns with frequency are given in figures 4.32(a) to 4.32(c).

From the above studies it is clear that most of the radiation characteristics of a strip-loaded horn can be controlled by simply adjusting the extent of metallisation of the E-plane walls near the throat region. It is also well understood that, except the gain characteristics, the horn H4A is exhibiting better radiation characteristics than the horn H4. In the earlier studies it was observed that, compared to the strip-loaded horns with uniformly thick E-plane walls, strip-loaded horns with tapered E-plane walls were exhibiting better radiation characteristics. Hence, inorder to explore the possibility of achieving further improvements in the radiation characteristics, another square pyramidal horn with tapered dielectric E-plane boundary walls is fabricated. The experimental results of this horn are presented in the next section.

4.5 OPTIMISATION OF GAIN AND IMPEDANCE MATCHING OF A SQUARE PYRAMIDAL HORN BY TAPERED E-PLANE WALLS

The comparative study of the radiation character-istics of the horns H3 and H4A (Section 4.4) has showed that the gain characteristic of the horn H4 is better than

S11   log MAG

REF -15.0 dB

1
▽ 3.0 dB/

 -13.182 dB

hp

C   MARKER 1

A   8.5725 GHz

D

S11   ∠

REF 1.0 Units

△ 200.0 mUnits/

1 46.287 Ω -21.305 Ω
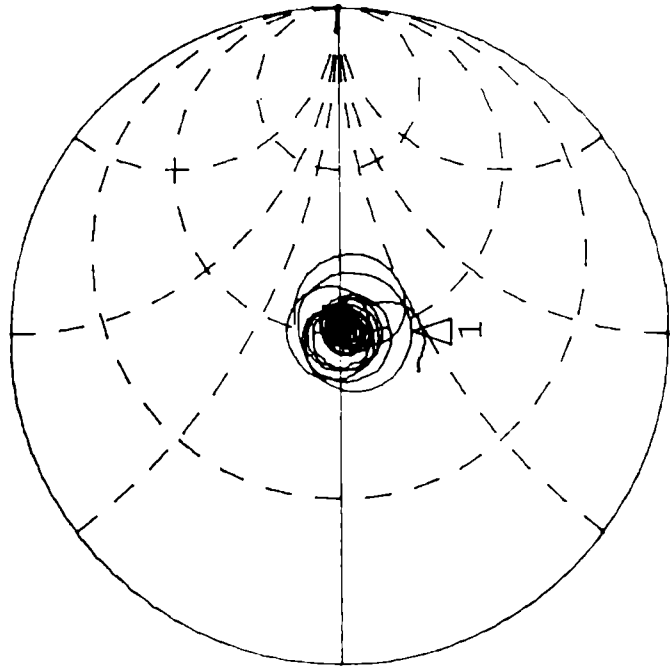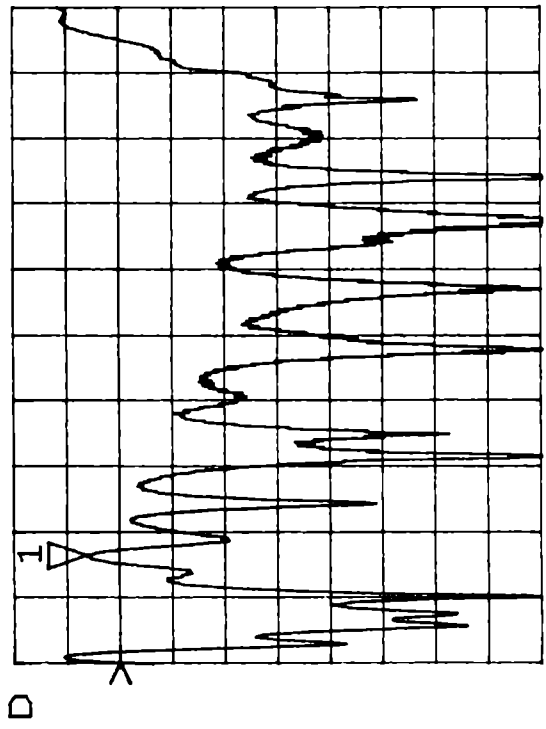
START   7.500000000 GHz

STOP   14.000000000 GHz

Fig.4.32(a): Variation of return-loss of horn H4 with frequency

S11   log MAG   S11
REF 0.0 dB   REF 1.0 Units   Z
△ 10.0 dB/   1 200.0 mUnits/
1 −11.62 dB   ▽ 62.729 Ω −27.197 Ω
hp

C   MARKER 1
    8.264 GHz
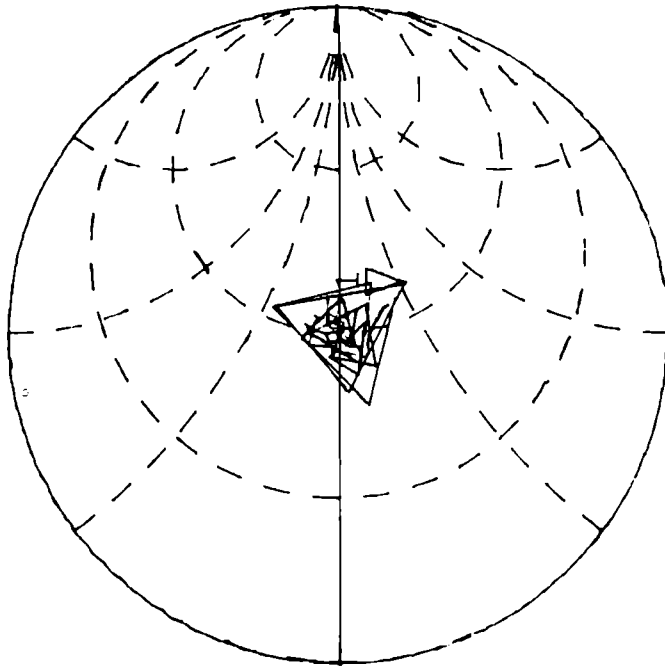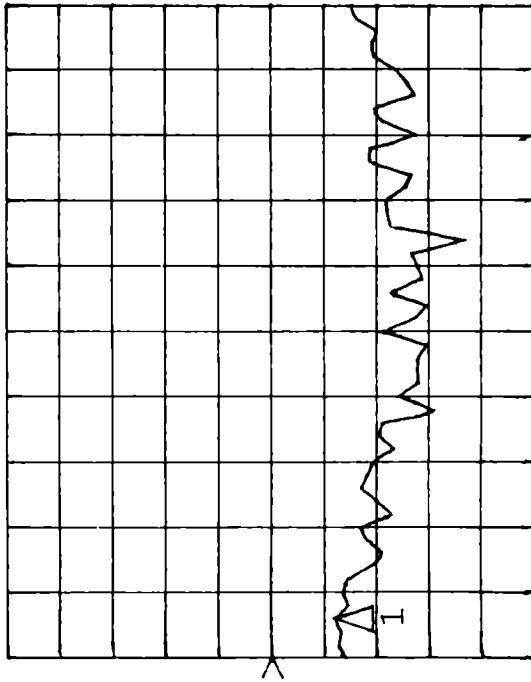
START   8.000000000 GHz
STOP   12.400000000 GHz

Fig.4.32(b): Variation of return-loss of horn H4A with frequency
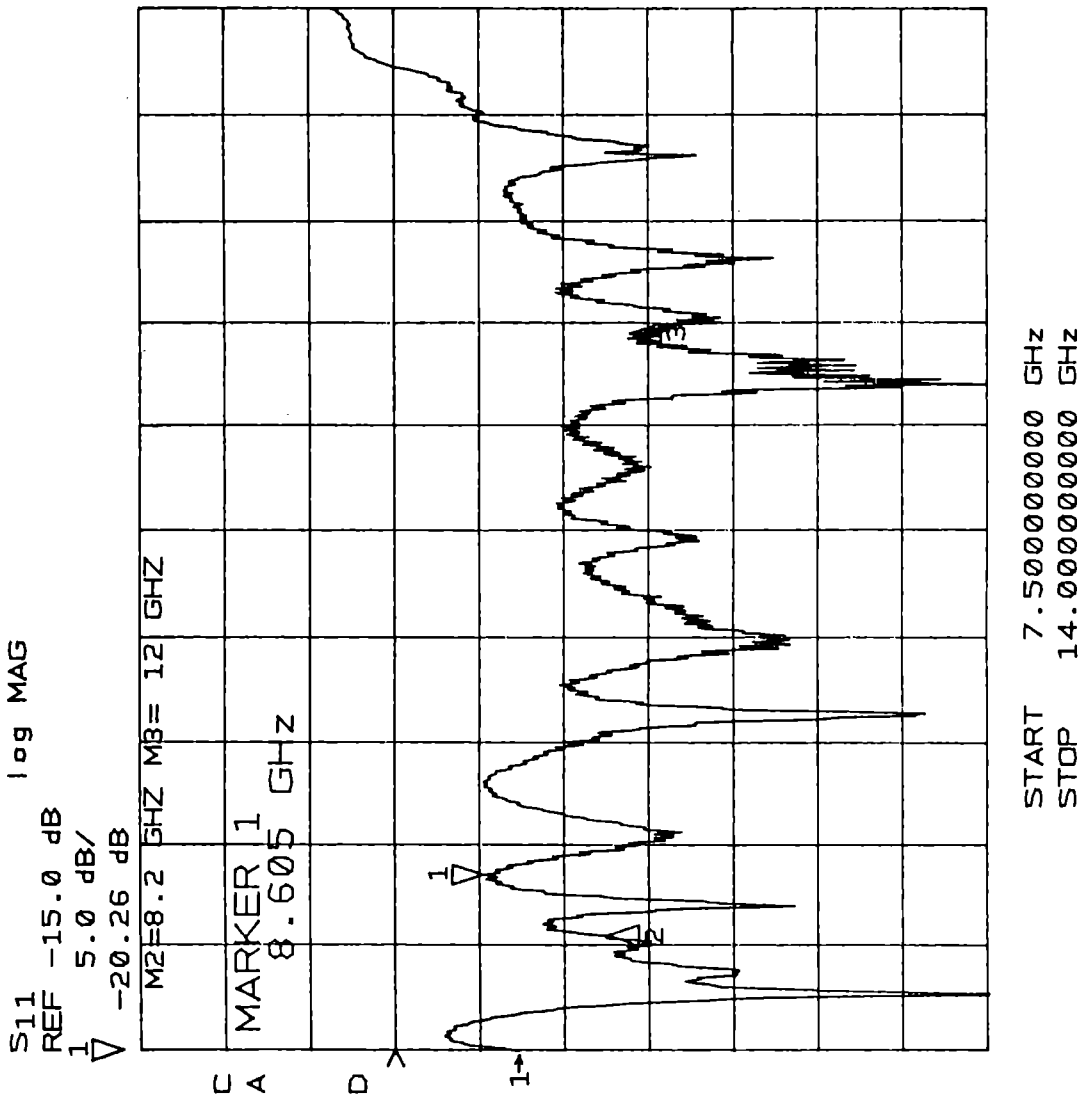
Fig.4.32(c): Variation of return-loss of conventional horn with frequency

that of the horn H4A. This observed improvement in gain of horn H4 may be due to the extended metallised portion at its throat region of the E-walls than that of the horn H4A. Moreover, its frequency response of return-loss was also within the tolerable limits. Also, the earlier studies have revealed that the radiation characteristics of horns with tapered dielectric E-plane walls are better than that with uniformly thick dielectric E-plane walls. Hence, for optimising the radiation characteristics, the present square pyramidal horn is fabricated with strip-loaded tapered dielectric E-plane walls having 3 cm metallisation at its throat region.

The aperture dimensions of the present square pyramidal horn (H5) are $a_1 = b_1 = 5.9$ cm. The E and H-plane slant lengths are $\rho_E = \rho_H = 12.8$ cm. The corresponding semiflare angles in these planes are $\psi_E = \psi_H = 25°$ respectively. All the basic physical dimensions of this square pyramidal horn H5 are identical to that of the horn considered in the previous section.

As stated earlier, at the throat region of the E-plane walls of the horn H5, 3 cm portion is metallised. After the metallised portion, the thickness of the

dielectric substrate is 0.75 cm. This is then gradually tapered to a thickness of 0.55 cm at the aperture of the horn so that the mean thickness h = 0.65 cm satisfies the balanced hybrid mode condition approximately at the frequency of 9.2 GHz. The entire remaining inner surface of the E-plane walls are then periodically loaded with thin conducting strips at a period d = 0.061 λ and a/d = 0.5, where 'λ' is the free-space wavelength at the design frequency.

Typical return-loss variation of the horn with frequency is shown in figure 4.33. The return-loss is better than -15.69 dB in the entire X-band frequency region. For all the frequencies above this, in the entire X-band, the return-loss is well within the tolerable limits.

The typical E-plane radiation pattern of the horn H5 at the design frequency, 9.2 GHz, is shown in figure 4.34. As the basic physical dimensions of the present horn H5 are identical to that of the conventional horn of previous section 4.4, for comparison, the E-plane radiation pattern of the conventional horn at 9.2 GHz is also plotted in the same graph. As explained earlier, the radiation

S11   log MAG   S11   Z
REF -15.0 dB   REF 1.0 Units/
1   ▽
▽ -15.686 dB   △
                                       1 64.266 Ω -12.363 Ω
                                          200.0 mUnits/

* C
A   MARKER 1
    8.255625 GHz

D
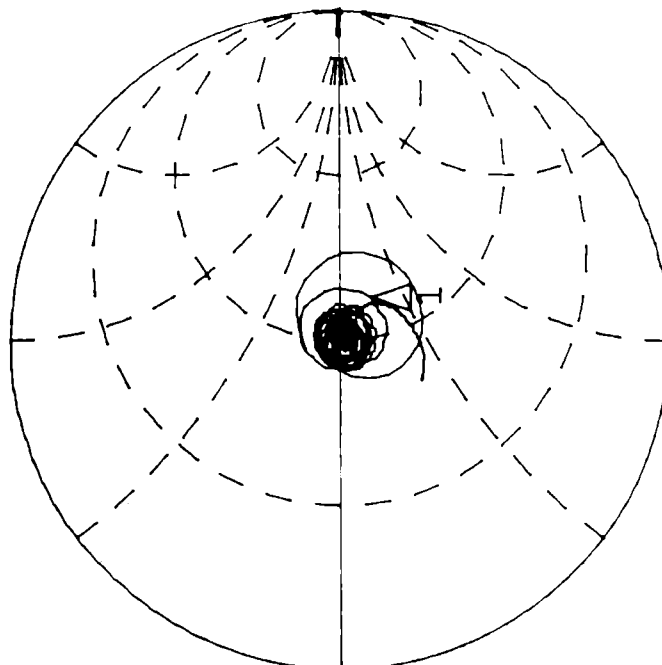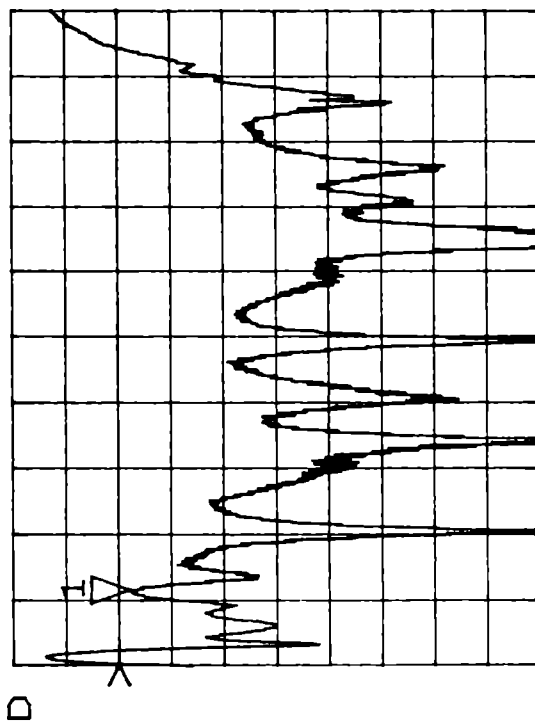
START   7.500000000 GHz
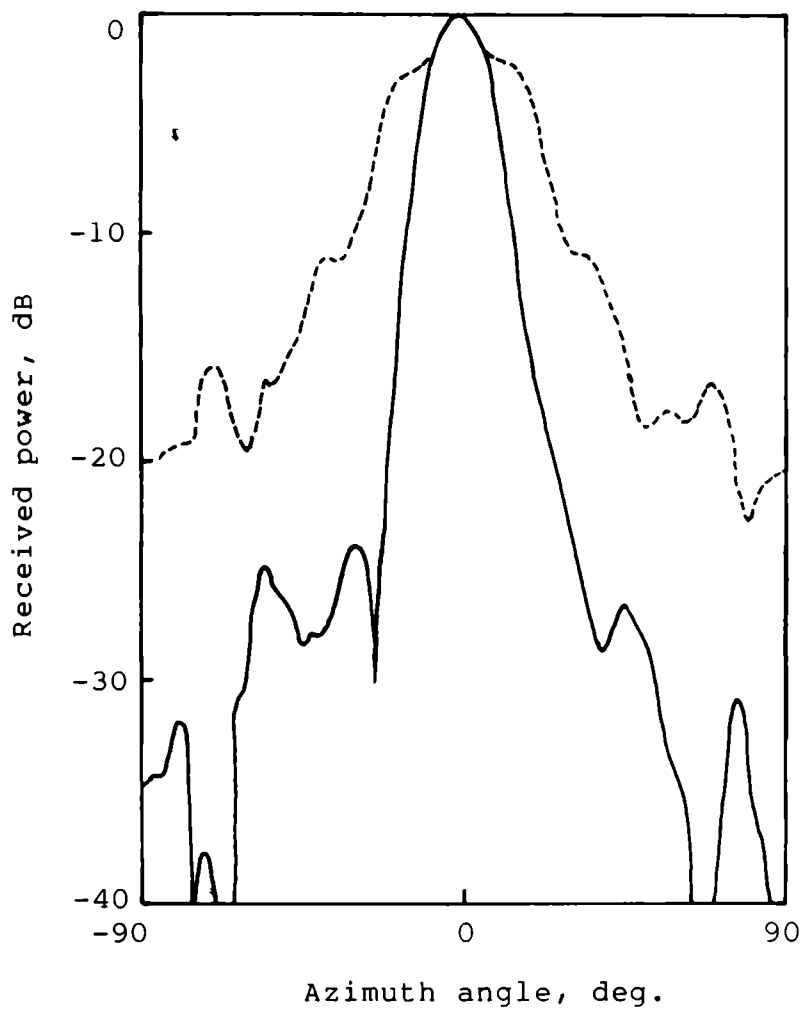STOP   14.000000000 GHz

Fig.4.33: Variation of return-loss of horn H5 with frequency

Fig.4.34. E-plane radiation patterns of horns H5 and CH at 9.2 GHz.

————— Horn H5,   --------- Horn CH.

pattern of the new strip-loaded horn H5 is narrow without any shoulderlobes or saddle in the main beam. The H-plane radiation patterns of this horn are found to be identical to the H-plane patterns of the conventional horn. Hence they are not presented here (refer section 4.1, page 103). It is also observed that the E-plane radiation patterns of this horn, in the entire X-band of frequency, are narrower than its H-plane radiation patterns.

In figure 4.35, the variation of sidelobe and backlobe levels of the present strip-loaded horn H5 and the conventional horn is shown. Compared to the conventional horn, the sidelobe and backlobe levels of horn H5 are found to be considerably improved. The sidelobe level of horn H5 is found to be better than -20 dB in the entire 8 GHz to 12 GHz frequency range. As shown in figure 4.36 the cross-polarisation level of horn H5 is better than -25 dB in the entire 8.5 GHz to 12 GHz frequency range. Moreover, its variation with frequency is also found to be smoother than that of the conventional horn.

Frequency response of the 3 dB and 10 dB beam-widths of horn H5 compared with that of conventional horn is shown in figure 4.37. In the entire X-band frequency
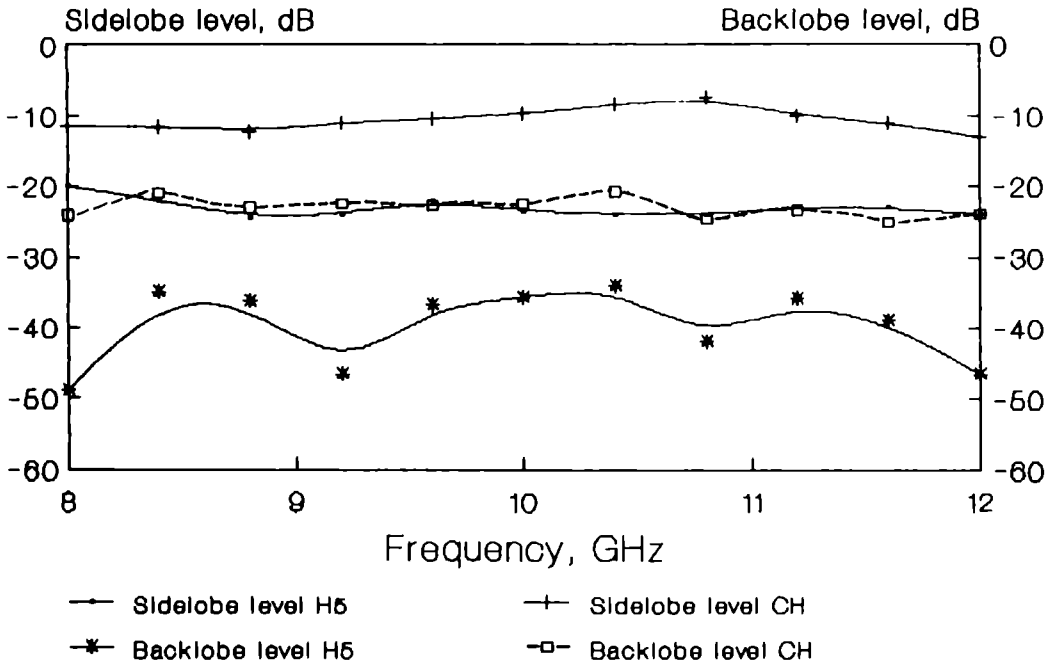
Fig.4.35 Variation of sidelobe and backlobe levels of horns H5 and CH with frequency.
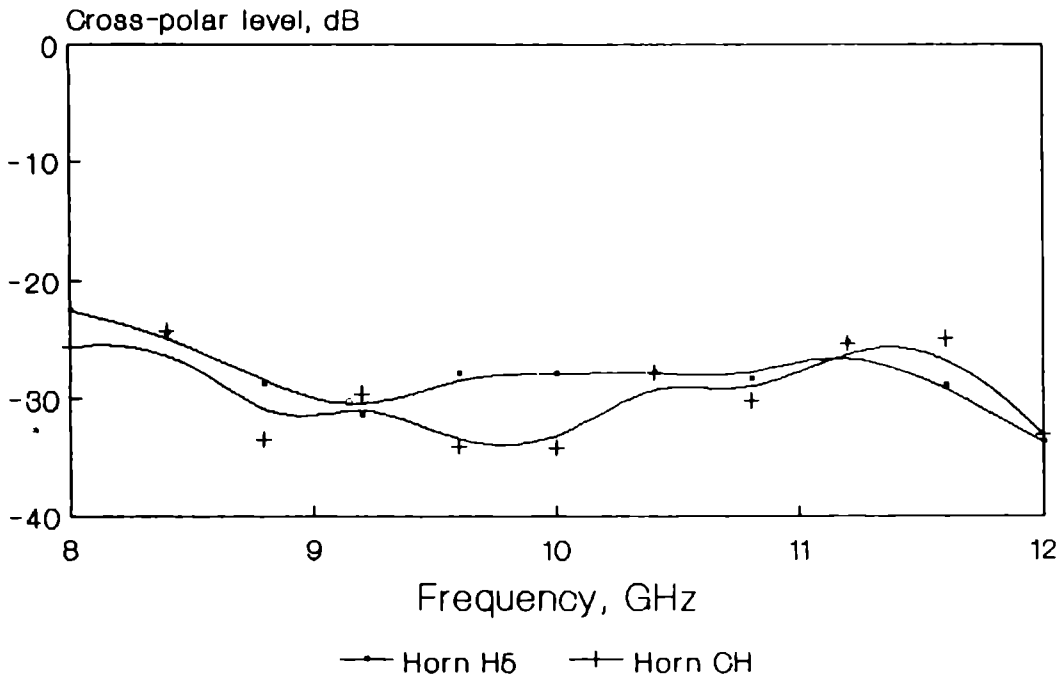
Fig.4.36 Variation of cross-polarisation level of horns H5 and CH with frequency.

region, the 3 dB beamwidth is found to be decreasing with increase of frequency. However, above 10.4 GHz, the 10 dB beamwidths are found to be widened with increase of frequency.

The typical variation of gain with frequency of horn H5 and conventional horn is given in figure 4.38. In the entire frequency range of 8.5 GHz to 12 GHz, the gain of the present horn is better than that of the conventional horn and it is found to be gradually increasing with frequency.

From the above experimental results it is evident that the radiation characteristics of the present strip-loaded horn H5, fabricated with tapered dielectric E-plane walls, are much better than that of the horns H4 or H4A of previous section 4.4, which are fabricated with uniformly thick dielectric E-plane walls.

4.6 EFFECT OF INTERIOR TAPERING AND EXTERIOR TAPERING PROFILE OF THROAT REGION

In the case of a metallic corrugated horn it is observed that the impedance matching is poor if the corrugation depth is kept uniform at $\lambda/4$. This is
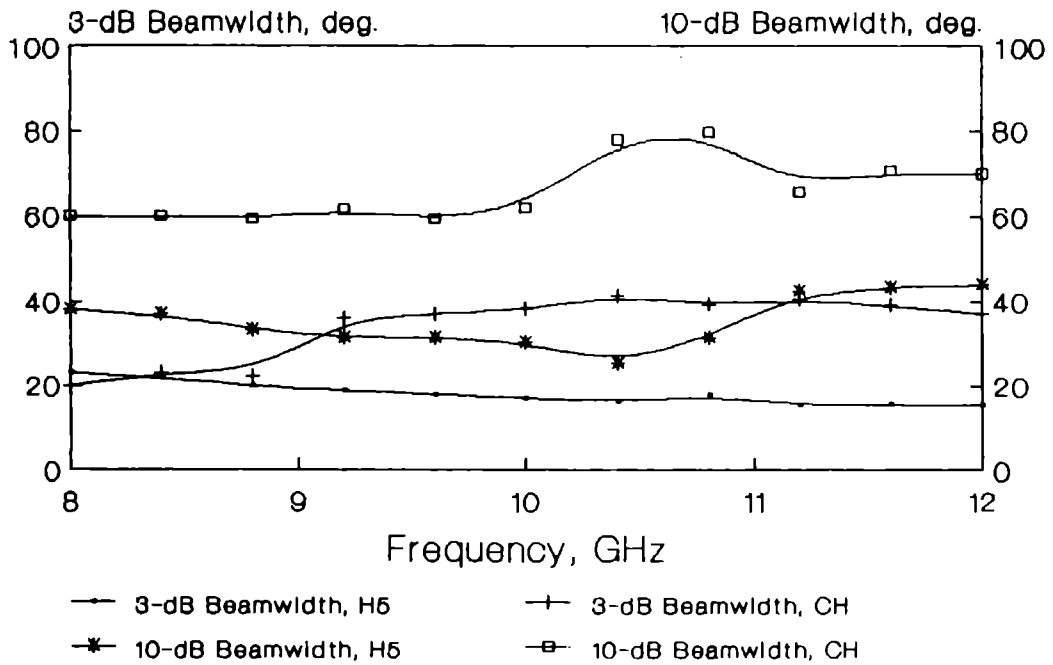
Fig.4.37   Variation of 3 dB and 10 dB beamwidths of
horns H5 and CH with frequency.
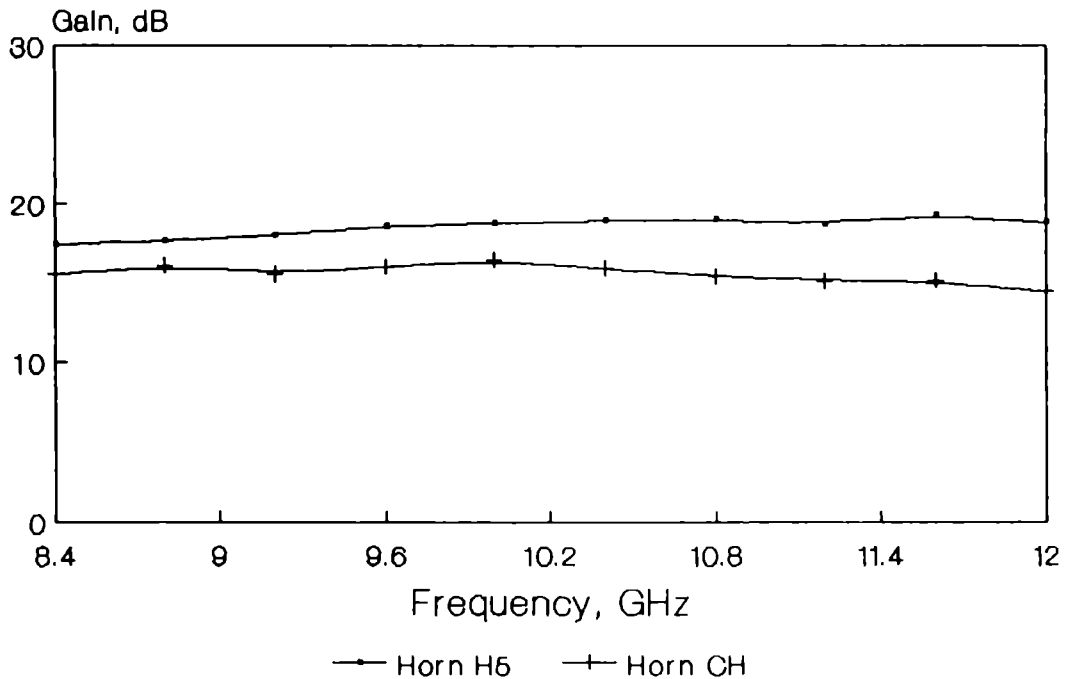
Fig.4.38   Variation of gain of horns H5 and CH with
frequency.

because, a $\lambda/4$ deep corrugation will act as a surface impedance of infinity and causes high mismatch at the throat region of the horn [89]. On the other hand, if the corrugation depth at the throat region is $\lambda/2$, it will act as zero surface impedance and hence it behaves as a plane surface. So scientists [89,101] proposed a gradual tapering of corrugation depth from $\lambda/2$ to $\lambda/4$ in the vicinity of the throat region, and thereafter constant at $\lambda/4$ upto the aperture of the horn to improve the impedance mismatch.

This technique is extended to improve the impedance bandwidth of the simulated scalar horns. However, the earlier studies have proved that the balanced hybrid mode condition is obtained when the thickness of the dielectric substrate is $\lambda/4\sqrt{\epsilon_r - 1}$ instead of $\lambda/4\sqrt{\epsilon_r}$. However, in the design of the present horn, in order to provide the tapered profile structure in the vicinity of the throat region, instead of metallising 3 cm portion, only 1 cm portion is metallised. After the 1 cm metallised portion, in the vicinity of the throat region the $\lambda/2\sqrt{\epsilon_r - 1}$ to $\lambda/4\sqrt{\epsilon_r - 1}$ tapering profile is employed for improving the impedance matching of the horn.

The horn H6 is a square pyramidal horn with aperture dimensions $a_1 = b_1 = 5.9$ cm. The E and H-plane slant lengths are $\rho_E = \rho_H = 12.8$ cm. The corresponding semiflare angles in the above planes are $\psi_E = \psi_H = 25°$. The E-plane cross-sectional view of the horn H6 with interior tapering profile for the throat region is shown in figure 3.39(a). At the throat region of the horn, after the 1 cm metallised portion, the thickness of the dielectric substrate (h_1) is $\lambda/2\sqrt{\epsilon_r-1}$. This is then gradually tapered to a thickness of $h_2 = \lambda/4\sqrt{\epsilon_r-1}$ at the point of P. From the point P to the aperture of the horn, the thickness is kept constant at $\lambda/4\sqrt{\epsilon_r-1}$ so that the balanced hybrid mode condition is satisfied at 8.4 GHz. $'\lambda'$ is the free-space wavelength at the above frequency.

The $\lambda/2\sqrt{\epsilon_r-1}$ to $\lambda/4\sqrt{\epsilon_r-1}$ tapering section used at the throat region of the horn causes an abrupt angular variation at the throat region. This may reduce the impedance matching of the horn. On the other hand, if the dielectric tapering is done on the outer surface of the E-plane walls, this can be avoided and hence there is a possibility of improvement in the impedance bandwidth. The horn H6A is another square horn of identical physical

dimensions as that of the horn H6, but the tapered profile structure is at the exterior side of the E-plane boundary walls. The E-plane cross-sectional view of the horn H6A with exterior tapering is shown in figure 4.39(b).

The variations of the return-loss of the two horns H6 and H6A with frequency are compared in figure 4.40. From the comparative study it is well understood that the abrupt angular variation caused by the interior tapered profile structure at the throat region of the horn H6 is not degrading its return-loss characteristic as expected. Actually, compared to the horn H6A, which is designed with an exterior tapered profile structure for the throat region, slight improvement is observed, especially, for frequencies around the design value. In the entire X-band of frequency, the maximum return-loss level exhibited by the horn H6 is -19.16 dB, whereas by the horn H6A it is -18.6 dB.

The E-plane aperture electric field distribution of both the horns H6 and H6A at different frequencies were measured. The measured electric field distributions of the horns, at 8.4 GHz, 8.8 GHz and 10 GHz along with the theoretical cosine distribution are given in figure 4.41.
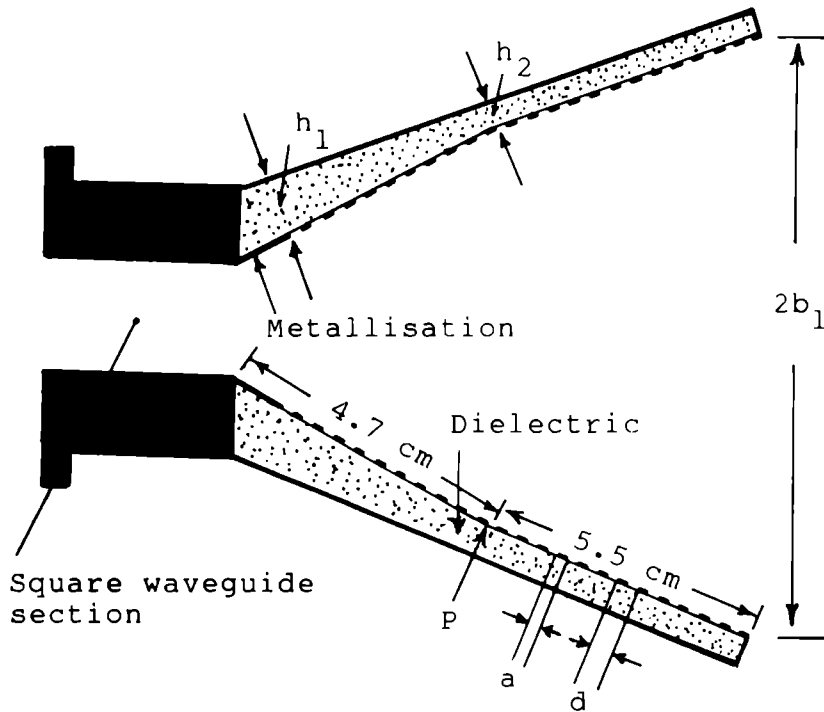
(a)   Horn H6
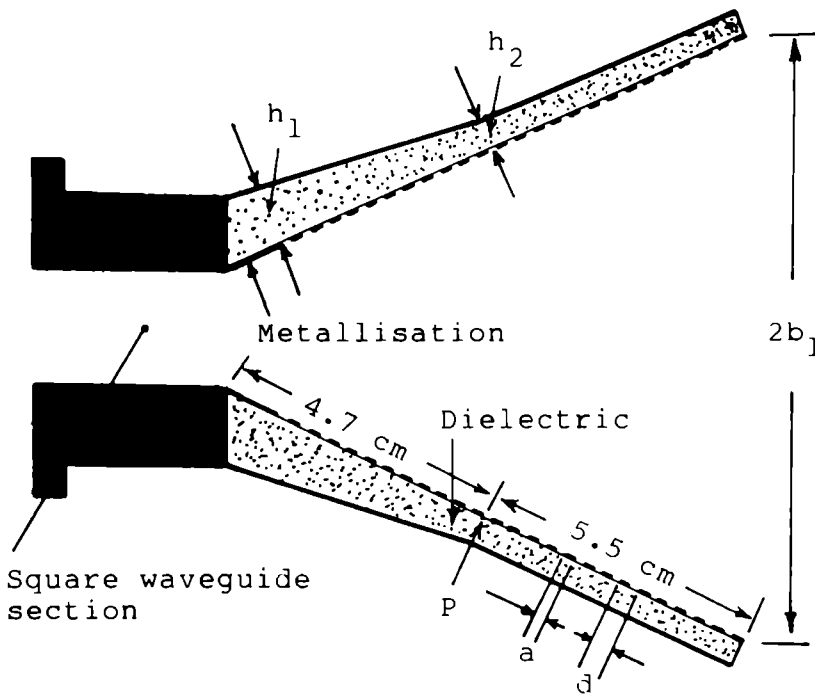
(b)   Horn H6A

Fig.4.39: E-plane view of horn H6 with interior
throat tapering profile and horn H6A
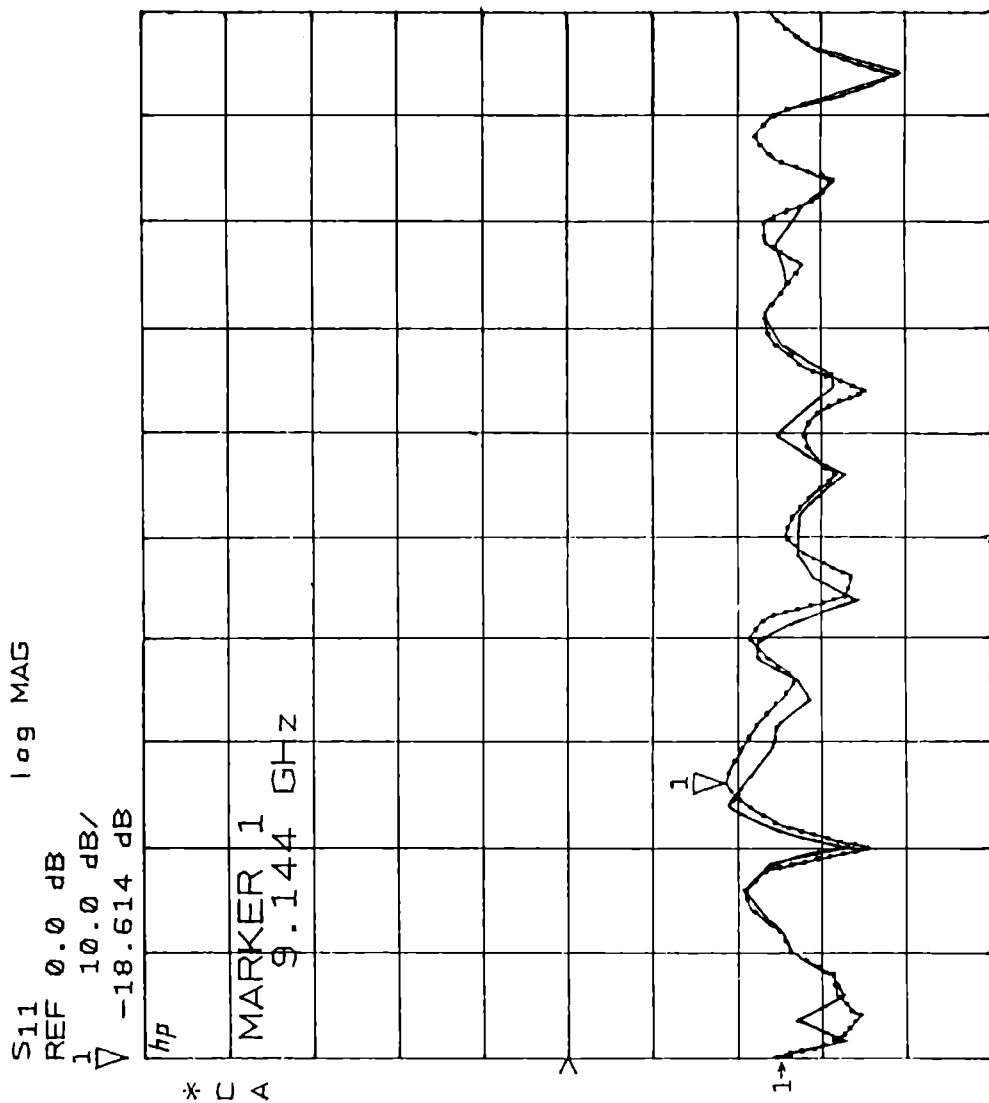with exterior throat tapering profile

S11   log MAG
REF 0.0 dB
1   10.0 dB/
▽ -18.614 dB

hp

MARKER 1
9.144 GHz

START 8.0000000000 GHz
STOP 12.4000000000 GHz

Fig.4.40: Variation of return-loss of horns H6 and H6A with frequency

————— Horn H6 ; ------- Horn H6A
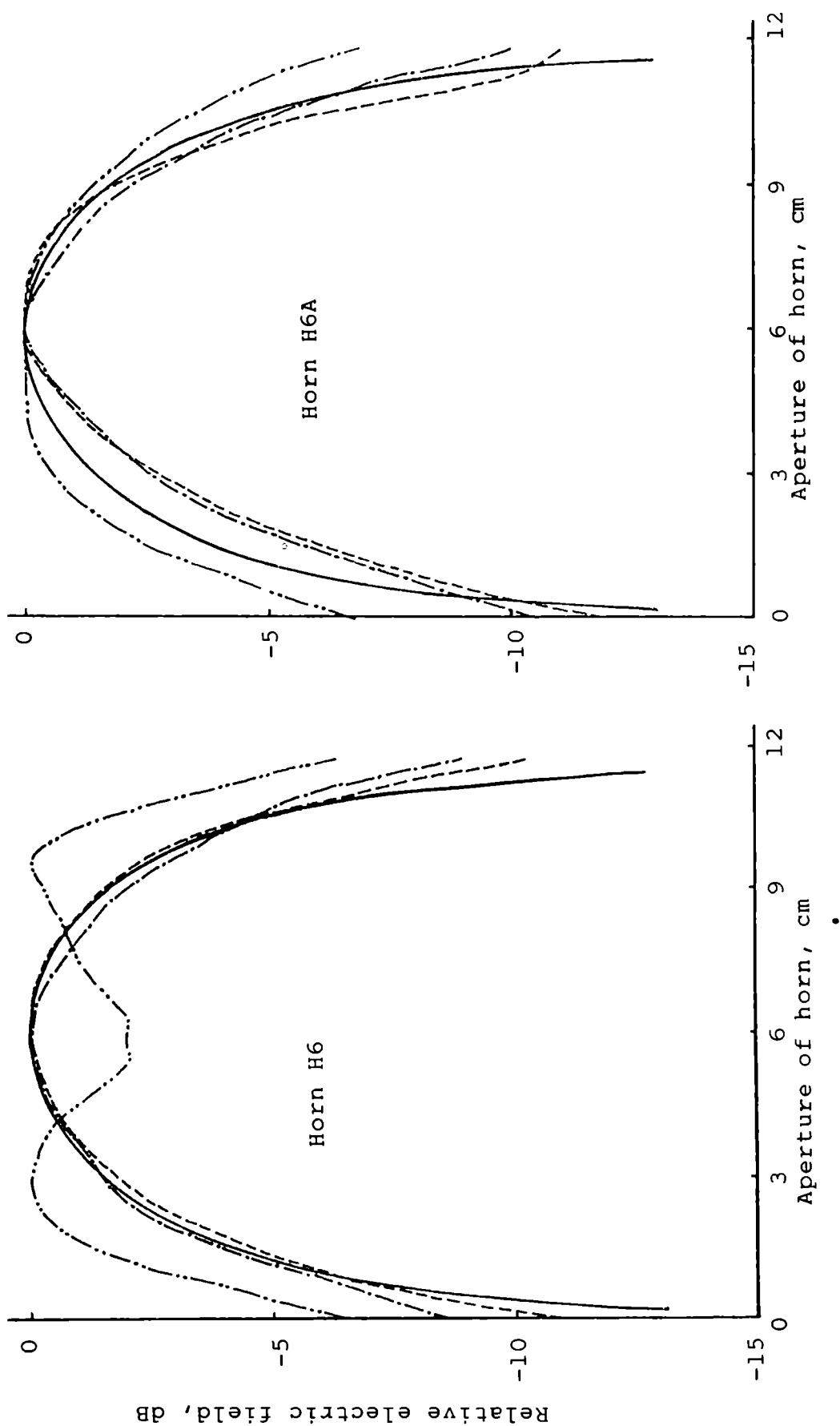
Fig.4.41: Comparison of measured E-plane aperture electric field distribution of horns H6 and H6A at different frequencies with cosine distribution

——— Cosine ; ————— 8.4 GHz ; —·—·— 8.8 GHz ; —··—··— 10 GHz

In the case of both the horns, at the design frequency, 8.4 GHz, the measured E-plane aperture electric field distributions are found to be almost cosine in nature. But at this frequency, the aperture distribution of the horn H6A is exhibiting slightly increased tapering than the horn H6. In the higher frequencies, it is also observed that the deviation of aperture distribution of horn H6A from the theoretical cosine distribution is less compared to that of horn H6. In the case of horn H6, at 10 GHz, at the centre of the aperture, a dip in the aperture field distribution is observed.

The typical E-plane radiation patterns of the horns H6 and H6A along with that of the conventional horn (CH) at different frequencies in X-band are shown in figures 4.42(a) to 4.42(d) and figures 4.43(a) to 4.43(d). It was observed that at the design frequency, the aperture distribution of both the horns H6 and H6A are nearly cosine in nature. As expected the sidelobes of the two horns at this frequency are found to be very low. As observed, because of the reduced tapering of the aperture electric field at higher frequencies, the sidelobe levels of the two horns are also found to be increasing with frequency.
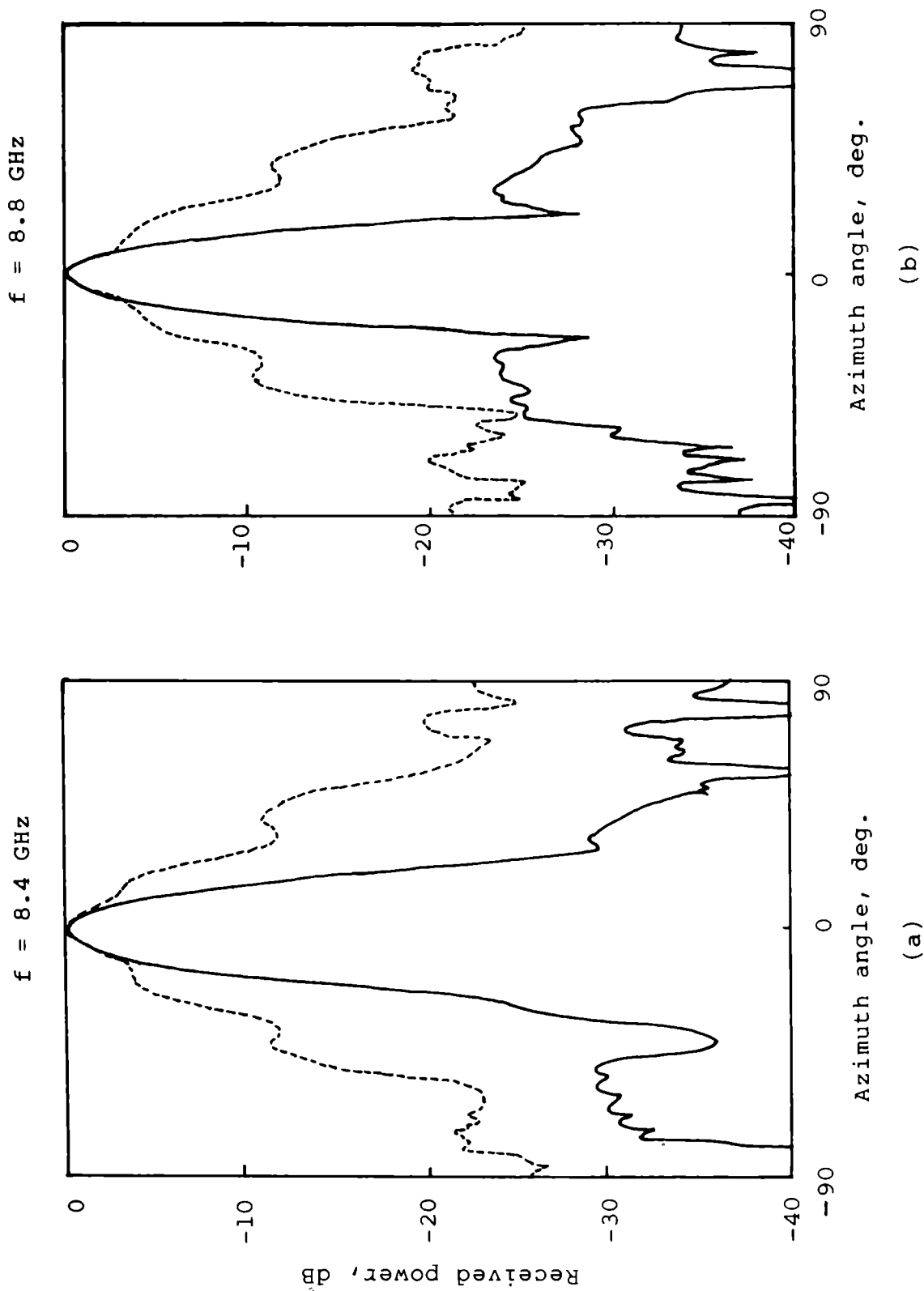
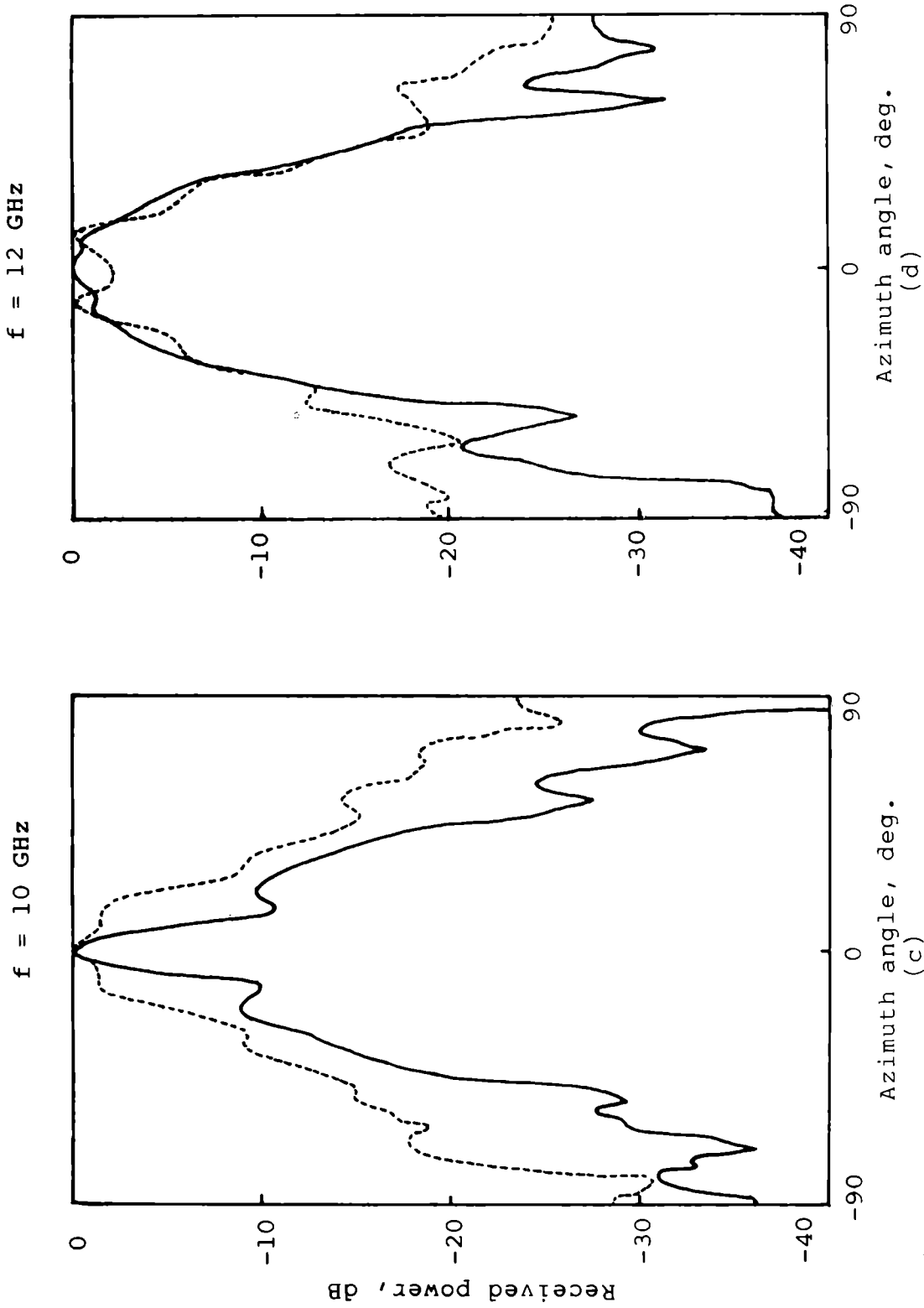Fig.4.42(a)&(b) E-plane radiation patterns of horns H6 and CH at different frequencies ——— Horn H6, —————— Horn CH.

Fig.4.42(c) & (d): E-plane radiation patterns of horns H6 and CH at different frequencies
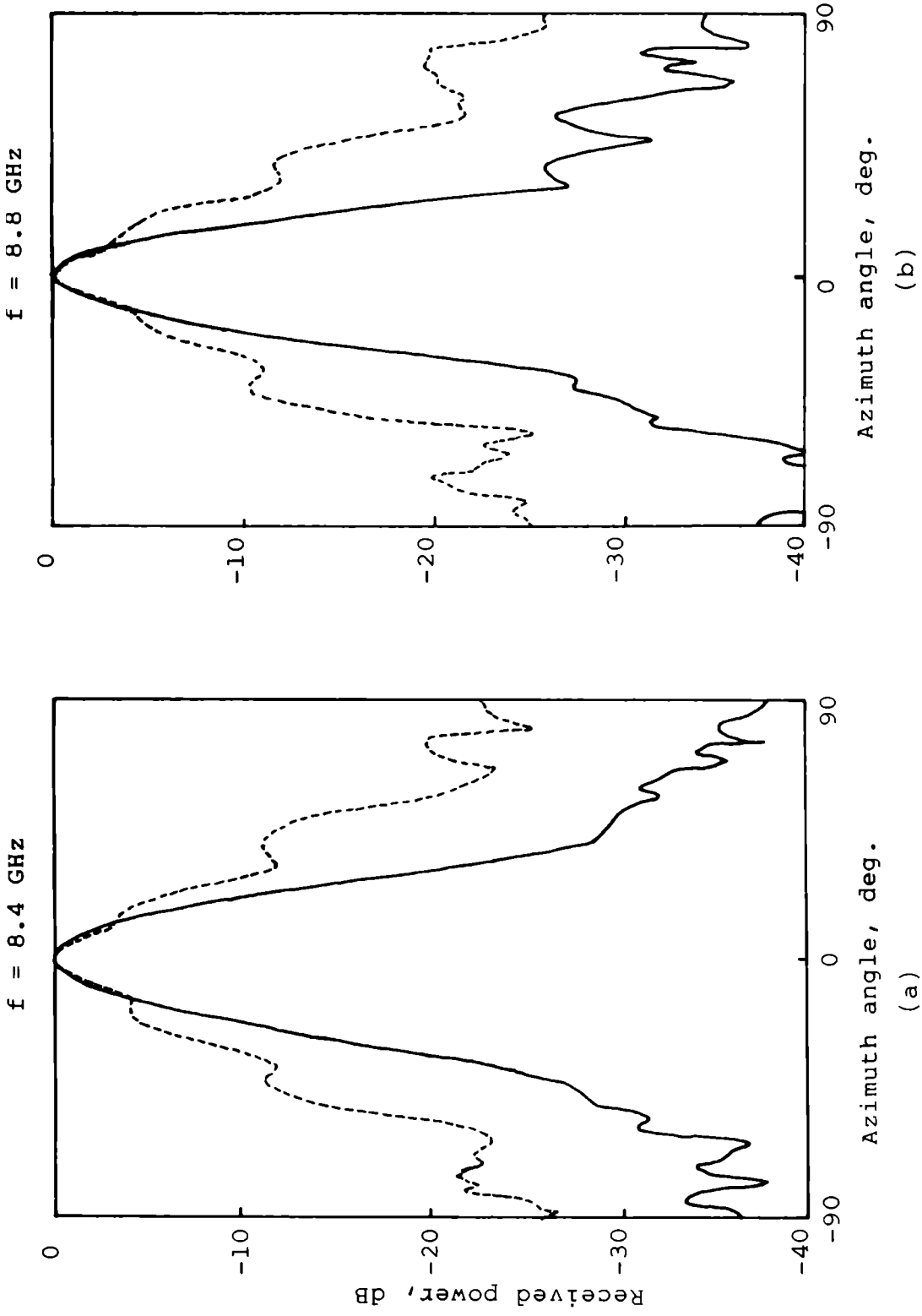
——————— Horn H6 ; ------- Horn CH

Fig.4.43(a)&(b) E-plane radiation patterns of horns H6A and CH at different frequencies.
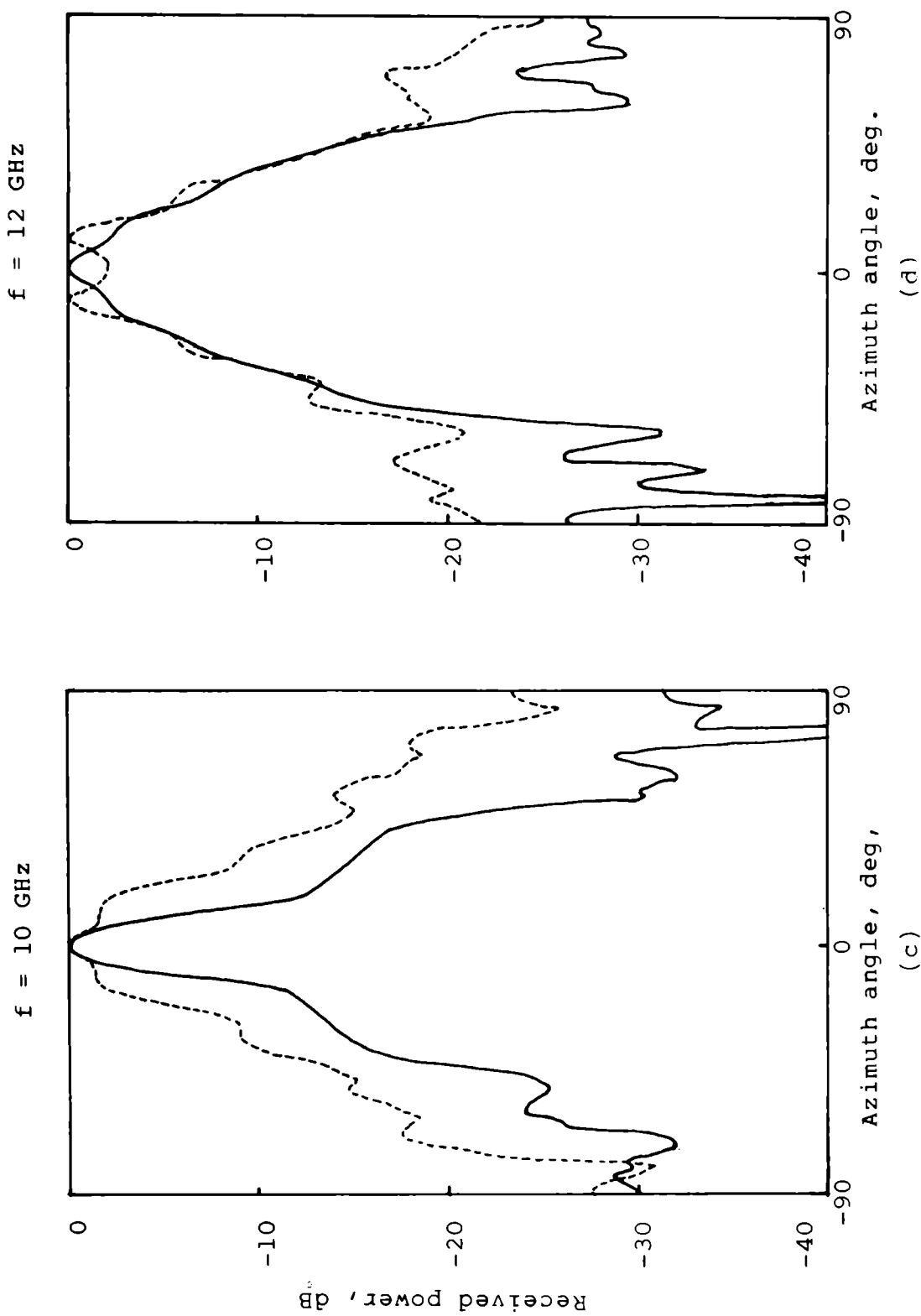
————— Horn H6A ;   -------- Horn CH

Fig.4.43(c) & (d) E-plane radiation patterns of horns H6A and CH at different frequencies.

——— Horn H6A,   - - - - - Horn CH.

However, at higher frequencies, in the radiation pattern of the horn H6, the presence of shoulderlobes are observed. The level of the shoulderlobes are found to be increasing with frequency. At 11 GHz, the observed shoulderlobe level of this horn is -3.2 dB and it is increased to -1.25 dB at 12 GHz. Though the sidelobes of the horn H6A are also increasing with frequency, such shoulderlobes are not observed in the radiation patterns. At higher frequencies, eventhough it shows a "bottle-neck nature" (BNN) in its radiation patterns, the 3 dB beamwidths are found to be reduced. The BNN of the patterns may be due to the merging of shoulderlobes with the mainlobe. Nevertheless, as in the earlier cases, the H-plane radiation patterns of both the horns H6 and H6A are found to be identical to that of the conventional horn. In the case of these horns also, throughout the frequency range of interest, the expected beam symmetry in the two principal planes is not observed.

The frequency response of sidelobe levels of the three horns is plotted in figure 4.44. At the design frequency, the sidelobe levels exhibited by the horns H6 and H6A are -29 dB and -30 dB respectively. As explained earlier, due to the presence of shoulderlobes, for frequencies above 8.8 GHz the sidelobe characteristic of the horn H6 is found to be deteriorated.

The variation of backlobe levels of the horns with frequency is presented in figure 4.45. Compared to the conventional horn, the backlobe characteristics of both the horns H6 and H6A are found to be improved. However, the horn H6A shows a better characteristic than the other two horns.

The frequency response of cross-polarisation of the three horns is shown in figures 4.46. Nevertheless, the -25 dB cross-polarisation bandwidth of the horn H6 is better than the other horns. At the design frequency, 8.4 GHz, the cross-polar level of the horn H6 is -32 dB, whereas that of the horn H6A is -23.3 dB.

The variation of 3 dB beamwidth of the three horns with frequency is given in figure 4.47. In the entire frequency range of interest, the 3 dB beamwidth of the horn H6A is gradually decreasing with frequency. But, in the case of the horn H6, from 8.4 GHz to 10.8 GHz its 3 dB beamwidth is decreasing with frequency and above 10.8 GHz it is found to be increasing. The large beamwidths at higher frequencies are attributed to the shoulderlobes of the radiation patterns. Above 9 GHz the patterns of the conventional horn also possess shoulderlobes. The
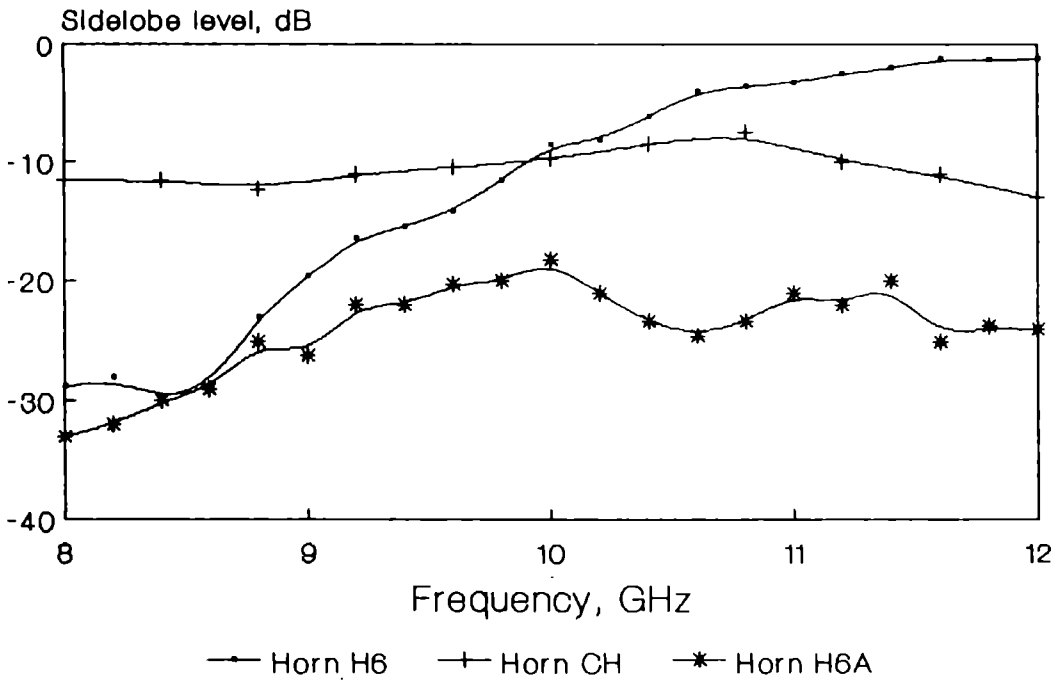
Fig.4.44 Variation of sidelobe level of horns H6, CH
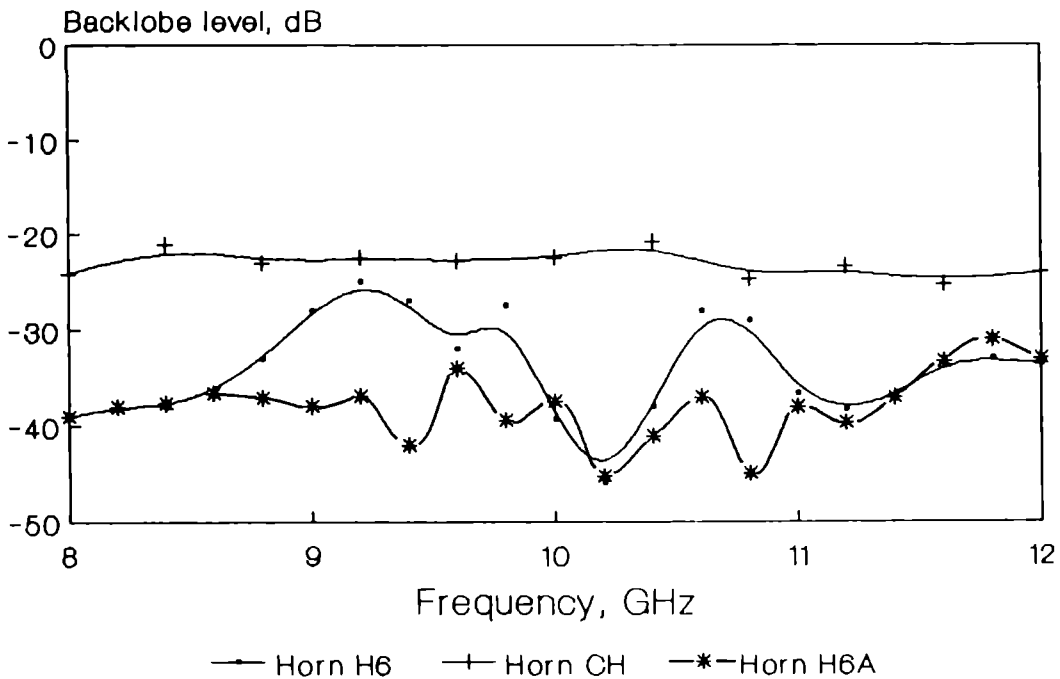and H6A with frequency.

Fig.4.45 Variation of backlobe level of horns H6, CH
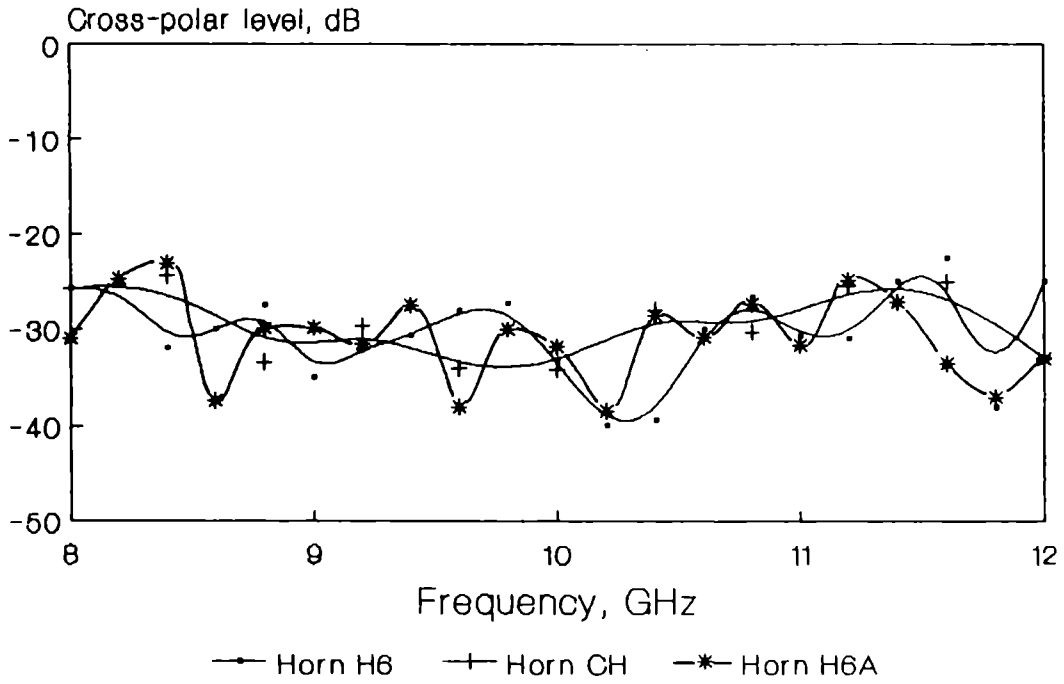and H6A with frequency.

Cross-polar level, dB

Fig.4.46 Variation of cross-polar level of horns H6, CH and H6A with frequency.
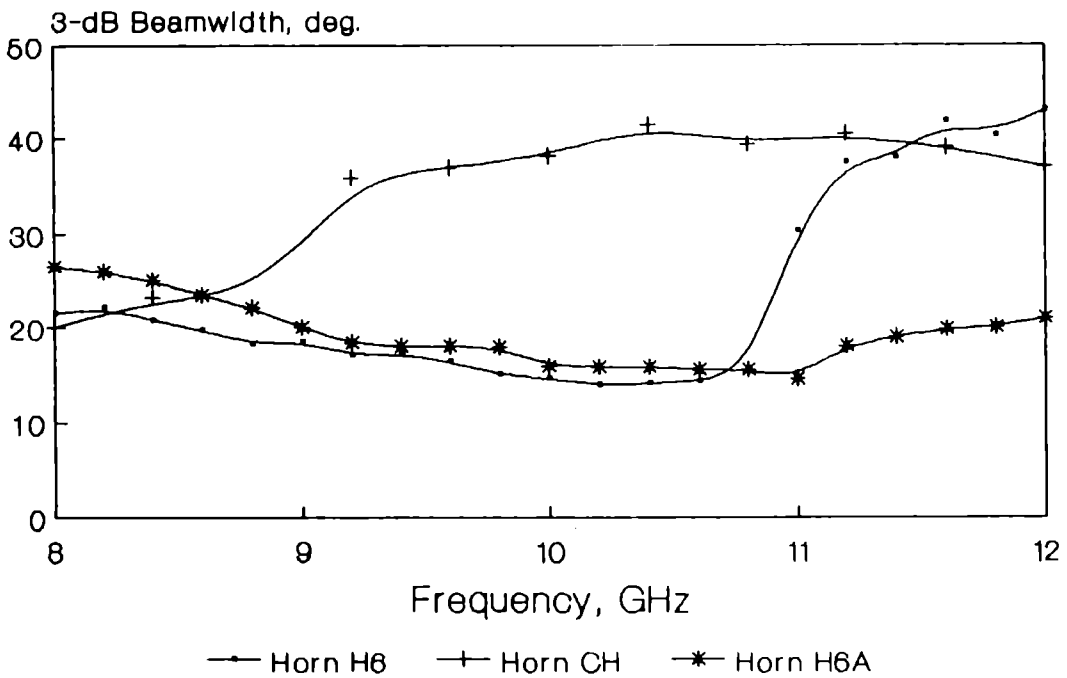
3-dB Beamwidth, deg.

Fig.4.47 Variation of 3 dB beamwidth of horns H6, CH and H6A with frequency.

variation of 10 dB beamwidth of the horns with frequency is given in figure 4.48. In this case also, upto 9.8 GHz, both the horns H6 and H6A show a decrease in beamwidths with frequency and above this frequency, the beamwidths are found to be increasing considerably.

The frequency response of gain of the horns is presented in figure 4.49. In the entire 8.4 GHz to 12 GHz frequency range, the gain of both the horns H6 and H6A are better than that of the conventional horn. Moreover, as expected, in the lower part of the frequency band horn H6 shows better gain characteristic than horn H6A and in the upper part, the horn H6A shows gain improvement.

From the above analysis it is observed that both the horns H6 and H6A are exhibiting better radiation characteristics only in the lower edge of the frequency band. This is because of the fact that the design frequency, 8.4 GHz, is also at the lower edge of the frequency band. Hence, in the further investigations, the design frequency selected is that of at the central region of the frequency band of interest. Another significant observation of the above analysis is that, for better radiation characteristics, the exterior tapering is preferable to the interior tapering profile.
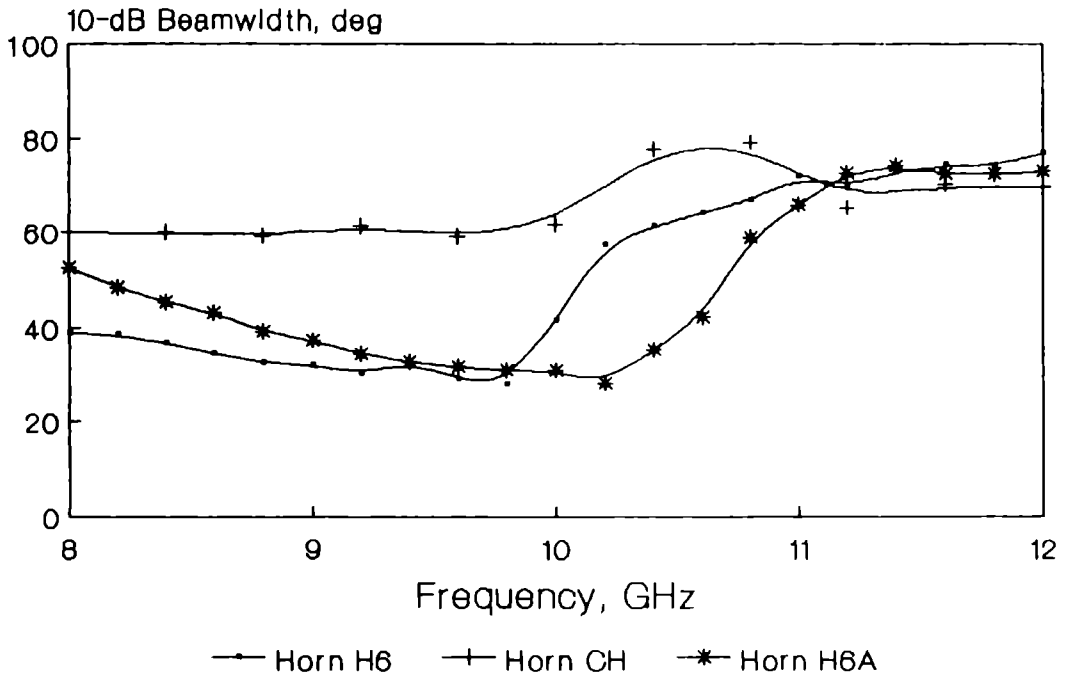
10-dB Beamwidth, deg

Frequency, GHz

— Horn H6   — Horn CH   —*— Horn H6A

Fig.4.48   Variation   of   10   dB   beamwidth   of   horns   H6,
CH and H6A with frequency.

Gain, dB

Frequency, GHz

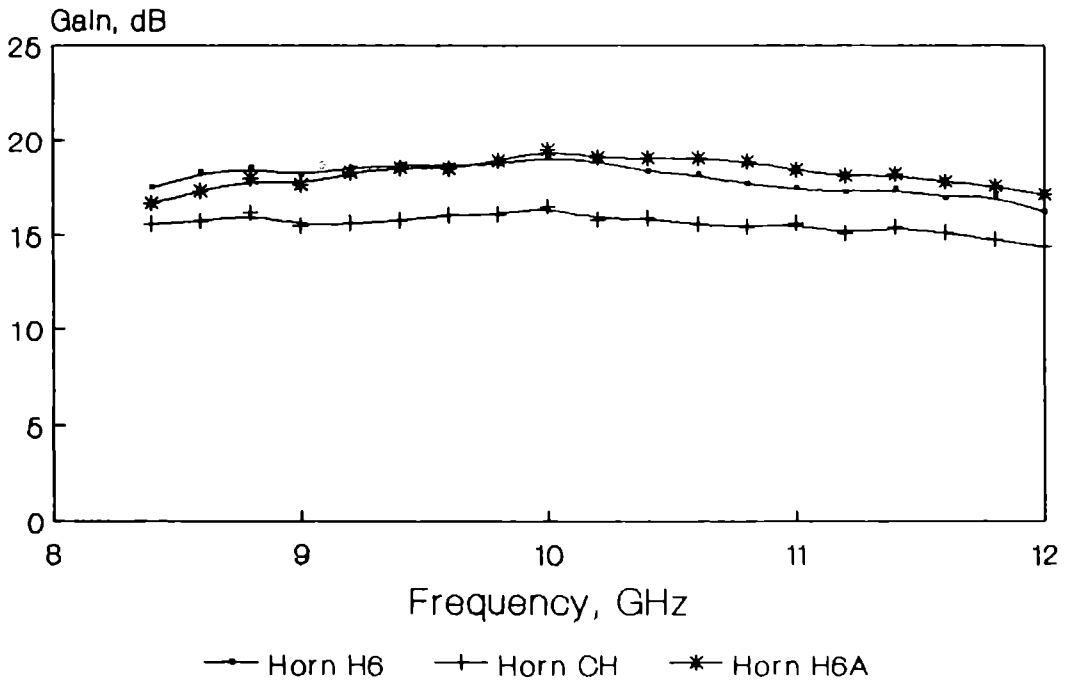— Horn H6   — Horn CH   —*— Horn H6A

Fig.4.49   Variation   of   gain   of   horns   H6,   CH   and   H6A
with frequency.

4.7 OPTIMISATION OF RADIATION CHARACTERISTICS OF HORN ANTENNA WITH INTERIOR TAPERING AT THE VICINITY OF THE THROAT REGION

The analysis of the experimental results of the horns with interior and exterior tapering profile structure for the throat region has revealed that, for better radiation characteristics, the exterior tapering is preferable to the interior tapering profile. Nevertheless, in the present investigation of the thesis, the chief interest is to develop a strip-loaded horn that simulates the radiation characteristics of a metallic corrugated horn of identical physical dimensions and design criteria. As the corrugations of a metallic corrugated horn are usually machined on the inner surface of the E-plane boundary walls, in the present investigation stress is given in the development of a strip-loaded horn with interior tapering profile structure.

The present strip-loaded square pyramidal horn (H7) is a small aperture horn of aperture dimensions $a_1 = b_1 = 3.5$ cm. The E and H-plane slant lengths are $\rho_E = \rho_H = 20.3$ cm and the corresponding semiflare angles in the above planes are $\psi_E = \psi_H = 9.5°$. The E-plane cross-sectional

view of the horn H7 is given in figure 4.50. It is fabricated with dielectric E-plane boundary walls having an interior tapering profile structure at the vicinity of the throat region. As in the case of horn H6 of the previous section 4.6, after the 1 cm metallised portion at the throat region, the thickness of the dielectric substrate (h_1) is $\lambda /2\sqrt{\epsilon_r-1}$ where λ is the free-space wavelength at the design frequency, 10 GHz, which is the centre frequency of the 8 GHz to 12 GHz frequency range. This thickness is then gradually tapered to a thickness $h_2 = \lambda /4\sqrt{\epsilon_r-1}$ at the point P. From the point P to the aperture of the horn, the dielectric thickness is kept constant at $\lambda /4\sqrt{\epsilon_r-1}$ so that the balanced hybrid mode condition is also satisfied at 10 GHz. The entire remaining inner surface of the E-plane walls is then loaded with thin conducting strips at a period d = 0.133 λ and a/d = 0.5. As in the case of earlier horn antennas, the entire outer surface of the horn is completely metallised.

The typical E and H-plane radiation patterns of the horn at the design frequency are given in figure 4.51. From the figure it is clear that the E and H-plane patterns of the present horn are almost identical. The variation of the 3 dB and 10 dB beamwidths of the E and H-plane
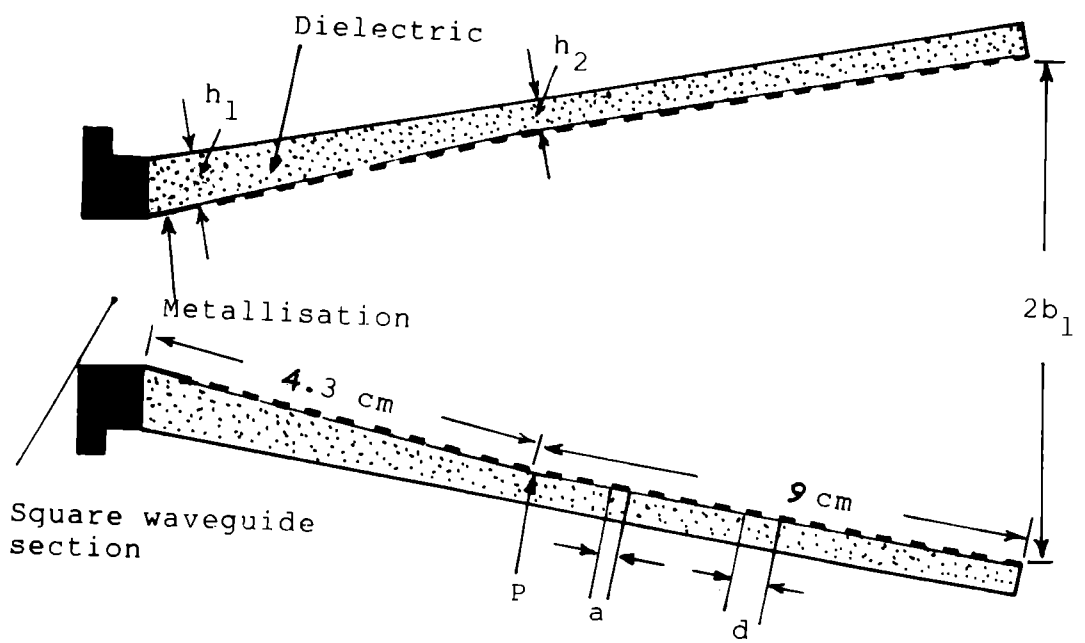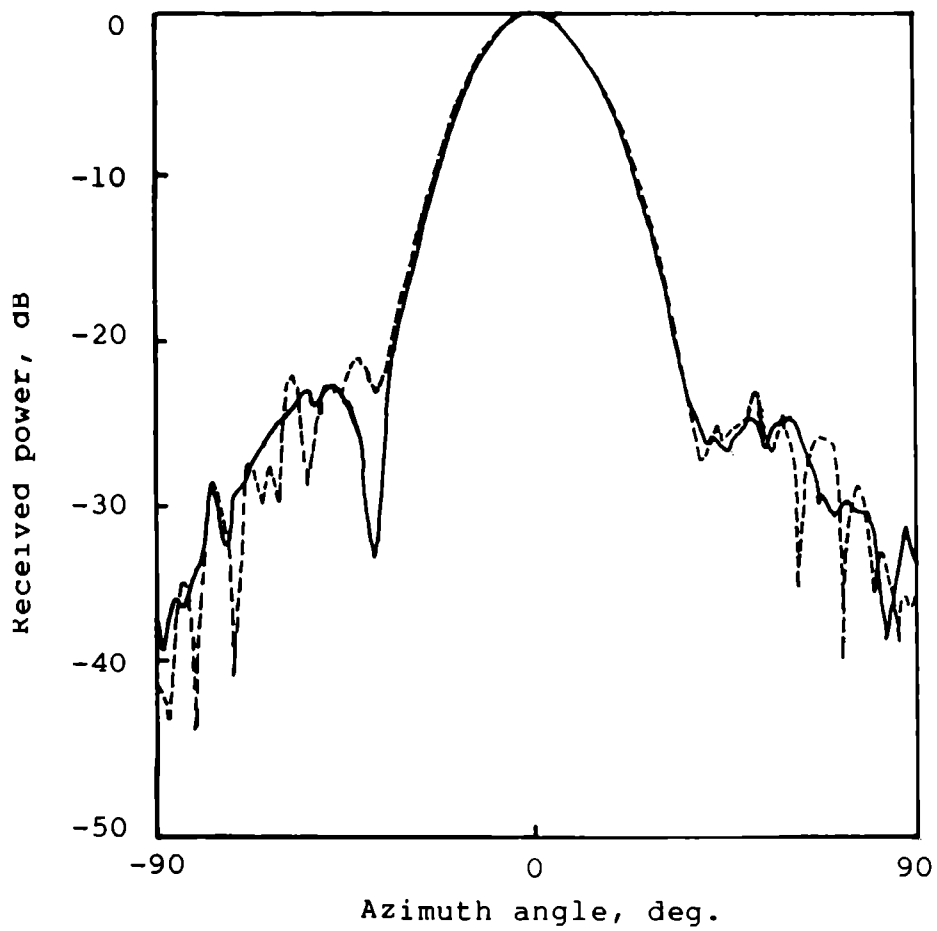
Fig.4.50: E-plane view of horn H7

Fig.4.51   E- and H-plane radiation patterns of horn H7
at 10 GHz.

———————— E-plane ; ——————H-plane.

radiation patterns of the horn is presented in figure 4.52. In the central region of the 8 GHz to 12 GHz frequency band, the 3 dB and 10 dB E-plane and H-plane beamwidths of the horn are found to be more or less same. The deviation from the beam symmetry is observed to be much more predominant in the lower edge of the frequency band than the upper edge.

The frequency response of the sidelobe, backlobe and cross-polarisation levels of the horn is shown in figure 4.53. As in the above case, the horn is found to be exhibiting better sidelobe and backlobe characteristics in the central region of the 8 GHz to 12 GHz frequency band. However, in this region, the cross-polar level is found to be slightly high. In the entire 8 GHz to 12 GHz frequency band the maximum sidelobe level exhibited by the horn is -17.5 dB. Though the horn is designed at 10 GHz, the observed minimum level of sidelobe level, -30.7 dB, is observed at 9.8 GHz. At the design frequency the exhibited sidelobe level is -22.5 dB.

The variation of the return-loss of the horn with frequency is shown in figure 4.54. In the entire X-band of frequency, the maximum level of return-loss is better than -19.75 dB.
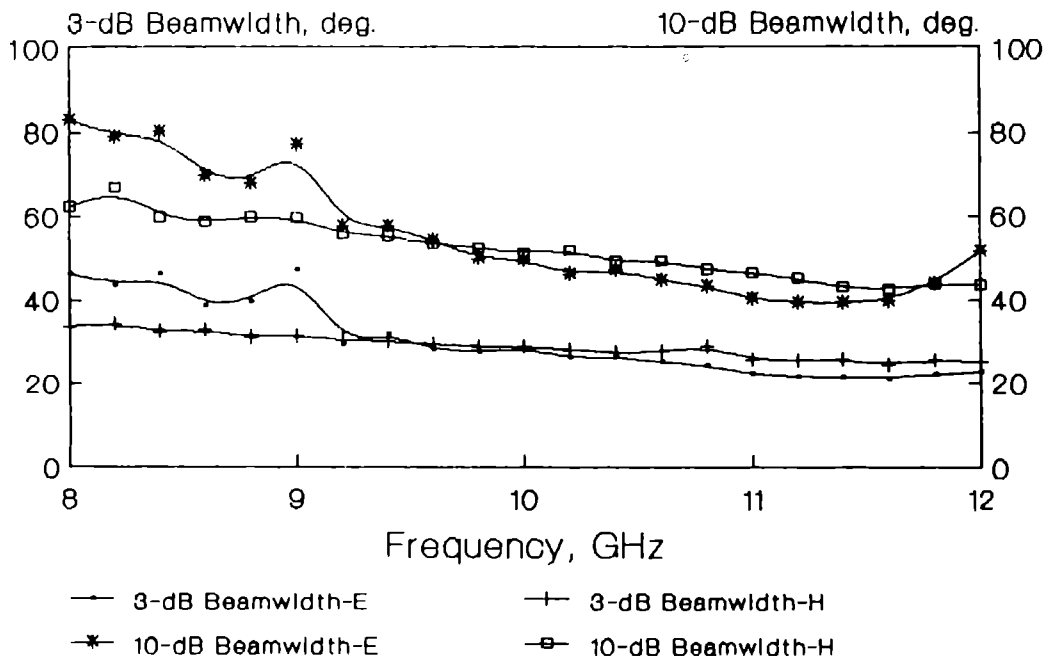
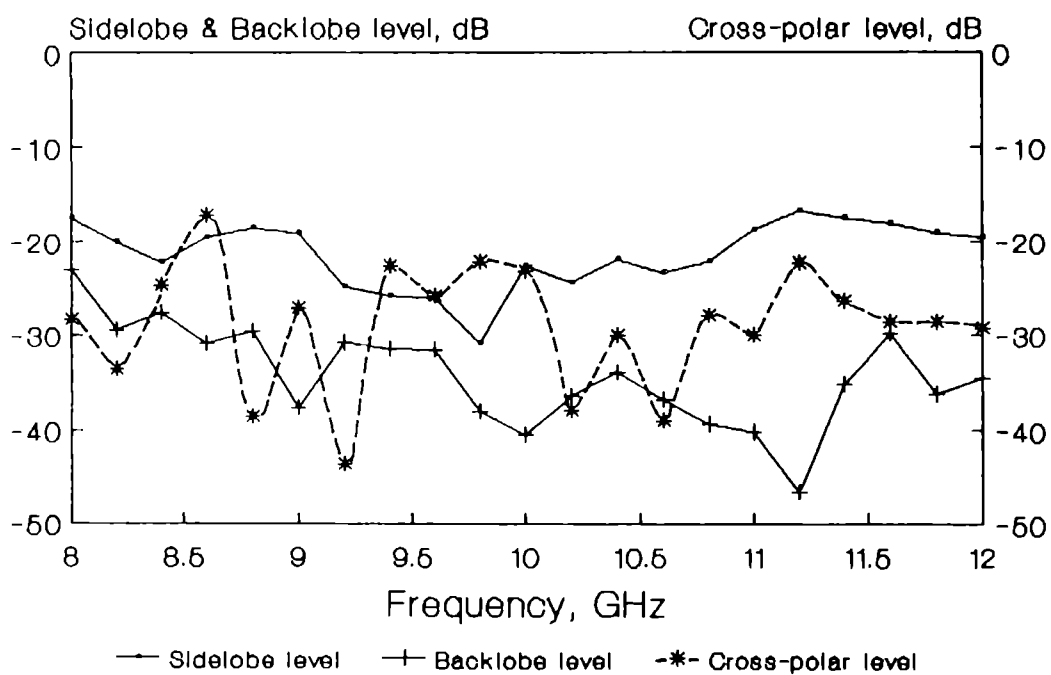Fig.4.52 Variation of 3 dB and 10 dB beamwidths of horn H7 with frequency.

Sidelobe & Backlobe level, dB   Cross-polar level, dB

Frequency, GHz

—•— Sidelobe level   —+— Backlobe level   -*- Cross-polar level

Fig.4.53 Variation of sidelobe, backlobe and cross-
polarisation levels of horn H7 with frequency.

S11   log MAG

S11
REF 0.0 dB   REF 1.0 Units
△   10.0 dB/   1   200.0 mUnits/
1   -19.956 dB   ▽   52.279 Ω -10.076 Ω
  hp

* C   MARKER 1
      10.75 GHz
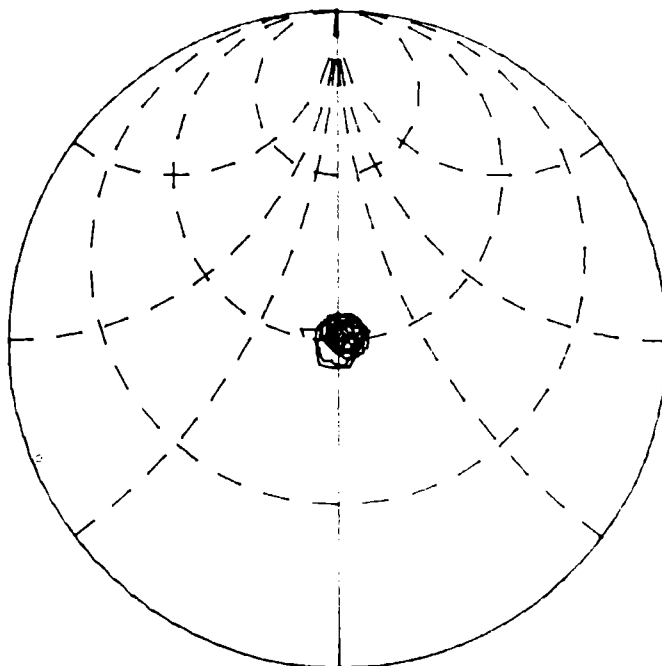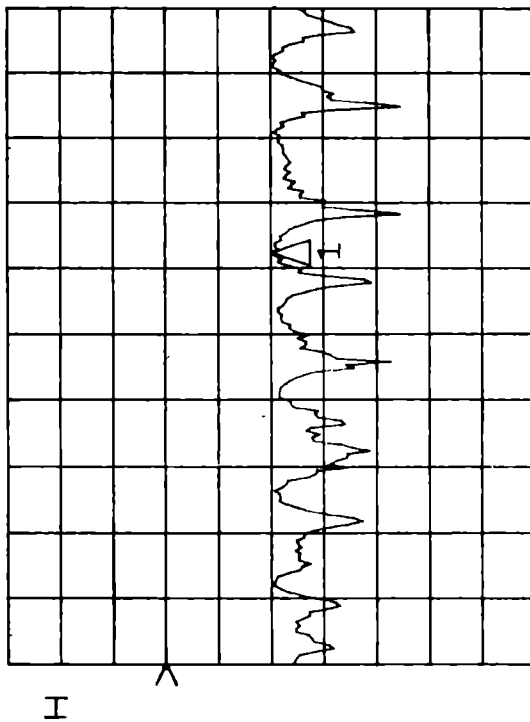
START   8.000000000 GHz
STOP   12.400000000 GHz

Fig.4.54: Variation of return-loss of horn H7 with frequency

The frequency response of the gain of the horn is plotted in figure 4.55. As expected, the gain is found to be increasing with frequency. At the design frequency, the gain of the horn is 16.3 dB.

From the analysis of the radiation characteristics of the horn H7, it is observed that its cross-polarisation characteristic in the frequency range considered is slightly high. Moreover, the achieved maximum sidelobe suppression level is only -17.5 dB. The small aperture of the horn 2.5 λ at the design frequency, may be the cause of such observed characteristics.

4.8 RADIATION CHARACTERISTICS OF A SIMULATED SCALAR FEED HORN ANTENNA

The study of the radiation characteristics of the horn H7 has revealed that, the achieved cross-polarisation and sidelobe level characteristics in the frequency band considered are poorer than -20 dB. The small aperture of the horn may be the root cause of the poor performance. In order to validate the observed results, a strip-loaded square pyramidal horn of larger aperture dimension is fabricated. The radiation characteristics of this strip-loaded horn antenna in the X-band frequency is studied in
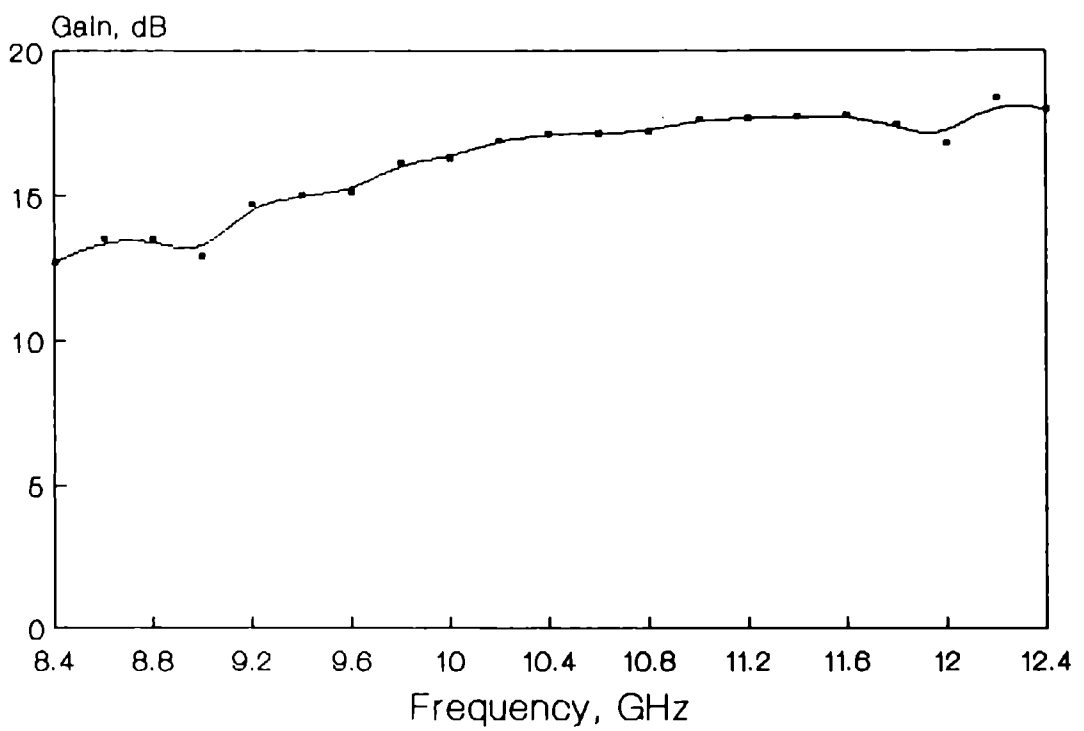
Fig.4.55 Variation of gain of horn H7 with frequency.

detail. From the study, it is well understood that this horn antenna is simulating the radiation characteristics of a scalar feed horn antenna. Hence, the new strip-loaded horn antenna is designated as 'Simulated Scalar Feed' horn antenna (SSF horn antenna).

The E-plane cross-sectional view of the SSF horn antenna is given in figure 4.56. The aperture dimensions of the SSF horn antenna are $a_1 = b_1 = 1.965\lambda$, where 'λ ' is the free-space wavelength at the design frequency, 10 GHz. Its E and H-plane slant lengths are $\rho_E = \rho_H = 4.27\lambda$ and the corresponding semiflare angles in the above planes respectively are $\psi_E = \psi_H = 25°$. The same design criteria employed for the horn H7 of previous section 4.7 is extended in the fabrication of the E-plane boundary walls of the SSF horn antenna also. At the throat region of the horn, after the 1 cm metallised portion, the thickness of the dielectric substrate h_1 is $\lambda/2\sqrt{\epsilon_r-1}$. This is then gradually tapered to a thickness $h_2 = \lambda/4\sqrt{\epsilon_r-1}$ at the point P. From the point P to the aperture of the horn, the dielectric thickness is kept constant at $\lambda/4\sqrt{\epsilon_r-1}$ so that the balanced hybrid mode condition is satisfied at 10 GHz. Thin conducting strips
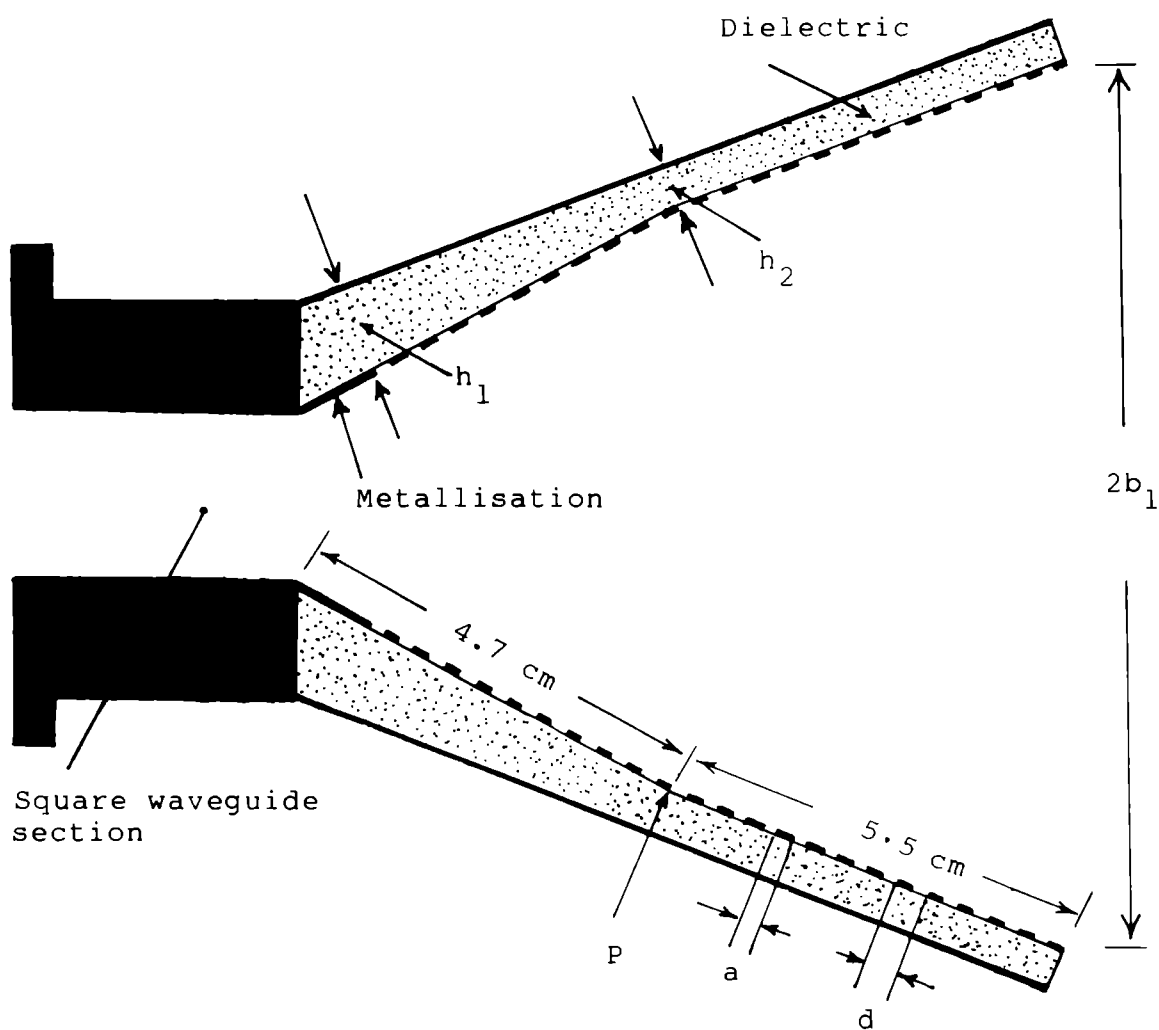
Dielectric

h_2

h_1

Metallisation

$2b_1$

Square waveguide
section

4.7 cm

5.5 cm

P

a

d

Fig.4.56: E-plane view of simulated scalar feed horn antenna

are periodically loaded on the entire inner surface of the E-plane walls at a period d = 0.133 λ and a/d = 0.5. The outer surface is completely metallised.

The E-plane aperture electric field distribution of the horn at different frequencies in X-band were measured. The measured aperture field distributions at different frequencies, compared with that of the theoretical cosine distribution, are shown in figures 4.57(a) and 4.57(b). From the figures it is clear that the aperture field distributions of the horn at these frequencies are almost cosine in nature.

The radiation characteristics of the SSF horn antenna are found to be very much improved than that of the corresponding identical conventional horn. Hence, no attempt has been made to compare the radiation characteristics with that of the identical conventional horn. However, for a direct information about its frequency response of gain, a comparison with the gain characteristic of the identical conventional horn is made in figure 4.58. The gain of the SSF horn antenna, in the entire 8.4 GHz to 12 GHz frequency range, is found to be better than that of the conventional horn.
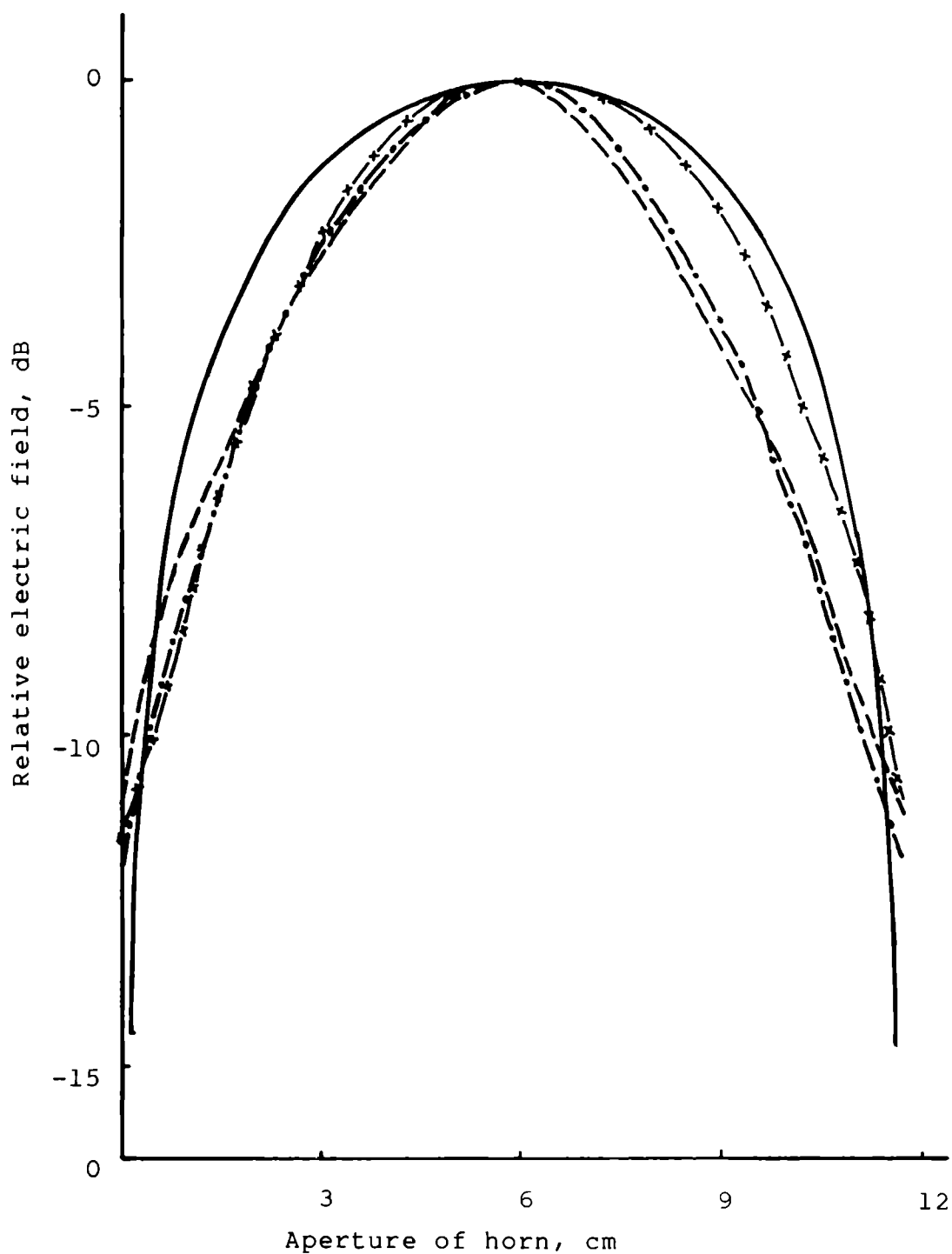
Fig.4.57(a) Comparison of measured E-plane aperture electric
field distribution of SSF horn at different
frequencies with cosine distribution.

————— cosine,   ——————— 8.8 GHz,
·—·—·—·— 9.2 GHz, x—x—x—x—x— 9.6 GHz.

Fig.4.57(b) Comparison of measured E-plane aperture electric
field distribution of SSF horn at different
frequencies with cosine distribution.

———————— cosine,   —————— 10 GHz
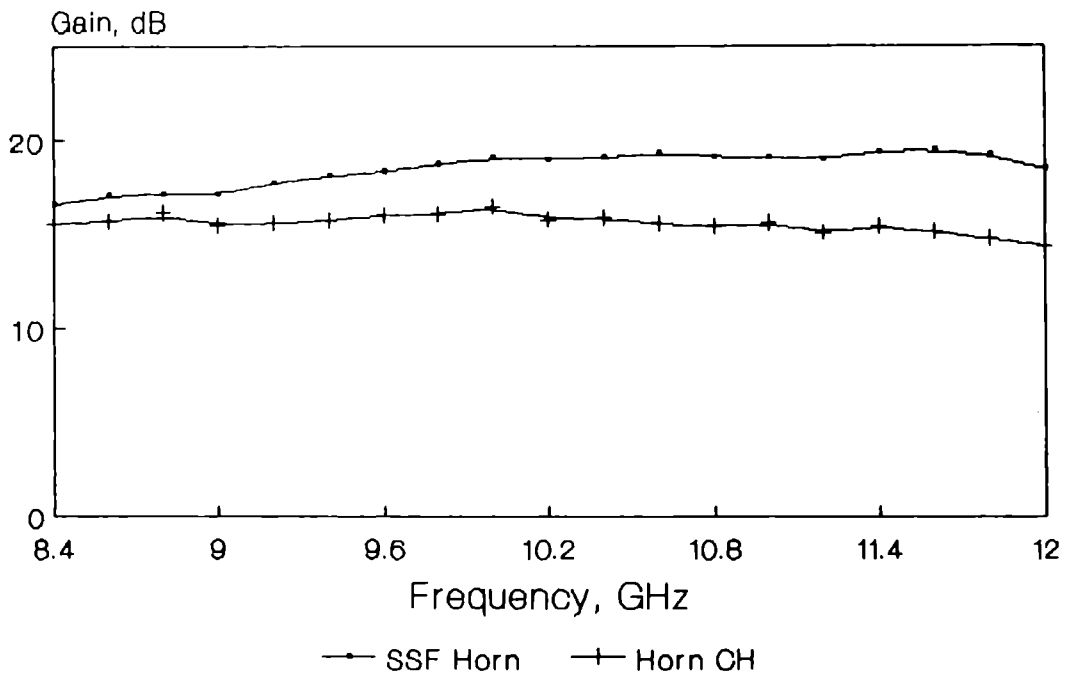—··—·—·— 10.4 GHz,   —×—×— 11 GHz.

Fig.4.58 Variation of gain of SSF horn and horn CH with frequency.

The typical E and H-plane radiation patterns, along with the cross-polar pattern, of the SSF horn antenna at the design frequency, 10 GHz, are shown in figure 4.59. From the figure it is clear that the expected beam-symmetry of the radiation patterns in the E and H-planes is not achieved. In the entire 8 GHz to 12 GHz frequency band, the beamwidths of the E and H-plane patterns are observed to be unequal. The shoulderlobes and saddle observed on the mainlobe of the E-plane radiation patterns of the conventional horn of identical dimensions, which are attributed to the out-of-phase relation between the direct and edge diffracted rays, are found to be totally absent in the E-plane radiation patterns of the SSF horn antenna, in the entire 8 GHz to 12 GHz frequency band. Since the E-plane radiation patterns of the SSF horn antenna at other frequencies in X-band, compared with that of an identical metallic corrugated horn are presented in the next section of the thesis, they are not shown in this section. Moreover, as observed in the earlier cases, the H-plane radiation patterns of the SSF horn antenna are found to be similar to the H-plane patterns of the identical conventional horn.

The variation of the sidelobe and backlobe levels of the horn with frequency is shown in figure 4.60. The
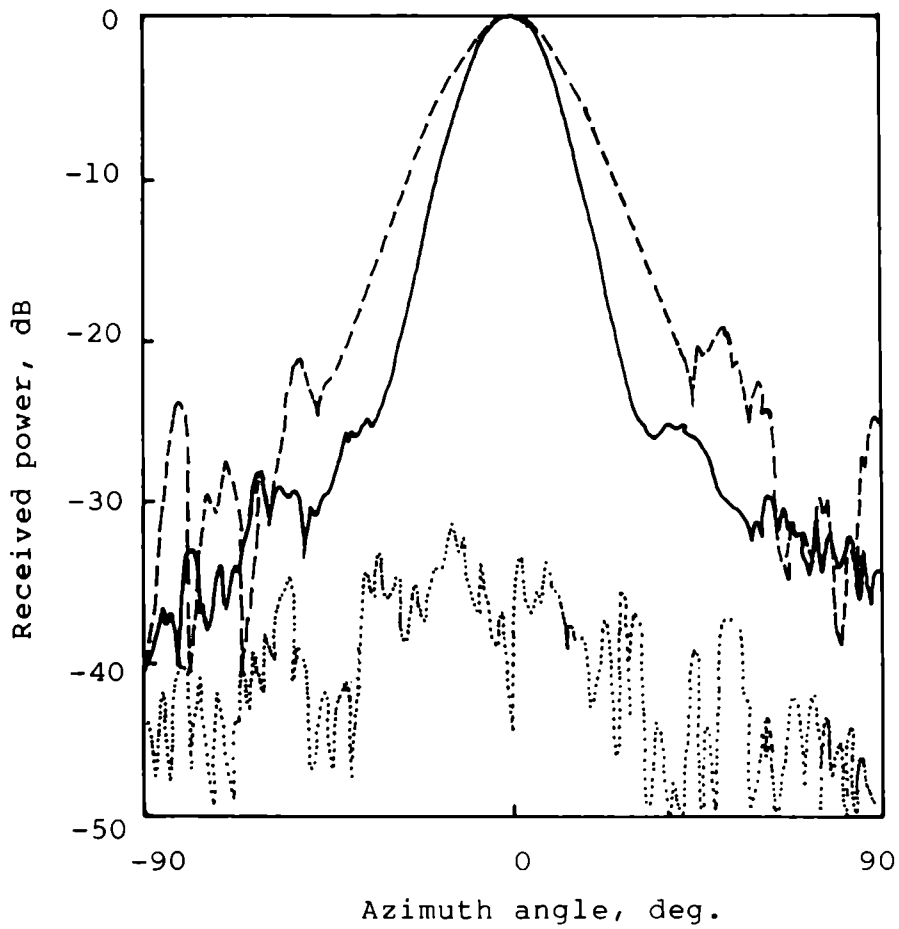
Fig.4.59   E-   and   H-plane   radiation   patterns   along   with
cross-polar pattern of SSF horn at 10 GHz.

——— E-plane, ––––– H-plane,·············· cross-polar.

maximum level of sidelobe exhibited by the SSF horn antenna, in the entire 8 GHz to 12 GHz frequency band, is -25 dB and the corresponding backlobe level is -29 dB.

The frequency response of the cross-polarisation of the SSF horn antenna is found to be better than -25 dB, in the entire 8 GHz to 12 GHz frequency band. At the design frequency, 10 GHz, the observed cross-polar level is -32 dB. The cross-polarisation level variation of the SSF horn antenna with frequency is presented in figure 4.61.

The 3 dB and 10 dB beamwidth variation of the E-plane radiation patterns of the SSF horn antenna is given in figure 4.62. Since the E and H-plane patterns are found to be asymmetrical in the entire frequency band, as stated earlier (refer page 103) H-plane beamwidth characteristics of the SSF horn antenna are not presented in the thesis. The E-plane 3 dB beamwidths of the horn are found to be decreasing with increase of frequency. On the otherhand, from 8.5 GHz to 10.6 GHz the 10 dB beamwidth decreases with frequency and above 10.6 GHz it increases with frequency.

The return-loss characteristic of the SSF horn antenna in the 7.5 GHz to 14 GHz frequency range is shown
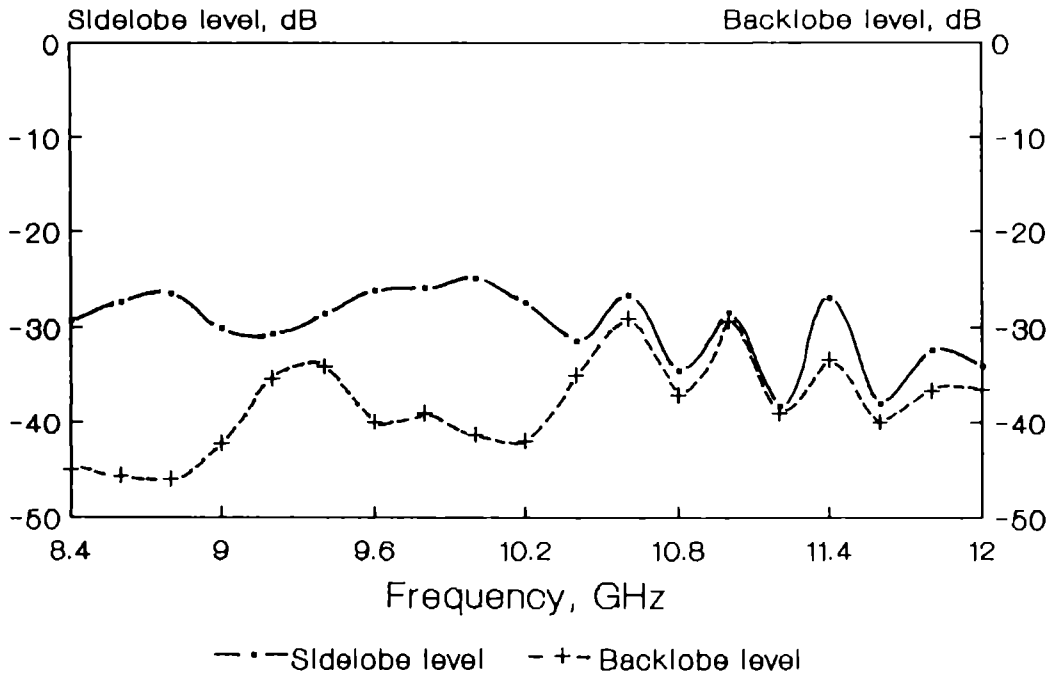
Fig.4.60   Variation of sidelobe and backlobe levels
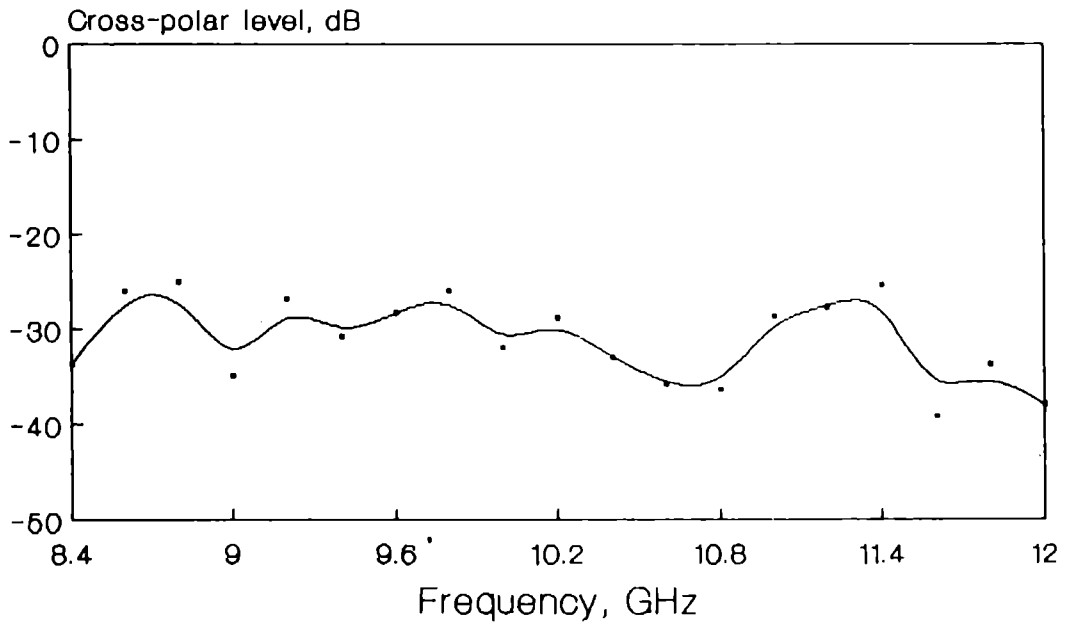of SSF horn with frequency.

Fig.4.61   Variation of cross-polarisation level of SSF
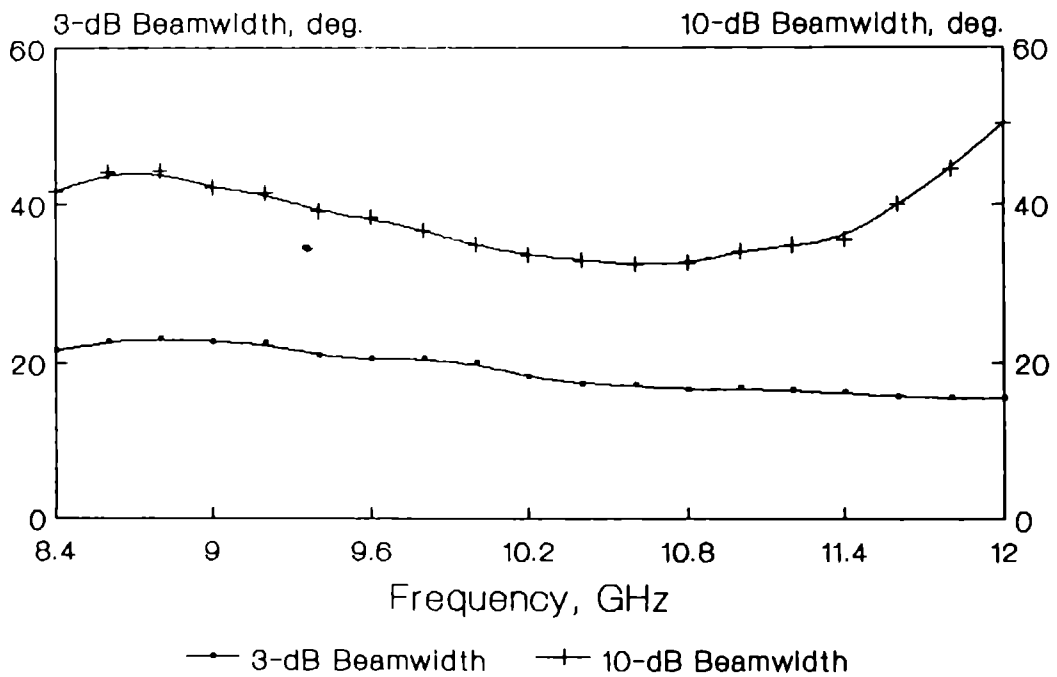horn with frequency.

Fig.4.62   Variation of 3 dB and 10 dB beam widths of SSF
            horn with frequency.

in figure 4.63. From the figure it is observed that in the worst case, the return-loss is -17.29 dB in the useful X-band region.
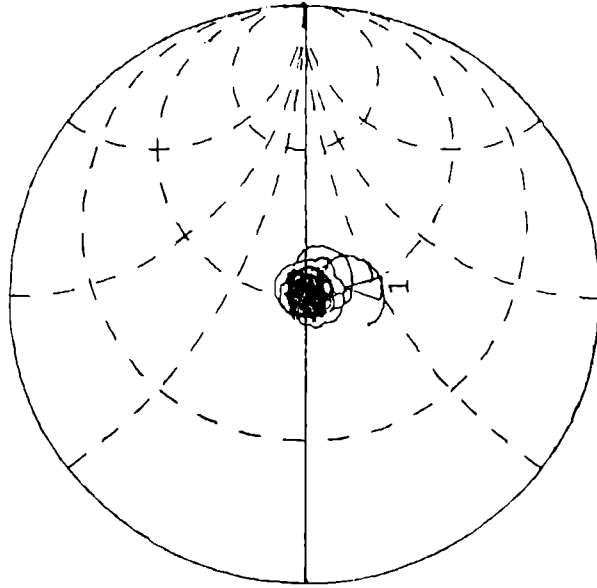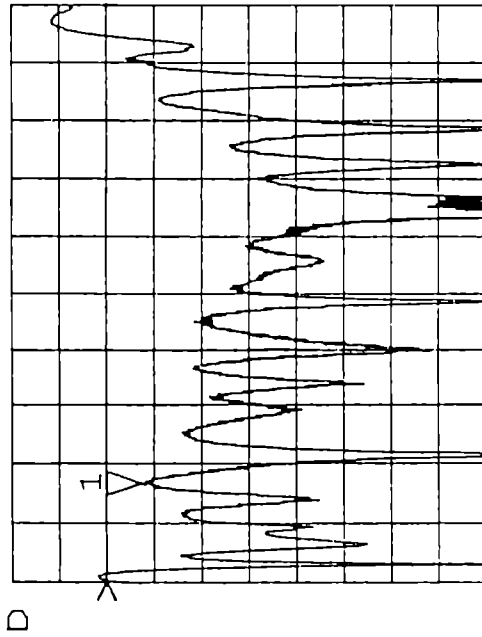
From the analysis of the above experimental results of the SSF horn antenna, it is obviously clear that it is simulating the radiation characteristics of a scalar feed horn antenna like a metallic corrugated horn antenna. Hence, in order to validate the observed results, a metallic corrugated horn (MCH) antenna of identical physical dimensions and design criteria as that of the SSF horn antenna is fabricated. The radiation characteristics of the MCH antenna and the SSF horn antenna are compared and are presented in the next section.

4.9 COMPARISON OF RADIATION CHARACTERISTICS OF A SIMULATED SCALAR FEED HORN ANTENNA AND A METALLIC CORRUGATED HORN ANTENNA

A close look on the radiation characteristics of the SSF horn antenna reveals the fact that it is simulating identical radiation characteristics of a metallic corrugated horn antenna. Hence, it will be of interest if we compare its radiation characteristics with that of a metallic corrugated horn (MCH) antenna of identical

S11   log MAG

REF −15.0 dB
1
▽ 3.0 dB/
▽ −17.292 dB

hp   SC HORN

S11   Z
REF 1.0 Units
200.0 mUnits/
△
1 51.693 Ω −13.92 Ω

C
A MARKER 1
    8.58875 GHz

D

START   7.500000000 GHz
STOP   14.000000000 GHz

Fig.4.63: Variation of return-loss of SSF horn antenna with
       frequency

physical dimensions. For this purpose, an identical metallic corrugated horn antenna is fabricated and its radiation characteristics are compared with that of the SSF horn antenna. The observed results are presented in the following section of the thesis.

The E-plane boundary walls of the MCH antenna are fabricated with a metallic corrugated surface of corrugation period d = 0.133λ and a/d = 0.5, where 'λ' is the free-space wavelength at the design frequency 10 GHz. At the throat region of the horn, after 1 cm of plane metallic portion of the E-plane walls, the slot depth of the first corrugation is 0.5 λ. As in the case of the SSF horn antenna, this is gradually tapered to a slot depth of 0.25λ at the point P. From the point P to the aperture of the horn, the slot depth is kept constant at 0.25 λ so that the balanced hybrid mode condition is also satisfied at the design frequency, 10 GHz.

The E-plane aperture electric field distribution of the MCH antenna at different frequencies in X-band are measured. These measured aperture field distributions are compared with that of the corresponding aperture field distributions of the SSF horn. In figure 4.64, the aperture electric field distributions of the two horns at
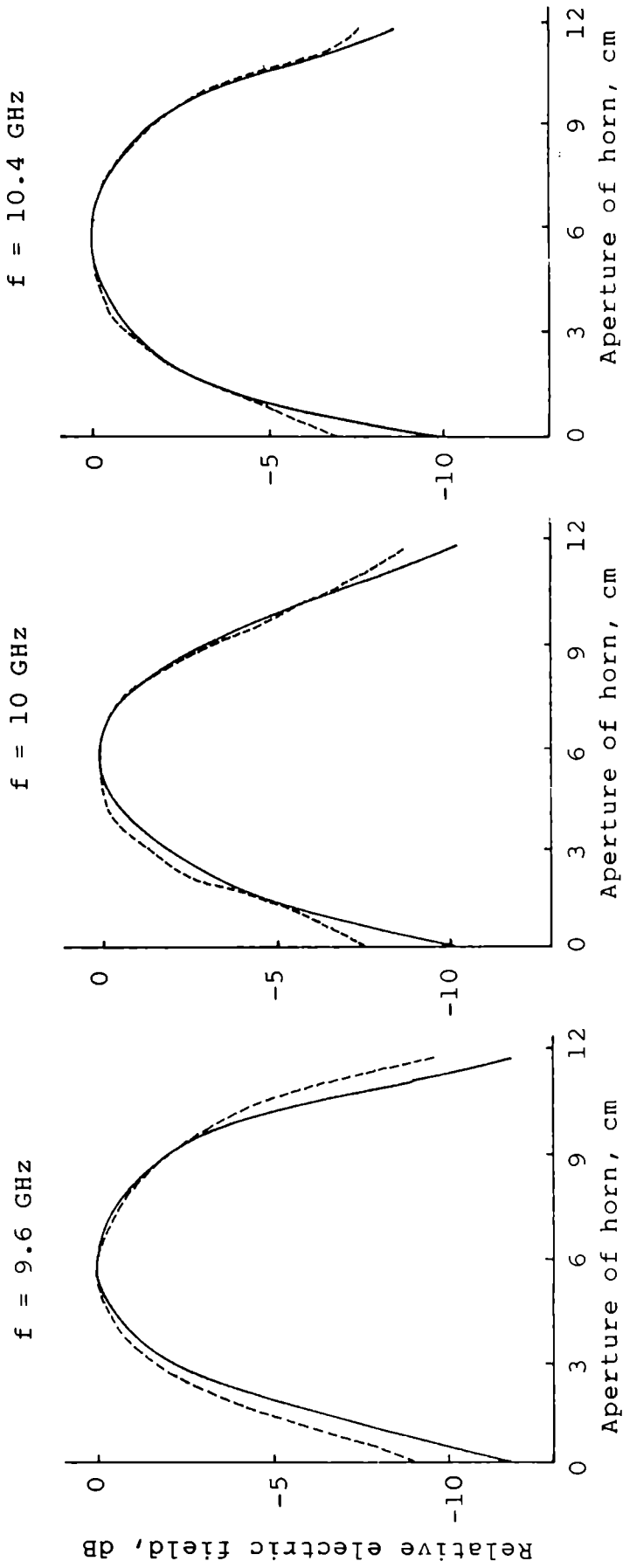
Fig.4.64: Measured E-plane aperture electric field distribution of SSF horn antenna and MCH antenna

———— SSF horn antenna ; –––––––– MCH antenna

9.6 GHz, 10 GHz and 10.4 GHz are compared. From the figure, it is observed that the E-plane aperture electric field distributions of the two horns are almost identical and cosine in nature. However, the tapering level of the electric field at the aperture edges of the SSF horn antenna is found to be slightly better than that of the MCH antenna.

The typical E-plane radiation patterns of the two horn antennas at different frequencies in X-band are compared in figures 4.65(a) and 4.65(b). Though slight dissimilarities are observed, the radiation patterns are found to be more or less identical in nature. For frequencies above 9 GHz, as observed in the case of E-plane aperture electric field distributions, the sidelobe levels of the SSF horn antenna are found to be slightly better than that of the MCH antenna.

The variations of the sidelobe and backlobe levels of the two horns with frequency are shown in figure 4.66. In the entire 8 GHz to 12 GHz frequency band, the sidelobe characteristics of the SSF horn antenna are found to be more or less identical to that of the MCH antenna. However, as observed in the case of E-plane aperture electric field
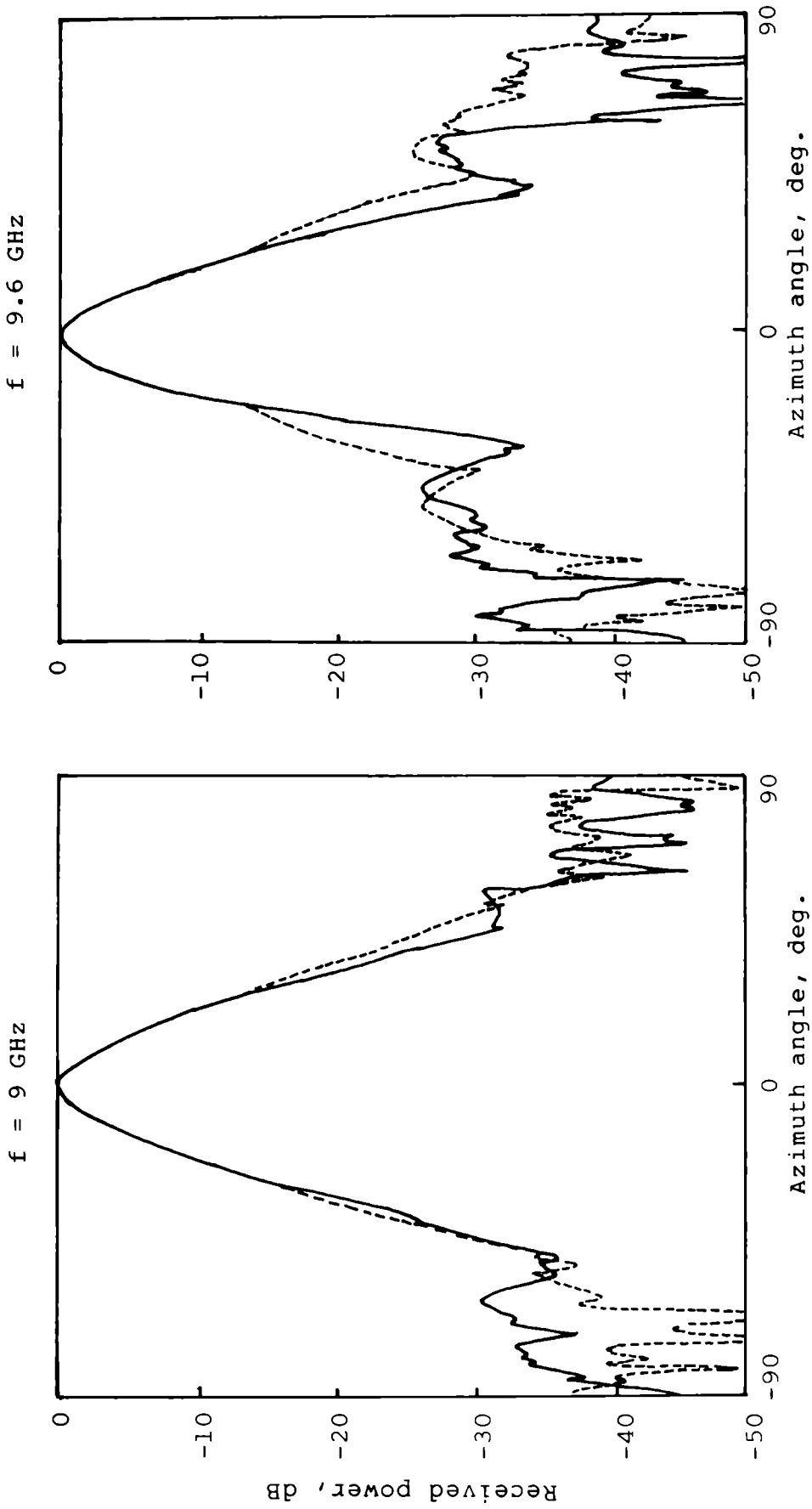
Fig.4.65(a): E-plane radiation patterns of SSF horn antenna and MCH antenna at different frequencies

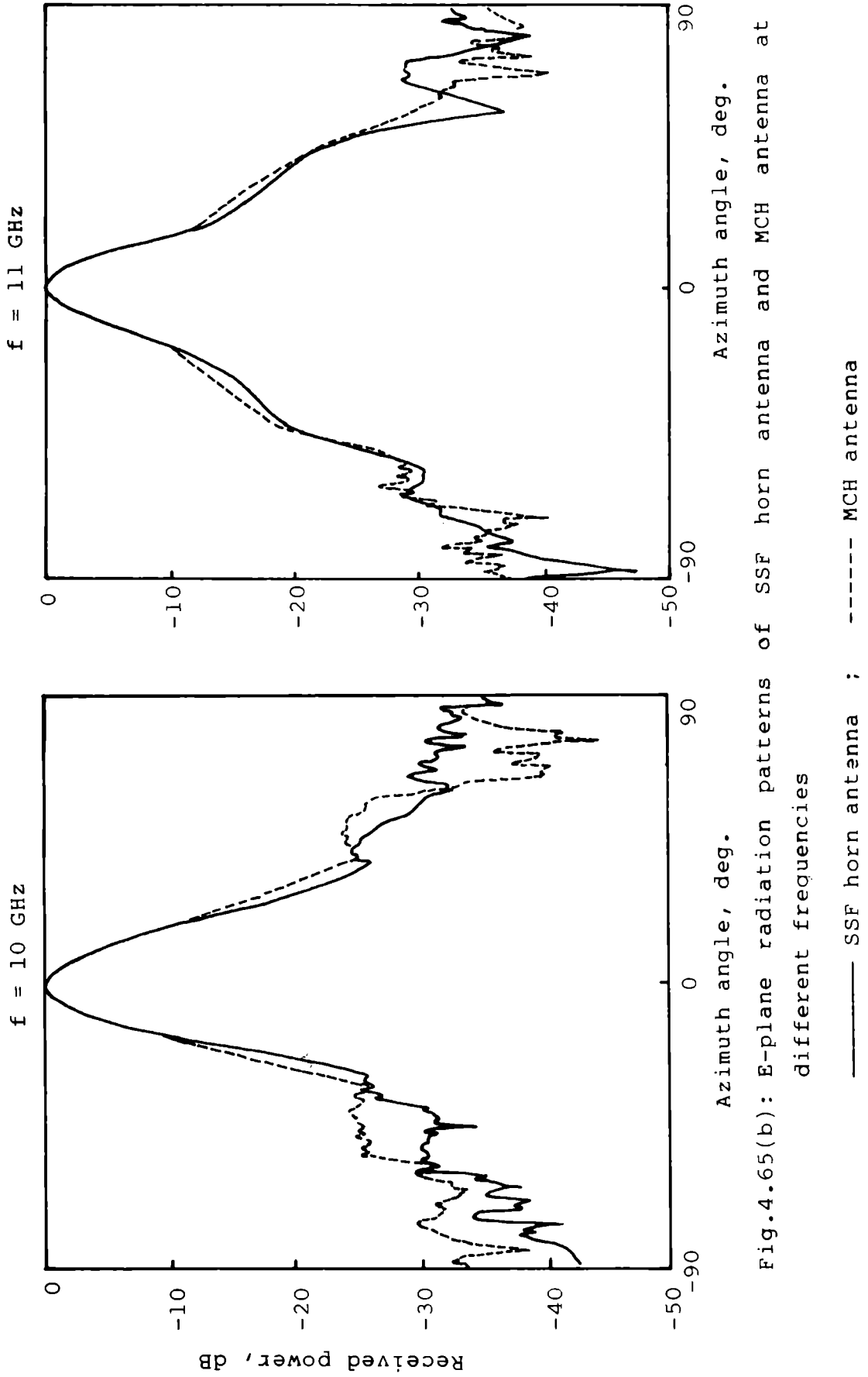————— SSF horn antenna ; ------- MCH antenna

Fig.4.65(b): E-plane radiation patterns of SSF horn antenna and MCH antenna at different frequencies

————— SSF horn antenna ;   —————— MCH antenna

distribution of the horns, almost in the entire 9 GHz to 12 GHz frequency range, the SSF horn antenna shows a slight improvement than the MCH antenna. At the design frequency, 10 GHz, the sidelobe level of the SSF horn antenna is -25 dB, whereas, that exhibited by the MCH antenna is -24 dB. Eventhough, above 10.2 GHz, the backlobe level of the SSF horn antenna is slightly higher than that of the MCH antenna, in the entire 8 GHz to 12 GHz frequency range, the observed maximum backlobe level of the SSF horn antenna is -29 dB.

The frequency response of the cross-polarisation levels of both the horns are presented in figure 4.67. Here also, in the entire frequency band of interest, 8 GHz to 12 GHz, the SSF horn antenna shows better character- istics than the MCH antenna. The maximum cross-polar level exhibited by the SSF horn antenna in the above frequency range is -24.3 dB, whereas that exhibited by the MCH antenna is -23 dB.

The typical variation of the 3 dB and 10 dB beamwidths of the two horns with frequency is shown in figure 4.68. From the figure it is well understood that, in the entire 8 GHz to 12 GHz frequency range, the 3 dB and 10 dB beamwidths variations of both the horns are identical.

Sidelobe level, dB   Backlobe level, dB

Frequency, GHz

—•— Sidelobe level-SSF   —+— Sidelobe level-MCH

—*— Backlobe level-SSF   —□— Backlobe level-MCH
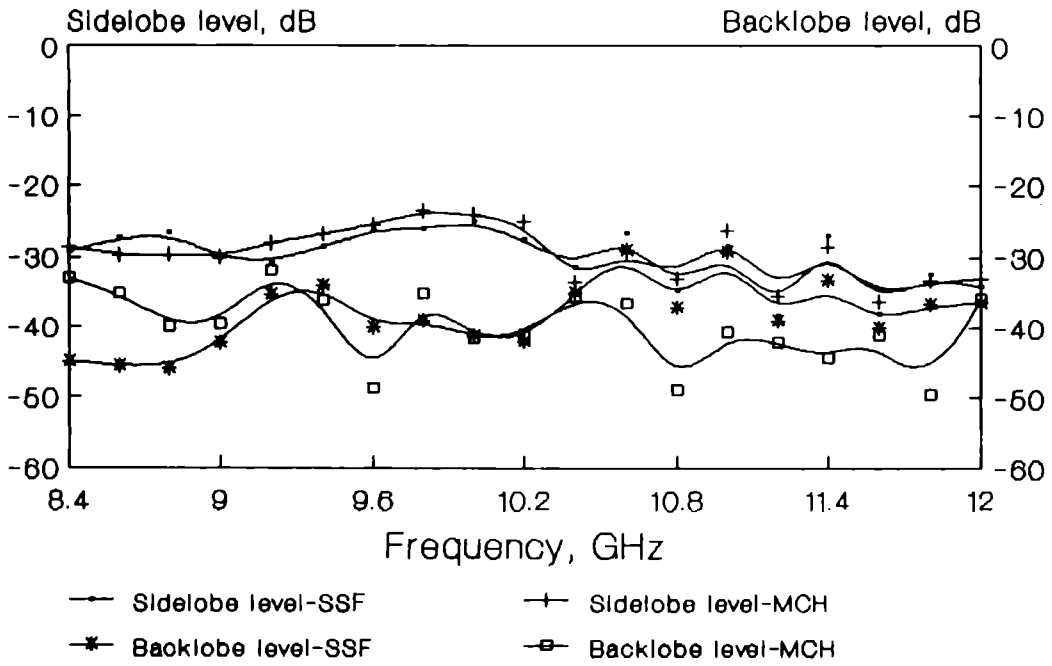
Fig.4.66: Variation of sidelobe and backlobe levels
of horns SSF and MCH with frequency

Cross-polar level, dB
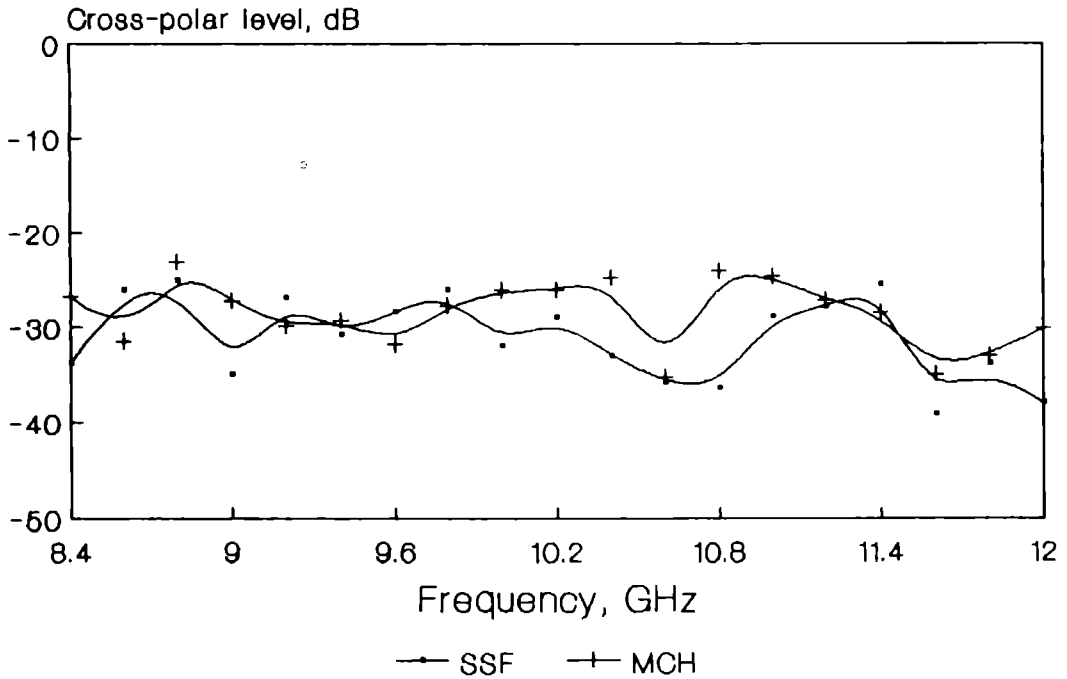

Frequency, GHz

—•— SSF   —+— MCH

Fig.4.67: Variation of cross-polarisation level of
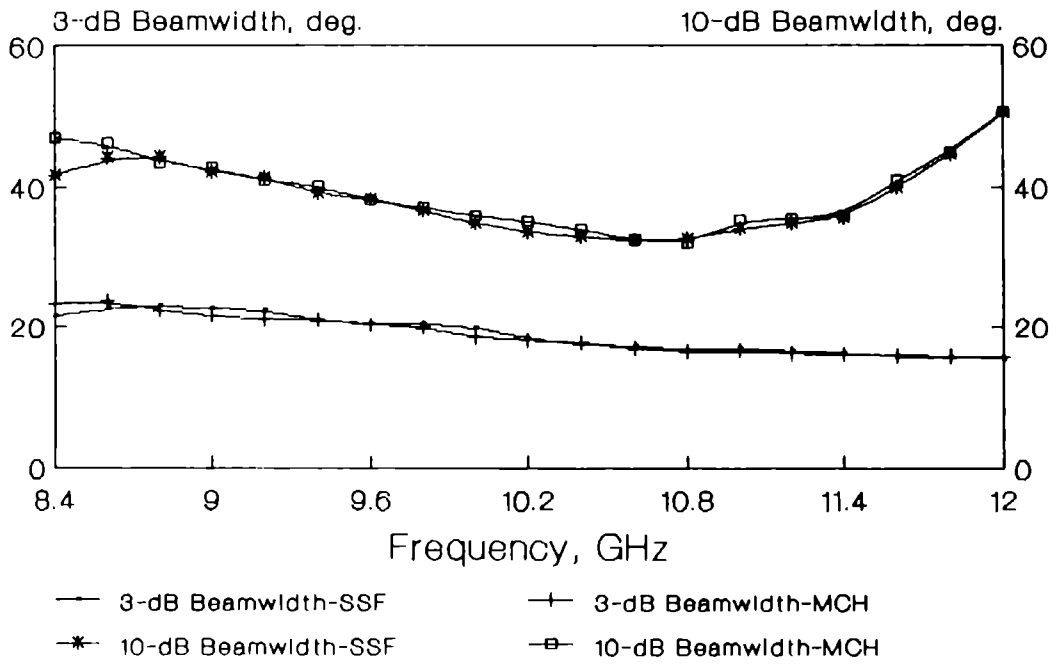hrons SSF and MCH with frequency

Fig.4.68: Variation of 3 dB and 10 dB beamwidths of horns SSF and MCH with frequency

The return-loss variation of the MCH antenna with frequency is given in figure 4.69. In this case, compared to the case of SSF horn antenna (figure 4.63) the MCH antenna shows slightly better matching characteristics.

The typical variation of gain of the two horns with frequency is plotted in figure 4.70. Throughout the 8 GHz to 12 GHz frequency band the gain variations of the two horns are almost identical in nature. The slight reduction of gain observed in the case of SSF horn antenna may be due to the dissipation of power in the dielectric substrate used for its E-plane wall construction.

The comparative study of the radiation character-istics of the SSF horn antenna and the corresponding identical MCH antenna has validated the simulating behaviour of the SSF horn antenna. Moreover, compared to the metallic corrugated horn antenna, the newly developed "Simulated Scalar Feed" horn antenna possesses the advantages of low production cost, ease of fabrication, light-weight etc. Mass production of this type of simulated scalar feeds with the required precision in the strip parameters is inexpensively possible if photolitho-graphic technique is employed.
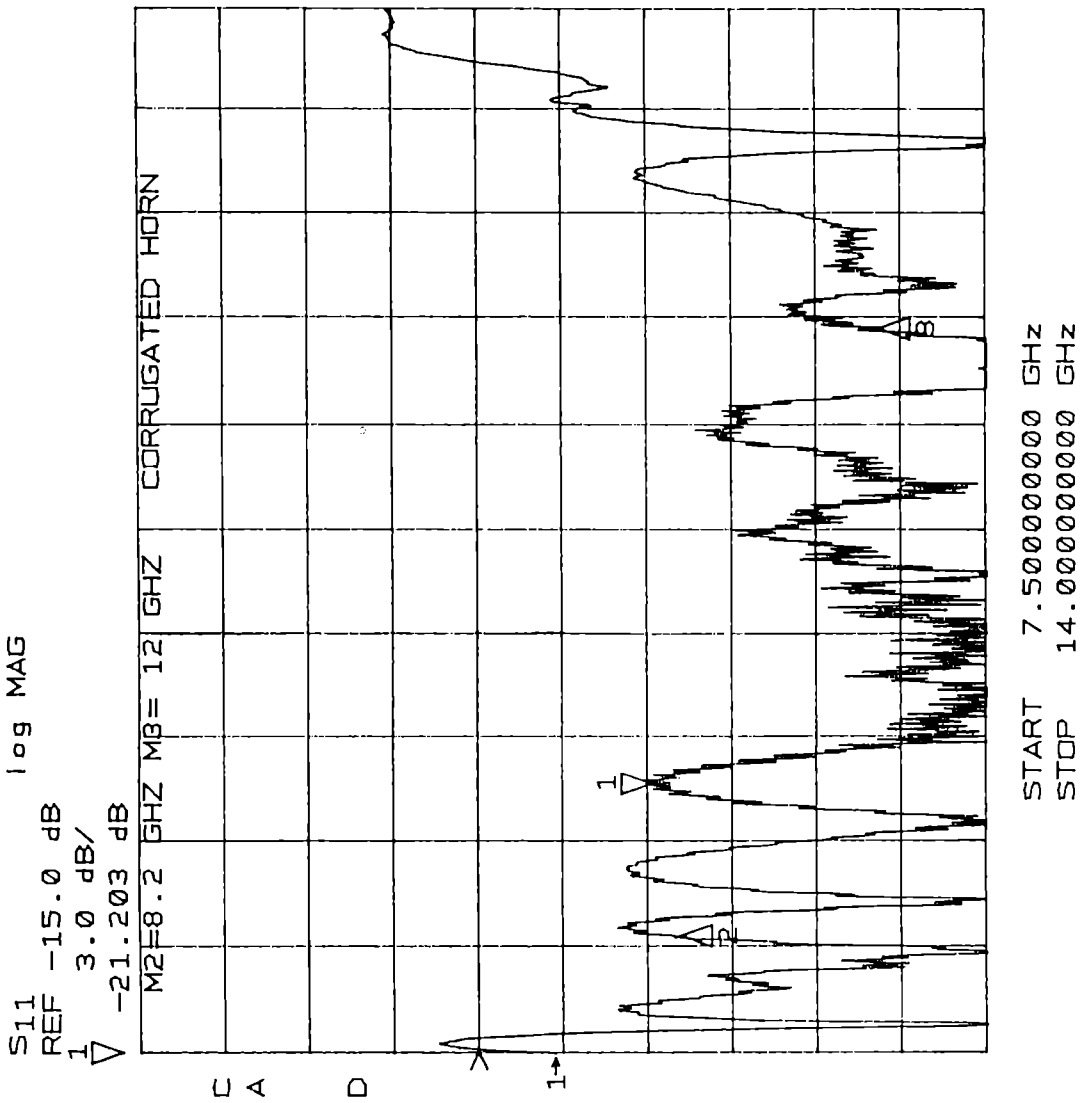
Fig.4.69: Variation of return-loss of MCH antenna with
          frequency
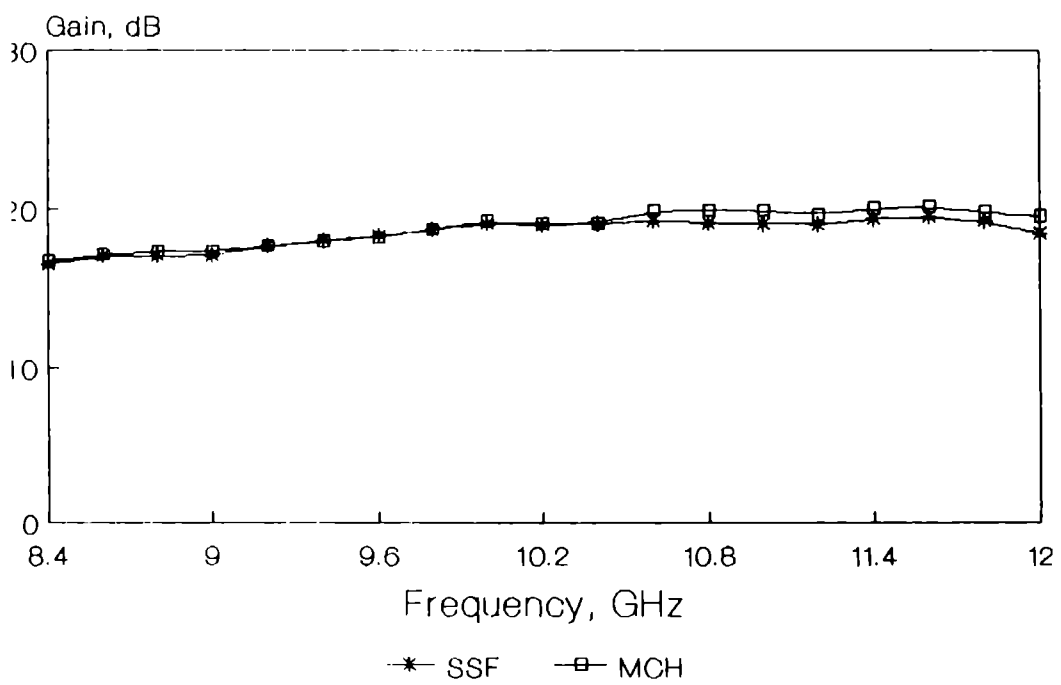
Fig.4.70: Variation of gain of horns SSF and MCH with frequency

As the newly developed scalar feed horn antenna is simulating the radiation characteristics of an identical metallic corrugated horn antenna, the theoretical explanation of the newly developed scalar feed horn antenna is tried on the basis of the theory of metallic corrugated horn antennas with appropriate modifications.   The theoretical analysis is presented in the next chapter.

Chapter 5

THEORETICAL ANALYSIS

Chapter 5

THEORETICAL ANALYSIS

Theoretical explanation for the E-plane radiation
patterns of newly developed simulated scalar feed horn
antenna is presented in this chapter. A comparative study
of the experimental results of the simulated scalar feed
horn antenna with those of an identical metallic corrugated
horn antenna has showed that the simulated scalar feed is
simulating the radiation characteristics of the metallic
corrugated horn antenna. Hence the theoretical explanation
is based on the theory of metallic corrugated horn antenna
with appropriate modifications. A comparison between the
experimental   and   the   theoretically   computed   E-plane
radiation   patterns   of   the   simulated   scalar   feed   horn
antenna at different frequencies in X-band is given as the
last part of this chapter.

5.1   ANALYSIS OF E-FIELD DISTRIBUTION OF E-PLANE APERTURE

It   is   well   known   that   the   E-plane   aperture
electric field distribution of a metallic corrugated horn
antenna whose corrugation depth is judiciously selected for
the balanced hybrid mode of operation is cosine in nature.

In the present investigation, the E-plane aperture electric field distribution of the newly developed simulated scalar feed is also found to be almost cosine in nature. This is well understood from the comparison of E-plane electric fields of the SSF horn antenna and the identical metallic corrugated horn antenna. [Section 4.9; figures 4.65]. Hence, as stated earlier, the E-plane radiation patterns of the present SSF horn antenna are explained on the basis of theory of metallic corrugated horn antennas.

In order to calculate the radiation pattern, first the E-plane aperture electric field distribution of a square waveguide with simulated corrugated surface as its E-plane boundary walls is calculated. For this, the theory suggested by Dragone [104] in the case of a metallic corrugated waveguide is used. Once the aperture electric field is obtained, the flaring of the horn in the two principal planes are also accounted and the E-plane far-field radiation patterns are calculated on the basis of vector diffraction formula.

The sketch of the waveguide with strip-grating structure on its E-plane boundary walls is shown in figure 5.1. The waveguide is directed along Z-axis and ν and τ
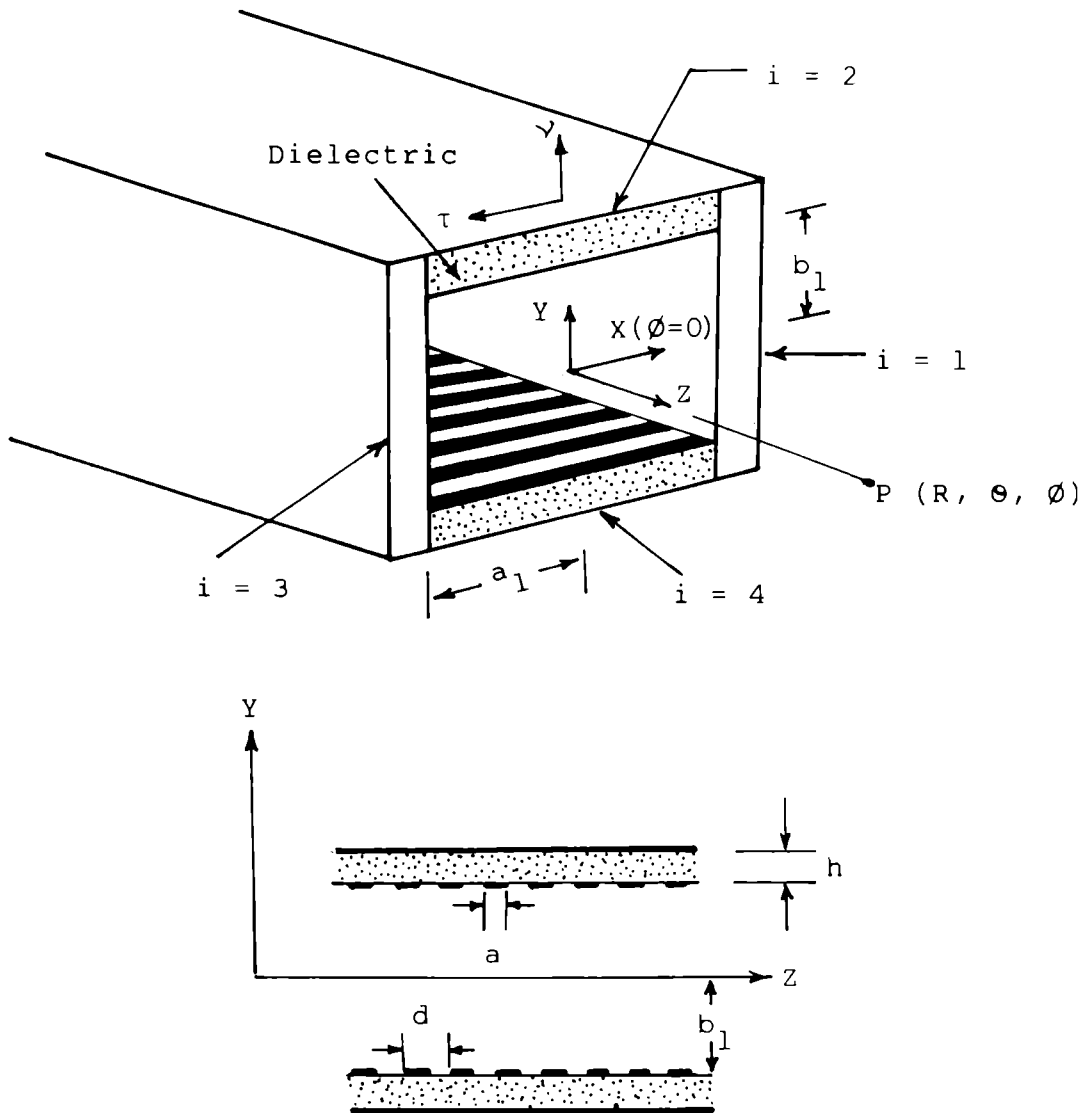
Fig.5.1: Sketch of a waveguide with strip-grating structure on its dielectric E-plane walls

are the unit vectors which are respectively directed normally and tangentially to the boundary surface such that $\tau = I_z \times \nu$, where I_z is the unit vector along Z-axis.

The surface impedances Z_τ and Z_z are defined by the longitudinal field components E_τ and H_τ and are given by,

$$Z_\tau = \frac{E_\tau}{H_z} \qquad \text{and} \qquad Z_z = \frac{E_z}{H_\tau} \qquad (5.1)$$

Since at the boundary surface. $E_\tau = 0$, only the impedance Z_z exists. However, as Z_z is imaginary, a real parameter Y is introduced and it is defined as,

$$jY = \frac{Z}{Z_z} \qquad (5.2)$$

where $Z = \sqrt{\mu/\epsilon}$ is the free space impedance.

As per the indices given to the four walls of the waveguide in figure 5.1, Y_n denote Y of the nth wall. Since the opposite walls are identical in nature, $Y_1 = Y_3$ and $Y_2 = Y_4$. Now for a wave polarised in the Y direction, $Y_1 = \infty$. Then the transverse components of the electric field are given by,

$$E_x = 0 \; ; \qquad E_y = \cos \alpha x \, \cos \gamma y \; e^{-j\beta z} \qquad (5.3)$$

where α, β and γ are the propagation constants.

Other field components can be determined using Maxwell's equations:

$$E_z = \frac{j\omega\mu}{\beta} \cos \alpha x \, \cos \gamma y \; e^{-j\beta z}$$

$$H_x = -\frac{1}{\beta}(\epsilon\omega + \frac{\alpha^2}{\omega}) \cos \alpha x \, \cos \gamma y \; e^{-j\beta z}$$

$$H_y = \frac{\alpha\gamma}{\omega\beta} \sin \alpha x \, \sin \gamma y \; e^{-j\beta z}$$

$$H_z = \frac{j\alpha}{\omega} \sin \alpha x \, \cos \gamma y \; e^{-j\beta z} \qquad (5.4)$$

For the dominant HE_{11} mode,

$$\alpha \, a_1 = \pi/2$$

As E_z varies with x as $\cos \alpha$ x, we get

$$\gamma_2 = \frac{-1}{1-a/d} \; \frac{\gamma_c}{k \, \tan(\gamma_c h)} \qquad (5.5)$$

where $\gamma_c^2 = k^2 - \alpha^2$

k is the free-space propagation constant. As stated earlier, for the dominant HE_{11} mode, for large ka_1 and kb_1

$$\alpha\, a_1 \;=\; \pi/2 \quad \text{and} \quad \gamma\, b_1 \;=\; \pi/2(1-\frac{\gamma_2}{kb_1}) \tag{5.6}$$

In the case of a square waveguide, $a_1 = b_1$.

Hence, the aperture electric field of the waveguide under consideration is given by the equation,

$$E_y \;=\; \cos\alpha x \;\; \cos\gamma y \;\; e^{-j\beta z} \tag{5.7}$$

5.2 ANALYSIS OF FAR-FIELD E-PLANE RADIATION PATTERNS

Equation (5.7) is the E-plane aperture electric field distribution of the waveguide fabricated with strip-loaded dielectric substrate as its E-plane boundary walls. In the case of a horn antenna, due to the flaring, a quadratic phase shift for the aperture field along the aperture is accounted by the factor $e^{-j4\pi y^2/\lambda L}$. Incorporating this quadratic phase variation, the E-plane aperture electric field of the horn antenna is given by,

$$E'_y \;=\; \cos\alpha x \, \cos\gamma y \;\; e^{-j\beta z}\, e^{-j4\pi y^2/\lambda L} \tag{5.8}$$

In the above expression, L is the distance from the phase centre to the aperture of the horn. As a rectangular to square waveguide transition is used to feed the SSF horn antenna, the effective phase centre of the SSF horn antenna along with the transition is experimentally determined by plotting its phase patterns for different axes of rotation. The E-plane radiation pattern of the SSF horn antenna along with its phase pattern plotted for at an axis of rotation of L = 18 cm at 10 GHz is given in figure 5.2.

The far-field radiation pattern in the E-plane ($\emptyset = \pi/2$) of the simulated scalar feed horn antenna, based on the vector diffraction formula [80,166,169] is given by,

$$E_\theta = \frac{jk \exp (-jkR)}{\pi R} (1 + \frac{k_r}{k}\cos \theta)\iint_S E'_y \exp(jky \sin \theta)dx.dy$$

(5.9)

where $k_r = (k^2 - \pi^2/4a_1^2)^{\frac{1}{2}}$

The theoretically calculated E-plane radiation patterns compared with the experimental ones at different frequencies in X-band are given in figures 5.3 and 5.4. The theoretically obtained 3 dB and 10 dB beamwidths of the SSF
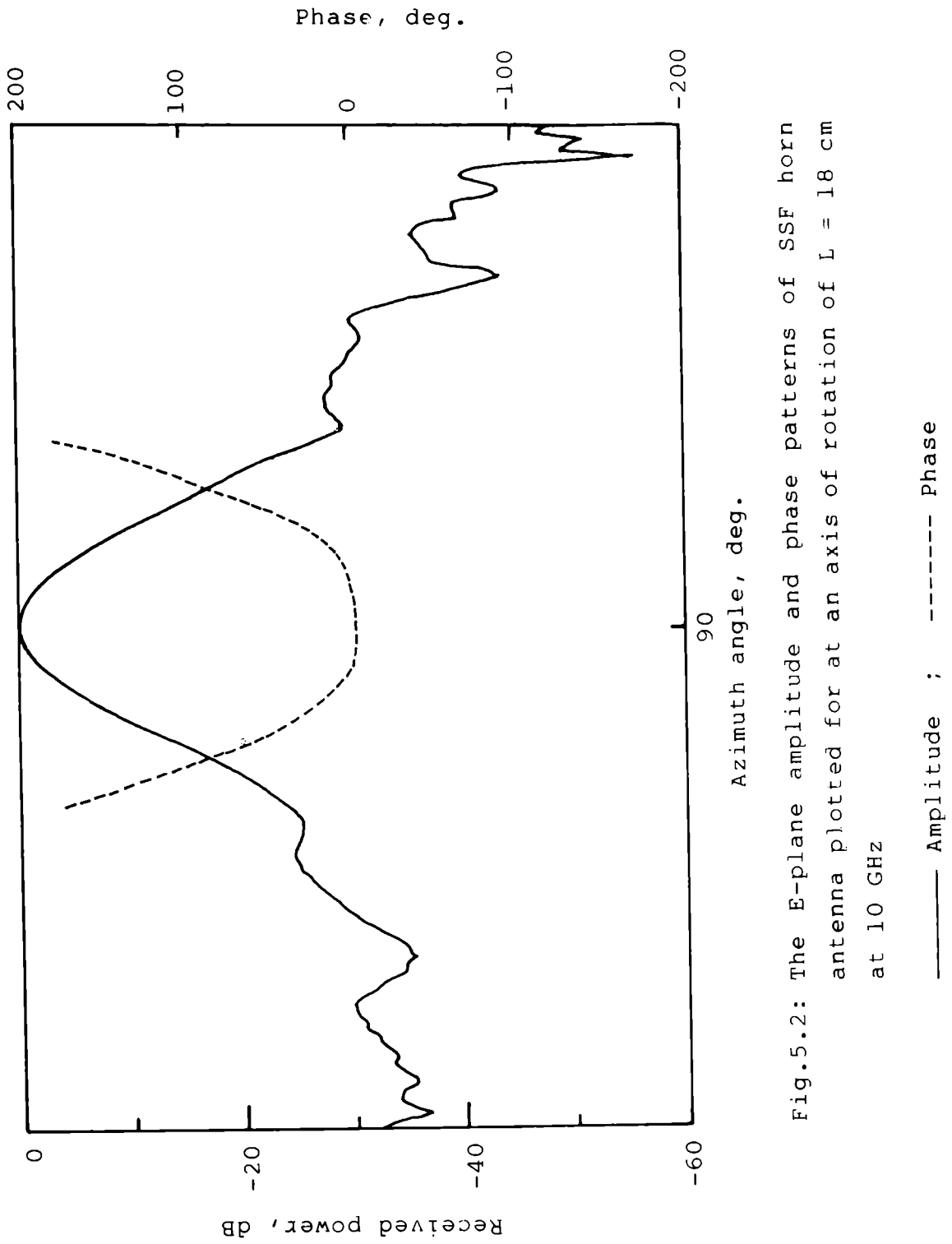
Fig.5.2: The E-plane amplitude and phase patterns of SSF horn antenna plotted for at an axis of rotation of L = 18 cm at 10 GHz

————— Amplitude ;   ------ Phase

f = 9.6 GH

f = 9 GHz

Received power, dB

Azimuth angle, deg.

Azimuth angle, deg.
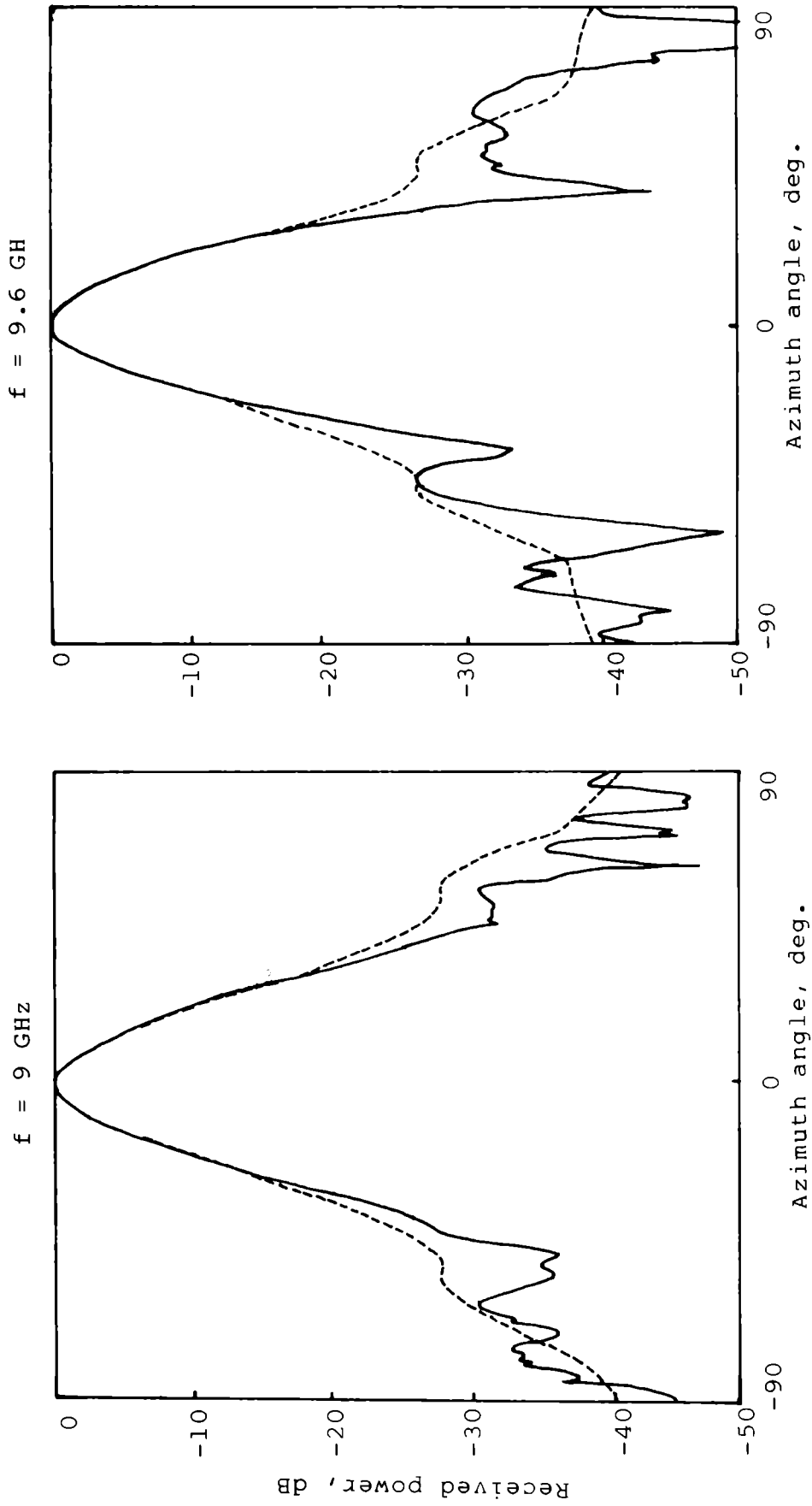
Fig.5.3: E-plane radiation patterns of SSF horn antenna

————— Experimental ; ———— Theory

217
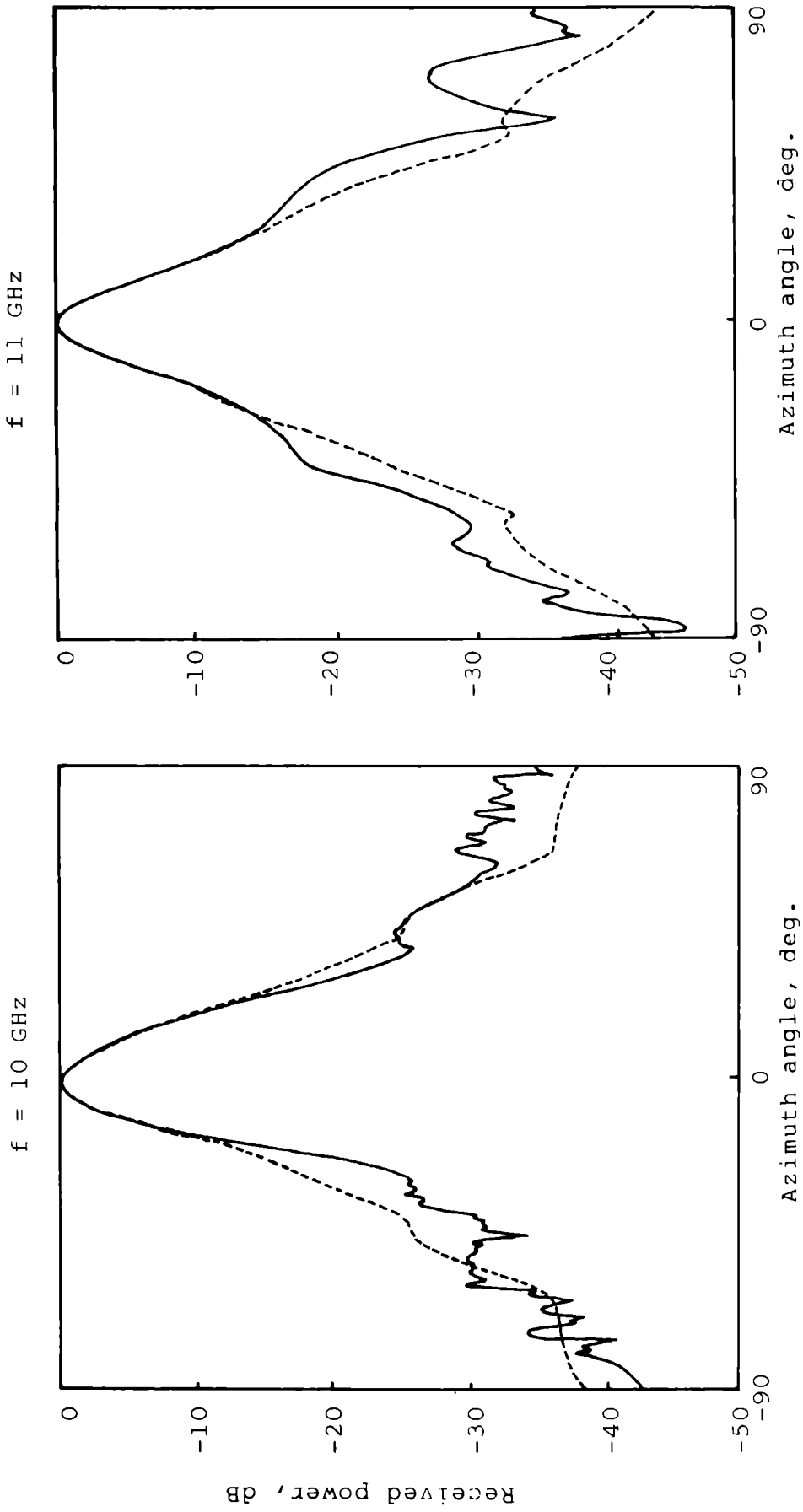
Fig.5.4: E-plane patterns of SSF horn antenna

——— Experiment ; ------ Theory

horn antenna compared with that of the experimental ones are presented in the table 5.1. From the table it is clear that the theoretical beamwidths are almost agreeing with the experimental values. In the theoretical calculations, the fields within the dielectric substrate are neglected. This may be the reason for the small discripencies between the theoretical and experimental radiation patterns. Eventhough the theoretical calculations cannot predict the nulls of the patterns, the main beams are well predicted with a good accuracy.

Table 5.1: Comparison of theoretical and experimental 3 dB
and 10 dB beamwidths of the SSF horn antenna

Frequency (GHz)	3 dB BEAMWIDTH (DEG.)		10 dB BEAMWIDTH (DEG.)	
	Theory	Experiment	Theory	Experiment
8.4	23.6	21.6	42.2	41.7
9.0	22.1	22.8	39.9	42.2
9.4	20.6	20.9	38.0	39.2
10.0	18.8	20.0	36.0	34.9
10.4	17.5	17.4	36.0	33.0
10.8	18.1	16.6	36.5	32.6
11.2	16.2	16.5	37.0	34.9
11.6	15.4	15.7	36.5	40.0
12.0	15.4	15.5	37.0	50.0

Chapter 6

CONCLUSIONS

Chapter 6

CONCLUSIONS

6.1 INTRODUCTION

The conclusions drawn and the comments on the results of the investigations carried out for the development of the 'Simulated Scalar Feed' horn antenna are presented. The advantages of the newly developed simulated scalar feed horn antenna over the existing feed horn antennas are examined in this chapter. The chapter concludes with the description of scope for further work in the field of simulated scalar feed horn antennas.

6.2 CONCLUSIONS FROM EXPERIMENTAL INVESTIGATIONS

From the experimental observations, it has been found that horns with E-plane wall thickness $\lambda/4\sqrt{\epsilon_r}$ are poor in gain characteristics compared to identical conventional horns. However, if one is interested only in sidelobe supression, this technique is successful upto a certain level.

Pyramidal horns with rectangular throat and square aperture are investigated later. They are fabricated with

221

tapered E-plane walls whose mean thicknesses satisfied the balanced hybrid mode condition $\lambda/4\sqrt{\epsilon_r-1}$ at their corresponding design frequencies. As the balanced hybrid mode condition is satisfied at their design frequencies, compared to the identical conventional horn, these horns have showed considerable improvements in their radiation characteristics. Though the return-loss characteristics of these horns are slightly deteriorated, around design frequencies, they are well within the tolerable limits. In the entire 8 GHz to 12 GHz frequency range, the gain characteristics of the horns are found to be considerably better than that of the identical conventional horn.

Pyramidal horn with square throat and aperture is also constructed and studied. The E-plane walls of this horn are fabricated from a flat dielectric substrate satisfying the balanced hybrid mode condition at 11.5 GHz. At the throat region of this horn, about one wavelength portion of the E-walls are metallised. Experiment is repeated for different metallisation lengths at the throat region of E-plane walls. It is found that the optimum metallisation length required at the throat region is nearly equal to one wavelength. In brief, it can be concluded that some of the radiation characteristics of a

strip-loaded horn can be controlled by simply adjusting the extent of metallisation of E-plane walls at its throat region.

Since the H-plane walls of the horns investigated are not altered, the H-plane radiation patterns are found to be identical to that of corresponding identical conventional horns.

To study the possibility of obtaining improvement in impedance matching, a square pyramidal horn with tapered dielectric E-plane walls is fabricated. The mean thickness of the E-plane wall of this horn satisfied the balanced hybrid mode condition at 9.2 GHz. The radiation characteristics like sidelobe level, bakclobe level, cross-polarisation level and return-loss of this horn are found to be considerably improved than that of earlier horns and the identical conventional horn. The exhibited improvements in its radiation characteristics may be due to the tapered nature of its E-plane walls.

In order to explore further improvements in the radiation characteristics, especially in impedance matching, two square pyramidal horns with a $\lambda/2\sqrt{\epsilon_r - 1}$ to

$\lambda \big/ 4 \sqrt{\epsilon_r - 1}$ tapering structure in the vicinity of the throat region are fabricated and tested. For the first horn this tapering is at the interior side of the horn, whereas for the second one it is at the exterior side of the horn. The return-loss studies of both the horns have clearly proved that the abrupt angular variation caused by the interior tapering is not degrading its matching characteristics as expected. Both the horns are found to be exhibiting good sidelobe level characteristics in the lower side of the 8 GHz to 12 GHz frequency region. This is due to the fact that the design frequency, 8.4 GHz, of both the horns is also at the lower side of the frequency region considered. The radiation characteristics of the horn having exterior tapering are found to be slightly better than that of the horn with interior tapering.

The SSF horn antenna is found to be well matched with a maximum return-loss of -17.29 dB in the useful X-band region. Compared to the identical conventional horn, its gain characteristic is considerably improved. From the analysis of the experimental results it is clear that the SSF horn antenna is simulating the radiation characteristics of a scalar feed horn like a metallic corrugated horn antenna.

In order to validate the observed radiation characteristics of the SSF horn antenna, its radiation characteristics are compared with that of a metallic corrugated horn antenna fabricated with identical physical dimensions and design criteria. The comparative study of the E-plane aperture electric field distributions, E-plane radiation patterns and other radiation characteristics like sidelobe, backlobe and cross-polar levels and also the 3 dB and 10 dB beamwidths of both the horns has showed that they are exhibiting identical radiation characteristics. Compared to the metallic corrugated horn, the slight reduction of gain observed in the case of SSF horn antenna may be due to the dissipation of power in the dielectric substrate used for its E-plane wall construction.

Compared to the metallic corrugated horn antenna the newly developed simulated scalar feed horn antenna possesses advantages like light-weight, low production cost, ease of fabrication etc. Mass production of this class of feed horn antennas with the required precision in the strip parameters of grating structure is inexpensively possible if the techniques of photolithography and etching are employed.

6.3 CONCLUSIONS FROM THEORETICAL ANALYSIS

The theoretical explanation of the SSF horn antenna is based on the theory of metallic corrugated horn antennas as suggested by Dragone with appropriate modifications. Eventhough the nulls of the radiation patterns were not fully realised by this theory, the main beam characteristics are well explained. Losses that may occur in the dielectric substrate of the E-plane walls of the SSF horn antenna are not considered in the theoretical explanation. This may be the cause of slight discripencies observed in the theoretical and experimental 3 dB and 10 dB beamwidths.

6.4 SCOPE OF FURTHER WORK IN THE FIELD

Though the newly developed strip-loaded SSF horn antenna is a square pyramidal horn antenna, beam symmetry is not observed in its E and H-plane radiation patterns. The possibility of obtaining symmetrical radiation patterns in the two principal planes can be explored. Moreover, in the present SSF horn antenna, conducting strips are loaded transversely (with respect to the axis of the horn) in the E-plane boundary walls. The effect of longitudinal or

inclined orientation of the conducting strips can be investigated. The possibility of obtaining elliptically or circularly polarised wave by the use of 45° orientation of strips can also be investigated.

In the present investigation, only the E-plane boundary walls of the SSF horn antenna are fabricated with strip-loaded dielectric walls. The same technique can be employed on the H-plane boundary walls of the horn and its effect on H-plane radiation patterns can be studied. Such strip-loaded surfaces can also be used for fabricating sectoral horn antennas and the resulting radiation characteristics can be studied.

Appendix I

DEVELOPMENT OF A NEW REFLECTING POLARISER

FOR E.M. WAVES

Appendix 1

DEVELOPMENT OF A NEW REFLECTING POLARISER FOR E.M.WAVES

A1.1 INTRODUCTION

Metallic surfaces with rectangular corrugations have many applications in antenna engineering, especially in the design of corrugated feed horn antennas. This type of reflecting surfaces are also capable of rotating the plane of polarisation of an incident linearly polarised electromagnetic wave or producing a circularly polarised wave [92,97]. However, the fabrication of such metallic corrugated surface with the required precision is a time consuming and tedious job. Moreover, a large amount of material is wasted in the process of fabrication. The possibility of obtaining identical results from alternative reflecting surfaces which are less expensive and easier to fabricate are explored and the experimental results of the investigation are presented here.

The newly developed reflecting surface is found to be simulating identical properties of a metallic corrugated reflecting surface. Hence it is termed as "Simulated Corrugated Reflecting Surface" (SCRS). Compared to a

228

metallic corrugated surface, the SCRS is less expensive, easy to fabricate and lighter.

A1.2 DESIGN DETAILS OF SCRS

The schematic representation of a SCRS is given in figure A1.1. One surface of a low-loss dielectric plate of uniform thickness 'h' is periodically loaded with thin conducting wires (or strips) at a period 'd' and gap 'g'. The parameter 'd' is such that d $< \lambda/2$, so that higher order modes are not propagated. 'λ' is the free-space wavelength of the incident electromagnetic wave. The other surface of the dielectric plate is completely metallised with copper. Depending on the grating parameters g, d and the thickness 'h' of the dielectric plate, the SCRS is found to be capable of tilting the plane of polarisation of the incident wave or producing circular polarisation.

The phenomenon of rotation of plane of polarisation of a linearly polarised incident wave or production of circular polarisation is qualitatively explained as follows. As stated earlier, if the linearly polarised incident electric field is at an angle of $\emptyset = 45°$ to the length of the strips, it can be resolved into two components namely TE (component parallel to the length of
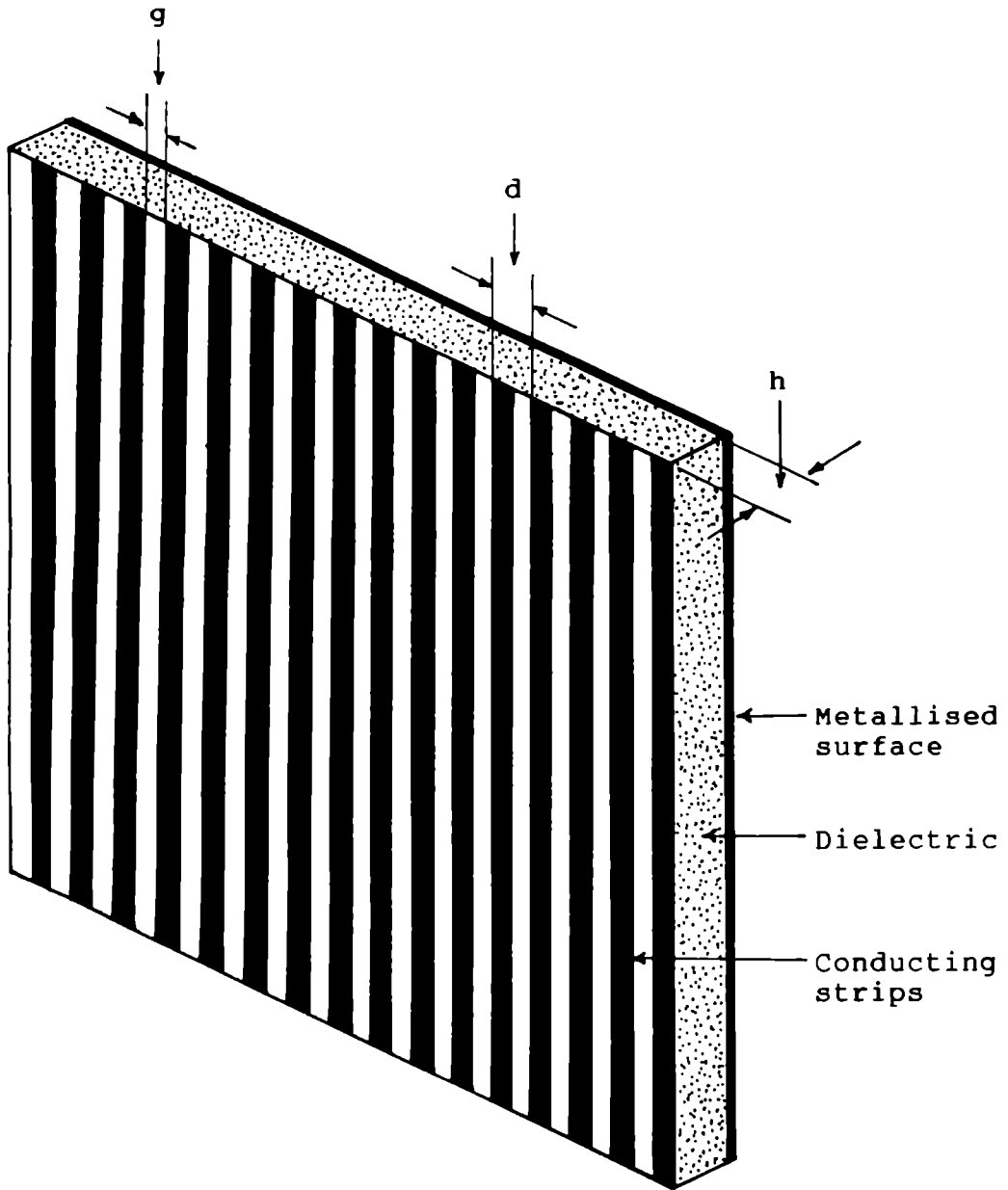
Fig.A1.1: Schematic representation of a simulated
corrugated reflecting surface

the strip) and TM (component perpendicular to the length of the strip) components. During reflection, the TE component is totally reflected from the top of the conducting strips, while the TM component penetrates into the dielectric substrate and gets reflected from the conducting ground plane. Hence, the reflected TM component is lagging the corresponding TE component by a phase of $4\pi h/\lambda_d$, where λ_d is the wavelength inside the dielectric medium. By adjusting the thickness 'h' of the dielectric plate, any desired polarisation can be achieved at a particular frequency.

A1.3 EXPERIMENTAL ARRANGEMENT

The experimental arrangement used for measuring the polarisation characteristics of the wave reflected from the SCRS is shown in figure A1.2. The equipment used and the measurement technique employed for the polarisation study are discussed in the following sections.

A1.3.1 The Transmitter

A small X-band rectangular pyramidal horn antenna of high cross-polarisation discrimination of -30 dB is used as the transmitting antenna of electromagnetic radiation.
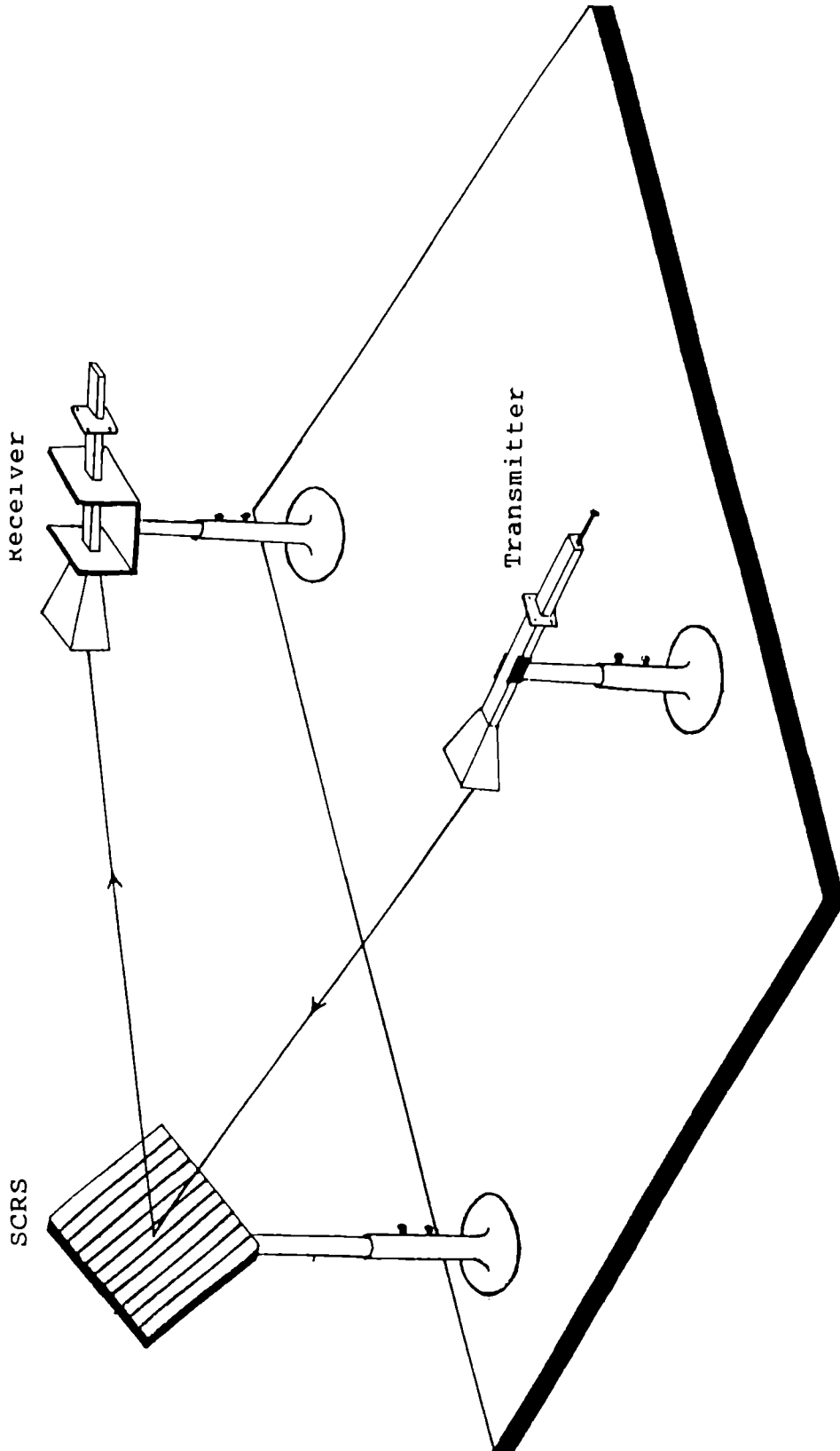
Fig.Al.2: Experimental arrangement for measuring the polarisation characteristics of waves reflected from SCRS

A1.3.2 The Receiver

Another small X-band rectangular pyramidal pick-up horn antenna is employed for receiving the reflected waves from the SCRS. This pick-up horn is mounted on a polarisation positioner, which can be automatically rotated about its axis using a remote control unit.

In order to avoid the direct coupling between the transmitting and receiving antennas, they are placed in such a way that the angle of incidence is 9° as suggested by Jull [92] for corrugated plate. Moreover, for total elimination of the coupling, microwave absorbing materials are interposed between them. It has been established that, for angles of incidence less than 10°, the differential change in phase shift between the TE and TM components is less than 1°. Hence the above experimental arrangement nearly satisfies the condition of normal incidence. The entire experiment is conducted in a microwave anechoic chamber.

A1.3.3 Antenna Polarisation Positioner

For studying the polarisation characteristics of the reflected wave, it is necessary to rotate the receiving antenna about its axis. A motorised antenna polarisation
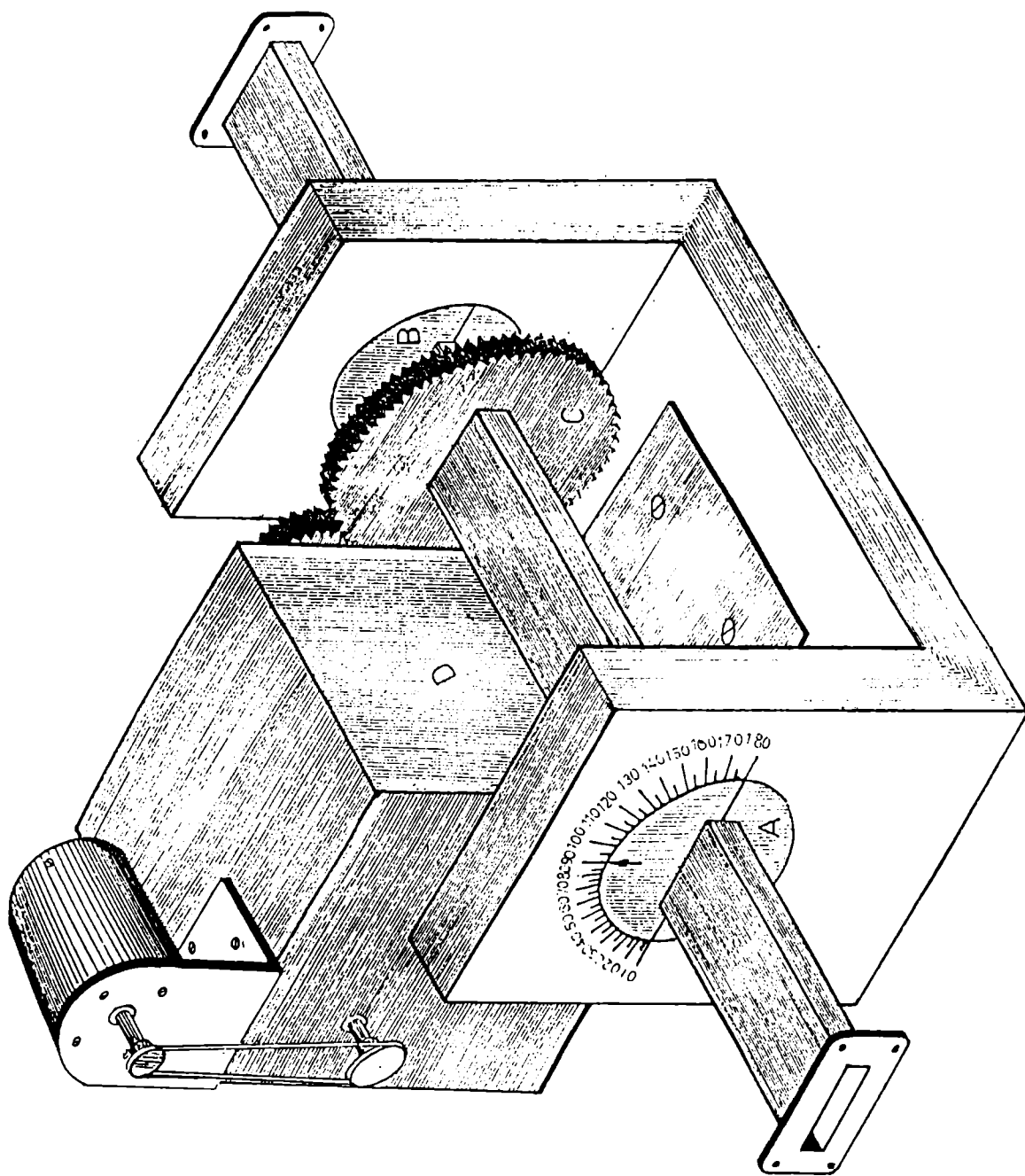
Fig.Al.3: View of the antenna polarisation positioner

positioner with a remote control facility is used for this purpose. A view of the antenna polarisation positioner is given in figure Al.3. In this, a rectangular waveguide piece is passed through two bearings A and B which are fitted on a metallic frame. One of the ends of the waveguide piece is connected to a pyramidal horn and the other end to a crystal detector with an adjustable short. The circular tooth wheel fitted to the waveguide is coupled to the gear box D. The gear box is connected to a 6 V DC motor through a pulley and belt. A wire wound linear potentiometer connected to the end of the adjustable short rotates in synchronization with the horn.

Al.3.4 X-Y Plotter

The signal received by the receiver antenna mounted on the polarisation positioner is plotted using an HP 7047A X-Y plotter. For this, the DC voltage from the potentiometer connected to the end of the adjustable short of the receiver horn is given to one of the axes of the X-Y plotter. The signal detected by the crystal detector of the receiving horn is given to the other axis of the plotter. Hence, as the receiver horn mounted on the polarisation positioner is rotated through 360°, the signals received at different angular positions of the

receiver horn in a vertical plane can be plotted. This plot between the received signal and the angle of rotation is the polarisation pattern of the wave reflected from the SCRS.

A1.4 EXPERIMENTAL RESULTS

This section is presented into two parts. In the first part, the experimental results of SCR surfaces which are capable of converting a linearly polarised incident electromagnetic wave into a circularly polarised wave are presented. In the second part, the experimental results of an SCRS which tilts the plane of polarisation of an incident linearly polarised e.m. wave are discussed.

A1.4.1 Production of Circularly Polarised Waves

The experimental arrangement shown in figure A1.2 is employed to study the circular polarisation characteristics of the waves reflected from the SCR surfaces of different grating parameters and dielectric thickness. The design parameters of the different SCR surfaces used for the experimental investigation are given in the table A.1.

Table Al.1:   Design parameters of different SCR surfaces
               investigated

SCR surface	d/λ	h/λ	g/d	Frequency (GHz)
1.a	0.093	0.1085	0.96	9.3
1.b	0.165	0.1155	0.96	9.9
2.a	0.1092	0.1092	0.96	10.92
2.b	0.1958	0.1175	0.96	11.75
3.a	0.1373	0.103	0.892	10.3
3.b	0.1587	0.0992	0.892	11.9

The typical variation of axial ratio with frequency of the reflected wave from the different SCR surfaces investigated are presented in figures Al.4 to Al.6. From the figures it is evident that the newly developed SCR surfaces are almost capable of producing circularly polarised wave by reflection. When h = d = 0.1092λ, and g/d = 0.96, the minimum axial ratio obtained is 0.145 dB at 10.92 GHz. For analysing the sense of circular polarisation of the reflected wave, left and right handed circularly polarised helical antennas were used as the receivers. The observations have showed that when the conducting wires or strips of the grill structure on the surface of the dielectric substrate is at an angle of 135° with respect to the H-vector in the clockwise direction, a left handed circular polarisation is obtained. On the other hand, when this angle is 45°, a right handed circular polarisation is resulted.

Al.4.2 Rotation of Plane of Polarisation by SCRS Technique

It has been observed that, for an optimum dielectric substrate thickness, the SCR surfaces are producing circularly polarised waves for g/d ≃ 1. However, when the value of q/d is decreased, the SCRS is found to be

Fig.Al.4: Variation of axial ratio with frequency of SCR surfaces l.a and l.b.

l.a ; d/ λ = 0.093, h/ λ = 0.1085, g/d = 0.96

l.b ; d/ λ = 0.165, h/ λ = 0.1155, g/d = 0.96

Fig.Al.5: Variation of axial ratio with frequency of
SCR surfaces 2.a and 2.b.

2.a ; d/λ = 0.1092, h/λ = 0.1092, g/d = 0.96
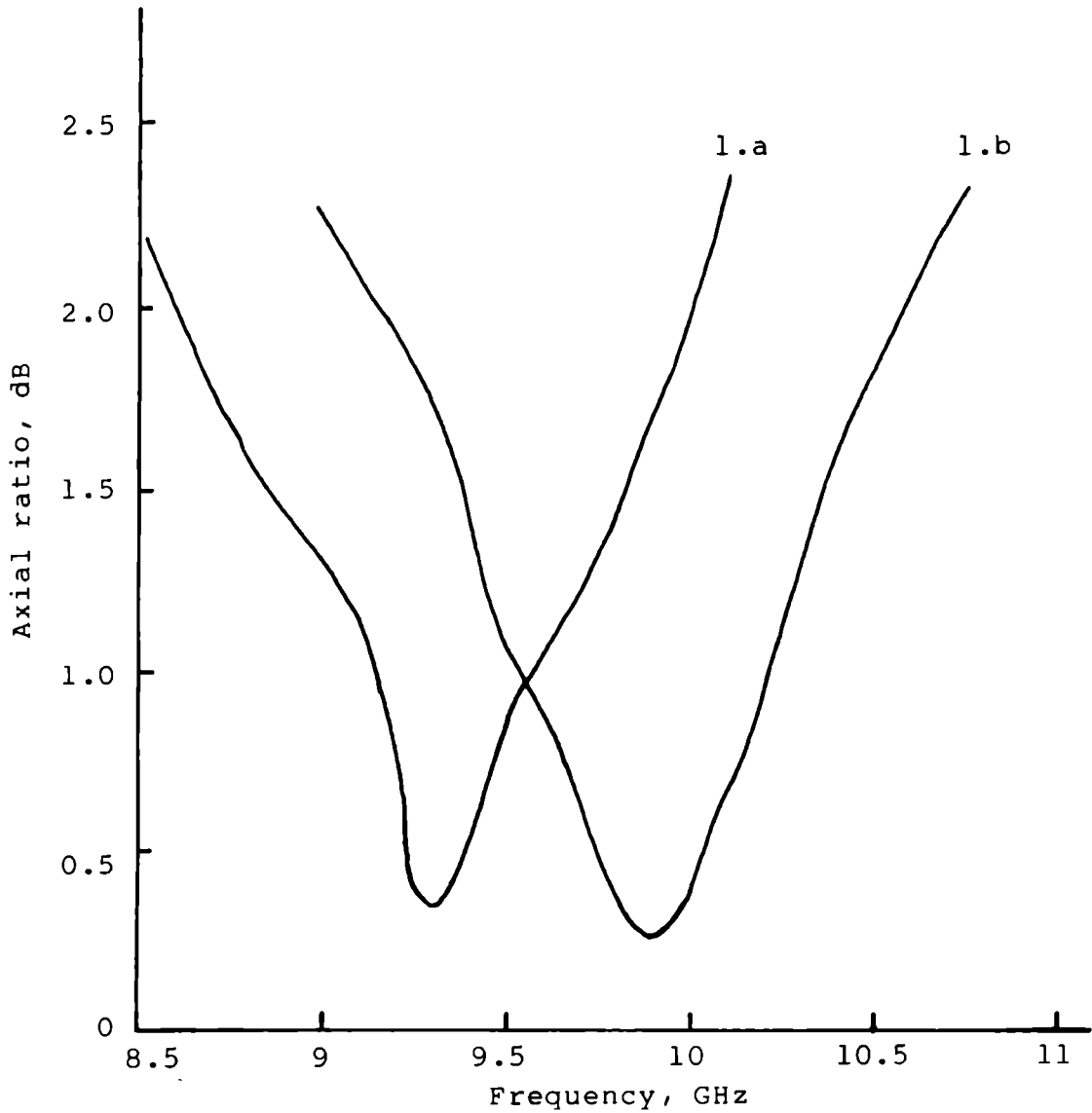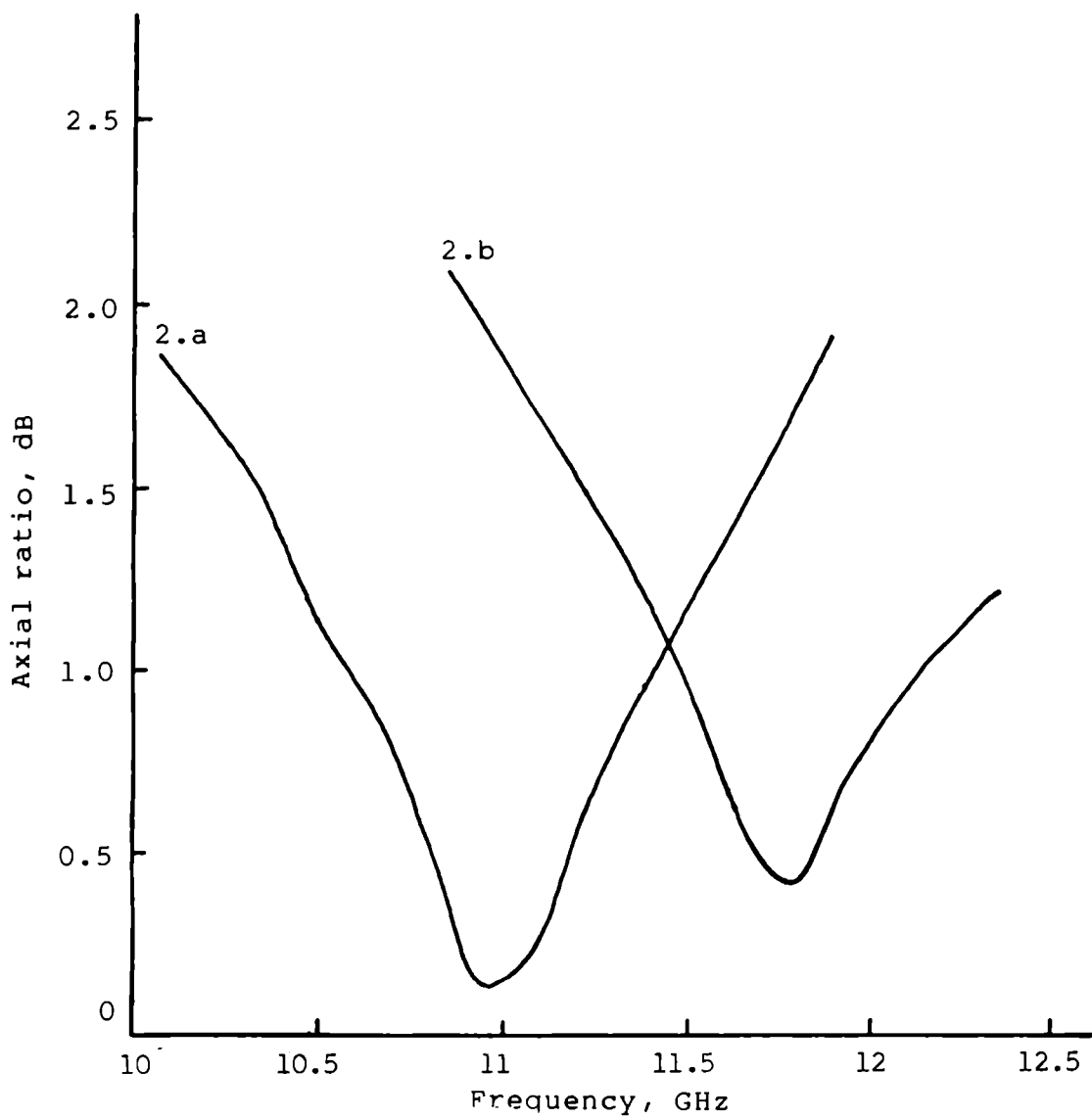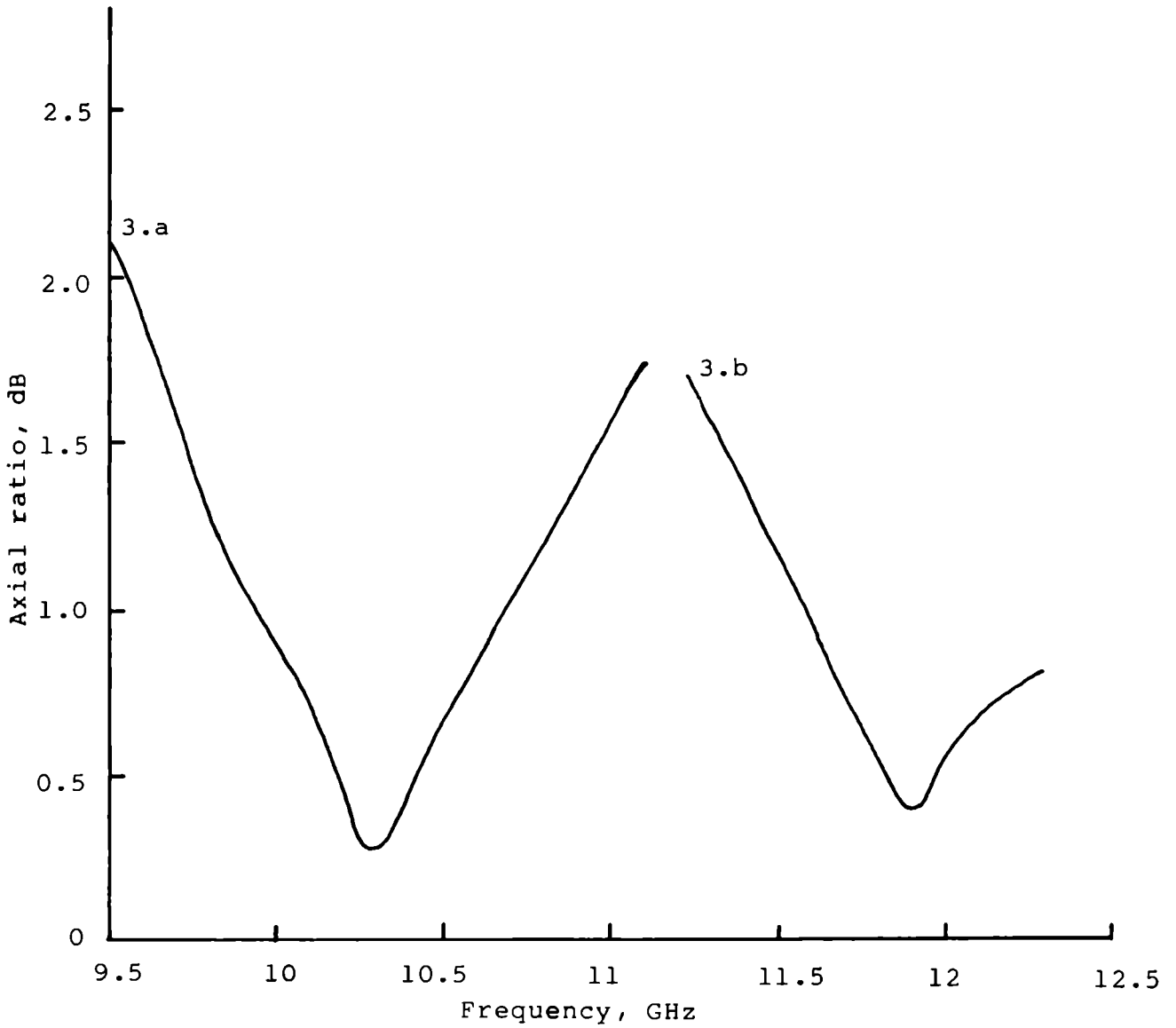2.b ; d/λ = 0.1958, h/λ = 0.1175, g/d = 0.96

Fig.Al.6: Variation of axial ratio with frequency of SCR
surfaces 3.a and 3.b.

3.a ; d/λ = 0.1373,   h/λ = 0.103,   g/d = 0.892

3.b ; d/λ = 0.1587,   h/λ = 0.0992,   g/d = 0.892

exhibiting the property of tilting the polarisation of the linearly polarised incident wave. The experimental arrangement shown in figure A1.2 is also utilized for studying the polarisation tilting characteristics of the SCRS.

SCRS with different grating parameters and dielectric substrate thickness were fabricated and tested. A SCRS with $d/\lambda = 0.1433$, $h/\lambda = 0.1082$ and $g/d = 0.5$, at an angle of incidence of 20° exhibited a polarisation tilt of 90° for 48° orientation of the incident electric field with the length of the strip. When the incident electric field is parallel or perpendicular to the length of the strip, the reflected wave is found to be plane polarised in the same plane as the incident wave and the surface behaves just like a conducting surface. The results are shown in figure A1.7. The experiment is repeated for different angles of incidence. It is observed that, as the angle of incidence is increased, the angle of orientation ($\emptyset$) of the incident electric field with the length of the strip, required for 90° tilt of plane of polarisation is also increased. As in the case of corrugated surface [92], here also, it is observed that, for small angles of incidence ($< 10°$), the angle of orientation of the incident electric

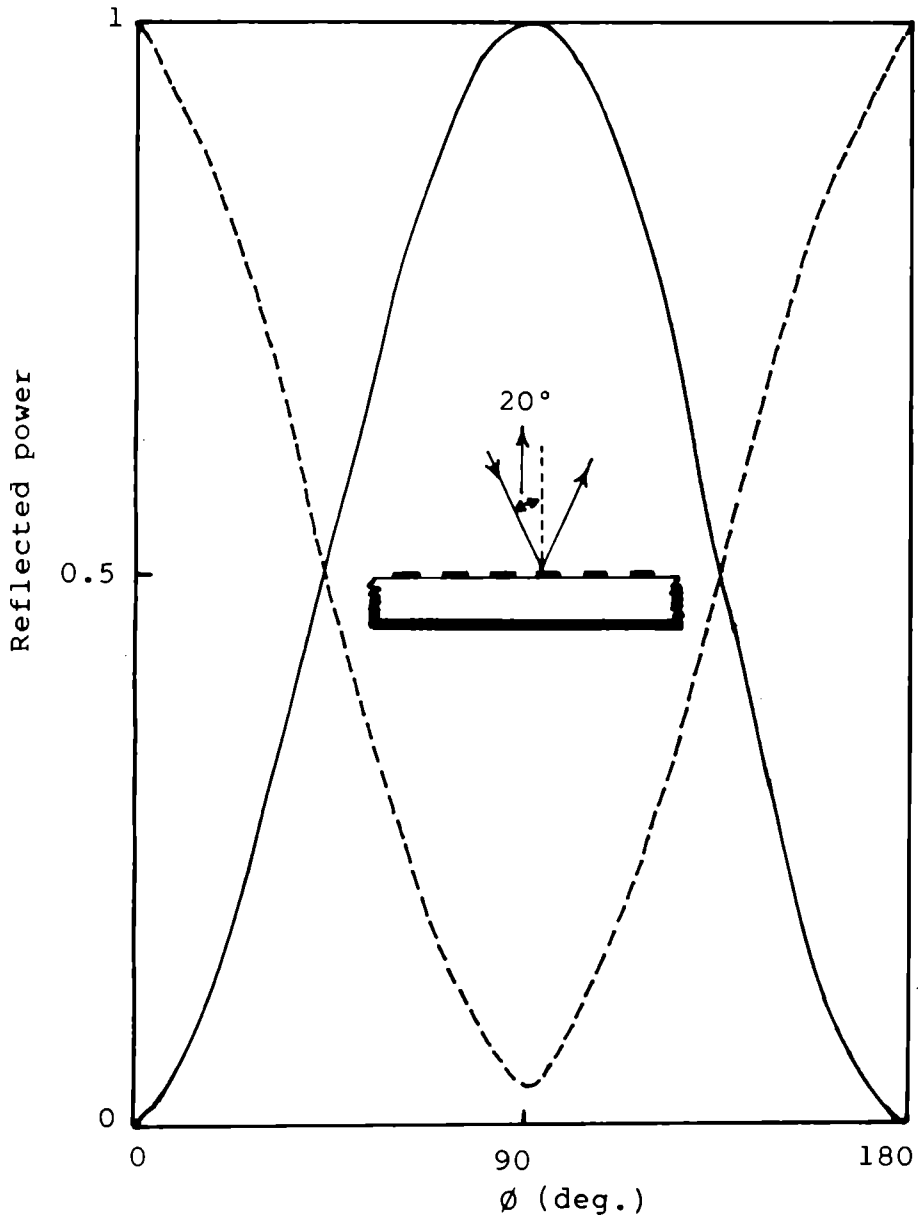Fig.A1.7: Reflected power from a SCRS (g/λ = 0.07163, d/λ = 0.1433 and h/λ = 0.10823) at an angle of incidence 20° from normal

———— Incident electric field parallel to the length of strips

- - - - - Incident electric field at 48° to the length of strips

field required for the 90° tilt of plane of polarisation of the reflected wave is found to be nearly 45° and beyond that it increases. The variation of the required angle of orientation $\emptyset$ of the incident electric field with the angle of incidence is given in figure A1.8.

A1.5 CONCLUSIONS

The experimental investigation on the reflection characteristics of SCRS has showed that the newly developed SCRS simulates the identical reflection characteristics of a metallic surface with rectangular corrugation. However, SCRS are much light, less expensive and easy to fabricate. This type of surface can be easily fabricated by photolithographic technique with high precision. The tedious job of corrugation cutting can be avoided if the technique of SCRS is adopted. These SCRS's may find applications in cassegrain antenna design, in the reduction of radar cross-section of targets, in the development of simulated corrugated scalar feed horns and in reduction of permanent echoes from buildings at airports provided with instrument landing systems.
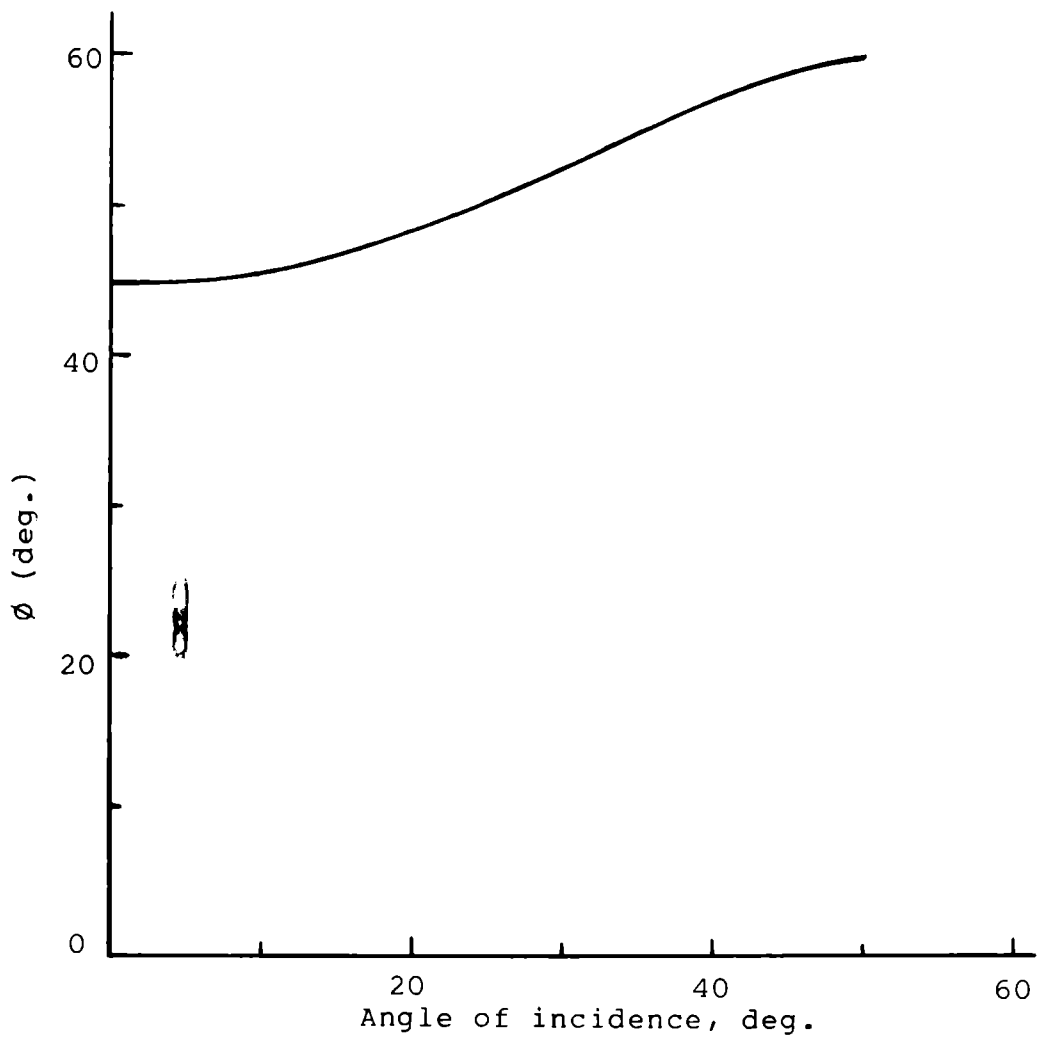
Fig.Al.8: Variation of optimum angle (∅) with angle of
incidence

Appendix   II

ANTENNA RADIATION MEASUREMENT USING VECTOR

NETWORK ANALYSER

Appendix II

ANTENNA RADIATION PATTERN MEASUREMENT USING

VECTOR NETWORK ANALYSER

The experimental measurements determine the actual performance of an antenna. In this appendix the technique/flow chart used for radiation pattern measurement using HP 8510 B Network Analyser and Scientific Atlanta Positioner controlled by HP 9000, 300 series Instrumentation Computer is presented. A new software was developed for the measurement. The measurements are made properly and precisely taking care of all precautions.

The flow chart of the radiation pattern measurement procedure of an antenna is presented in figure A2.1. At the start of the measurement, the following input data are given to the computer,

i)   Start frequency, Stop frequency, Step frequency

ii) Start angle, Stop angle, Step angle

iii) Source power, Averaging, Smoothing etc.

After entering all these parameters the measurement set-up is calibrated in the frequency band of

```
                    ┌─────────────┐
                    │    Start    │
                    └──────┬──────┘
                           │
    ┌──────────────────────▼──────────────────────────┐
    / Start frequency, Stop frequency, Step frequency  /
   /      Start angle, Stop angle, Step angle         /
  /        Source power, Averaging, Smoothing        /
 └─────────────────────────┬────────────────────────┘
                           │
                     ◇ Calibration ◇ ──Yes──▶ Boresight the antenna
                           │                         │
                          No                   Response Calibration
                           │                         │
                  ◇ Instrumental state ◇ ──No──┐     │
                           │ Yes               │     │
              No ◀─── ◇ Time domain analysis ◇ │     │
                           │ Yes               │     │
                    Boresight the antenna      │     │
                           │                   │     │
                    Time domain mode           │     │
                           │                   │     │
                    Proper window              │     │
                           │                   │     │
                    Gate                       │     │
                           │                   │     │
                    Frequency domain mode      │     │
                           │                   │     │
                           ▼                   │     │
                          (A)◀────────────────┘─────┘
```
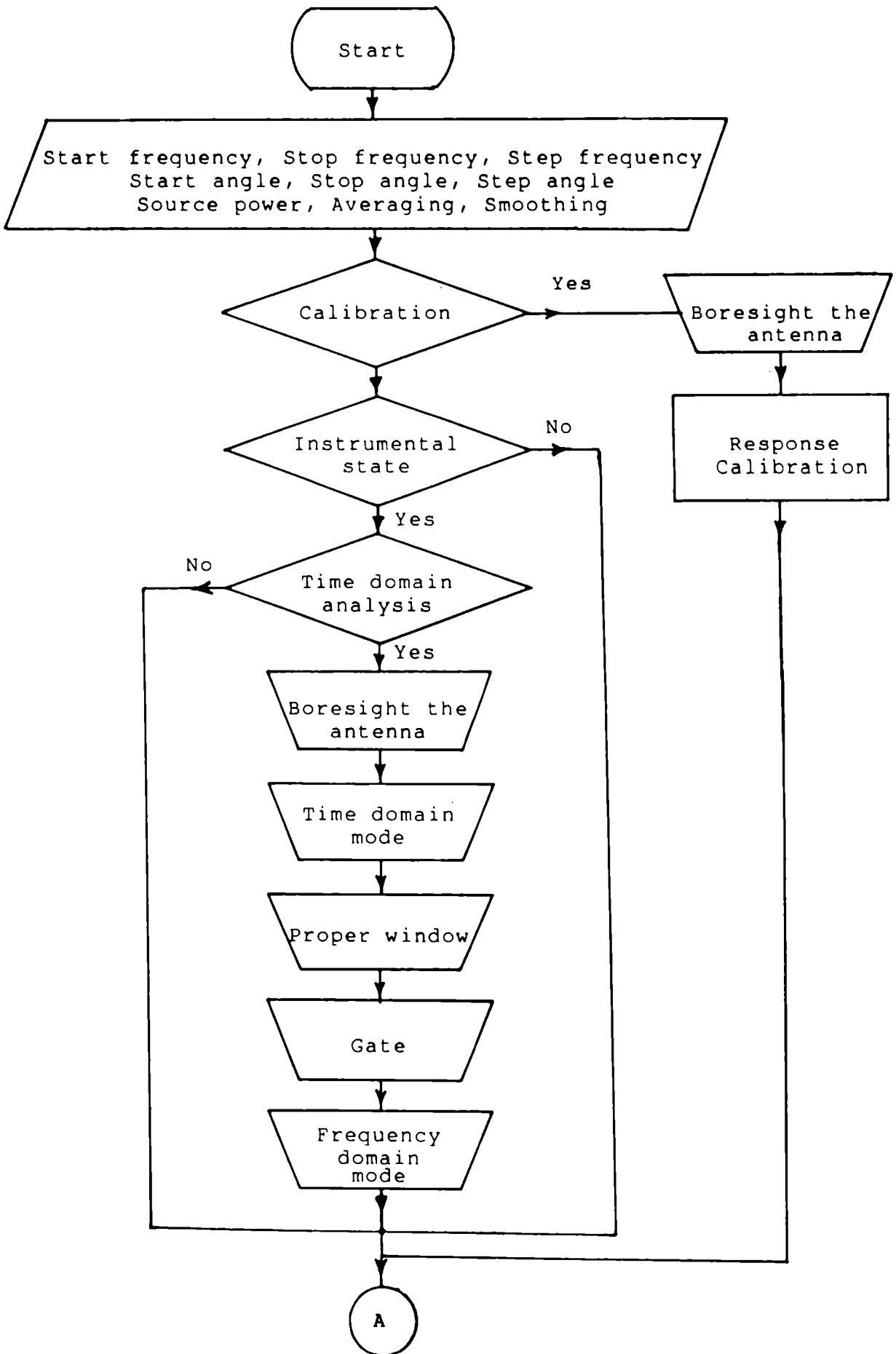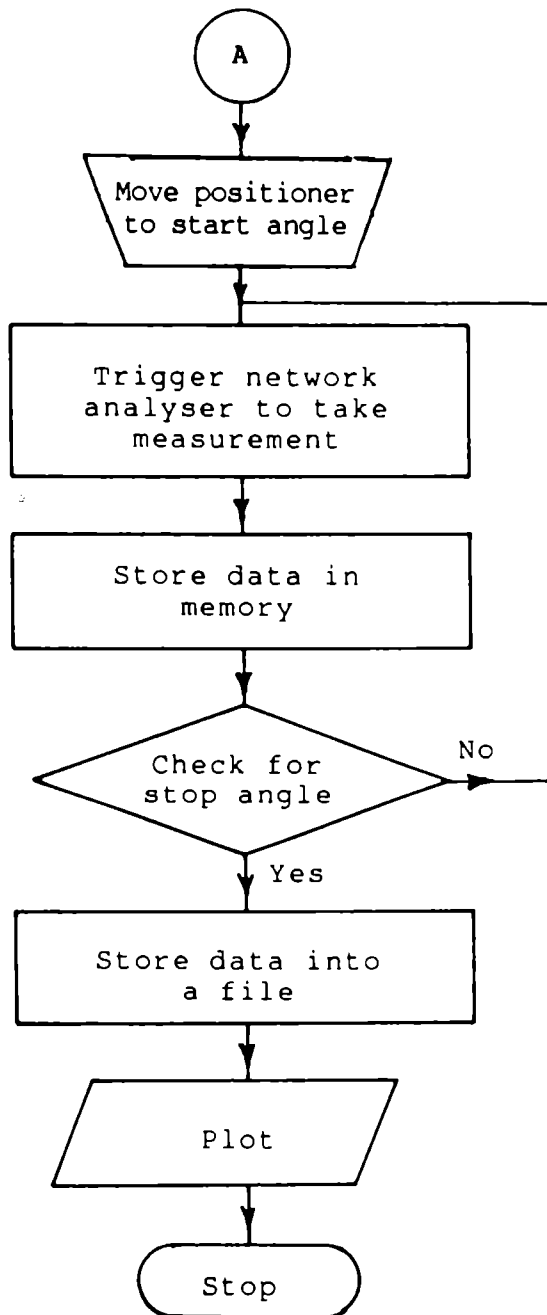
Fig.A2.1: Flow chart of radiation pattern measurement procedure
using HP 8510 B network analyser

interest. Now the transmitting and receiving antennas (antenna under test) are boresighted and a response calibration is done for S_{21}. For starting the measurement, now the positioner is moved to the start angle of the measurement. The calibration of the measurement set up can be avoided if instrumental state is called. In instrumental state, the calibration stored in any of the eight CAL SET in the network analyser can be recalled. If time domain analysis is required, it can be selected in the network analyser. For doing time domain analysis, the antenna under test is boresighted. Now the network analyser is set for time domain mode operation. In this mode, for eliminating unwanted reflections, proper windowing and gating are possible. After selecting the proper window and gate, the network analyser is brought back to the frequency domain and the positioner is moved to the start angle of measurement. Now the network analyser will be triggered to take measurement and the computer will acquire the data of each step angle from the network analyser. The positioner will wait until the data is taken. After that, a control pulse will be sent to the positioner to move through the next step angle and another pulse will be sent back to the computer for taking the data. Like this, the data will be taken for each and every

step angles of measurement. At each step, the measurement will be done 64 times (or the averaging factor given). The measured data can be stored in computer, which can be used for obtaining the radiation pattern of the desired frequency. The hard copy of the radiation pattern can be plotted by the HP 7475A plotter. The experimental arrangement used for plotting the radiation pattern in the present study is shown in figure A2.2. A typical radiation pattern of a horn antenna plotted using the above measurement procedure is presented in figure A2.3.

A2.1 CONCLUSION

A procedure for radiation pattern measurement of an antenna integrating an HP 8510 B Network Analyser and a Scientific Atlanta Positioner along with an HP 9000, 300 series Instrumentation Computer is described in this appendix.
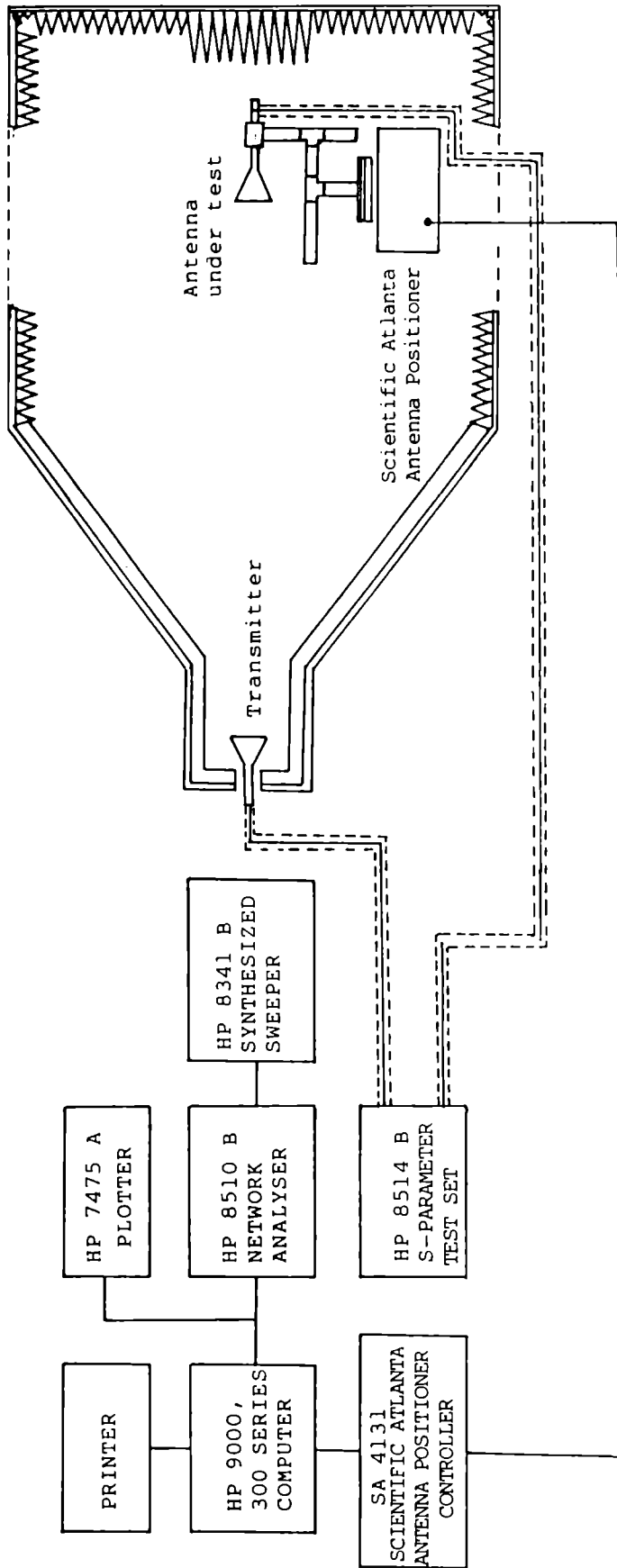
Fig.A2.2: Experimental arrangement used for plotting antenna radiation pattern measurement using HP 8510 B network analyser
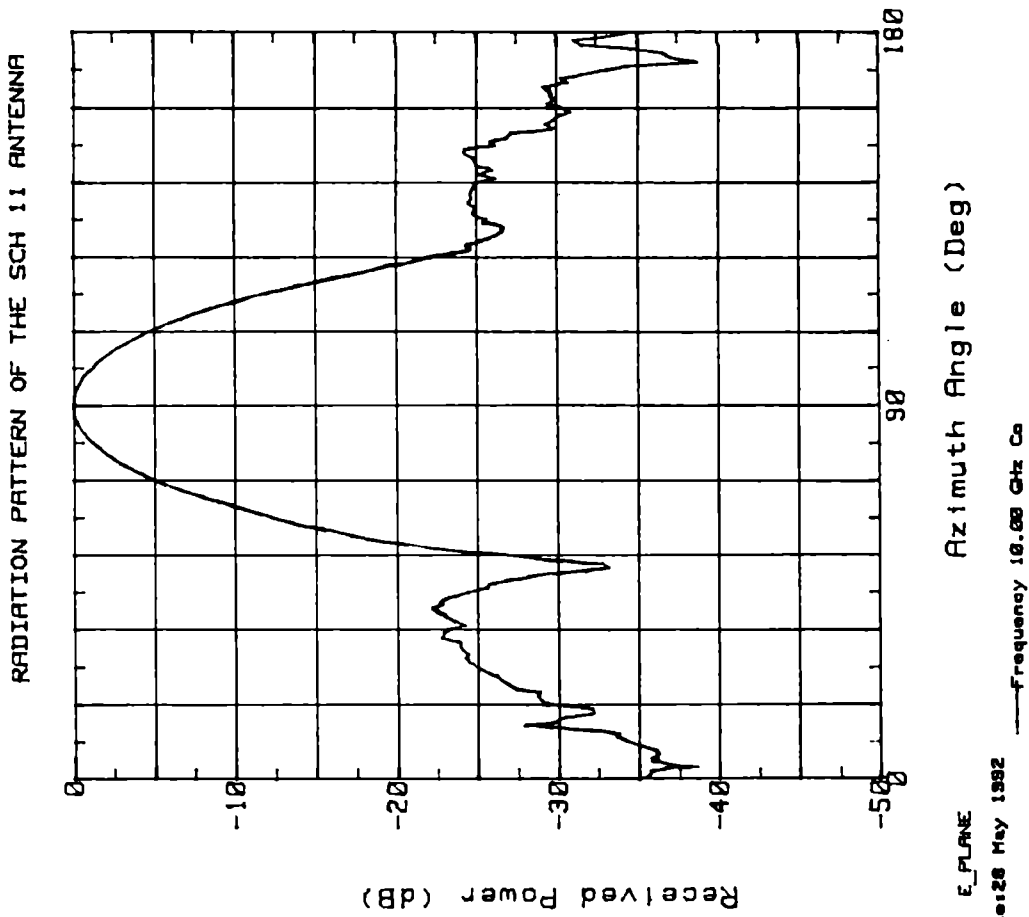
Fig.A2.3: A typical radiation pattern of horn antenna plotted using HP 8510 B network analyser

REFERENCES

1. J.F.Ramsay, "Microwave antenna and waveguide technique before 1900", Proc. IRE, Vol.46, pp.405-415, Feb. 1958.

2. G.C.Southworth, "Hyper-frequency waveguides--General considerations and experimental results", Bell. Syst. Tech. J. Vol.15, pp.284-309, April 1936.

3. W.L.Barrow, "Transmission of electromagnetic waves in hollow tubes of metal", Proc. IRE, Vol.24, pp.1298-1328, Oct. 1936.

4. W.L.Barrow and F.M.Greene, "Rectangular hollow pipe radiators", ibid., Vol.26, pp.1948-1519, Dec. 1938.

5. W.L.Barrow and L.J.Chu, "Theory of electromagnetic horn", ibid., Vol.27, pp.51-64, Jan. 1939.

6. W.L.Barrow and F.D.Lewis, "The sectoral electromagnetic horn", ibid., Vol.27, pp.41-50, Jan. 1939.

7. G.S.Southworth and A.P.King, "Metal horns as directive receivers of ultra short waves", ibid., pp.95-102, Feb. 1939.

254

8. L.J.Chu and W.L.Barrow, "Electromagnetic horn design", Trans. AIEE, Vol.58, pp.333-338, July 1939.

9. L.J.Chu, "Calculation of the radiation properties of pipes and horns", J. Appl. Phys., Vol.2, pp.603-610, Sept. 1940.

10. D.R.Rhodes, "An experimental investigation of the radiation patterns of electromagnetic horn antennas", Proc. IRE, Vol.36, pp.1101-1105, Sept. 1948.

11. G.A.Woonton, D.R.Hay and E.L.Vogan, "An experimental investigation of formulas for the prediction of horn radiation patterns", J. Appl. Phys. Vol.20, pp.71-78, Jan. 1949.

12. C.W.Horton, "On the theory of the radiation patterns of electromagnetic horns of moderate flare angle", Proc. IRE, Vol.37, pp.744-749, July 1949.

13. Herbert S.Bennett, "Transmission line characteristics of the sectoral horn", ibid., Vol.37, pp.738-749, July 1949.

.4. S.O.Rice, "A set of second order differential equations associated with reflection in rectangular waveguides-- Application to guide connected to a horn", Bell Syst. Tech. J. Vol.18, pp.136-156, Jan. 1949.

15. A.P.King, "The radiation characteristics of conical horn antennas", Proc. IRE, Vol.38, pp.249-251, March 1950.

16. Marvin G.Schorr and Fred J.Beck Jr., "Electromagnetic field of conical horn", J. Appl. Phys. Vol.21, pp.795-801, Aug. 1950.

17. W.C.Jakes, "Gain of electromagnetic horns", Proc. IRE, Vol.39, pp.160-162, Feb. 1951.

18. E.H.Braun, "Gain of electromagnetic horns", ibid., Vol.41, pp.109-115, Jan. 1953.

19. E.H.Braun, "Some data for the design of electromagnetic horns", IEEE Trans. Antennas Propagat., Vol.AP-4, pp.29-31, Jan. 1956.

20. James J.Epis, "Compensated electromagnetic horns", Microwave J., Vol.4, pp.84-89, May 1961.

21. K.L.Walton and V.C.Sundberg, "Broadband rigid horn design", ibid., Vol.7, pp.96-101, March 1964.

22. P.M.Russo, R.C.Rudduck and L.Peters Jr., "A method for computing E-plane patterns of horn antennas", IEEE Trans. Antennas Propagat., Vol.AP-13, pp.219-224, March 1965.

23. L.I.Tingye and R.H.Turrin, "Near-zone field of the conical horn", ibid., Vol.AP-12, pp.800-802, Nov. 1964.

24. Y.S.Yu, R.C.Rudduck and L.Peters Jr., "Comprehensive analysis for E-plane of horn antennas by edge diffraction theory", ibid., Vol.AP-14, pp.138-149, March 1966.

25. M.A.K.Hamid, "Diffraction by a conical horn", ibid., Vol.AP-16, pp.520-528, Sept. 1968.

26. T.S.Chu and R.A.Semplek, "Gain of electromagnetic horns", Bell Syst. Tech. J., Vol.44, pp.527-537, March 1965.

27. E.V.Jull, "On the behaviour of electromagnetic horns", Proc.IEEE, Vol.56, pp.106-108, Jan. 1968.

28. E.V.Jull, "Finite-range gain of sectoral and pyramidal horns", Electron. Lett., Vol.6, pp.680-681, Oct. 1970.

29. E.I.Muehlodorf, "The phase centre of horn antennas", IEEE Trans. Antennas Propagat., Vol.AP-18, pp.753-760, Nov. 1970.

30. M.S.Narasimhan and B.V.Rao, "Modes in a conical horn: new approach", Proc. Inst. Elect. Eng., Vol.118, pp.287-292, Feb. 1971.

31. M.S.Narasimhan and B.V.Rao, "Radiation from conical horns with large angles", IEEE Trans. Antennas Propagat., Vol.AP-19, pp.678-681, Sept. 1971.

32. M.S.Narasimhan and B.V.Rao, "A correction to the available radiation formula for E-plane sectoral horns", ibid, Vol.AP-21, pp.878-879, Nov. 1973.

33. John L.Kerr, "Short axial length broad-band horns", ibid., Vol.AP-21, pp.710-715, Sept. 1973.

34. E.V.Jull, "Errors in the predicted gain of pyramidal horns", ibid., Vol.AP-21, pp.25-31, Jan. 1973.

35. M.F.Iskander and M.A.K.Hamid, "Numerical solution for the near-field transmission between two H-plane sectoral electromagnetic horns", ibid., Vol.AP-24, pp.87-89, Jan. 1976.

36. E.V.Jull and L.E.Allen, "Gain of an E-plane sectoral horn: a failure of Kirchoff's theory and a new proposal", ibid., Vol.AP-22, pp.221-226, March 1974.

37. C.A.Mentzer, L.Peters Jr., and R.C.Rudduck, "Slope diffraction and its application to horns", ibid., Vol.AP-24, pp.153-159, March 1976.

38. J.C.Mather, "Broad-band flared horn with low sidelobes", ibid., Vol.AP-29, pp.967-969, Nov. 1981.

39. R.C.Menendez and S.W.Lee, "Analysis of rectangular horn antennas via uniform asymptotic theory", ibid., Vol.AP-30, pp.240-250, March 1982.

40. A.W.Love, "The diagonal horn antenna", Microwave J., Vol.5, pp.117-122, March 1962.

41. P.D.Potter, "A new horn with suppressed sidelobes and equal beamwidths", Microwave J., Vol.6, pp.71-78, June 1963.

42. P.D.Potter and A.C.Ludwig, "Beam shaping by use of higher order modes in conical horns", Northeast Electron. Res. and Eng. Meeting, pp.92-93, Nov. 1963.

43. P.A.Jensen, "A low-noise multimode cassegrain monopulse feed with polarisation diversity", Northeast Electron. Res. and Eng. Meeting, pp.94-95, Nov. 1963.

44. A.C.Ludwig, "Radiation pattern synthesis for circular aperture horn antennas", IEEE Trans. Antennas and Propagat., Vol.AP-14, pp.434-440, July 1966.

45. R.H.Turrin, "Dual mode small aperture antennas", ibid., Vol.AP-15, pp.307-308, March 1967.

46. K.Tomiyasu, "Conversion of TE_{11} mode by a large diameter conical junction", IEEE Trans. Microwave Theory Tech., Vol.MTT-17, pp.277-279, May 1969.

47. K.K.Agarwal and E.R.Nagelberg, "Phase characteristics of a circularly symmetric, dual-mode transducer", ibid., Vol.MTT-18, pp.69-71, Jan. 1970.

48. S.B.Cohn, "Flare-angle changes in a horn as a means of pattern control", Microwave J., Vol.13, pp.41,43,44,46, Oct. 1970.

49. C.C.Han and A.N.Wickert, "A new multimode rectangular horn antenna generating a circularly polarised elliptical beam", IEEE Trans. Antennas Propagat., Vol.AP-22, pp.746-751, Nov. 1974.

50. W.J.English, "The circular waveguide step-discontinuity mode transducer", IEEE Trans. Microwave Theory Tech., Vol.MTT-21, pp.633-636, Oct. 1973.

51. G.F.Koch, "Co-axial feeds for high aperture efficiency and low spillover of paraboloidal reflector antennas", IEEE Trans. Antennas Propagat., Vol.AP-21, pp.164-169, March 1973.

52. R.W.Gruner, "A 4- and 6 GHz, prime focus, CP feed with circular pattern symmetry", IEEE, AP-S Symp. Program and Dig, pp.72-74, June 1974.

53. A.J.Simmons and A.F.Kay, "The scalar feed--A high performance feed for large paraboloidal reflectors", Design and construction of large steerable aerials, IEE Conference Publ. Vol.21, pp.213-217, 1966.

54. R.E.Lawrie and L.Peters, Jr., "Modification of horn antennas for low sidelobe levels", IEEE Trans. Antennas Propagat., Vol.AP-14, pp.605-610, Sept. 1966.

55. V.H.Rumsey, "Horn antennas with uniform power patterns around their axis", ibid., Vol.AP-14, pp.656-658, Sept. 1966.

56. H.C.Minnet and B.Mac A.Thomas, "A method of synthesizing radiation patterns with axial symmetry", ibid., Vol.AP-14, pp.654-656, Sept. 1966.

57. P.J.B.Clarricoats and P.K.Saha, "Theoretical analysis of cylindrical hybrid modes in a corrugated horn", Electron. Lett., Vol.5, pp.187-189, May 1, 1969.

58. P.J.B.Clarricoats and P.K.Saha, "Analysis of spherical hybrid modes in a corrugated conical horn", ibid., Vol.5, pp.189-190, May 1, 1969.

59. P.J.B.Clarricoats and P.K.Saha, "Radiation from wide-flare-angle scalar horns", ibid., Vol.5, pp.376-378, 1969.

60. M.E.J.Jeuken, "Experimental radiation pattern of the corrugated conical horn antenna with small flare-angle", ibid., Vol.5, pp.484-485, Oct. 2, 1969.

61. M.E.J.Jeuken and C.W.Lambrechtse, "Small corrugated conical horn with wide flare-angle", ibid, Vol.5, pp.489-490, Oct. 2, 1969.

62. B.MacA.Thomas, "Bandwidth properties of corrugated conical horns", ibid., Vol.5, pp.561-563, Oct. 30, 1969.

63. M.S.Narasimhan and B.V.Rao, "Hybrid modes in corrugated conical horns", ibid., Vol.6, pp.32-34, Jan. 22, 1970.

64. R.Baldwin and P.A.McInnes, "Surface wave excitation from a corrugated horn", ibid., Vol.6, pp.259-260, April 1970.

65. B.MacA.Thomas, "Prime focus one and two hybrid mode feeds", ibid., Vol.6, pp.460-461, July 23, 1970.

66. M.S.Narasimhan and B.V.Rao, "Diffraction by wide flare angle corrugated conical horns", ibid., Vol.6, pp.469-471, July 23, 1970.

57. P.J.B.Clarricoats, A.D.Olver and P.K.Saha, "Near-field radiation characteristics of corrugated horns", ibid., Vol.7, pp.446-448, Aug.12, 1971.

58. P.J.B.Clarricoats and P.K.Saha, "Propagation and radiation behaviour of corrugated feeds, Part I--Corrugated waveguide feed", Proc. IEE, Vol.118, pp.1167-1176, Sept. 1971.

59. P.J.B.Clarricoats and P.K.Saha, "Propagation and radiation behaviour of corrugated feeds", Part II--corrugated conical feed", ibid., Vol.118, pp.1177-1186, Sept. 1971.

70. J.K.M.Jansen, M.E.J.Jeuken and C.W.Lambrechtse, "The scalar feed", Arch. Elek Ubertragung, Vol.26, pp.22-30, Jan. 1972.

71. B.MacA.Thomas, "Mode conversion using circumferentially corrugated cylindrical waveguide", Electron Lett. Vol.8, pp.394-396, July 27, 1972.

72. C.M.Knop and H.J.Wiesenfarth, "On the radiation from an open-ended corrugated pipe carrying the HE_{11} mode", IEEE Trans. Antennas Propogate., Vol.AP-20, pp.644-648, Sept. 1972.

73. P.J.B.Clarricoats and L.M.Seng, "Propagation and radiation characteristics of corrugated horns", Electron Lett., Vol.9, No.1, Jan. 11, 1973.

74. M.S.Narasimhan, "Corrugated conical horns with arbitrary corrugation depth", Radio Electron. Eng., Vol.43, pp.188-192, March 1973.

75. M.S.Narasimhan and V.V.Rao, "Radiation characteristics of corrugated E-plane sectoral horns", IEEE Trans. Antennas Propagat., Vol.AP-21, No.3, pp.320-327, May 1973.

76. R.Caldecott, C.A.Mentzer and L.Peters, Jr., "The corrugated horn as an antenna range standard", ibid., Vol.AP-21, pp.562-564, July 1973.

77. T.B.Vu and N.V.Hien, "A new type of high performance monopulse feed", ibid., Vol.AP-21, pp.855-857, Nov. 1973.

78. C.A.Mentzer and L.Peters, Jr., "Properties of cut off corrugated surfaces for corrugated horn design", ibid., Vol.AP-22, pp.191-196, March 1974.

79. AMB AL HARIRI, A.D.Olver, P.J.B.Clarricoats, "Low attenuation properties of corrugated rectangular waveguide", Electron. Lett., pp.304-305, July 25, 1974.

80. M.S.Narasimhan and V.V.Rao, "Radiation from wide flare corrugated E-plane sectoral horn", IEEE Trans. Antennas Propagat., Vol.AP-22, pp.603-608, July 1974.

81. M.S.Narasimhan, "Corrugated conical horn as a space feed for phased array illumination", ibid., Vol.AP-22, pp.720-722, Sept. 1974.

82. Z.Frank, "Very wideband corrugated horns", Electron Lett., Vol.11, No.6, pp.131-133, March 1975.

83. R.Baldwin and P.A.McInnes, "Corrugated rectangular horns for use as microwave feeds", Proc. IEE, Vol.122, pp.465-469, May 1975.

84. P.Baldwin and P.A.McInnes, "A rectangular corrugated feed horn", IEEE Trans. Antennas Propagat., Vol.AP-23, pp.814-817, Nov. 1975.

85. C.G.Parini, P.J.B.Clarricoats and A.D.Olver, "Cross-polar radiation from open-ended corrugated waveguides", Electron. Lett., Vol.11, No.23, pp.567-568, Nov. 13, 1975.

86. F.Takada and T.H.Moto, "Broadbanding of corrugated conical horns by means of the ring-loaded corrugated waveguide", IEEE Trans. Antennas Propagat., Vol.AP-24, No.6, pp.786-792, Nov., 1976.

87. G.L.James, "Radiation Properties of 90° conical horns", Electron. Lett., Vol.13, No.10, pp.293-294, May 12, 1977.

88. A.J.Terzuoli, Jr. and L.Peters, Jr., "VSWR properties of E-plane dihedral corrugated horns", IEEE Trans. Antennas Propagat., Vol.AP-26, No.2, pp.239-243, March 1978.

89. B.MacA.Thomas, "Design of corrugated conical horns", ibid., Vol.AP-26, No.2, pp.367-372, March 1978.

90. R.F.E.Guy and R.W.Ashton, "Cross-polar performance of an elliptical corrugated horn antenna", Electron Lett., Vol.15, No.13, pp.400-402, June 21, 1979.

91. S.C.J.Worm, "Compact dual-hybrid mode feeds with low cross-polar radiation", ibid., Vol.15, No.23, pp.740-741, Nov.8, 1979.

92. E.V.Jull, "Reflection circular polarisers", ibid., Vol.15, pp.423-424, 1979.

93. G.L.James, "Surface reactance of corrugated planes", ibid., Vol.15, No.23, pp.751-753, Nov.8, 1979.

94. C.Dragone, "Attenuation and radiation characteristics of the HE_{11} mode", IEEE Trans. Microwave Theory Tech., Vol.MTT-28, No.7, pp.704-710, July 1980.

95. G.L.James, "Analysis and design of TE_{11} to HE_{11} corrugated cylindrical waveguide mode converters", ibid., Vol.MTT-29, No.10, pp.1059-1066, Oct. 1981.

96. G.L.James and Bruce M.Thomas, "TE_{11}-to-HE_{11} cylindrical waveguide mode converters using ring-loaded slots", ibid., Vol.MTT-30, No.3, pp.278-285, March 1982.

97. P.O.Paul and K.G.Nair, "Rotation of plane of polarisation of a beam of microwaves by corrugated reflector surfaces", Electron. Lett., Vol.18, No.8, pp.338-339, April 1982.

98. K.A.Iskander, L.Shafai, A.Frandsen and J.E.Hansen, "Application of impedance boundary conditions to numerical solution of corrugated circular horns", IEEE Trans. Antennas Propagat., Vol.AP-30, No.3, pp.366-372, May 1982.

99. T.A.Shing Chu and W.E.Legg, "Gain of corrugated conical horns", ibid., Vol.AP-30, No.4, pp.698-703, July 1982.

100. G.Morris, "A broad-band constant beamwidth corrugated rectangular horn", IEEE Trans. Antennas Propagat., Vol.AP-30, No.5, pp.966-974, Sept. 1982.

101. G.L.James, "TE_{11}-to-HE_{11} mode converters for small angle corrugated horns", ibid., Vol.AP-30, No.6, pp.1057-1062, Nov. 1982.

102. B.MacA.Thomas, "A curved-aperture corrugated horn having very low cross-polar performance", ibid., Vol.AP-30, No.6, pp.1068-1072, Nov. 1982.

103. C.Dragone, "Scattering at a junction of two waveguides with different surface impedances", IEEE Trans. Microwave Theory Tech., Vol.MTT-32, No.10, pp.1319-1329, Oct. 1984.

104. C.Dragone, "A rectangular horn of four corrugated plates", IEEE Trans. Antennas. Propagat., Vol.AP-33, No.2, pp.160-164, Feb. 1985.

105. A.A.S.Obaid, T.S.M.Maclean and M.Razaz, "Propagation characteristics of rectangular corrugated waveguides", Proc. IEE, Vol.132, Pt.H(7), pp.413, Dec. 1985.

106. C.Witebsky, G.F.Smoot, S.Levin and M.Bensadoun", A large L-band rectangular corrugated horn", IEEE Trans. Antennas Propagat., Vol.AP-35, No.11, pp.1310-1313, Nov. 1987.

107. A.D.Olver and J.Xiang, "Wide angle corrugated horns analysed using spherical modal matching", Proc. IEE, Vol.135, Pt.H(1), pp.34-40, Feb. 1988.

108. P.S.Kildal and E.Lier, "Hard horns improve cluster feeds of satellite antennas", Electron. Lett., Vol.24, No.8, pp.491-492, April 14, 1988.

109. F.Manshadi and R.Hartop, "Compound taper feed horn for NASA 70 m antennas", IEEE Trans. Antennas Propagat., Vol.36, No.9, pp.1213-1216, Sept. 1988.

110. M.A.Toral, R.B.Ratliff, M.C.Lecha, J.G.Marusehak, C.L.Bennet and G.F.Smoot, "Measurements of very low-sidelobe conical horn antennas", ibid., Vol.37, No.2, pp.171-177, Feb. 1989.

111. J.M.Arnold and A.Dendane, "Intrinsic mode theory of conical corrugated horns", Proc. IEE, Vol.136, Pt.H(3), pp.250-256, June 1989.

112. P.J.B.Clarricoats and P.K.Saha, "Attenuation in corrugated circular waveguide", Electron. Lett., 25th year of publication, pp.S9-S11, Nov. 22, 1989.

113. O.W.Ata, T.M.Benson and A.Marincic, "Sidelobe supression in an E-plane sectoral horn antenna", ibid., Vol.26, No.4, pp.231-233, Feb. 15, 1990.

114. B.MacA.Thomas, K.J.Greene and G.L.James, "A wide-band prime-focus horn for low noise receiver applications", IEEE Trans. Antennas Propagat., Vol.38, No.11, pp.1898-1900, Nov. 1990.

115. E.J.Zachariah, K.Vasudevan and K.G.Nair, "Beam shaping and impedance matching of sectoral electromagnetic horn antennas using corrugated flanges", Ind. J. Radio & Space Phys., Vol.8, pp.24-28, Feb. 1979.

116. E.J.Zachariah, K.Vasudevan and K.G.Nair, "Metal flanges with more parameters for beam shaping", IEEE Trans. Antennas Propagat., Vol.AP-27, No.9, pp.708-710, Sept. 1979.

117. P.A.Pravinkumar, P.Mohanan and K.G.Nair, "Corrugated flanged horn feed for paraboloidal reflectors", Ind. J. Radio & Space Phys., Vol.10, pp.246-247, 1981.

118. K.Vasudevan and K.G.Nair, "An analysis of radiation patterns of corrugated corner reflector antenna systems", Ind. J. Radio & Space Phys. Vol.11, pp.156-158, Aug. 1982.

119. P.Mohanan, P.A.Pravinkumar and K.G.Nair, "Axially Symmetric radiation patterns from flanged E-plane sectoral horn feeds", ibid., Vol.11, pp.112-115, 1982.

120. P.Mohanan, C.K.Aanandan and K.G.Nair, "Axially symmetric radiation patterns from corrugated flanged H-plane sectoral horns", ibid., Vol.13, pp.13-15, Feb. 1984.

121. P.Mohanan, C.K.Anandan and K.G.Nair, "Circularly polarised corrugated flanged feed horn", ibid., Vol.13, pp.137-138, Feb. 1984.

122. H.E.Bartlett and R.E.Mosley, "Dielguides--High
efficient low noise antenna feeds", Microwave J.,
Vol.9, pp.53-58, Dec. 1966.

123. G.N.Tsandoulas and W.D.Fitzgerald, "Aperture
efficiency enhancement in dielectrically loaded
horns", IEEE Trans. Antennas Propagat., Vol.AP-21,
pp.69-74, Jan. 1972.

124. M.A.K.Hamid, S.J.Towaiji and G.O.Martens, "A
dielectric loaded circular waveguide antenna", ibid.,
Vol.AP-20, pp.96-97, Jan. 1972.

125. T.Satoh, "Dielectric loaded horn antenna", ibid.,
Vol.AP-20, pp.199-201, March 1972.

126. J.R.James, "Engineering approach to the design of
tapered dielectric-road and horn antennas", Radio
Electron Eng., Vol.42, pp.251-259, June 1972.

127. R.Ashton and R.Baldwin, "Rectangular horn with
dielectric slab insert", Electron. Lett. Vol.9, No.2,
pp.26-27, Jan. 1973.

128. R.Baldwin and P.A.McInnes, "Radiation patterns of dielectric-loaded rectangular horns", IEEE Trans. Antennas Propagat., pp.375-376, May 1973.

129. P.J.B.Clarricoats and C.E.R.C.Salema, "Antennas employing conical dielectric horns, Part I - Propagation and radiation characteristics of dielectric cones", Proc. Inst. Ele. Eng., Vol.120, pp.741-749, July 1973.

130. P.J.B.Clarricoats and C.E.R.C.Salema, "Antennas employing conical dielectric horns, Part 2 - The cassegrain antenna", Proc. Inst. Ele. Eng., Vol.120, pp.750-756, July 1973.

131. N.Brooking, P.J.B.Clarricoats and A.D.Olver, "Radiation patterns of pyramidal dielectric waveguides", Electron. Lett. Vol.10, pp.33-34, Feb. 7, 1974.

132. R.J.Collier and P.D.Potter, "Attenuation measurement of dielectric waveguide", ibid., Vol.10, No.25/26, pp.526-527, Dec. 12, 1974.

133. V.J.Vokurka, "Dual-frequency-band feed with partially dielectric loaded grooves", ibid., Vol.11, No.16, pp.376-378, Aug. 1975.

134. A.G.Martin, "Radiation from dielectric sphere loaded horns", ibid., Vol.14, No.1, pp.17-18, Jan. 1976.

135. K.K.Sabnani and R.K.Arora, "Radiation characteristics of a rectangular aperture centrally loaded with a dielectric slab in the H-plane", J. Inst. Electron. and Telecom. Engrs., Vol.24(7), pp.302-304, 1978.

136. R.A.Nair, A.K.Kamal, and S.C.Gupta, "A high gain multimode dielectric coated rectangular horn antenna", The Radio and Electronic Engr., Vol.48(9), pp.439-443, 1978.

137. R.A.Nair, S.C.Gupta and A.K.Kamal, "Radiation characteristics of dielectric-coated conical horn", J. Inst. Electron. and Telecom. Engrs., Vol.24(8), pp.331-333, 1978.

138. A.Kumar, "Dielectric-lined waveguide feed", IEEE Trans. Antennas Propagat., Vol.AP-27, No.2, pp.279-282, March 1979.

139. K.K.Chan, C.C.Huang and A.R.Raab, "Dielectric loaded trifurcated horn for H-plane stacked reflector feed array", Proc. IEE, Vol.127, Part H(1), pp.61-64, 1980.

140. M.S.Aly and S.F.Mahmoud, "Propagation and radiation behaviour of a longitudinally slotted horn with dielectric filled slots", ibid., Vol.132, Pt.H(7), pp.477-479, Dec. 1985.

141. E.Lier, "A dielectric hybrid mode antenna feed: A simple alternative to the corrugated horn", IEEE Trans. Antennas Propagat., Vol.AP-34, No.1, pp.21-29, Jan. 1986.

142. K.Raghavan, A.D.Olver and P.J.B.Clarricoats, "Compact dual mode dielectric-loaded horn", Electron.Lett., Vol.22, No.21, pp.1131-1132, Oct. 9, 1986.

143. C.M.Knop, Y.B.Cheng and E.L.Ostertag, "Performance of corrugated and dielectric-loaded metallic conical horns", ibid., Vol.22, No.23, pp.1253-1254, Nov. 6, 1986.

144. K.A.Jose and K.G.Nair, "Reflector-backed perfectly blazed strip gratings simulate corrugated reflector effects", ibid., Vol.23, No.2, pp.86-87, Jan. 15, 1987.

145. S.F.Mahmoud and M.S.Aly, "A new version of dielectric lined waveguide with low cross-polar radiation", IEEE Trans. Antennas Propagat., Vol.AP-35, No.2, pp.210-212, Feb. 1987.

146. E.Lier and T.S.Pettersen, "The strip-loaded hybrid mode feed horn", ibid., Vol.AP-36, No.9, pp.1086-1088, Sept. 1987.

147. C.S.Lee, S.W.Lee and D.W.Justice, "A simple circular polarised antenna: circular waveguide horn coated with lossy magnetic material", ibid., Vol.36, No.2, pp.297-300, Feb. 1988.

148. E.Lier, "Hard waveguide feeds with circular symmetry for aperture efficiency enhancement", Electron. Lett., Vol.24, No.3, pp.166-167, Feb. 4, 1988.

149. P.S.Kildal, "Definition of artificially soft and hard surfaces for electromagnetic waves", ibid., Vol.24, No.3, pp.168-170, Feb. 4, 1988.

150. O.W.Ata and T.M.Benson, "Novel phase-corrected horn antenna of short length", ibid., Vol.24, No.5, pp.292-293, March 3, 1988.

151. P.S.Kildal and E.Lier, "Hard horns improve cluster feeds of satellite antennas", ibid., Vol.24, No.8, pp.491-492, April 14, 1988.

152. A.D.Olver, P.J.B.Clarricoats and K.Raghavan, "Dielectric cone loaded horn antennas", Proc. IEE, Vol.135, Pt.H(3), pp.158-162, June 1988.

153. A.Kumar, "Compact horn for earth coverage", Electron Lett., Vol.24, No.14, pp.868-869, July 7, 1988.

154. P.S.Kildal, "Bandwidth of a square hard horn", Proc. IEE, Vol.135, Pt.H(4), pp.275-278, Aug. 1988.

155. E.Lier and P.S.Kildal, "Soft and hard horn antennas", IEEE Trans. Antennas Propagat., Vol.36, No.8, pp.1152-1157, Aug. 1988.

156. J.J.H.Wang, V.K.Tripp and R.P.Zimmer, "Magnetically coated horn for low sidelobes and low cross-polarisation", Proc. IEE, Vol.136, Pt.H(2), pp.132-138, April 1989.

157. R.Cahill, "Design of core support mechanism for mm-wave dielectrically loaded horn", Electron Lett., Vol.25, No.18, pp.1248-1249, Aug. 31, 1989.

158. A.K.Singh, B.Jha and R.K.Jha, "E-plane sectoral hollow dielectric horn antenna", IETE Tech. Review, Vol.6, No.6, pp.457-461, 1989.

159. S.I.Ghobrial and H.R.Sharolim, "Radiation patterns of a paraboloidal reflector fed by a pyramidal horn with lossy walls", IEEE Trans. Antennas Propagat., Vol.37, No.10, pp.1316-1317, Oct. 1989.

160. T.S.Bird and S.G.Hay, "Mismatch in dielectric-loaded rectangular waveguide antenna", Electron. Lett., Vol.26, No.1, pp.59-61, Jan. 4, 1990.

161. A.K.Singh, B.Jha and R.K.Jha, "Near-field analysis of H-plane hollow sectoral dielectric horn antennas", Int. J. Electron. Vol.68, No.6, pp.1055-1061, June 1990.

162. E.Lier, "Analysis of soft and hard strip-loaded horns using a circular cylindrical mode", IEEE Trans. Antennas Propagat., Vol.38, No.6, pp.783-793, June 1990.

163. E.Lier, "Broad-band elliptical-beamshape horns with low cross-polarisation", ibid., Vol.38, No.6, pp.800-805, June 1990.

164. R.A.Nair, "Dielectric-sphere-mounted corrugated conical horn", Int. J. Electron, Vol.68, No.4, pp.585-593, 1990.

165. C.M.Knopp, "On the performance of metallic wall conical horns with centrally loaded dielectric material", Proc. IEE, Pt.H(1), Vol.138, pp.23-31, Feb. 1991.

166. S.Silver, "Microwave Antenna Theory and Design", McGraw Hill Book Co., New York, 1949.

167. R.C.Johnson and H.Jasik, (Eds): "Antenna Engineering Handbook", McGraw Hill Book Co., New York, 1961.

168. E.C.Jordan and K.G.Balmain, "Electromagnetic Waves and Radiating Systems", Prentice-Hall of India, New Delhi, 1967.

169. R.E.Collin and E.J.Zucker, "Antenna Theory Part I", McGraw-Hill Book Co., New York, 1969.

170. C.A.Balanis, "Antenna Theory, Analysis and Design", John Wiley and Sons Inc., New York, 1982.

171. P.J.B.Clarricoats and A.D.Olver, (Eds): "Corrugated Horns for Microwave Antennas", Peter Peregrinus Ltd., London, UK, 1984.

172. R.Chatterjee, "Dielectric and Dielectric Loaded Antennas", John Wiley and Sons Inc., New York, 1985.

173. Y.T.Lo and S.W.Lee, (Eds): "Antenna Hand Book", Van Nortrand Reinhold Co., New York, 1988.

LIST OF PUBLICATIONS OF THE AUTHOR

1. "Reflector Backed Dielectric Plate with a Surface Grill Structure for Producing Circular Polarisation of E.M. Waves", Proc. Int. Symp. on Electronic Devices, Circuits and Systems, (ISELDECS-87), IIT, Kharagpur, 1987, pp.465-466.

2. "Design of SLCS Horn Antennas", Presented in National Symp. on Microwave Antennas and Propagation, CUSAT, Cochin, 1988.

3. "Development of a New Polariser for E-M Waves Using SCRS Techniques", Proc. Int. Conf. on Electromagnetics in Aerospace Applications", Torino, Italy, 1989, pp.359-360.

4. "A Novel Feed Horn-Substrate for Metallic Corrugated Horn", Proc. National Conference on Electronic Circuits and Systems (NACONECS-89), Roorkee, 1989, pp.379-381.

5. "Simulated Corrugated Feed Horn Antenna", Proc. IEEE AP-S Int. Symp. Texas, USA, 1990, pp.984-987.

6. "A New Scalar Feed with Low Sidelobe Level", Proc. of National Symp. on Microwave Antennas and Propagation (APSYM-90), CUSAT, Cochin, 1990, pp.259-262.

7. "A Strip-Loaded Feed-Horn Antenna", IEEE Microwave and Guided Wave Letters, Vol.1, No.11, pp.318-319, Nov. 1991.

INDEX